Novel Glass Ionomer Cements for Biomedical Applications

Kathryn Hurrell-Gillingham

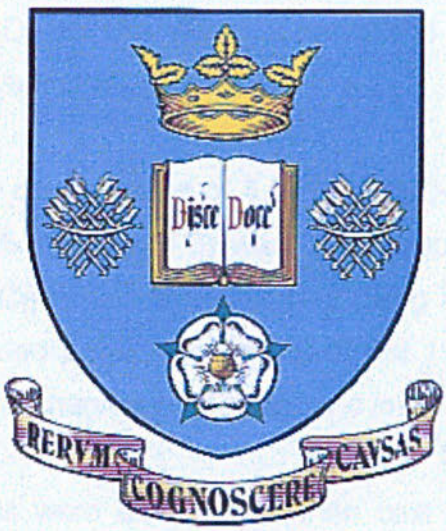

Departments of Engineering Materials & Restorative Dentistry

University of Sheffield

A thesis submitted for the degree of Doctor of Philosophy

January 2004

Abstract

Since their invention in the late 1960's, glass ionomer cements (GICs) have been used extensively in dentistry but recently they have also been utilised as bone cements in ear nose and throat (ENT) surgery. Unfortunately, Al^{3+}, a component of conventional ionomer glasses, has been linked to poor bone mineralisation and neurotoxicity. Consequently, the aim of the research was to modify the glass composition in GIC bone cements to reduce the amount of Al^{3+} present and therefore its potential release during clinical usage. Fe_2O_3 was therefore substituted for Al_2O_3 in the glass formulations and the resulting cements compared with conventional GIC's

Glasses with molar compositions of $4.5SiO_2{\cdot}XM_2O_3{\cdot}YP_2O_5{\cdot}3CaO{\cdot}2CaF_2$ (M = Al or Fe, X = 3 or 1.5 Y = 0 – 1.5) were fabricated using a conventional glass-processing route. Cements were prepared using a standard ratio; 1 g of glass powder: 0.2 g of dried polyacrylic acid: 0.3 g of 10% tartaric acid solution, and their setting times, mechanical properties, and *in-vitro* biocompatibility evaluated.

Al_2O_3-based glasses were amorphous when cast into water but crystallised to apatite and mullite when heat treated at 750°C and 950°C, respectively. In contrast, Fe_2O_3-based glasses devitrified to magnetite and apatite on cooling irrespective of the quench rate. Cements could be fabricated from all glasses and glass ceramics. GIC's based on Fe_2O_3 containing glasses gave similar mechanical properties to conventional Al_2O_3 based GIC's and several compositions were identified whose setting times were appropriate for clinical usage. Good *in vitro* biocompatibility was observed for all Fe_2O_3 - based cements and for those formed from Al_2O_3-based ionomer glasses crystallised at 750°C to form apatite.

Declaration

This research was carried out at the University of Sheffield during the period of October 1999 to January 2004. This research is all my own work and has not been previously submitted to any university for any award.

Kathryn Hurrell-Gillingham
January 15th 2004

To Alan and Phoebe without whom this would have been a lot easier but would be meaningless.

The most exciting phrase to hear in science, the one that heralds new discoveries, is not 'Eureka!' but 'That's funny ...'

- Isaac Asimov

Acknowledgements

I would like to thank my supervisors Dr Ian Reaney and Prof. Paul Hatton. Their guidance and advice over the past 4 years has been unending. Special thanks are owed to them both for being so supportive during my pregnancy and their continued encouragement once Phoebe was born. I would also like to thank Prof. Sharp for his help and advice.

I am grateful for the guidance and support shown by all of the technical staff in the department. Especially to Mr I Watts and Mr D Haylock for their expert guidance in glass melting and furnace operation Even when my glasses melted through crucibles and resulted in black gunk in the bottom of the furnace! Mr H Bagshaw for all of his help, Miss B Lane for helping with DTA, Mr B Keeley for his advice with XRD and Miss D Bussey and the other Sorby Centre technicians for showing me how to prepare EM samples and teaching me how to operate the microscopes. Thanks also to Mrs S Bodell for her help with cell culture.

Thanks to everyone in the Engineering Materials Department. To everyone on L and I floor for the long chats over coffee and help when the computers ate my work. To all the other staff who have helped me be the confident researcher I now am. I would also like to thank everyone involved with the SCAFCART project, although I'm not truly one of you, you made me feel very welcome.

To my long suffering husband, thank you and I promise I will now go and get a proper job! To my beautiful daughter, thank you for being so good and allowing me to finish this. My final thanks go to my friends and family, this thesis is as much yours as it is mine, as it would never have been started or completed without your love and support.

Table of Contents

1. Introduction

Human life expectancy is increasing and as a result ever-greater demands are being placed on medical science. 'Miracle cures' and improved treatments are no longer desired but expected. These expectations have driven the development of biomaterials throughout the 20th century. The ability to repair or replace damaged body parts is however not new but has existed for thousands of years. The Romans, Chinese and Aztecs used gold in dentistry more than 2000 years ago and the use of prosthetics can be dated back to 300BC [Ratner 1996].

Biomaterials have evolved over centuries, with the most significant advances made in the latter part of the 20th century. The field of biomaterials has evolved from one of simple 'trial and error' to an interdisciplinary science based upon an understanding of the interaction between tissue and biomaterials. The development and sale of medical devices is now a multimillion-pound industry and it is continuing to grow.

Natural tissue is difficult to replicate and biomaterials are relatively poor substitutes. The desire to improve currently available biomaterials is therefore great. One area of significance is the replacement and repair of bone. Bone is a vital and complex body tissue. While bone has relatively good healing properties compared to other tissues, it is not always capable of self-repair. Many attempts have been made to develop the ideal artificial material for the replacement or repair of bone tissue [Tartaro *et al* 1996]. Biomaterials have been employed in a wide range of bone repair applications including simple

fracture repair, defect filling and the cementation of implant materials. This large range of operations necessitates the use of a number of biomaterials and devices in the skeletal system e.g. steel, aluminium, polymethylmethacrylate (PMMA) and hydroxyapatite (HA). The use of bone cements for fixing implant materials is one area however, where the ideal material has not yet been developed.

PMMA is the currently the most widely used material for cementing applications. It has been used in total joint replacements for over 30 years. This operation has revolutionised the treatment of joint disease by improving quality of life for many thousands of people [Charnley 1961]. This material, however, acts as a filler or grout, rather than a true cement, as it has no adhesive properties. In addition, it is not osteoconductive and is therefore unable to encourage bone healing. Further disadvantages include thermal necrosis of bone due to the exothermic reaction of the setting cement [Jonck *et al* 1989], which in turn has been linked to the pathogenesis of failure [Wilson and Nicholson 1993]. There is therefore an interest in the development of a bone cement with good biocompatibility, the ability to bond to both organic and inorganic matter, and possessing the appropriate mechanical properties. One class of materials suggested as having the potential to meet these requirements are the glass-ionomer cements (GICs).

GICs have been used as a direct restorative material for dental applications for over 30 years [Blades *et al* 1998, Mount 1998, and Nicholson 1998a]. The main reason for their popularity is their ability to adhere to both enamel and dentine and to release fluoride. GICs are also considered to be more

biocompatibile than many alternative restorative materials [Sasanaluckit *et al* 1993]. These are all desirable properties for use in biomedical applications. In addition GICs have been proven to have 'good handling', a low setting exotherm and can also bond with metallic implants. This long history has led to the development of medical grade GICs. Medical grade GIC bone cement (Serenocem®) manufactured by Corinthian Surgical is available throughout Europe. It has been successfully used as bone cement in middle ear surgery. This material is closely related to its dental predecessor and has potential for further use in medical applications.

While GICs have been used successfully for many years in dentistry, there are concerns regarding GIC biocompatibility in non-dental applications. In particular, Al^{3+} release has been associated with poor local bone mineralisation and neurotoxicity [Carter *et al* 1997, Blades *et al* 1998, Loescher *et al* 1994 a & 1994b]. A detailed summary is given in section 2.3.4.

Cements with reduced or no Al^{3+} release are therefore desirable. One route to achieving this might be the crystallisation of the Al component within the glass. Hill and co-workers [1991a and b, 1995, 2001a and b] have described crystallisation following heat treatment of a number of ionomer glasses. They reported that most compositions crystallised to apatite and mullite, with occasional formation of fluorite and anorthite. While much of this work has focussed on the development of castable glass-ceramics for medical and dental applications, it seems likely that devitrification of ionomer glasses represents a route to improve biocompatibility [Hurrell-Gillingham *et al* 2003].

A second route would be to find an alternative setting agent to Al^{3+}. The main ion considered for the replacement of Al^{3+} is Fe^{3+} since it can also adopt a four or six fold co-ordination in the glass, structurally replacing Al^{3+}. The body already has a mechanism for removal of iron since Fe is a major constituent of haemoglobin and the release into the body should not produce as serious an effect as Al^{3+}. Another consideration in choosing Fe is because the resulting cement would be black, a sharp contrast from the off-white colour of bone. Should revision surgery be necessary, a coloured cement would be more visible to assist the surgeon.

Surprisingly, little effort has been directed at understanding the interaction of these biomaterials with tissues, or the design of safer bone cements, despite the current debate concerning GIC bone cement biocompatibility. The aims of this research were therefore to first investigate modifications to existing commercial GIC bone cement composition to reduce the amount of Al^{3+} released, and second to develop a non-aluminium containing GIC with the potential for use as a bone cement. Specific aims and objectives are discussed in section 2.5.

However, before considering the results of this study, it is important to review the scientific literature surrounding the repair of bone tissue with biomaterials including GICs. Glasses, glass-ceramics, biomaterials and bone tissue are all reviewed in the following chapter. Glass science underpins the whole basis of GIC chemistry and therefore will be discussed in detail.

2. Literature Review

2.1 Bone

Bone is a complex and vital tissue within the human body. It performs many important functions; providing support, shape, and the ability to move. Another important role played by bone tissue is to protect the body from external forces that could damage internal organs, e.g. the skull around the brain. Bones are used for mineral storage, and the central cavity of long bones is employed for the formation of erythrocytes or red blood cells. Both these functions are essential in maintaining life.

2.1.1 Composition and Structure of Bone Tissue

Bone is composed of living cells and matrix containing both organic and inorganic components. The living cells found within bone are osteoblasts, osteocytes, and osteoclasts. Osteoblasts are responsible for the formation of the organic constituent of the matrix, osteoid. Osteoid includes proteoglycans, glycoproteins, and collagen fibres [Marieb 1998]. Osteocytes are osteoblasts which have become trapped in the mineralised bone matrix [Abercrombie *et al* 1984]. The osteoclasts are involved in eroding the bone, helping to maintain bone mass [Alberts *et al* 1994].

One third of the bone matrix is composed of the organic osteoid. The role of osteoid is not confined to providing structural properties such as strength. It also gives the bone flexibility and increases the toughness allowing the bone to be able to resist stretching and twisting [Marieb 1998]. The inorganic

component consists of a calcium phosphate mineral, hydroxyapatite. This is found in the form of small crystals that are associated with the collagen fibres. The mineral component of bone provide hardness and resistance to compression. [Marieb 1998]

The body is made up of four main types of bone commonly termed long, short, flat and irregular according to their shape. Every bone, irrespective of its shape has a dense outer layer, comprising compact or cortical bone and an internal spongy layer known as cancellous or trabecular bone. The structure of these two regions is shown in Figure 2.1.

The compact region is made up of osteons or Haversian systems. Each osteon consists of an elongated cylinder of bone matrix or lamellae with a central or Haversian canal. Within the canals are blood vessels and nerve fibres. Perpendicular to the Haversian canal are Volksmann's canals, these serve to connect the vascular and nerve supplies to the central canals and medullary cavity [Marieb 1998]. The small cavities between the lamellae known as lacunae contain osteocytes that help to maintain the bone matrix. The lacunae are connected to each other and the central canal by canaliculi. [Alberts et al 1994] These canaliculi connect all the osteocytes in an osteon permitting the passage of nutrients and waste products. This is an important function as bone is impermeable to nutrients and these structures allow the bone cells to be fully nourished [Marieb 1998].

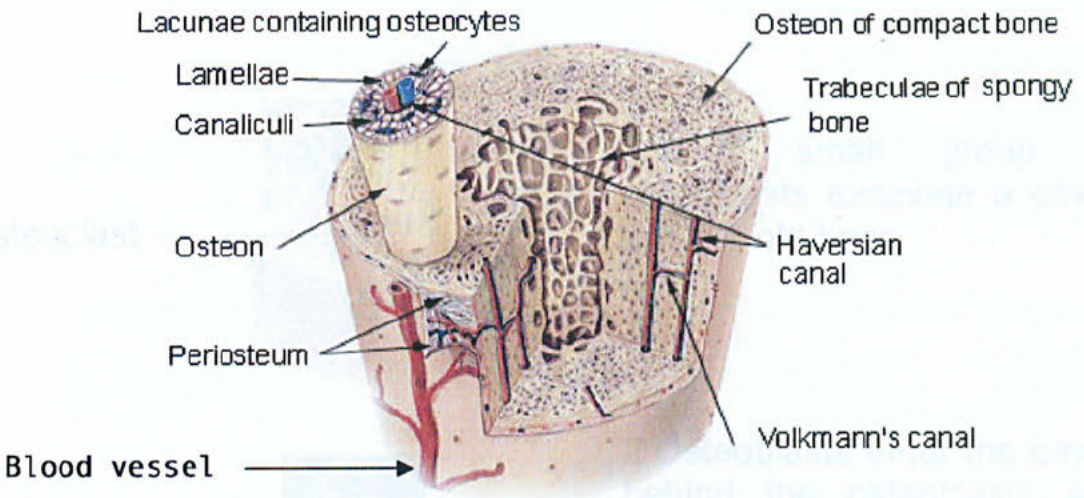

Figure 2.1: Microscopic structure of bone showing both cortical and cancellous bone. [adapted from http://training.seer.cancer.gov]

2.1.2 Physiology of Bone

Bone is a dynamic tissue, constantly remodelling in response to external forces. The process by which this occurs is summarised in Figure 2.2. Osteoclasts secret enzymes and acids onto the surface of the bone causing resorption. This creates a cavity in the bone that is then filled with migrating osteoblasts. These cells lay down concentric layers of new bone which slowly fill the cavity. Osteoblasts can become trapped within the bone matrix and become osteocytes [Alberts *et al* 1994]. This process is continuous and as one cavity is filled another is created. New bone is deposited and resorbed in response to both mechanical and hormonal stimuli. Every week the body recycles around 5 – 7 % of its bone mass. [Marieb 1998]

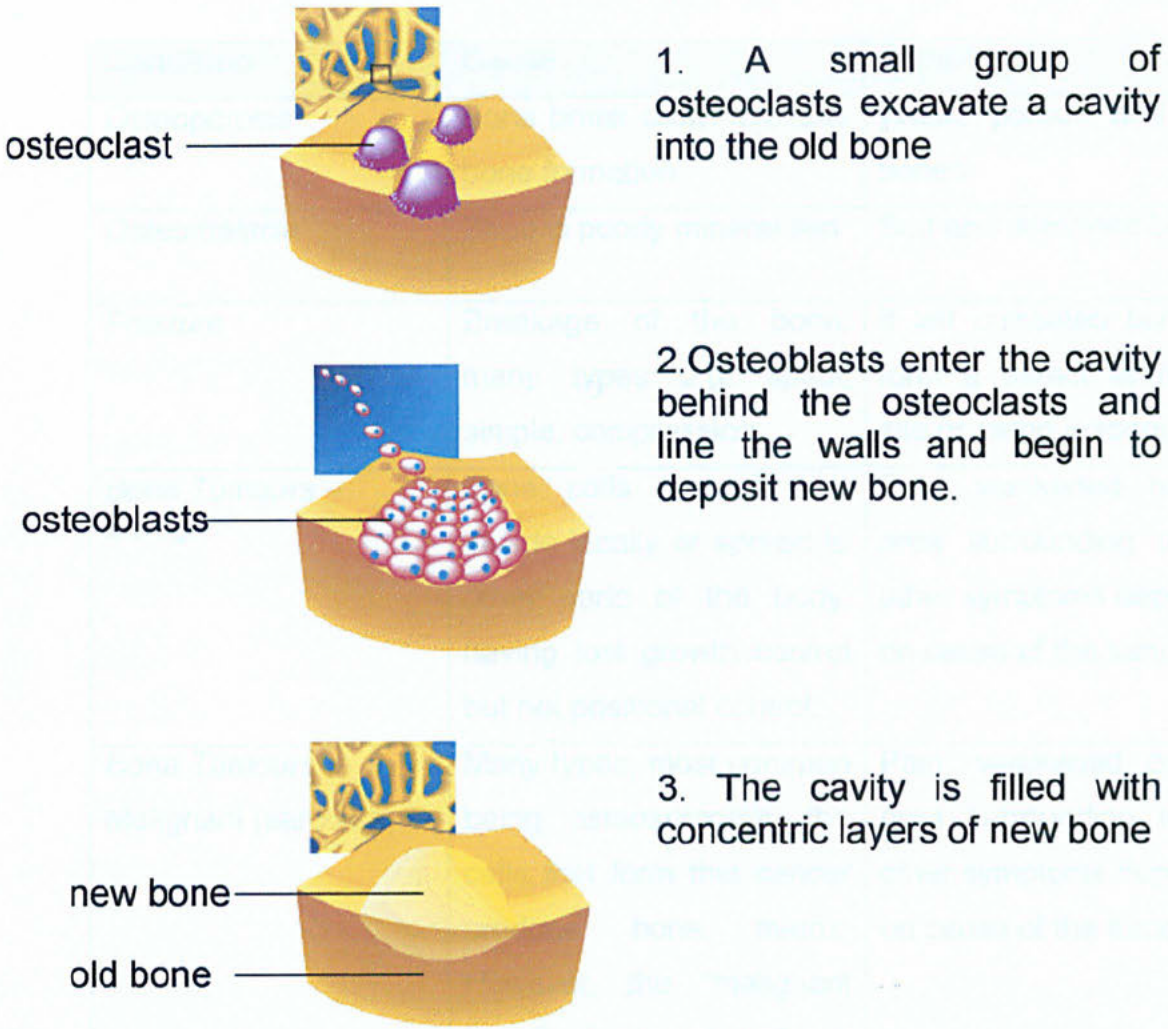

Figure 2.2: A schematic diagram depicting the remodelling of compact bone. [adapted from www.ostex.com and Alberts *et al* 1994]

2.1.3 Bone Injury

Bone can become damaged through a number of mechanisms. The most common is fracture and generally the body can self-repair breakages of this type. Bone can also become damaged through imbalances between bone formation and resorption. Table 2.1 gives a summary of some conditions.

Table 2.1: Examples of conditions causing defects in bone tissue

Condition	**Cause**	**Symptoms**
Osteoporosis	Bone break down exceeds bone formation	Weak, porous and brittle bones
Osteomalacia	Bone is poorly mineralised	Soft and deformed bones
Fracture	Breakage of the bone, many types e.g. spiral, simple, compression	If left untreated bone can form a defect at fracture site or mend inadequately.
Bone Tumours – Benign	Bone cells that do not invade locally or spread to other parts of the body, having lost growth control but not positional control.	Pain, weakened bone in area surrounding tumour, other symptoms depending on cause of the tumour.
Bone Tumours – Malignant (sarcoma)	Many types, most common being osteosarcoma, the cells that form this cancer produce bone matrix. However, the "malignant bone" tissue is not as strong as normal bones.	Pain, weakened bone in area surrounding tumour, other symptoms depending on cause of the tumour.
Osteogenesis Imperfecta	Genetic condition with little or no apparent cause	Bones that break easily
Paget's Disease	Excessive bone break down and abnormal bone formation	Abnormally high ratio of woven to compact bone, spot weakening of bones

Bone has relatively good reparative properties. However the body is not always capable of self-repairing defects and breaks within bone tissue. There is therefore a need for intervention to aid the repair of non-healing bone defects.

2.2 Biomaterials in Bone Repair

Orthopaedic surgeons use a variety of materials in the repair of bone defects. These include autologous and allogenic bone grafts, demineralised bone matrix and alloplastic biomaterials [Finkemeier 2002]. Table 2.2 details some of the currently employed synthetic and natural materials used in the skeletal system for bone defect repair. No one material is suitable for all bone repair applications. The approach to repairing the defect and material selection is based on a number of factors. These include the age and condition of the bone, the nature of the injury, the availability of materials and also on the requirements of the material, whether they are structural or bone forming or both.

Table 2.2: Examples of applications of synthetic and modified natural biomaterials in the skeletal system. [Adapted from Ratner 1996]

Application	**Types of Material**
Joint replacement	Titanium, Ti-Al-V alloy, Steel, Polyethylene
Bone plate for fracture fixation	Steel, Co-Cr Alloy
Bone Cement	Poly(methyl methacrylate), GIC
Bony Defect Repair	Bone Grafts, Hydroxyapatite, Glass-Ceramics
Dental implant for tooth fixation	Titanium, Alumina, calcium phosphate, Glass-ceramics

2.2.1 Bone Grafts and Natural Biomaterials

Autogenous grafts, bone taken from the patient, are regarded as being the ideal material to use [Ducheyne and Qui 1999]. However the removal of bone tissue is both painful and time consuming and involves an additional operation.

Another consideration is that it may not be possible to obtain enough bone to fill the void. For these reasons allogenic bone grafts, biomaterials and combinations of the two have been developed. Allografts are retrieved from cadaver or donor tissue and therefore do not match the tissue of the recipient exactly. Additionally there is a perceived increase risk of infections, such as HIV and hepatitis however there is very little evidence to backup the fears [Finkemeier 2002].

Modified natural tissue also offers an alternative to bone grafts. Demineralising bone leaves the basic bone matrix that can be used as a scaffold. The risk of infection is eliminated and problems associated with tissue matching are minimised. The scaffold can be directly implanted into the defect to encourage the growth of the patient own bone into the pores. Alternatively cells can be pre-seeded into the scaffold. This is cultured and then implanted when cells populate the scaffold. Demineralised bone scaffolds do however tend to lack structural support and can not be used in weight bearing applications.

2.2.2 Alloplastic Biomaterials

The development of biomaterials described in Table 2.2 has advanced the repair of bone defects where more tradition methods, e.g. bone grafts, were just not possible. However the implantation of biomaterials within the body causes a response between the biological environment and the material. This interaction can either be the material affecting the host or the host affecting the material. A summary of these interactions is given in Table 2.3. Some

materials are specially designed to reabsorb whilst others are chosen because they induced a very minor response from the biological environment. The ideal response is when the needs of the biological environment are met [Williams 1987].

Table 2.3: Biomaterial-Tissue Interactions [Adapted from Schoen 1996]

Effect of the implant on the host	**Effect of the host on the implant**
Local a. *Blood-Material Interactions* protein aborption coagulation fibrinolysis platelet adhesion, activation, release complement activation leukocyte adhesion/activation haemolysis b. *Toxicity* c. *Modifications to Normal Healing* Encapsulation foreign body reaction pannus formation d. *Infection* e. *Tumour Growth*	**Physical –Mechanical** a. *Abrasive Wear* b. *Fatigue* c. *Stress – corrosion cracking* d. *Corrosion* e. *Degeneration and dissolution*
Systemic and Remote a. *Embolization* b. *Hypersensitivity* c. *Elevation of implant elements in blood* d. *Lymphatic particle transport* e. *Tumours*	**Biological** a. *Absorption of substances from tissues* b. *Enzymatic degradation* c. *Calcification*

Table 2.2 shows that all classes of materials are used in the repair and replacement of bone. There is an abundance of literature on all of these materials. However this study is concerned with the use of bone cements and the components which make up bone cements therefore no further review of alternative materials will be given.

One class of materials used in bone tissue repair are the glasses, ceramics and glasses-ceramics. These materials have been engineered to interact with the host environment. The relative chemical activity of the different types of ceramics, glasses and glass ceramics is shown in Figure 2.3. Four types of tissue responses have been identified and these can be used for material selection.

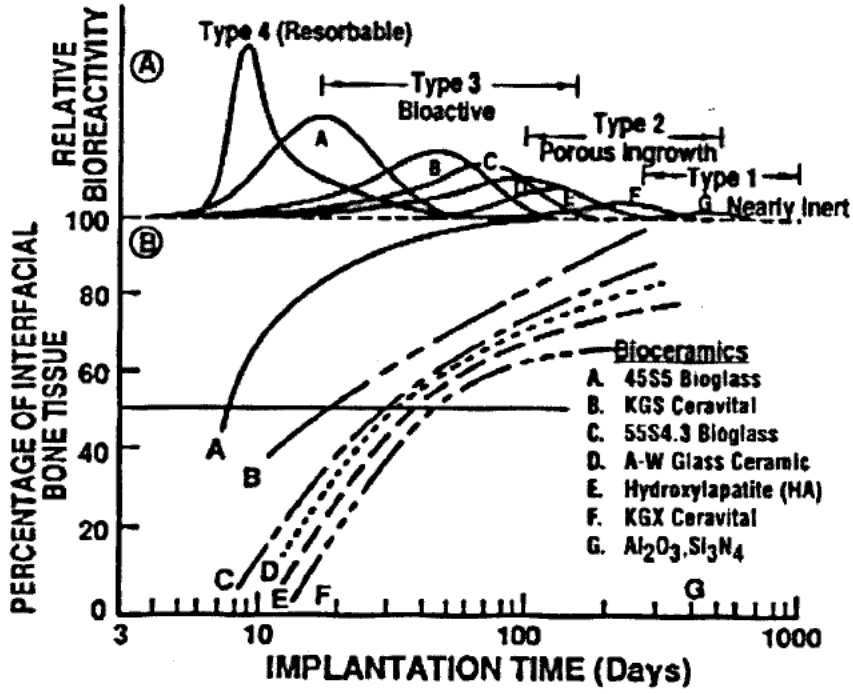

Figure 2.3: Bioactivity spectra for various bioceramic implants [Hench 1996]

A number of different types of ceramics, glasses and glass-ceramics are used in medical applications [Hench 1993]. Ceramics and glass-ceramics are employed because they have high strength. In addition the chemistry of the implant can be tailored to obtain the biological response required.

Most glass-ceramic systems are based on glasses that crystallise to form an apatite phase [Hill and Wood 1995]. The glasses can be cast into specific intricate shapes and then crystallised. A more detailed review of the processing of glass-ceramics is given in section 2.4.2.

Bone Cement

Bone cements can be used for the fixation of implants to bone. This can either be by using the cement to directly glue the implant onto the bone or by acting as grout, filling the void between the implant and the bone. Several biomaterials have been referred to as 'bone cements'. These generally fall into three categories, acrylic bone cement (polymethylmethacrylate (PMMA)), calcium phosphate cements (CaP) or glass-ionomer cements (GIC). Bone cements are also used when repairing bone defects. .

Acrylic Bone Cement

PMMA bone cement provides the fixation into the bone as a grouting agent rather than a glue [Higgs *et al* 2001]. It has enjoyed wide spread use because it is inexpensive to manufacture and easy to use. Polymerisable beads of PMMA are added to liquid MMA monomer. The polymer dissolves into the liquid monomer and in the presence of an initiator addition polymerisation is

started. As it proceeds the mix becomes 'dough-like' and is suitable for introduction into the body or mould. [Kuhn 2000].

PMMA is a relatively biocompatible material, however the presence of residual MMA monomer can cause extensive problems *in vivo*. The monomer is known to be cytotoxic and its release has also been identified as a factor in decreasing blood pressure [Nicholson 2002]. A second problem associated with the setting reaction of this cement is the high exotherm exhibited during polymerisation. This can be in excess of 75°C, causing localised heating to the surround tissue when implanted resulting in tissue death. Additional problems are coagulation of blood that occurs from 56°C and denaturing of collagen which occurs at 72°C [Nicholson 2002]. A further problem specific to orthopaedic implants is that of aseptic loosening. PMMA bone cement has been attributed to this cause of failure. Both the death of the surrounding tissue and shrinkage of the setting cement can cause a gap to appear between the implant and the surrounding bone. The implant is then able to move causing it to fail.

Calcium Phosphate Cements

Calcium phosphate cements have a similar composition to the bone they replace [Nicholson 2002]. Several types of cement formulations exist. Powders are mixed from different calcium phosphate derivatives. For example tetracalcium phosphate (TTCP), dicalcium phosphate anhydrate (DCPA), dicalcium phosphate dihydrate (DCPD) or β – tricalcium phosphate (β – TCP). Combinations of these powders are reacted in the presence of water to form

hydroxyapatite [Kenny and Buggy 2003]. One advantage of this system is that no acidic or basic products are formed.

Calcium phosphate bones cement offers several advantages as bone graft and repairing materials. They are able to adapt to the defect size and shape, and also have a low setting exotherm. [Santos *et al* 2003]. These cements have been shown to be osteoconductive and biocompatible [Kenny and Buggy 2003]. An additional property exhibited by these cements the ability to be remodelled intraoperatively.

2.3 Glass Ionomer Cements

2.3.1 Historical Development

The invention and development of the glass-ionomer cement (GIC) was part of the revolution in dental materials that occurred over the past three decade's [Wilson 1991]. The GIC came into being due to the dissatisfaction with the clinical performance of dental silicate cements. Wilson and co-workers concluded that no further improvements of the silicate cement were possible and began examining alternatives [Wilson and Nicholson 1993]. The initial development took place in the late 1960's by Wilson and Kent, in the Laboratory of the Government Chemist, and in the mid 1970's the first GIC was launched on the market. The original cements were known as ASPA, an acronym for Alumino-Silicate Polyacrylic Acid, this being taken as the trade name for the early commercial materials. The International Standards Organisation has adopted the name glass polyalkenoate cement. However the most commonly used and accepted term to describe these cements is glass-ionomer cement and will be used throughout this research. Both names are now generally expected to describe cements that set via an acid-base reaction

2.3.2 Composition

The cement consists of cross-linked polyacrylate chains reinforced by aluminosilicate glass particles [Neve *et al* 1993]. The original GICs comprise an aqueous solution of poly(acrylic) acid (~45 m/m%) which was reacted with a calcium fluoroaluminosilicate glass [Kent and Wilson 1973]. The resulting cements however set very slowly and were too opaque for use as filling

materials [Nicholson 1998b]. Modifications therefore have been made to produce current commercial compositions.

Ionomer Glasses

Currently all commercially available GIC are based on aluminosilicate glasses which may in addition include calcium, phosphate, strontium and lanthanum oxides. The latter two are generally included because they increase radio-opacity. A typical dental ionomer glass composition is given in Table 2.4.

Table 2.4: Typical GIC glass composition (G200) the basis for ASPA IV glass [adapted from Wilson and Nicholson 1993]

Oxide	Weight percent	Mole percent
SiO_2	30.1	22.3
Al_2O_3	19.9	24.9
AlF_3	2.6	2.7
CaF_2	34.5	33.2
NaF	3.7	1.9
$AlPO_4$	10.0	15.1

There are two main types of glasses, SiO_2-Al_2O_3-CaO and SiO_2-Al_2O_3-CaF_2 from which all ionomer glasses have been derived [Wilson and Nicholson 1993]. The composition of the glass is largely restricted to the region indicated on Figure 2.4. Compositions outside of this tend to crystal or phase separate, resulting in a more opaque glass.

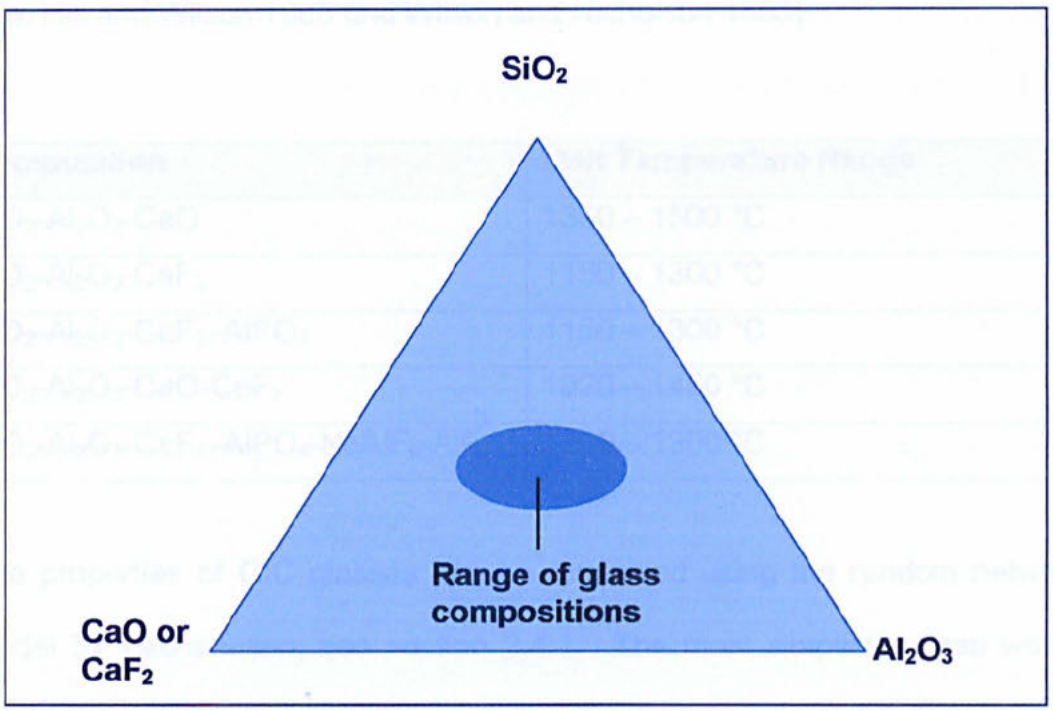

Figure 2.4: Schematic diagram showing the role of glass composition in the production of glass-ionomer cements [adapted from van Noort 1994]

The glasses are prepared using traditional glass processing routes. Raw batch materials are placed into a ceramic crucible, generally composed of sillimanite and melted at a temperature suited to the composition, Table 2.5. The resulting glasses are fast quenched to avoid devitrification. The glass is then ball milled and sieved to obtain a powder with a maximum particle size of 45 μm.

Table 2.5: Glass melt temperatures based on glass composition [adapted from Hill and Wilson 1988 and Wilson and Nicholson 1993]

Composition	**Melt Temperature Range**
SiO_2-Al_2O_3-CaO	1350 – 1500 °C
SiO_2-Al_2O_3-CaF_2	1150 – 1300 °C
SiO_2-Al_2O_3-CaF_2-$AlPO_4$	1150 – 1300 °C
SiO_2-Al_2O_3-CaO-CaF_2	1320 – 1450 °C
SiO_2-Al_2O_3-CaF_2-$AlPO_4$-$NaAlF_6$-AlF_3	1100 – 1300 °C

The properties of GIC glasses can be explained using the random network model by Zachariasen, see section 2.4.1. The most simplistic glass would solely consist of tetrahedra however, these would be unsuitable for use in a GIC since they would not be susceptible to acid attack. The addition of Al into a purely SiO_2 glass alters the behaviour. Al produces only a 3+ charge but can be forced to take up a tetrahedral co-ordination within the glass structure. This leaves the glass with a net negative charge disrupting electroneutrality. This is balanced by introducing positively charged ions e.g. Ca^{2+} and Na^{2+}. [Nicholson 1998a] The Al:Si substitution is limited to a ratio of 1:1. Above this Al^{3+} ions no longer adopts a tetrahedral structure [Wilson and Nicholson 1993].

The Si:Al ratio is believed to alter the length of time taken for the cement to set fully. High Si to Al ratios have been shown [Wilson and Nicholson 1993 and Ellis *et al* 1991] to give a slower set but as the ratio decreases the setting time also decreases. This is attributed to the basic nature of the Al_2O_3 species. The optimum ratio for setting (that which allows manipulation of the cement in-situ but hardens quickly after implantation) is composition dependent and is

linked to the other elements present, mainly Ca^{2+} [Wood and Hill 1985]. Studies by Griffin and Hill [1999 and 2000a] have shown that the Si:Al ratio in the glass did not have a significant influence on cement properties when P_2O_5 was added to the glass formulation. These authors suggested that the Al_2O_3 and P_2O_5 form tetrahedral $AlPO_4$ units and form part of the network in this manner. This reduces the number of Al-O-Si bonds in the glass, which are responsible for Al^{3+} ion release. From their study, they have proposed that a new model of degradation in which the P-O bond hydrolysis is an important mechanism of glass degradation.

Another constituent, F, often added in the form of CaF_2, also confers beneficial properties. The fluorine has two major roles within the set cement. First it lowers the refractive index giving rise to optically lucent cements. Second it is able to form complexes in the set cement that can be released [Griffin and Hill 2000b]. The resulting release of F^- from set cements is believed to have a beneficial effect on tooth tissue, protecting against caries. It has also been shown in experimental glass-ionomer bone cements that osteoconduction does not occur when fluorine is omitted from the glass [Brook *et al* 1991a]. In a more practical aspect, fluorine also lowers the melting temperature of the glass. The setting reaction is also improved by the addition of fluorine as it breaks up the glassy network within the glass allowing the acidic attack to occur more readily [Hill and Wilson 1988].

Up until 2000, all ionomer glass compositions conferred to the above observations. However, during the course of this PhD the has been one report

of an Fe-based GIC [Kamitakahara *et al* 2000]. The glass reported by Kamitakahara *et al* does not contain all the components commonly associated with ionomer glasses. It lacked the presence of both fluoride and phosphate species. In addition very little characterisation was reported and the effect of biocompatibility was not investigated.

Polyacid

The glass component is the main focus of this research, however there has been extensive research into the polymer component. A short review of the polyacids that have been employed in GIC's is given here. The most useful polyacids used are derived from poly(acrylic acid) or copolymers of acrylic and itaconic acids [Crisp *et al* 1975], acrylic and malelic acid [Culbertston 2001]. Figure 2.6 shows the chemical structure of the commonly used polyacids.

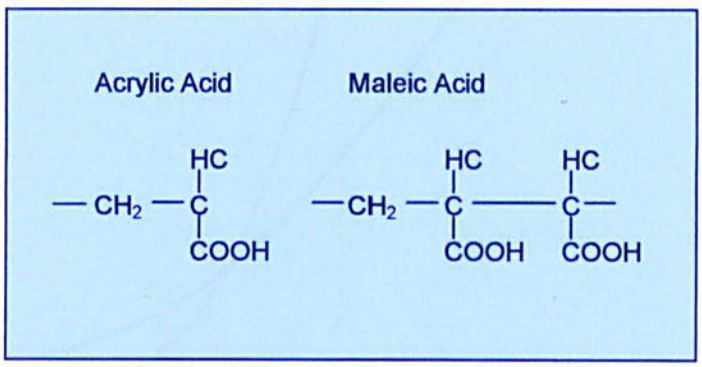

Figure 2.6: Acid components used in glass ionomer cements [adapted from van Noort 1994]

There is not an optimum concentration of polyacid but strength and resistance to aqueous attack increase with increasing polyacid concentration. The limiting factor is the consistency of the cement paste [van Noort 1994].

Early cements were slow to set and Wilson investigated the effects of chelating agents on setting characteristics [Walls 1986]. Tartaric acid was found to improve the cement's handling properties. The working time was extended and the setting was sharpened [Nicholson 1998]. The effect of tartaric acid is shown graphically, Figure 2.7.

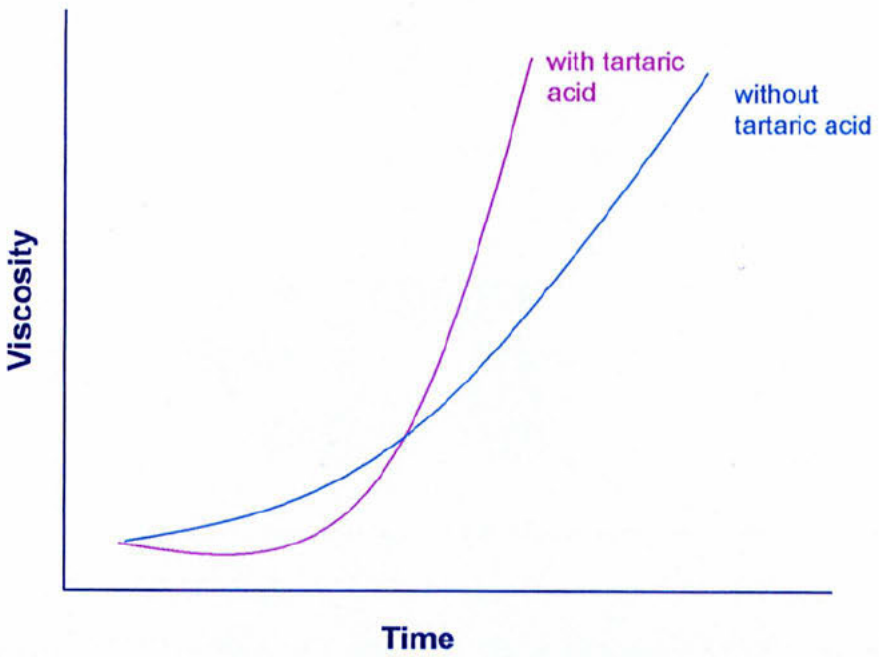

Figure 2.7: The effect of tartaric acid on the viscosity-time curve for a setting glass ionomer cement [van Noort 1994]

2.3.3 Setting Reaction

The setting reaction of a GIC is fundamental in determining the microstructure of the material. The material sets by an acid-base reaction, which can be summarised by the equation, $MO.SiO_2 + H_2A \rightarrow MA + SiO_2 + H_2O$. Most dental textbooks describe the overall setting process as three overlapping stages dissolution, gelation and then finally hardening. The rate at which the processes occur is dependent on the rate of ion release from the materials. Dissolution is the process where the acidic group on the polyacid is attacked by water resulting in the formation of hydrogen ions, as summarised in Figure 2.8.

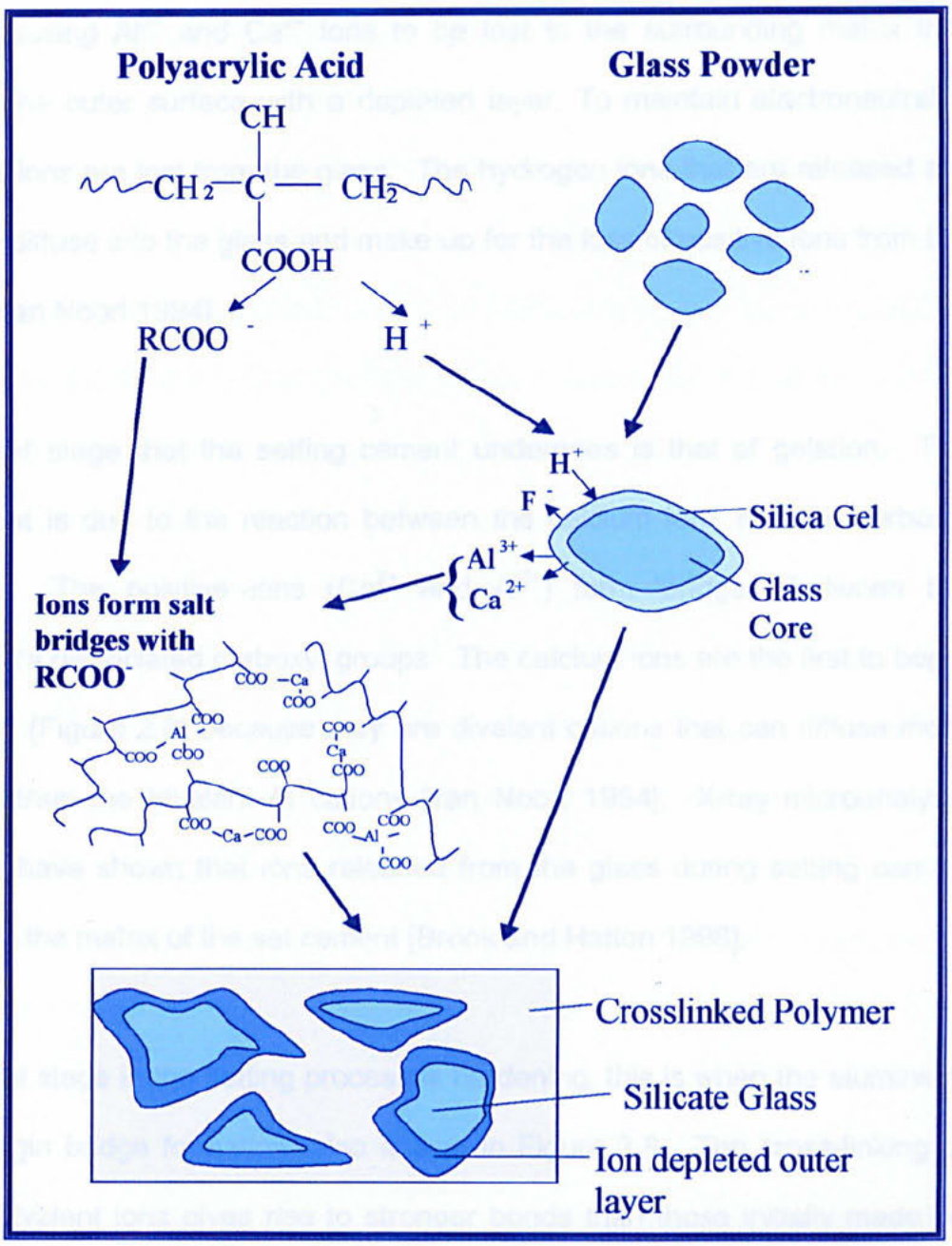

Figure 2.8: The setting reaction of a glass ionomer cement, showing the three main stages dissolution, gelation and hardening

The presence of water causes the acid to go into solution [van Noort 1994]. The water is either present in the powder or in the solution added to form the

glass-ionomer cement. The acid then begins to attack the outer surface of the glass causing Al^{3+} and Ca^{2+} ions to be lost to the surrounding matrix that leaves the outer surface with a depleted layer. To maintain electroneutrality fluoride ions are lost from the glass. The hydrogen ions that are released are able to diffuse into the glass and make up for the loss of positive ions from the glass [van Noort 1994].

The next stage that the setting cement undergoes is that of gelation. The initial set is due to the reaction between the calcium ions and the carboxyl groups. The positive ions (Ca^{2+} and Al^{3+}) form 'bridges' between the polyacid's dissociated carboxyl groups. The calcium ions are the first to begin bridging (Figure 2.8) because they are divalent cations that can diffuse more quickly than the trivalent Al cations [van Noort 1994]. X-ray microanalysis studies have shown that ions released from the glass during setting can be found in the matrix of the set cement [Brook and Hatton 1998].

The final stage in the setting process is hardening, this is when the aluminium ions begin bridge formation, also shown in Figure 2.8. The cross-linking of these trivalent ions gives rise to stronger bonds than those initially made by the divalent Ca cations. There is a continuation of the forming of the salt bridges and water becomes bound to the silica gel that now surrounds the core of the glass particle. [Wilson and Nicholson 1993] The final structure of a set glass-ionomer cement is shown schematically in Figure 2.8 and has also been observed in the transmission electron microscope by Hatton and Brook

[1992]. A non-electron dense region surrounds the glass particles. This has given rise to the expression 'the glass displays a halo'.

More recent data suggests that GIC setting is more complex than the simple textbook definition. Wasson and Nicholson [1990] have shown that by acid-washing the glasses a number of ions in addition to Al and Ca are released. They suggested that these ions could also contribute the setting of the cement. In a later study [Wasson and Nicholosn 1991] they proposed that silica is also involved in the setting and maturation of GICs. Hatton and Brook [1992] have also suggested that the Si ions could also be involved in the setting process. They proposed that the Si were not confined to the outer depleted layer but also had a role in the cross-linking. Matsya et al [1996] further investigated the role of Si ions in the hardening and maturation using IR and NMR. They showed that the silicate network is restructured during the setting and maturation process and could therefore be involved in the increase in strength.

In more recent studies, Griffith and Hill [1999, 2000a 2000b and 2000c] have investigated the role of compositional variation on the properties of GICs. They concluded that phosphate is also important in the setting and maturation of GICs. The phosphate disrupts the cross-linking by competing with the carboxylate groups for the metal cations.

2.3.4 Medical Glass Ionomer Cements

GICs have been used in dentistry since the early 1970's, mainly as a direct restorative material but also in other dental applications (see section 1). The main reason for their popularity is their ability to adhere to both enamel and dentine, and GIC's are considered to be more biocompatible than many alternative materials [Sasanaluckit *et al* 1993]. This successful development has led to further research into the use of this class of materials for wider medical applications.

Ionocem (ESPE GmbH and Co, Seefeld Germany) was the first medical grade GIC developed for use in bone surgery [Engelbrecht 2000]. Early animal studies of GIC bone cements provided evidence of good biocompatibility [Brook et al 1992, Jonck *et al* 1989, 1990 & 1992]. The cement was used in clinical trials that concluded that the materials exhibited good biocompatibility. One trial involving 167 patients undergoing reconstructive middle-ear surgery concluded 'the glass-ionomer cement had proved its value as a well tolerated, easily handled bone replacement material' [Geyer and Helms 1990]. The cement continued to be employed in a number of low-load bearing applications in otorhinolaryngology until 1994.

In 1994 concerns were raised over the *in vivo* neurotoxicity of the setting cement [Loescher 1994a & 1994b]. The most serious manifestations of this problem were clinical reports of complications and death following skull base surgery where relatively large volumes of a GIC bone cement were apparently placed in direct contact with cerebral spinal fluid (CSF) or brain tissue

[Hantson *et al* 1994, Renard *et al* 1994 and Reuscher *et al* 2001]. While doubts have been expressed over the surgical approach taken, and current GIC bone cements are contra-indicated for these clinical applications, concerns remain regarding the biocompatibility of these biomaterials.

Reviews of numerous cell culture studies of cytotoxicity have reported cell inhibition by specific GIC compositions [Brook and Hatton 1998]. It appeared that the *in vitro* toxicity of GICs was due to a complex mechanism based on both ion release (in particular, Al^{3+} and F^-) and pH effects [Brook *et al* 1998 & 1992, Sasanaluckit *et al* 1993, Devlin *et al* 1998].

In addition, *in vivo* work showed a mineral defect in bone adjacent to GICs caused by Al^{3+} release [Carter *et al* 1997, Blades *et al* 1998]. Carter et al [1997] also went on to suggest that the effects of the ions are not confined solely to the surrounding tissue but may have far reaching consequences in the body.

In 1997 a second medical grade GIC was launched onto the market but strict recommendations were suggested to reduce the risk of fatalities. These included not placing the 'wet' cement near or on unprotected nerve tissue and avoiding moisture contamination during setting. However, the clinical needs which the original medical GICs were employed still exist and, without Al, GICs may be a good biomaterial for these procedures. Further research is therefore required to develop GICs that do not release Al during and after setting.

2.3.5 Devitrification of Ionomer Glasses

Previous studies [Wood and Hill 1991a, Milne *et al* 1997 and Rafferty *et al* 2000] have shown that ionomer glasses readily crystallise following heat treatment. Glass-ceramic forming systems are discussed in more detail in section 2.4. The bulk of the literature is based on simple systems, i.e. non-phosphate containing. In non-phosphate glass systems, initial crystallisation of fluorite (CaF_2) occurs at about 700°C, this continues on heating until around 700 – 800°C when the formation stops due to exhausting all the CaF_2 available in the glass [Wood and Hill 1991a]. The residual glass therefore is made up of anorthite ($CaAl_2Si_2O_8$) that crystallises at around 850°C. The crystallisation of fluorite occurs readily because Ca^{2+} and F^- are mobile within the glass network. Anorthite formation however requires strong bonds within the glass network to be broken and as such occurs at a high temperature [Wood and Hill 1991b].

For phosphate containing glasses, the initial crystal to form is apatite ($Ca_5(PO_4)_3$ (OH, Cl, or F) most likely as fluorapatite [Wood and Hill 1991a]. The second crystalline phase to form is mullite ($Al_6Si_2O_{13}$). The high P_2O_5 content of these glasses favours apatite formation over fluorite.

2.4.6 An 'Ideal' Bone Cement

There is a desire to develop a cement for biomedical use. As discussed in the previous section GICs have potential for this application. Altering the chemistry of GIC is known to affect the mechanical properties, setting time and ion leaching of cements. A dental standard exists for the clinical requirements

of dental GIC. Handling is one of the more important properties; if the working time is too short then insufficient mixing can occur, whereas an excessive working time could impinge on the overall setting time of the cement. A setting time of less than 15 min would be desirable as this would allow ample time for placement of the cement. There is a need therefore to determine the properties required of developmental GIC for use in biomedical applications. An ideal bone cement would have a working time of between 90 – 300 s and a setting time not in excess of 900 s.

2.4 Glass and Glass Ceramics

2.4.1 Glass

Glass has been defined as *'the fusion product of an inorganic material which has been cooled to a rigid condition without crystallising'* [Vose 1980, & McMillan 1979]. This definition has been used to describe glasses for decades but with the advances that have been made in glass technology it has become a little dated. Most glasses are inorganic and non-metallic but it is possible to form glasses from organic materials e.g. glucose [Paul 1982]. This definition also makes assumptions about the method of glass formation. Traditionally they are formed through the reaction of raw materials (e.g. sand, soda, potash) at elevated temperatures and the resultant product cooled. However other methods exist through which glasses can be formed. Vapour deposition, sol-gel processing and neutron irradiation of crystalline materials [Shelby 1997] although very specialised techniques, can be used to produce glasses.

Every glass, regardless of the processing route or chemical composition have two common characteristics [Shelby 1997]. First they lack the regular arrangement of atoms characteristic of the crystalline state and exhibit atomic arrangements similar to liquids [Paul 1982]. This can be illustrated using X-ray diffraction (XRD) and electron diffraction, these techniques show that glasses lack long-range periodic order. A characteristic XRD pattern is shown in Figure 2.9, which exhibits an amorphous glassy hump and demonstrates the absence of peaks corresponding to crystal phases.

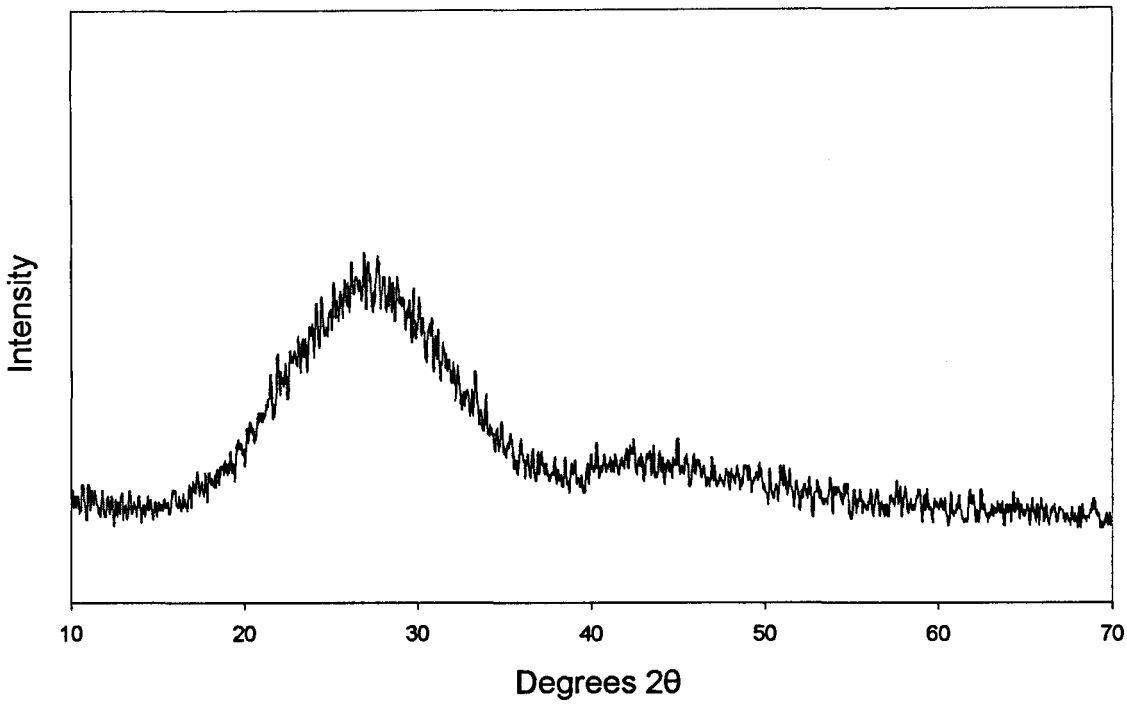

Figure 2.9: Typical X-ray diffraction curve obtained from a glass sample

Second, all glasses exhibit time-dependent behaviour known as glass transformation [Shelby 1997]. Unlike crystalline solids, glasses do not have sharp melting points. Glasses combine the short-time rigidity of the crystal state with a little long-time fluidity of the liquid state [Paul 1982].

Therefore a more accurate definition of a glass would be '*an amorphous solid, completely lacking in long range periodic structure which exhibits a region of glass transformation behaviour*'. [Shelby 1997]

Glasses tend to be transparent because they are isotropic structures. There are no planes and they lack internal structures e.g. grain boundaries that can

scatter light. Additionally glass has a homogenous structure and as such a crack, once started, will not meet an obstruction to hinder its progress [Vose 1980].

The glass transition behaviour and the relationship between crystal, glass and liquid can be explained via a volume-temperature diagram, Figure 2.10. On cooling a liquid from point A, the volume will slowly decrease along the line AB. If the rate is slow and nuclei are present then crystallisation will occur. This takes place at point B, also known as T_f the freezing or melting temperature. The liquid suddenly becomes a crystalline solid, causing a rapid decrease in volume (C). Further cooling (C $\rightarrow$ D) results in a gradual decrease in volume, due to contraction of the solid. A glass however forms if cooling is sufficiently rapid and crystallisation is avoided, passing through point B and continuing onto E. The volume of the super-cooled liquid decreases along line BE, upon reaching a certain temperature, T_g, the gradient of the line changes and becomes parallel to CD. The point T_g is where the material changes from a liquid to glass and is known as the glass transformation temperature. T_g varies with glass composition and is defined as the temperature at which the viscosity of the material is 10^{13} poise.

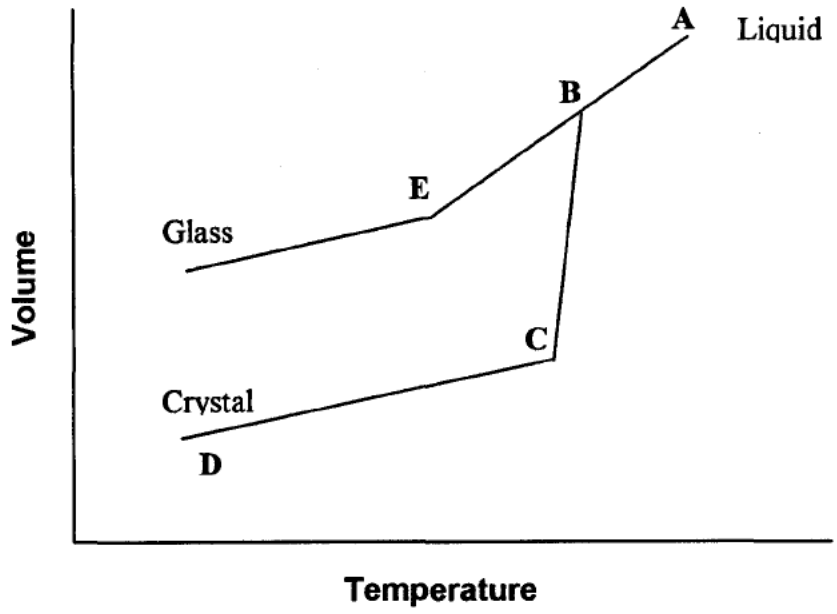

Figure 2.10: Relationship between glass, liquid and solid.

The ability of a substance to form a glass does not depend upon any particular chemical or physical properties. It is now generally agreed that almost any substance if cooled sufficiently fast could form a glass. A number of models have been proposed to explain the formation of glasses. The most highly regarded is the Zachariasen's random network hypothesis. Zachariasen proposed that since the mechanical properties and density of an oxide glass are similar to those of the corresponding crystal, the interatomic distances and interatomic forces must also be similar. Zachariasen postulated that as in crystals the atoms in glasses must also extend in three-dimensional networks. XRD however, shows that the network in glasses is not symmetrical and periodic as in crystals. [Paul 1990, Rawson 1967 and McMillan 1964]

In SiO_2 for example, the only difference between vitreous and crystalline silica, is that in the glassy form the relative orientation of adjacent silicon-oxygen tetrahedra is variable whereas in the crystalline form it is a constant structure, this difference can be shown schematically, Figure 2.11.

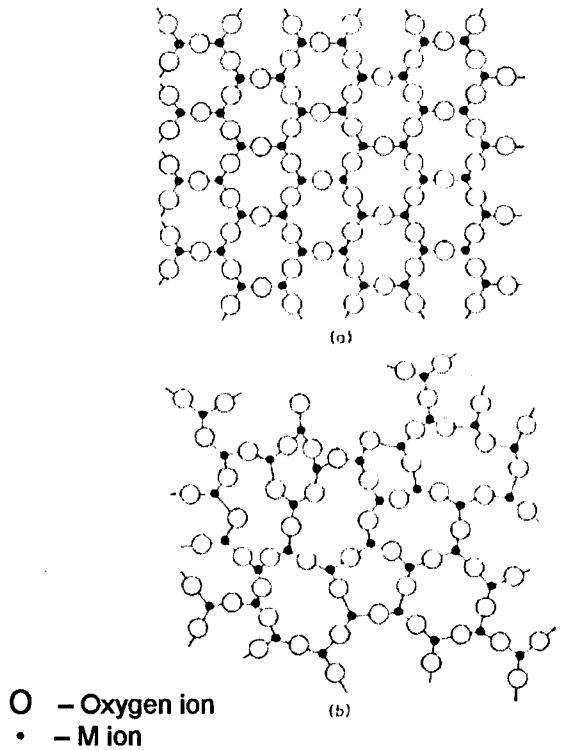

Figure 2.11: Two-dimensional representation of the structure of (a) a hypothetical crystalline compound M_2O_3 and (b) the glassy form of the same compound. [McMillan 1979]

Zachariasen went onto to propose certain conditions that an oxide must satisfy in order to form a glass:

1. No oxygen atom may be linked to more than two atoms of M.

2. The number of oxygen atoms surrounding M must be small (probably 3 or 4)
3. The oxygen polyhedra share corners with each other not edges or faces.
4. At least three corners of each polyhedron must be shared.

Oxides of the type A_2O and AO do not satisfy the rules laid out above and should therefore not form glasses. This is found to be correct as none of the group I or II elements form glasses on their own. A_2O_3 type oxides do form glasses, this is consistent with the criterion of rules 1,3 and 4 proposed by Zachariasen, provided that the oxygen's form a triangular arrangement around the M ions [McMillan 1979]. It is also possible for oxides of the type MO_2 and M_2O_5 to from glasses provided that the oxygen's form a tetrahedral arrangement [Rawson 1967]. The fourth condition proposed is not strictly applicable since glasses are known in which this condition would not be fulfilled. [Paul 1982 and McMillan 1979]

A second approach to determining the formation of glasses is based on the kinetics of glass formation. This approach does not use the ability of a liquid to form a glass but rather how fast must a liquid be cooled to avoid crystallisation [Paul 1990]. The theory was originally proposed by Staveley in the 1950's but has undergone a series of revisions and currently Uhlmann's interpretation is the most widely accepted [Paul 1990 and Uhlmann and Yinnon 1983]. Uhlmann suggested that theoretical time/temperature/% transformation (T-T-T) curves might provide a route in determining the cooling rate required avoiding devitrification. He devised an equation (equation 2.1)

which can be applied to the T-T-T curves to determine the rate required to avoid a given volume fraction of crystallisation.

$$X \sim \tfrac{1}{3} \pi I_v u^3 t^4 \qquad \text{Equation 2.1}$$

Where X is the volume fraction of X crystallised t is time I_v is the nucleation frequency and u is the rate of advance of the crystal – liquid interface. To construct the curves a known volume fraction of crystallisation is chosen and the time taken for that volume to form is measured at different temperatures. Figure 2.12 is an example of a T-T-T curve.

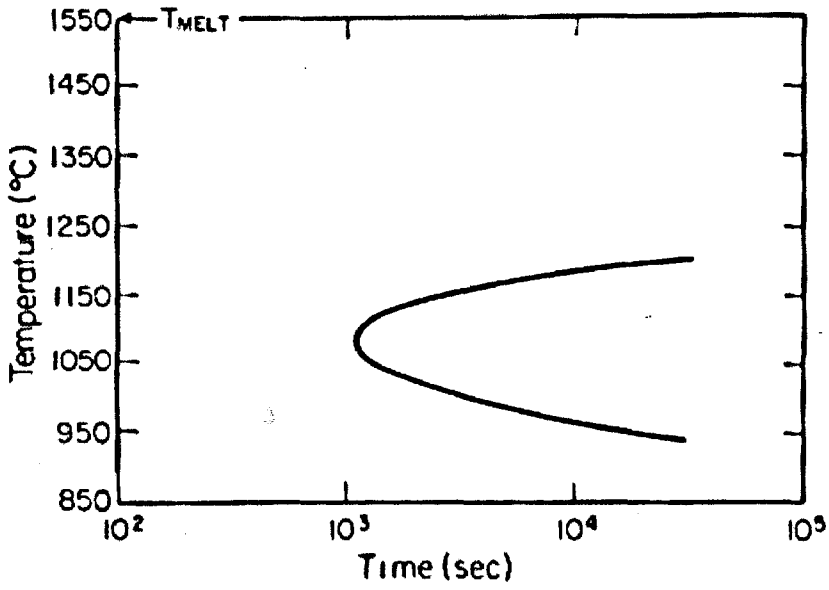

Figure 2.12: Isothermal time-temperature-transformation (T-T-T) curve for anorthite [Paul 1982]

The nose of the curve corresponds to the least time required to obtain the crystallisation. This results from the driving force to crystallise (increases with decreasing temperature) and the atomic mobility (decreases with decreasing

temperature). The critical cooling rate, R_c required to form a glass can be calculated using equation 2.2.

$$R_c \sim \frac{\Delta T_N}{\tau_N} \qquad \text{Equation 2.2}$$

Where $\Delta T_N = T_m - T_N$ and T_m is the melting temperature, T_N is the temperature at the nose of the curve and τ_N is the time at the nose of the curve. [Uhlmann 1983]

Glasses are made up three components, glass or network-formers, network-modifiers and intermediates [Shackelford 1996]. Glass formers provide the backbone in mixed oxide glasses [Paul 1990] but are equally capable of forming a glass on their own. Only B_2O_3, SiO_2, GeO_2 As_2O_3 and P_2O_5 readily become glasses [Babcock 1977], these all form oxide polyhedra and are capable of making a network of tetrahedra [Shackelford 1996]. The manufacture of single oxide glasses is expensive due to the high temperatures required to melt the oxides therefore network modifiers or fluxes are employed. Modifiers break up the continuity of the network and change the properties of the glass [McMillan 1964]. Modifiers also tend to have a lower melting temperature than the formers and provide a medium in which they can dissolve, thus producing a glass at a much lower temperature. The most commonly used fluxes are soda and potash. Until recently lead was used but due to concerns over safety it is less commonly employed. There is however a disadvantage to using a flux as they can decrease the durability of the glass. Na and Li ions are small and are easily leached by water. Intermediates have

a stabilising effect on the glass and are added to increase the chemical durability and also to decrease the possibility of unwanted devitrification. The oxides are usually alkali earth or transition metal oxides, lime and Al_2O_3 are also used. Al^{3+} for example is able to substitute for Si^{4+} within the glass network and this increases the network stability [Shackelford 1996].

Glasses are known to undergo a number of phase transformations, these are summarised in Figure 2.13. Modern experimental techniques have shown that glasses believed to be homogenous have actually undergone phase separation [Beall and Duke 1983]. Glass in glass phase separation is very similar to oil in water. Two types of separation exist and are formed either above or below the liquidus temperature. When phase separation occurs above the liquidus it is termed stable immiscibility and the resulting effect is to give the glass an opalescence appearance [Ford and Todhunter 1989]. Phase separation that occurs below the liquidus is called metastable immiscibility. Figure 2.14 shows an example of a dome of immiscibility. The latter is of more interest as it can be a precursor to crystallisation and may offer a route to forming glass-ceramics that will be discussed in section 2.3.

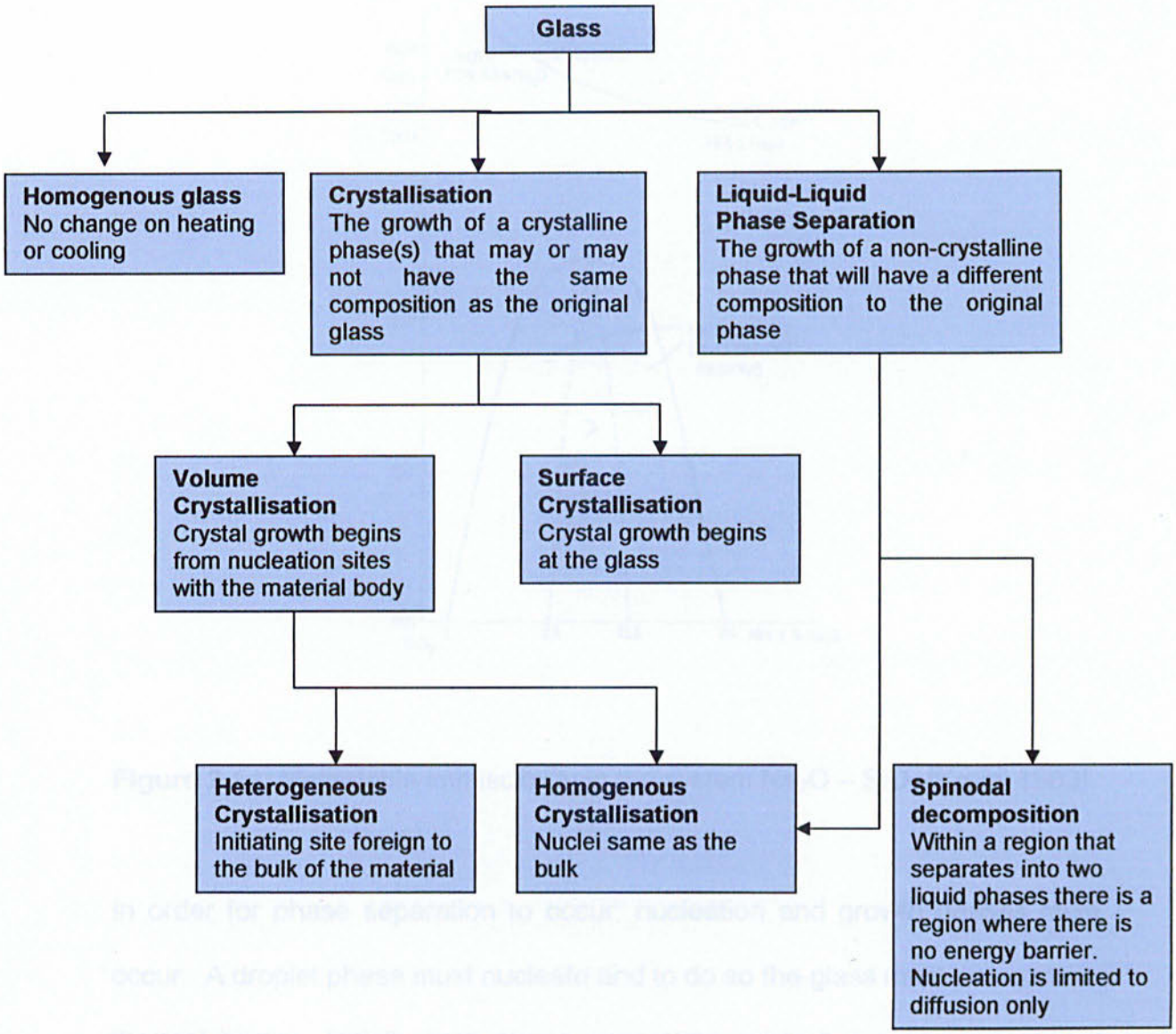

Figure 2.13: Phase transformations in glasses [adapted from Paul 1990]

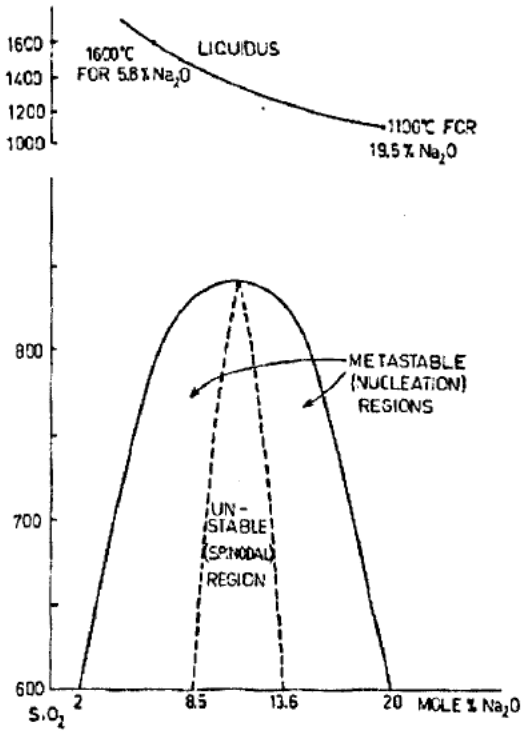

Figure 2.14: Metastable immiscibility in the system Na_2O – SiO_2 [Kreidl 1983]

In order for phase separation to occur, nucleation and growth phases must occur. A droplet phase must nucleate and to do so the glass must overcome a thermal barrier. Initially zero phase separation exists but once nucleated it grows until equilibrium is reached. Growth occurs through diffusion. The mechanism of phase separation can be determined using a free energy composition curve for a specific system, Figure 2.15.

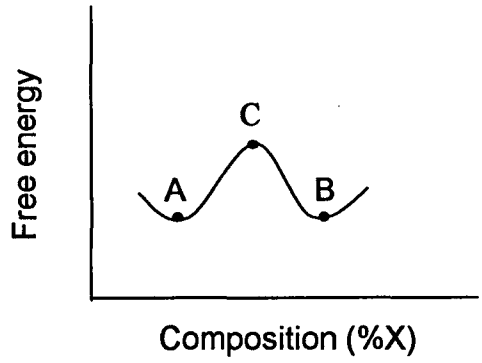

Figure 2.15: Free energy composition diagram for a binary glass of composition X and Y

Consider a binary system composed of X and Y. At a temperature above T_c, the glass will be uniform and single phase (point C on Figure 2.15). Decreasing temperature to just below T_c will cause a small fluctuation in composition to occur. The free energy will drop causing the system to become unstable eventually it ends up at points A and B. This phenomenon is known as spinodal decomposition. [Ford and Todhunter 1989]

2.4.2 Glass Formation

There are a number of methods and processing routes available to produce glass. The most common however is the traditional furnace method. A glass batch is placed into a crucible and is transferred to a furnace at the required melt temperature. The furnace can either be electrically or gas heated. Electric furnaces tend to be used more often for small experimental melts as they are cleaner and therefore do not contaminate the glass. Gas furnaces are more suited to larger scale melts. They are cheaper to run and heat up

more quickly than electrical counterparts. An additional advantage to using gas furnaces is that it is possible to alter the atmosphere within the furnace. It is possible therefore to have either a neutral, oxidising or reducing environment in which to melt the glass. However due to the design of a gas furnace, it is not possible to include a stirrer into the melt.

Crucibles are used as the reaction vessels in which the transformation from batch materials to liquid glass takes place. Crucibles can be manufactured from both ceramic and metallic materials. These materials are employed because they are durable at the elevated temperatures commonly used in the manufacture of glass. Platinum is often used to make crucibles because it is chemically and thermally stable. However they cannot be employed in the manufacture of P_2O_5–containing glasses because they are known to attack Pt-12%Rh crucibles [Babcock 1977].

Ceramic crucibles are susceptible to corrosion during the glass melting process [Cable 1998]. Four main types of ceramic refractory corrosion are known to exist, (i) direct or congruent (ii) indirect or incongruent (iii) flux-line corrosion and (iv) drilling [McCauley 1996]. All the mechanisms involve an interface between the refractory and the glass. In (i) the resulting interface is due to direct dissolution of all the refractory material into the glass, however in (ii) the interface arises from the indirect dissolution of one or more phases present in the refractory. Flux-line corrosion (iii) is related to the increased convection that occurs at the glass surface, this causes an increase in the surface energy that in turn causes an increase in dissolution of the refractory.

The final mechanism, drilling (iv), involves a further interface with gaseous bubbles present in the melt. When the glass comes into contact with a horizontal surface (e.g. the base of the crucible) gas bubbles can become trapped between the two. This can result in the downward drilling motion of the bubbles resulting in specific corrosion at the base of the crucible. [McCauley 1996]

Refractory corrosion is also related to melt temperature, viscosity and refractory defects. Corrosion rate doubles for every 50°C increase in temperature of the melt furnace and a decrease in the glass' viscosity also results in an increase in the corrosion rate. Crucible defects can act as loci for corrosion, examples include regions of chemical difference (residual glass after firing the crucible) which can be more susceptible to dissolution and physical defects such as a change in the surface topography of the crucible. This can causes changes in the convection flow patterns resulting in preferred areas of corrosion. [McCauley 1996 and Begley 1974]. In addition the composition of the glass can also contribute to the rate of corrosion.

2.4.2 Glass-Ceramics

All glasses will crystallise providing a high enough temperature is applied. Generally unwanted crystals grow in from the surface in a chaotic and disorganised manner (Figure 2.16a). Impurities and surface defects act as the nuclei for crystal growth. The glass-ceramics formed however are of poor quality and are generally weak therefore specific glass compositions have been designed to encourage volume or bulk nucleation (Figure 2.16b).

Crystals grown through this method are evenly distributed throughout the glass bulk and give rise to a finer more organised crystal structure. Generally a nucleating agent is required but some glass systems are able to homogeneously nucleate [McMillan 1979].

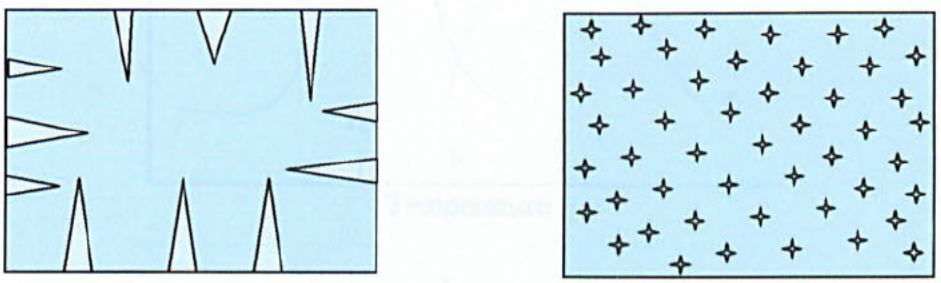

Figure 2.16: Crystal growth a. surface nucleated and b. volume nucleated

The first stage in forming a glass-ceramic is to ensure that the glass is homogenous. Second a high density of nuclei is desired. An optimum temperature for this can be calculated with the aid of a nucleation (I) temperature graph (Figure 2.17). The curves have been derived for various glass compositions and exhibit a maximum to coincide with the highest number of nuclei present. The glass is then held at this temperature for a set period of time. Following the period of nucleation the crystals need to be encouraged to grow, therefore a second hold temperature is derived from a crystal growth rate temperature chart (Figure 2.17). The graph also exhibits a maximum to correlate with the optimum amount of crystal growth.

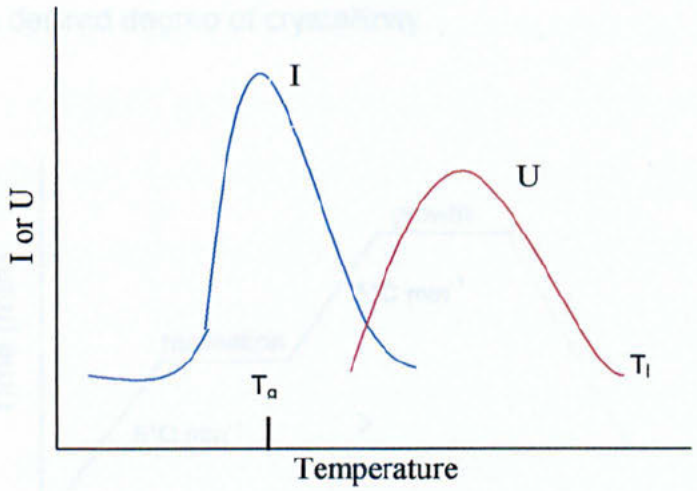

Figure 2.17: Schematic diagram showing the nucleation rate (I) and growth rate (U) curves versus temperature [adapted from McMillan 1979]

Using the temperatures derived from Figure 2.17 it is possible to obtain a heat treatment schedule required to produce a glass ceramic from a glass. Figure 2.18 shows a typical heat treatment schedule. Typically, a two step heat treatment is applies. The glass is heated from room temperature to the required nucleation temperature at a rate of around 2 – 10°C/min. The rate is not too important but care must be taken not to introduce stresses within the glass. The glass is then held at this temperature for a prolonged period of time to maximise the number of nuclei formed. The second stage is also preceded by a controlled increase in temperature. The heating rate is more important because if the glass is heated too quickly then volume changes associated with the formation of crystals can cause cracking in the glass. With a slower heating rate the internal stresses introduced due to the volume changes can be relieved by slow viscous flow in the residual glass [McMillan

1979]. The material is then maintained at a constant growth temperature to achieve the desired degree of crystallinity.

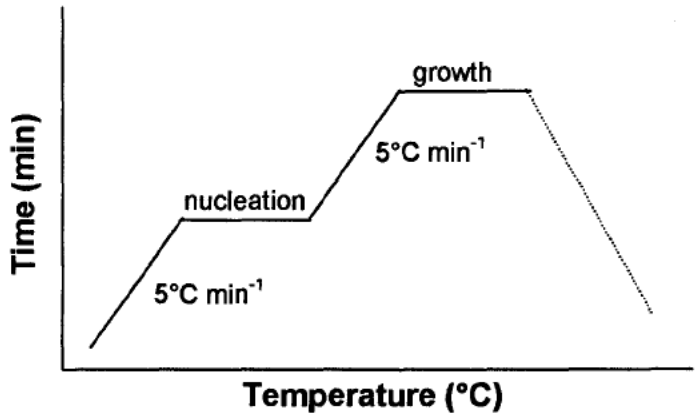

Figure 2.18: Double stage heat treatment schedule used to prepare a glass ceramic

In more complex glasses where more than one crystal phase may form, an isothermal heat treatment to the growth temperature may be employed, omitting the nucleation steps.

2.5 Aims

To summarise, glass ionomer cements have been developed for use as *in situ* setting bone cements for specific applications in otorhinolaryngology (ENT) surgery. However, there are still doubts regarding their biocompatibility. These concerns are based on the potential for Al^{3+} release, an ionic species associated with poor bone mineralization and neurotoxicity. The aim of this research was therefore to investigate routes to reduce or eliminate Al^{3+} release from GIC's. Specific objectives were therefore:

- To produce a series of glasses based on a commercial glass formulation (Serenocem®) and to use these to investigate the effect of composition and controlled crystallisation on ion release and *in vitro* biocompatibility of the resulting cements.
- To produce a series of ionomer glasses where Al_2O_3 is fully replaced by Fe_2O_3, and to evaluate their potential for cement formation with PAA.
- To study the effect of Fe-based glasses on ion release and their respective cements.
- With respect to these novel cement series, to investigate ion release and its relationship to *in vitro* biocompatibility.

On conclusion, this research will add significantly to existing knowledge of GIC's, and contribute to the development of a new class of biomaterials.

3. Experimental Procedure

3.1 Materials

3.1.1 Glass Formation

Table 3.1 shows the raw materials employed for the melting of all the glasses in this study. The amounts employed for each individual glass is given in Tables 3.4 – 3.6.

Table 3.1: Raw materials used for the fabrication of all glasses.

Raw Material	**Company**
$Al(OH)_3$	Fisher Scientific, UK
Fe_2O_3	Fisher Scientific, UK
$CaHPO_4$	Fisher Scientific, UK
$CaCO_3$	Fisher Scientific, UK
CaF_2	Fisher Scientific, UK
Sand (99.5% SiO_2)	Tilcon (south) Ltd, UK

3.1.2 Glass Characterisation

Table 3.2 shows the materials used in the characterisation of the glasses.

Table 3.2: Materials used in the preparation of electron microscopy samples

Material	**Information**	**Company**
Silver Dag	Silver in methylisobutanetone	Agar Scientific LTD, Essex UK
5 minute Epoxy Resin	epoxy and polyamine resin	Devcon, England

3.1.3 Cement Formation

Table 3.3 shows the materials used to fabricate the GICs.

Table 3.3: Materials used to fabricate cements

Material	Information	Company
Serenocem® glass	Batch 079920-5	Cera Dynamics Ltd, Northamptonshire, UK
Mercaptan-free Poly(acrylic acid) (PAA)	Mean MW 52,000 Batch 079915-2	Advanced Healthcare, Kent, UK
Tartaric acid solution	Ultra-pure water	Stenpak, Runcorn, UK
	Tartaric acid	BDH LTD, Poole, UK

3.1.4 Cement Characterisation

Ion Release

Total ionic strength adjustment buffer (TISAB II)(Orion Research Inc, Boston Ma, USA) was used as a decomplexing agent. This contains H_2O, NH_4Cl, CH_3COONH_4, $C_6H_{10}[N(CH_2COOH)_2]_2$ and Cresol red sodium salt. Protein standard solutions were made using protein solution (Orion Research Inc, Boston Ma, USA). HCl (10N, Aldrich Chemicals, Dorset, UK) was also used in the ion release.

Cell Culture

Table 3.4 shows the materials used for both culturing and processing of cultured samples.

Table 3.4: Materials used to perform and evaluate the cell culture studies

Name	Information	Supplier
Methylthiazolyldiphenyl - tetrazolium bromide (MTT)	3-(4,5-dimethylthiazol-2-yl)-2,5-diphenyltetrazolium bromide	Sigma Diagonostic Inc, St Louis, USA
Ca^{2+}/Mg^{2+}-free phosphate-buffered saline (PBS)	0.14 M NaCl, 2.7 mM KCl, 1.5 mM KH_2PO_4, 8.1 mM Na_2HPO_4, pH 7.2	Gibco BRL® Life Technologies, Paisley, UK
Dulbecco's modification of Eagle's medium (DMEM)	High glucose formula with 4500 mg/L glucose & sodium bicarbonate. Without L-glutamine	Gibco BRL® Life Technologies, Paisley, UK
Penicillin – Streptomycin – Glutamine	10000 units/ml penicillin, 10000 mg/ml streptomycin & 29.2 mg/ml L–glutamine in 85 % saline in a 10mM citrate buffer	Gibco BRL® Life Technologies, Paisley, UK
Foetal calf serum (FCS)	Heat-inactivated	Gibco BRL® Life Technologies, Paisley, UK
Trypsin-EDTA Solution	0.5 g/L trypsin 0.2 g/L EDTA in Ca^{2+} / Mg^{2+} - free Hanks balanced salt solution	Gibco BRL® Life Technologies, Paisley, UK
Protein Standard	Albumin (bovine)10 g 1.0 mg/mL in 0.15 M NaCl, 0.05% NaN_3	Sigma Diagonostic Inc, St Louis, USA
Biuret Reagent	$CuSO_4$ 0.75 mM, NaOH 94 mM, $KNaC_4H_4O_6$ 2.6 mM, KI 3.76 mM and Na_2CO_3 0.19 mM	Sigma Diagonostic Inc, St Louis, USA
Lowry Reagent	45% $CH_3(CH_2)_{11}OSO_3Na$, 38.5% Na_2CO_3, 15% $LiOH.H_2O$, 1.35% CuC_2H_2O6	Sigma Diagonostic Inc, St Louis, USA
Folin – Ciocaulteu's Phenol Reagent	57.5% H_2O, 15% $LiSO_4$, 10% $Na_2WO_4.2H_2O$, 10% HCl, 5% H_3PO_4, 2.5% $Na_2MoO_4.2H_2O$	Sigma Diagonostic Inc, St Louis, USA
Acidified Isopropanol	0.5 ml 0.04 – 0.1 N HCl in absolute Isoproponal	Aldrich Chemicals, Dorset UK
Osmium tetraoxide	1% OsO_4 (aq)	BDH, Poole UK
Cacodylate Buffer	0.1 M, pH 7.4, Sodium Cacodylate in H_2O	BDH, Poole UK
Gluteraldehyde Fixative	3% Gluteraldehyde in 0.1 M Cacodylate Buffer	BDH, Poole UK

3.2 Glass Melting

A premixed batch of raw materials was used to produce either 50, 100 or 300 g of glass. Glass batches were prepared from standard laboratory grade chemicals (section 3.1.1). The batch calculations can be found in Appendix I. 'Full' and zero P_2O_5-containing glasses were produced and ratios of these two glasses were melted to make intermediate compositions.

Crucible selection was an important factor in the formation of glass. It has been shown that Pt-12%Rh crucibles undergo flux line dissolution in P_2O_5–containing glasses and therefore it was necessary for P_2O_5–containing glasses to be melted in ceramic crucibles [Babcock 1977]. Sillimanite (Al_2SiO_5) crucibles were found to be the least susceptible to corrosion from the Al_2O_3–containing glasses. Fe_2O_3–containing glasses are more aggressive to sillimanite refractories [Volf 1984] and therefore alumina (Al_2O_3) crucibles were used in the production of these glasses. Lids were added to the ceramic crucibles to avoid the loss of batch components during melting. The crucibles were weighed before and after the melts to determine any losses that might have occurred.

All types of ceramic crucible (alumina, mullite and sillimanite) were heated to 1050°C (2°C min^{-1}) prior to melting to avoid thermally shocking the crucible. When using an Al_2O_3 crucible the batch also had to be preheated. This method was also used when sillimanite crucibles were employed. Preheating was found to reduce the loss of reactants during charging.

The crucible containing the batch was transferred to an electrically heated box glass-melting furnace at 1450°C. The length of the melt was composition dependent varying from 1 to 3 h. Fe_2O_3–containing glasses required a shorter melting time than the Al_2O_3–containing glasses. Melt time was kept to a minimum to reduce crucible corrosion and glass contamination.

Glass was made using a quenching method. The fluid glass was either poured into a container of cold water to form granular frit, or quenched between two pieces of steel. Some of the glass compositions were found to devitrify on cooling. Iced salt water (-3°C) was used as the quenching medium to minimise the formation of crystals.

3.3 Glass Composition

Glass melts were deemed successful if all the batch components had fully melted and the viscosity was sufficiently low for pouring. Glasses in the Al_2O_3 series that had opacity or crystallisation present on quenching were discarded.

3.3.1 Glass Series A – $4.5SiO_2{\cdot}3Al_2O_3{\cdot}(1.53 - X)P_2O_5{\cdot}3CaO{\cdot}2CaF_2$

Glass series A is based on a commercially available medical grade glass-ionomer bone cement, Serenocem® (Corinthian Surgical, UK). This glass composition was selected because Serenocem® is approved for clinical use in Europe and North America. While it has enjoyed clinical success, its performance is hindered by Al^{3+} ion release (see section 2.3.4). Compositional variations exist between glasses SC and A1 due to differences in raw material selection (see section 4.1.1). Phosphate content was varied as

it has been shown that P_2O_5 content in the final glass has a direct effect on the setting characteristics [Griffin and Hill 2000a]. Compositions are given in Table 3.5

Table 3.5 : Glass compositions used in the preparation of series A (mol %)

Oxide	Glass				
	SC **X = 0** **P_2O_5 = 1.5**	**A1** **X = 0** **P_2O_5 = 1.53**	**A2** **X = 0.38** **P_2O_5 = 1.15**	**A3** **X = 0.77** **P_2O_5 = 0.77**	**A5** **X = 1.53** **P_2O_5 = 0**
SiO_2	32.03	31.93	32.82	33.77	35.95
Al_2O_3	21.27	21.2	21.80	22.43	23.87
P_2O_5	10.92	10.88	8.39	5.75	0
CaF_2	14.26	14.22	14.62	15.04	16.00
CaO	21.54	21.76	22.37	23.02	24.18

3.3.2 Glass Series B – $4.5SiO_2{\cdot}3Fe_2O_3{\cdot}(1.53 - X)P_2O_5{\cdot}3CaO{\cdot}2CaF_2$

The presence of Al^{3+} ions in GICs used for biomedical applications have been at the centre of a recent debate. It is generally accepted that the presence of the Al^{3+} species is detrimental to biocompatibility (see section 2.3.4). It was therefore decided to replace the Al_2O_3 with Fe_2O_3. A mechanism for the removal of Fe exists within the body since Fe is a major constituent of haemoglobin. Therefore the release of Fe into the body should not cause as serious an effect as Al^{3+}. A trivalent ionic species (Fe^{3+}) is still available for the setting reaction. In this series of glasses Fe_2O_3 has wholly replaced Al_2O_3. Table 3.6 shows the compositions of the Fe_2O_3 substituted glasses. The P_2O_5

content was varied to offer a route to investigate its effect on working and setting times of the final cement.

Table 3.6: Glass compositions used in the preparation of series B (mol %)

Oxide	Glass				
	B1 **X = 0** **P_2O_5 = 1.53**	**B2** **X = 0.38** **P_2O_5 = 1.15**	**B3** **X = 0.77** **P_2O_5 = 0.77**	**B4** **X = 1.15** **P_2O_5 = 0.38**	**B5** **X = 1.53** **P_2O_5 = 0**
SiO_2	31.93	32.82	33.77	34.77	35.83
Fe_2O_3	21.21	21.80	22.43	23.09	23.80
P_2O_5	10.88	8.39	5.75	2.96	0
CaF_2	14.22	14.62	15.04	15.48	15.95
CaO	21.76	22.37	23.02	23.70	24.42

3.3.3 Glass Series C – $4.5SiO_2 \cdot 1.5Fe_2O_3 \cdot (1.53 - X)P_2O_5 \cdot 3CaO \cdot 2CaF_2$

All the glasses in series B were found to contain crystallised magnetite on quenching into both water and iced brine. A reduced Fe_2O_3–containing series of glasses (series C) was produced to retard the crystallisation and to potentially increase the amount of Fe^{3+} in the residual glass component. The compositions of the reduced Fe_2O_3 – containing glasses is given in Table 3.7.

Table 3.7: Glass compositions used in the preparation of series C (mol %)

Oxide	Glass				
	C1 **X = 0** **P_2O_5 = 1.53**	**C2** **X = 0.38** **P_2O_5 = 1.15**	**C3** **X = 0.77** **P_2O_5 = 0.77**	**C4** **X = 1.15** **P_2O_5 = 0.38**	**C5** **X = 1.53** **P_2O_5 = 0**
SiO_2	35.72	36.84	38.03	39.31	40.67
Fe_2O_3	11.86	12.23	12.63	13.05	13.51
P_2O_5	12.17	9.42	6.48	3.35	0
CaF_2	15.90	16.40	16.94	17.50	18.11
CaO	24.25	25.11	25.92	26.79	27.72

3.4 Glass Characterisation

3.4.1 Glass Composition

The composition of selected glasses (post–melt) was verified by x-ray fluorescence (XRF). A Philips PW2400 MagiXPro x-ray fluorescence spectrometer (Eindhoven, The Netherlands) fitted with a rhodium target end window x-ray tube and Philips X-40 analytical software was employed. Samples were prepared using the fusion technique [Giles *et al* 1995]. The sample was then irradiated with high energy primary x-ray photons over a wavelength range of 0.0877–1.4797 nm. The spectrometer was interfaced to a PC which recorded the weight percentages of the oxides present.

3.4.2 Differential Thermal Analysis

Differential thermal analysis was carried out on powdered glass (<45 μm) using a Perkin Elmer DTA7 running Pyris thermal analysis software in Unix, at

a heating rate of 10°C min^{-1} to 1000°C in an argon atmosphere. The data were recorded and temperatures assigned to the traces.

3.4.3 Heat Treatment

From the DTA traces a heat treatment schedule was derived for each glass composition. Fast-quenched pieces of glass for each composition were then heated to the appropriate temperature in a tube furnace (Lenton) at 5°C min^{-1} and held for 120 min before being cooled at 5°C min^{-1} to ambient temperature.

3.4.4 X-ray Powder Diffraction

The as-cast and heat-treated glasses were percussion mortared to produce powder (<75 μm) samples. X-ray powder diffraction was carried out on a Philips diffractometer (Philips, Holland) interfaced to a microcomputer. The samples were placed in holders and analysed using Cu radiation (λ – 1.541 A). The angles used were from 10°2θ to 70°2θ in 0.2°2θ intervals with a speed of 2°2θ/min. Plots were made and the peaks assigned using the JCPDS x-ray data files. Table 3.8 lists the JCPDS cards used in this study.

Table 3.8: JCPDS cards used to identify crystalline phases

Mineral Name	Chemical Formula	Card Number
Fluorite	CaF_2	35 – 816
Cristobalite	SiO_2	39 – 1425
Fluorapatite	$Ca_5(PO_4)_3F$	15 – 876
Mullite	$Al_6Si_2O_{13}$	15 – 776
Hematite	Fe_2O_3	33 – 664
Wollastonite	$CaSiO_3$	43 – 1460
Anorthite	$CaAl_2Si_2O_8$	41 – 1486
Magnetite	Fe_3O_4	19 – 629

3.4.5 Microstructural Analysis

Scanning Electron Microscopy

Pieces of glass frit were mounted into slow cold setting resin and left for 24 h to cure. The embedded samples were then ground on varying degrees of silicon carbide paper (120, 400, 800 and 1200 grades) and polished with diamond paste. The samples were then carbon coated. The samples were analysed using JEOL 6400 scanning microscope at an operating voltage of 20 kV and a working distance of 8 mm.

For ball – milled powder samples (see section 3.5.1), the glass powder was placed on an aluminium stub and gold sputter coated (SC500A EM scope) for 4 min prior to use. The samples were observed using a Camscan series II SEM at an operating voltage of 10 kV and a working distance of 10 mm.

The mechanical property rods post testing (see section 3.7.2) were prepared for SEM. The non-fracture surface was ground to achieve a rod length of ~ 5 mm in length using 400 grade silicone carbide paper and mounted in Q-compound onto steel mounting blocks. Silver dag was applied to the surface and the samples were gold sputter coated for 3 min prior to observation. The samples were observed using a Camscan series II SEM at an operating voltage of 20 kV and a working distance of 10 mm.

Transmission Electron Microscopy

Glass and glass-ceramic samples were ground and polished to less than 30 μm using varying degrees of silicon carbide paper. A Cu support ring was then glued onto the sample using an epoxy resin. After curing, the sample was removed from the glass slide and excess material chipped away using a razor blade. Thinning to perforation was achieved using an ion beam miller, operating at 6 kV with a total beam current of 0.6 mA, at an incidence angle of 15°. Once prepared the samples were carbon coated and then observed using a Philips EM400 and EM420 transmission electron microscope, operating at accelerating voltages of 100 kV and 120 kV respectively. The Philips 420 was equipped with a LINK energy dispersive x-ray detector.

3.5 Glass Powder Preparation and Characterisation

3.5.1 Milling

The glasses were powdered using a porcelain ball mill with an internal volume of 1 l. The frit was dry milled for 3 h. A charge volume of 0.5 l of balls with

diameters ranging from 1 mm to 15 mm was employed. The resulting ground glass was then sieved to remove particles over 45 μm.

3.5.2 Particle Size Analysis

Two methods were employed to determine the particle size distribution of the milled glasses. Qualitative SEM (see section 3.4.5) showed both the size and shape of the ground powders and quantitative laser diffraction particle size analysis allowed for an accurate assessment of the distribution of the particle sizes.

Laser Particle Size Analysis

The particle size and distribution were analysed using a laser particle sizing device (LS130, Coulter Electronics Ltd. Luton, Beds) with polarization intensity differential scattering (PIDS). Powder suspensions were dispersed into 2 litres of water and pumped round the diffraction and PIDS sample cells. Al_2O_3–containing glasses were analysed using the 'glass' optical module and Fe_2O_3–containing glasses were analysed using the Fraunhofen optical module. The different optical modules allow for a correction factor due to morphological differences in the two glass types. The optical model allows measurement of particles ranging in size from 1 to 800μm and the PIDS any sub micron particles present. Individual measurements were taken over 90 second periods and, between runs, the powder solution was sonically agitated to discourage agglomeration. Fine powders can agglomerate and deflocculants are added to reduce this. Different deflocculants were investigated for use

with all glass powders but were found to cause more agglomeration. The particle size of the glasses was calculated without the use of a deflocculant.

3.6 Cement Formation

Cement was made using an 'in house' ratio of glass: polyacrylic acid: tartaric acid solution. 1 g of glass powder was added to 0.2 g of dried polyacrylic acid and 0.3 g of dilute tartaric acid solution (0.1 M). The resulting cements were given a nomenclature relating to the glass used, e.g. GIC A1 – glass ionomer cement made from glass A1 and GIC A2 – glass ionomer cement made using glass A2.

3.7 Cement Characterisation

3.7.1 Working and Setting Time Determination

Gilmore Needle

The setting and working times were initially determined using a Gilmore Needle according to the dental material standard (BS EN29917 & 6039). The Gilmore needle works on the principle of two different sized needles with differing weights being placed onto the surface of the setting cement. Initially a large diameter needle (10 mm) with a weight of (28 g) is applied and the working time is determined when the needle no longer indents the surface. A second needle with a smaller diameter (1 mm) and larger weight (400 g) is then applied to the surface and the time when this needle no longer indents the surface is designated as the setting time. Both tests were carried out at ambient temperature 21±1°C. A schematic diagram is shown in Figure 3.1.

Based on the dental standard and the Gilmore needle times calculated for the commercial system, the viability of experimental cements was ascertained. If the working time was less than 1 min or greater than 5 min then the cement was deemed unworkable and no further investigation of its properties were carried. A setting time in excess of 20 min was also deemed too long for a viable cement.

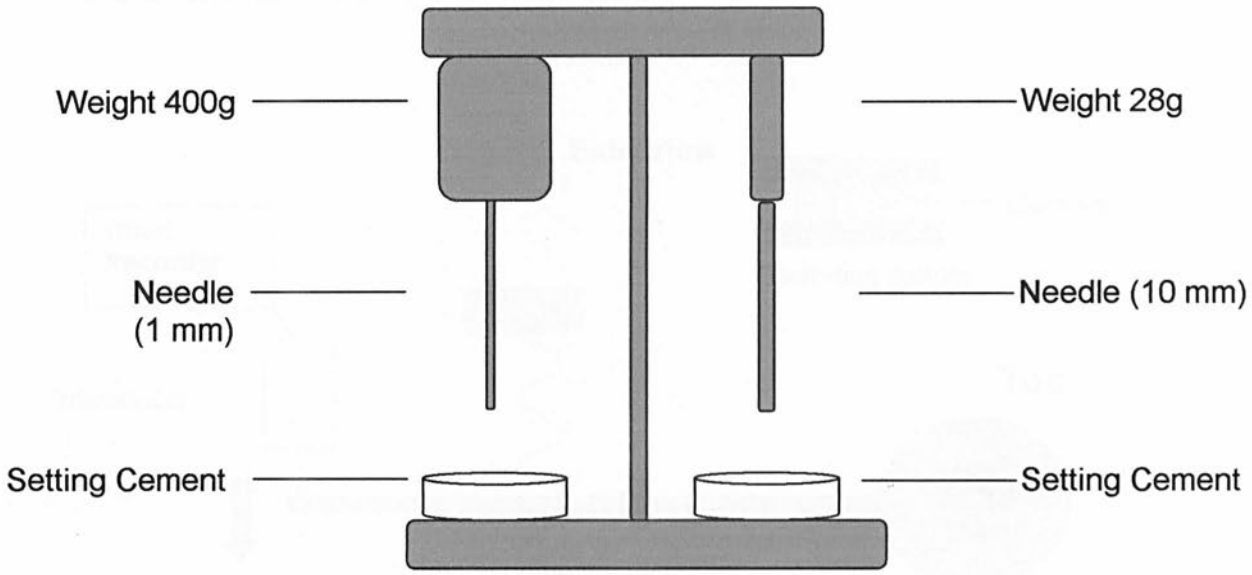

Figure 3.1 : Schematic diagram of a Gilmore needle.

Oscillating Rheometer

The working and setting times of selected cements were further characterised using an oscillating rheometer. This apparatus consists of two plates one fixed and the other capable of oscillating by means of an eccentrically driven spring. The movement of the lower plate of the rheometer varies with the

fluidity of the material and the amplitude of the oscillation was measured and plotted against time on a chart recorder. A zero time mark was made on the recording paper and the recorder was started at the beginning of the mix. The cement was mixed and within 30 s of completion transferred to the lower plate of the rheometer. The upper plate was lowered into position so that the thickness of the material between the plates was 1 mm. This produced a trace on the chart recorder which was wide when the material was fluid and whose width decreased as the material set. The equipment is shown in Figure 3.2 and an example trace is shown in Figure 3.3.

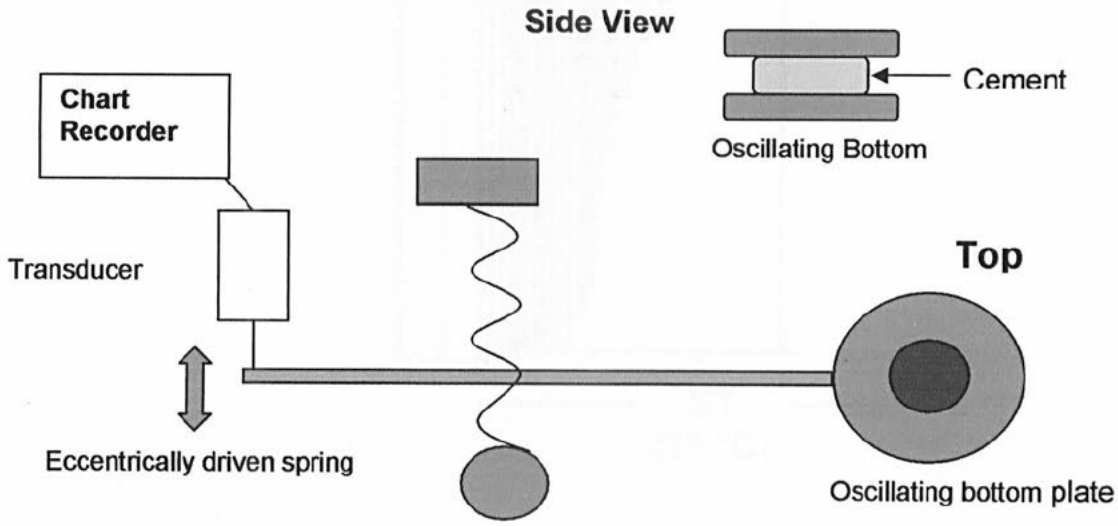

Figure 3.2: Schematic diagram of an oscillating rheometer, adapted from Griffin and Hill, 2000 (part 1).

The working time of the cement is carried out at ambient temperature (21 ± 1°C) and determined when the amplitude of the oscillation reduces to 95 % of the original value. The setting time of the cement is ascertained at 37 ± 1°C

when the amplitude reaches 0. Three measurements were carried out for each cement composition.

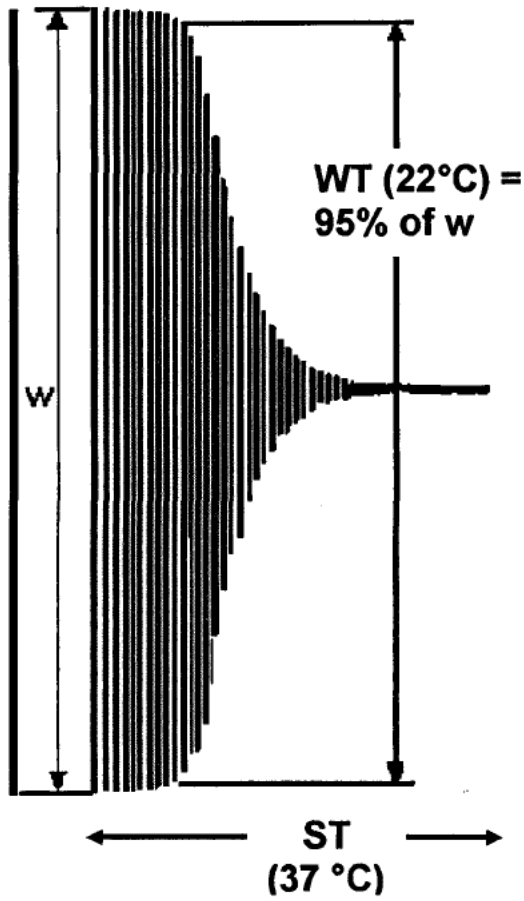

Figure 3.3: A typical trace from a glass ionomer cement showing w (initial trace width) WT (working time, (95% of w) and ST (setting time).

3.7.2 Mechanical Properties

Flexural Strength in 3 - Point Bend

Specimens were mixed in accordance with section 3.6, and placed into cylindrical moulds with a diameter of 4.6 ±0.05 mm and left to set for 1 h. Samples were then removed from the moulds and placed into water and

stored for two time periods, 1 d (unaged) and 28 d (aged). Ten rods of each material were fabricated.

Mechanical testing of specimens was carried out on a screw driven Hounsfield testing machine (Hounsfield, UK) interfaced to a PC. A 1 KN load cell was used to test the materials. The cements were tested using the compression to extension programme that calculates both the force and elongation to failure for the test sample. The test conditions used were Load range – 30 N, Extension – 5 mm, Test Speed – 1 mm min^{-1}, Test End Point – 4.5 mm, Preload – 2 N, Span – 25 mm.

The flexural strength was then calculated using equation 2.

$$FS = \frac{FL}{\Pi r^3} \qquad (2)$$

Where F is force to failure, L is the length between the two supports and r is the radius of the cylindrical test sample.

Samples were mounted into the load cell and the programme set to fracture the rod. The testing machine accurately monitors and records how the rod reacts and determines the force to failure.

The fracture surfaces of the materials were examined using SEM (see section 3.4.5).

3.7.3 Ion Release

Discs (12 mm diameter by 2 mm thickness) were produced from selected cements using standard ratios, see section 3.6. 4 discs of each material were made. All materials were cured at 37 °C in a humid environment for 24 h prior to use. One disc was placed in each of 4 bottles of 20 ml of de-ionised water. The bottles were then placed in an incubator at 37 °C. Samples were taken at three time intervals, 1 d (unaged), 7 d and 28 d (aged). Bottles containing only de-ionised water were set up as a control and these underwent the same water changes as the test bottles. This was to determine any background ion levels. At each time period the water was removed and replaced with fresh water.

0.1 ml of 10 N HCl was added to the 10 ml samples to stabilise any released ions. The samples were then analysed. Aluminium, iron, silicon, calcium and phosphorus ion levels were determined using inductively coupled plasma atomic emission spectroscopy (ICP-ES). This was undertaken by the Analytical Sciences Unit, Department of Chemistry, University of Sheffield.

Fluoride ion release was measured using an ion selective electrode (Orion Research Inc, Cambridge, USA). The probe was calibrated between 1 ppm and 10 ppm for fluoride from standard solutions. The standard solutions were prepared following the manufacturer's instructions (Orion Research Inc, Cambridge, USA) to give the desired concentrations. A decomplexing solution TISAB II was added.

All ion release results were collected in the form of ppm and the data was manipulated to express it as the mass of ion released per unit of surface area ($\mu mol.mm^{-2}$).

3.7.4 In Vitro Biocompatibility

Biocompatibility was investigated using cultured rat osteosarcoma cells (ROS 17/2.8, Merck Inc.). Cellular response was assessed using MTT assay, a measure of the respiratory rate of the cells, total protein assay (Biruet and Lowry methods) that gives a measure of the protein concentration and SEM that allows for observation of the cultured cells.

Materials

Cement discs were prepared using the method described in 3.6 and sterilised by autoclaving (15 min at 121°C/ 15 psi). Discs were cured for 24h in a humid atmosphere prior to use.

Cell Culture

ROS cells (P_8) were removed from storage in liquid nitrogen and defrosted. The freezing medium was removed and the cells were washed using sterile PBS. The Cells were cultured in a DMEM supplemented with 10% FCS and 1% Penicillin/Streptomycin/Glutamine. Cells were left to populate the surface of culture plates and when fully dense spilt using Trypsin-EDTA. Cells were seeded into wells of a 24 well plate containing test samples (seeding density of 1.25×10^4 cells/ml) with a total well volume of 1 ml. A non-material control

was included for comparison. The materials and cells were incubated at 37°C in a 5% CO_2 atmosphere for 72 h.

MTT Assay

100 mg of MTT powder was dissolved into 20 ml of DMEM media (5 mg/mL) and sterilised by filtration (20 µl filter). MTT solution (0.1 ml) was aseptically added to each well and left to incubate at 37°C for 4 h. The cells were then lysed with acidified isopropanol. The intensity of the coloured solution was measured using a photospectrometer at a wavelength of 570 nm.

Total Protein Assay

Two different methods were employed to measure the total protein in the test samples, Lowry and Biruet. The procedure for these two methods is the same but different reagents (Lowry and Biruet see Table 3.4) are employed for releasing the protein.

The test wells were washed 3 times PBS to remove any residual media. 1 ml de-ionised water was added to each well along with 1 ml of reagent (either Lowry or Biruets depending on test method). This was left for 20 min to react. 0.5 ml of Folin-Ciocalteu reagent was then added and left for 30 min for the colour to develop. Protein standards were also subjected to the same chemical additions. The standards and test samples were then measured using a photospectrometer at a wavelength of 750 nm. A protein standard curve was derived and protein concentrations calculated for the test samples.

Scanning Electron Microscopy

Post culturing, discs which had been incubated both with and without cells were processed for SEM analysis. The discs were washed in 0.1 M sodium cacodylate buffer (adjusted to pH 7.4) for 30 min. 1 ml of fixative was then added and left for 1 h. The fixative was then removed and the samples washed with buffer 3 times. 0.5 ml of osmium tetraoxide in 0.1 M cacodylate buffer was then added for 1 h. The osmium solution was then replaced with cacodylate buffer. The samples were then taken to J. Procter in the Biological Sciences department for further processing (see Appendix II for details of processing).

The samples were examined using a Camscan series II SEM at an operating voltage of 20 kV and a working distance of 10 mm.

4. Results and Discussion –

Glass series A: $4.5SiO_2{\cdot}3Al_2O_3{\cdot}(1.53 - X)P_2O_5{\cdot}3CaO{\cdot}2CaF_2$

This chapter deals with the formation and characterisation of the glasses in the series $4.5SiO_2{\cdot}3Al_2O_3{\cdot}(1.53 - X)P_2O_5{\cdot}3CaO{\cdot}2CaF_2$ (X = 0 – 1.53), and their ability to form GICs. Sections 4.1 and 4.2 describe the fabrication of the glass series and the problems encountered in reproducing a commercial composition. Characterisation of the glasses can be found in section 4.3. The preparation of glass powders is discussed in section 4.4, and in section 4.5 the ability of these glass powders to form cements and their resulting properties is reported. Finally in section 4.6 their *in vitro* biocompatibility is considered. Two different series of cements were used, cements based on glasses with a compositional variation and cements based on devitrified glasses.

4.1 Glass Melting

Glass A1 was based on the composition of a commercial system (SC). The fabrication of this glass was not straightforward. Two main problems were encountered, corrosion of the crucible and incomplete melting. Differences between the glass-melting procedure of the commercial system and the 'in-house' method were noted. Firstly, the raw materials employed were different (see section 4.1.1). In addition the type of reaction vessel and scale of the melt also differed. It was possible that these may have contributed to the difficulties described.

4.1.1 Raw Materials

Differences in raw materials were a potential factor affecting the fabrication of the glasses in series A. Research based on the same glass composition as A1 carried out in the University of Limerick in Ireland used P_2O_5 as a source of phosphate [Griffin and Hill 2000]. This was, however, considered to be too hazardous for use in our laboratory. Commercially, P_2O_5 is added in the form of $AlPO_4$, which is also a source of Al_2O_3. Since one objective of this research was to reduce or eliminate the use of aluminium it was decided not to use $AlPO_4$. Instead $CaHPO_4$ was used to provide phosphate.

A further difference was the decomposition/melting temperature (T_m) of the raw materials selected. $CaHPO_4$ has a T_m of 350°C, whereas P_2O_5 has a significantly higher T_m of 560°C [MSDS 2002]. This may have caused a difference in the reaction sequence during the formation of the glasses, resulting in the formation of different intermediate phases, altering the final glass structure.

4.1.2 Crucible Selection

A wide range of crucibles are available for fabricating glasses. Crucible selection is generally based on melt conditions, glass composition and cost. Platinum crucibles are used for high purity melts, as contamination from the crucible is low but they are expensive. Ceramic crucibles (e.g. mullite) are used commercially due to their low cost.

The crucibles employed commercially to manufacture SC are made from sintered mullite, and have a relatively porous structure compared to slip-cast ceramic crucibles. When used for smaller melts, the walls of commercial crucibles absorbed molten glass, resulting in a significant loss of the glass mass (measured to be between 20 and 40 wt %). This reduced the amount available for further characterisation and was considered as a potential source of contamination. Slip-cast crucibles have very few pores in their wall surfaces and the glass losses post-melting were found to be significantly reduced (measured to be between 1 and 10 wt %). Slip-cast crucibles were therefore, employed for all experimental melts described in this thesis. Whilst the decision to use less porous slip-cast crucibles was straightforward, selection of the crucible material was not.

Pt – 12%Rh crucibles are known to undergo flux line corrosion in the presence of P_2O_5 [Babcock 1977], which is related to an increase in convection near the glass surface. This mechanism is discussed in section 2.4. This type of attack ruled out the use of platinum crucibles for phosphate containing glasses and it was therefore necessary to employ ceramic crucibles for glasses A1 – A3.

Ceramic crucibles are also susceptible to corrosion during melting (see section 2.4). Table 4.1 documents the problems encountered when glass A1 was fabricated experimentally. Four corrosion mechanisms have been described and a detailed explanation of these is given in section 2.4. Melt temperature, viscosity and glass composition may also contribute to the dissolution of

ceramic crucibles. However, these three factors were kept constant during the melting of glass A1 and therefore the corrosion noted was attributed to one of the four corrosion mechanisms.

Table 4.1: Observations made related to crucible materials selection for glass A1 based on standard melt procedure[1].

Crucible Material	Observations
Platinum Pt-12%Rh	Undergoes flux-line corrosion in the presence of P_2O_5
Mullite ($Al_6Si_2O_{13}$)	Cavity in base of crucible noted post-melting (Figure 4.1a). Corrosion mechanism unknown – but thought to be either direct dissolution of the crucible or drilling.
Alumina (Al_2O_3)	Dissolution of base and walls resulting in thinning of the crucible noted post-melting. Corrosion mechanism unknown – but thought to be either direct or indirect dissolution of the crucible.
Silica (SiO_2)	De-lamination of crucible walls after 2 h melt rendering the crucible brittle, unsafe and difficult to handle.
Zirconia (ZrO_2)	Crucible cracked when transferred from pre-heat furnace to melt furnace. This was attributed to thermal shock.
Sillimanite (Al_2SiO_5)	Minimal dissolution of the base and walls, corrosion greatly reduced. Crucible chosen for all glass melts.

Alumina and mullite crucibles were found to be susceptible to refractory corrosion from glass A1, crucible loss was found to be 5 – 10 wt %. A reduction of 3 – 7 wt % was however observed when sillimanite crucibles were employed.

[1] Standard melt conditions: Preheat – 1050°C (2°C min^{-1}), Electric Furnace 2h @ 1450°C

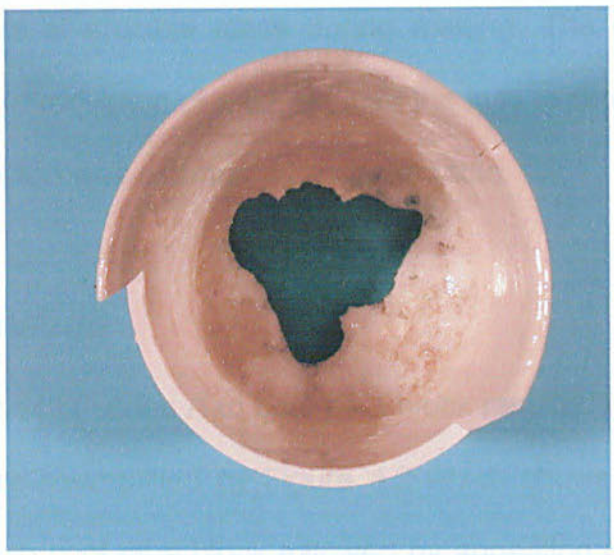

Figure 4.1: Photographs showing the appearance of a mullite crucible after melting a glass with the composition $4.5SiO_2{\cdot}3Al_2O_3{\cdot}1.53P_2O_5{\cdot}3CaO{\cdot}2CaF_2$

The introduction of a lid to the melt was found to decrease the corrosion of the crucible and also decrease the amount of glass mass lost. One explanation for the change can be related to the formation of a surface layer when a lid is not employed. Surface devitrification reactions caused by the loss of vapour from the glass melt surface can result in a layer forming on the surface. The presence of this layer can then cause a decrease in heat transmission through the melt causing increased corrosion beneath it [Begley 1974]. A further explanation is that the presence of both Al and F can prevent the formation of secondary bubbles and the liberation of gases at the point of contact with the refractory. The absence of the bubbles and gases reduces the dissolution of the crucible through drilling [Volf 1984]. It is believed that the presence of the lid retains fluoride within the melt and stops the loss of SiF_4.

In all glass melts the crucibles were weighed before and after melting to determine the loss of crucible mass during melting. The use of sillimanite crucibles and the introduction of a lid reduced the loss to around (1 – 5 wt %). This level of corrosion was determined as acceptable.

4.2 Glass Formation

Allowing the glasses in series A to cool as a block resulted in the formation of apatite crystals, as exemplified by Figure 4.2 which shows an XRD trace of glass A1 allowed to cool as a block followed by annealing (550°C/5 °Cmin^{-1}). The formation of apatite can be related to the presence of phosphate in the glass. An over saturated solution of phosphate (wt % > 1.5) on cooling slowly precipitates into heterogeneous particles (e.g. apatite), resulting in opacity in the glass [Volf 1984]. Fast quenching either into water or onto steel suppressed this devitrification, giving rise to amorphous glass (see section 4.3.4).

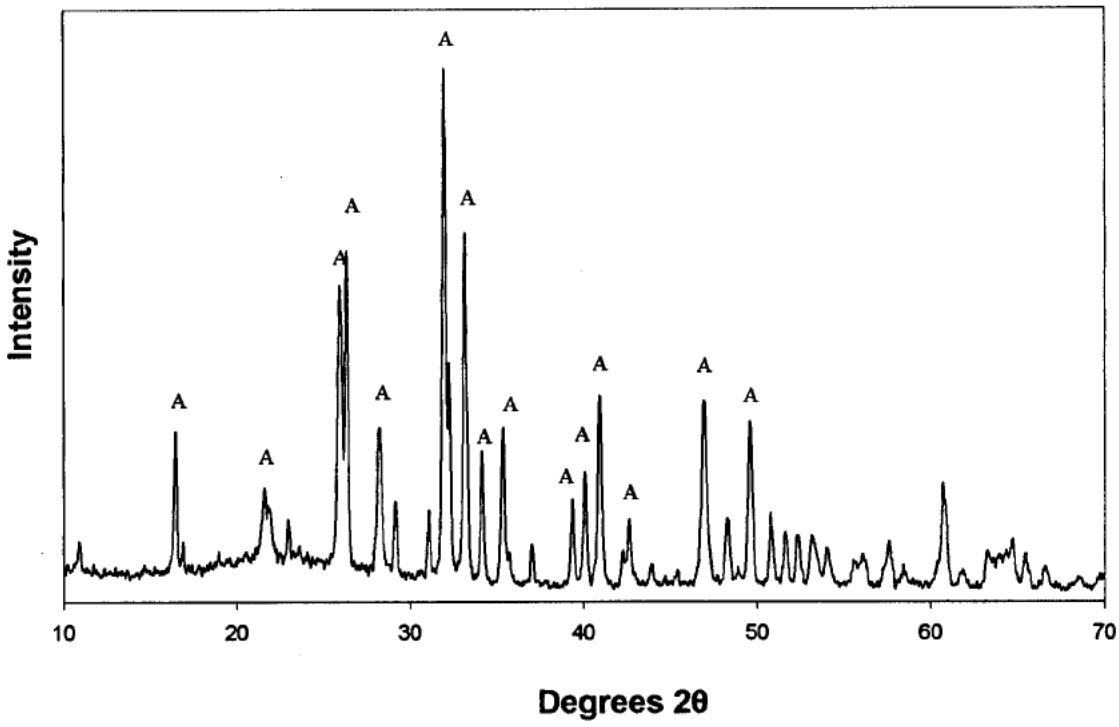

Figure 4.2: XRD trace of glass A1 after cooling at 5 °C min^{-1}. Principal peaks associated with the crystalline phase apatite are labelled (A).

4.3 Glass Characterisation

4.3.1 Glass Composition

X-ray fluorescence (XRF) showed a close similarity between SC, A1 and the theoretical molar composition. Table 4.2 indicated that very little volatilisation had occurred during melting. Although the loss of fluoride in the form of SiF_4 from ionomer glass melts has been widely reported [Barra and Hill 2000, Wilson and Nicholson 1993, Clifford *et al* 2001a, Clifford *et al* 2001b, Wood and Hill 1991], the glass composition used in this study has been optimised for minimal fluoride losses [Wood and Hill 1991]. Incorporating a basic oxide into the glass ensures that at least one non-bridging oxygen per silicon exists,

leaving sufficient aluminium atoms free to combine with the fluoride [Clifford *et al* 2001a].

Table 4.2: Glass compositions of SC and A1 determined by XRF compared to the calculated molar composition (mol %).

Oxide	SC	A1	Calculated
SiO_2	31.8	31.6	32.0
Al_2O_3	21.2	22.0	21.3
P_2O_5	9.5	9.2	10.9
CaO	27.2	25.9	21.5
CaF_2	10.3	11.3	14.3

4.3.2 Differential Thermal Analysis

Typical DTA traces are shown in Figure 4.3 for glasses SC and A1. The glass transition temperature, T_g, (SC – 665°C, A1 – 648°C) and the crystallisation exotherms, T_x (SC – 764°C & 913°C, A1 – 724°C & 898°C) are indicated on the diagram. Despite having similar compositions (Table 4.2), there was a significant difference between the T_g and T_x observed in SC and A1. The small compositional variations that exist between the two glasses (Table 4.2) may partially explain the differences noted. Glass SC had a 1 mol% less CaF_2 than glass A1. Studies by Hill and co-workers have shown that T_g falls linearly with an increase in CaF_2 content [Hill *et al* 1991, Clifford *et al* 1995, Hill *et al* 1996 and Barra *et al* 2000]. The reduction in T_g was attributed to Ca and F ions disrupting the glassy network.

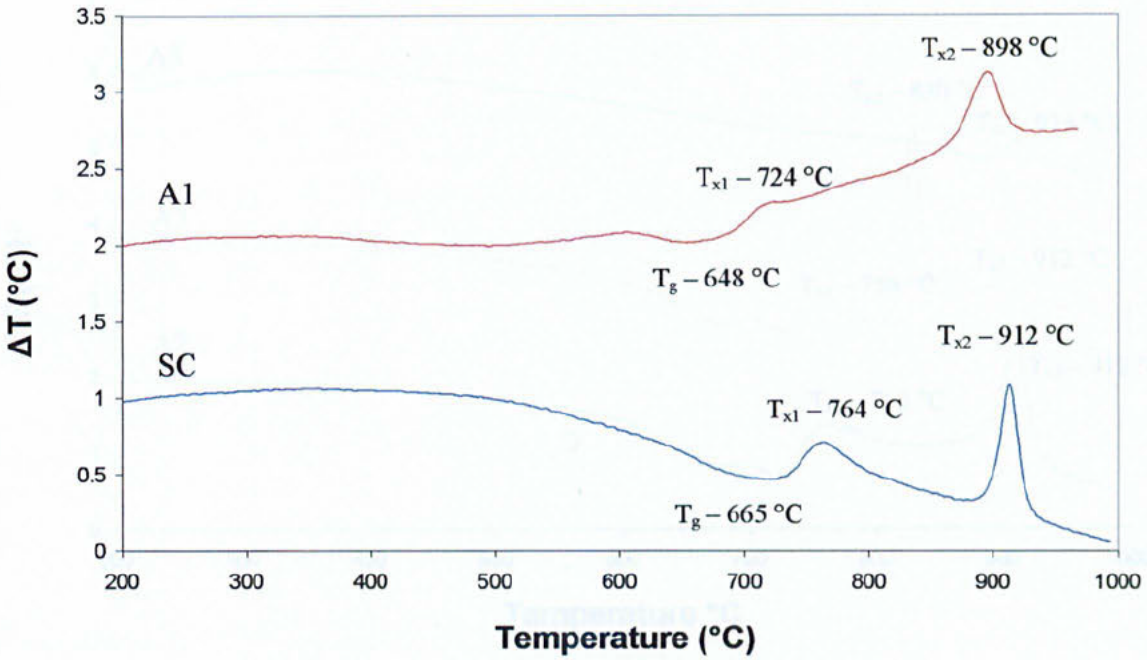

Figure 4.3: Differential thermal analysis of glasses SC and A1, showing the glass transition temperatures (T_g), and crystallisation exotherms (T_x).

Figure 4.4 shows the DTA traces obtained for glasses A2, A3 and A5 and a summary of the data is given in Table 4.3. The phosphate content of the glass was decreased as P_2O_5 has been shown to have an effect on the working and setting times of the cement [Griffin and Hill 2000a, Wilson *et al* 1980]. A variation in glass transition temperature across glass series A was noted and it was found that T_g is inversely proportional to P_2O_5 content, as shown in Figure 4.5. Griffin and Hill [2000a] have also reported a reduction in T_g with increasing phosphate content. They related the decrease in T_g to the incorporation of phosphate into the glass structure resulting in a weakening of the glass network.

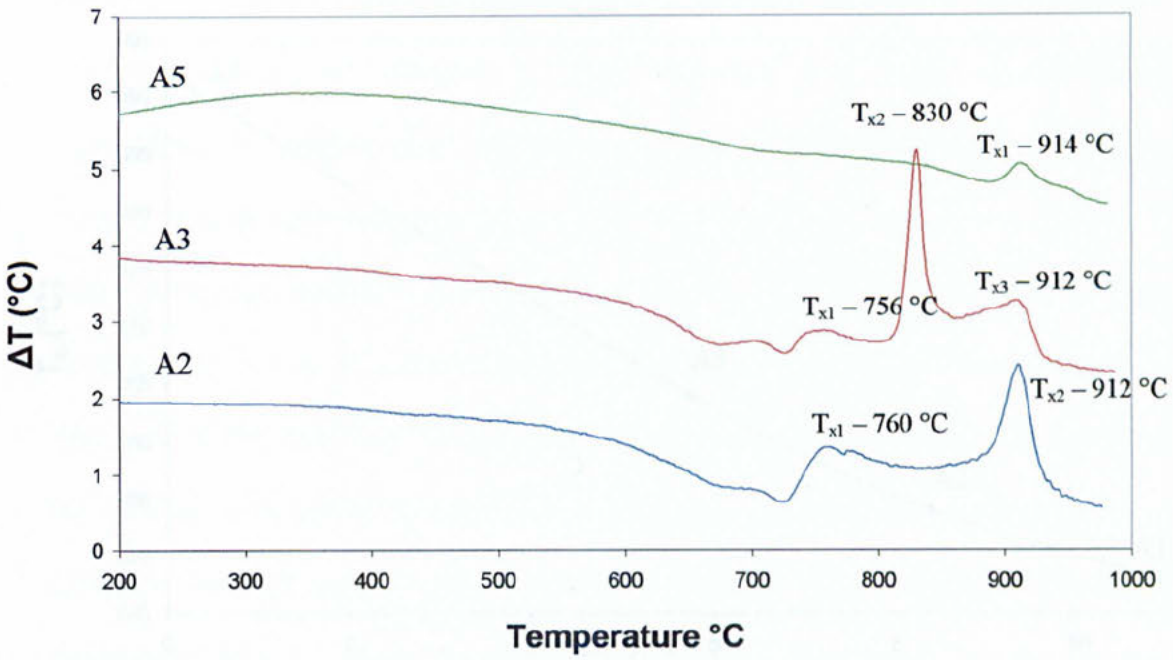

Figure 4.4: Differential thermal analysis of glasses A2, A3 and A5 showing the glass transition temperatures, (T_g) and crystallisation exotherms (T_x)

Table 4.3: Differential thermal analysis results for glass series A

Glass	P_2O_5 Mol %	T_g °C	T_{x1} °C	T_{x2} °C	T_{x3} °C
A1	10.9	648	724	898	
A2	8.4	654	760	912	
A3	5.8	664	756	830	912
A5	0	692	914		

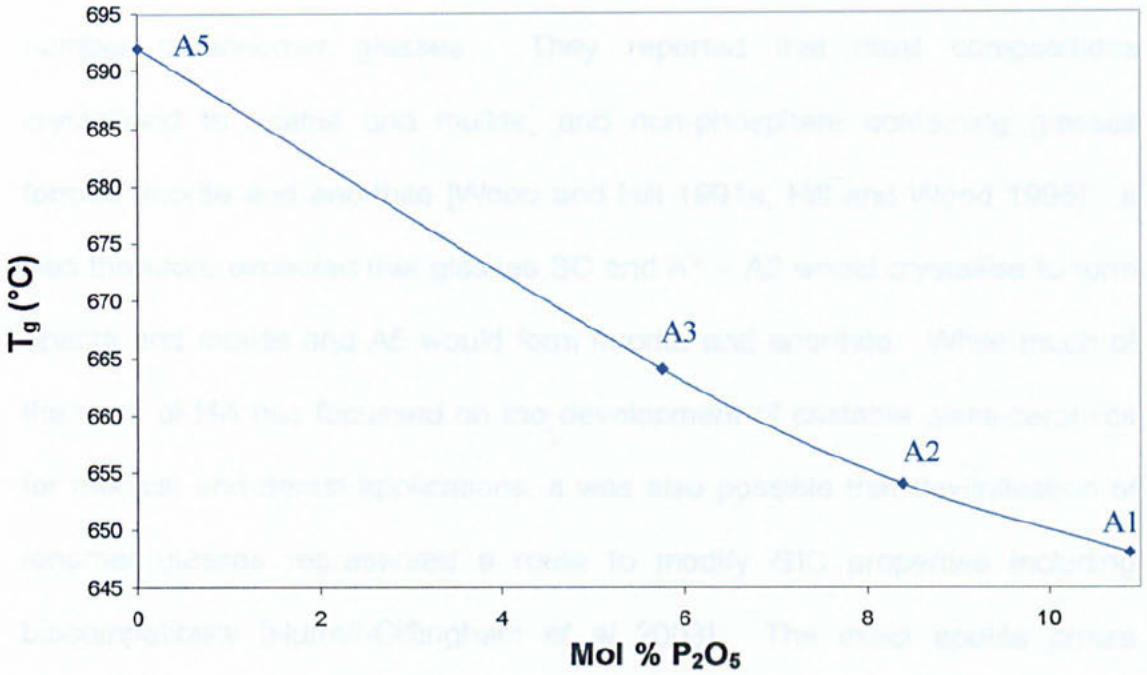

Figure 4.5: Relationship between glass transition temperature T_g and mol % of P_2O_5 in glass series A.

4.3.3 Heat Treatment

DTA demonstrated (Figures 4.3 and 4.4) that all the glasses in series A exhibited crystallisation exotherms (T_x). From the T_x values, isothermal heat treatment above and below the exotherms allowed characterisation of the crystals forming at these temperatures. Glasses A1 – A3 and SC had similar T_{x1} values, (725 – 760°C). All glasses in the series also exhibited an exotherm between ~900 – 915°C. Glasses SC, A1 and A5 were heat-treated to 700, 750, 800, 850, and 950°C and glasses A2 and A3 were heated to 750, 850 and 950 using the ramp detailed in section 3.5. The resulting crystal phases were identified using XRD.

Hill and co-workers have described crystallisation following heat treatment of a number of ionomer glasses. They reported that most compositions crystallised to apatite and mullite, and non-phosphate containing glasses formed fluorite and anorthite [Wood and Hill 1991a, Hill and Wood 1995]. It was therefore expected that glasses SC and A1 – A3 would crystallise to form apatite and mullite and A5 would form fluorite and anorthite. While much of the work of Hill has focussed on the development of castable glass-ceramics for medical and dental applications, it was also possible that devitrification of ionomer glasses represented a route to modify GIC properties including biocompatibility [Hurrell-Gillingham *et al* 2003]. The exact apatite phase formed in these glasses is unknown and could be fluorapatite, hydroxyapatite or a mixed apatite. All these crystals have similar powder diffraction patterns and therefore the crystal formed is given the generic term apatite.

4.3.4 X-Ray Diffraction

Figures 4.6 and 4.7 show XRD traces of SC and A1. The as cast glasses were amorphous and the two compositions generally followed similar phase evolutions. At 700°C peaks were recorded that corresponded to the presence of apatite ($Ca_5(PO_4)_3(F)$ – JCPDS #15-876). This is slightly before the crystallisation exotherm noted in the DTA for both glasses. This may be explained by the different heating rates employed for the two different techniques (5°C min^{-1} for heat treat, 10°C min^{-1} DTA). A slower heating rate can result in earlier crystallisation. At 950°C, mullite ($Al_6Si_2O_{13}$ – JCPDS #15-776) was the major phase present in addition to apatite and cristobalite (SiO_2 – JCPDS #39-1425).

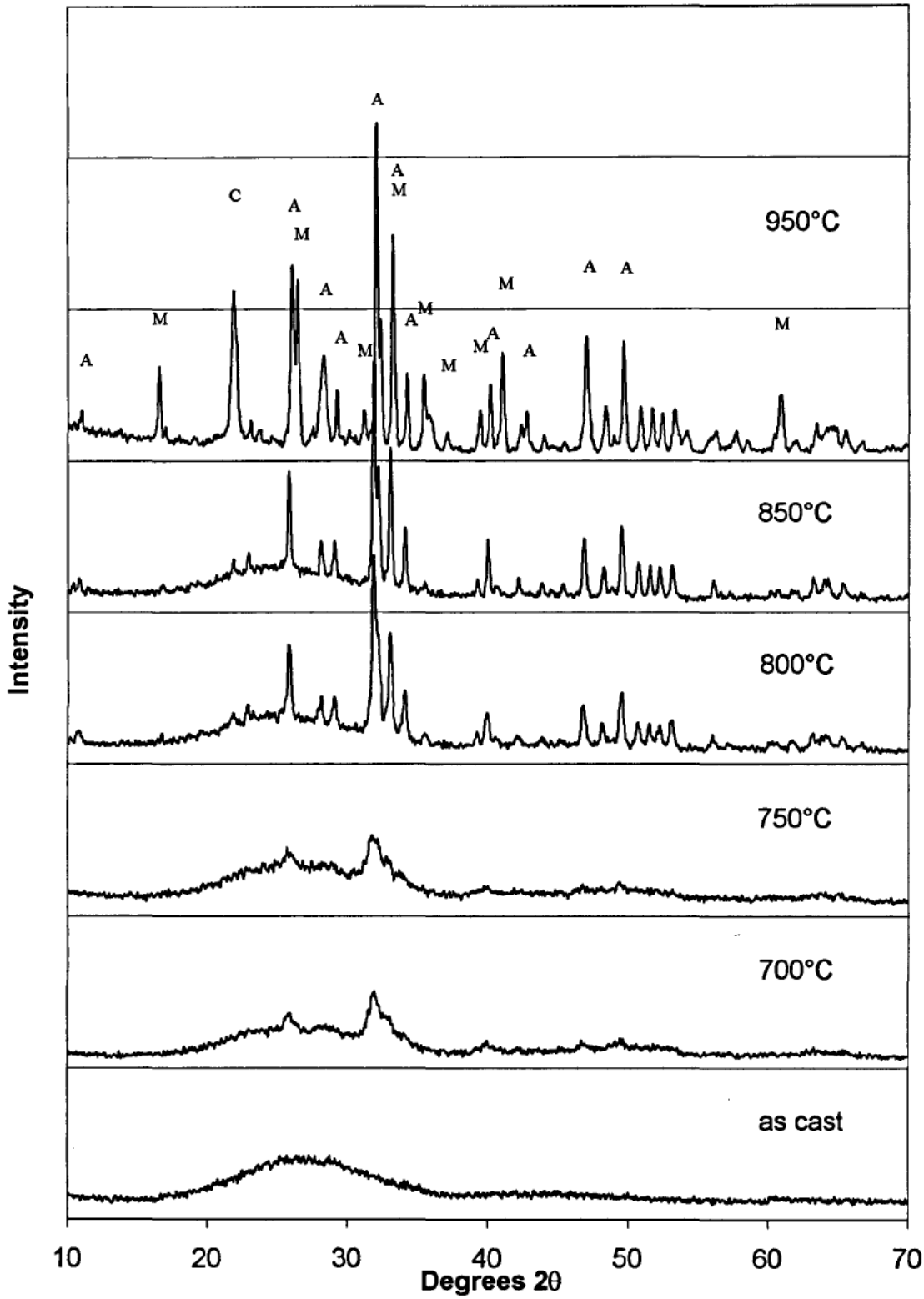

Figure 4.6: XRD spectra from the crystallisation of glass SC using isothermal heat treatments. Principal peaks associated with the crystalline phases are labelled A – Apatite M – Mullite C – Cristobalite.

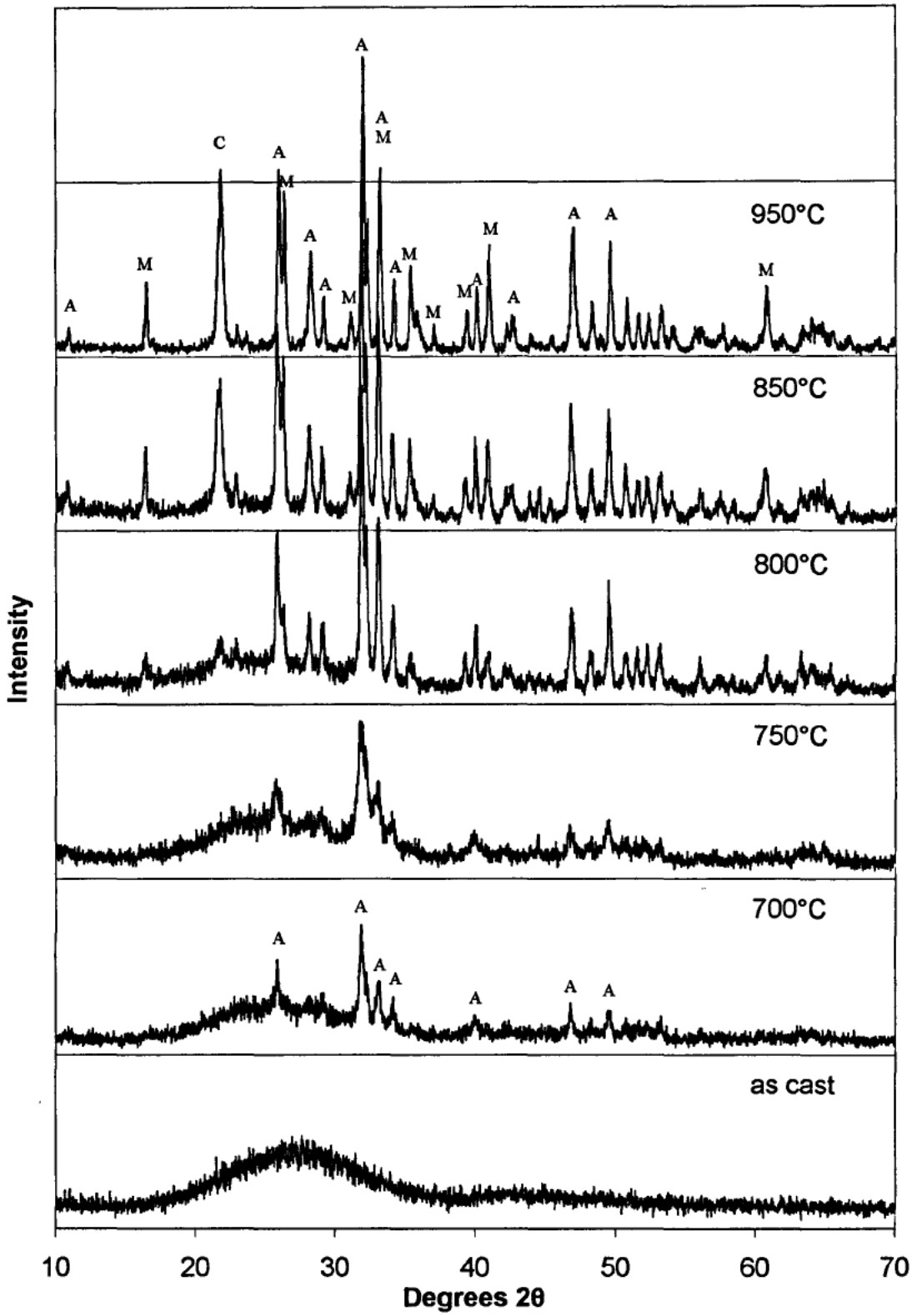

Figure 4.7: XRD spectra from the crystallisation of glass A1 using isothermal heat treatments. Principal peaks associated with the crystalline phases are labelled A – Apatite M – Mullite C – Cristobalite.

A peak with a d-spacing of ~4.05 Å (~22°2θ) was noted in both glasses when heated to 950°C. The powder diffraction file for apatite exhibits a peak at 4.05 Å with relative intensity of 8. However, the relative intensity of the 4.05 Å peak noted in glasses SC and A1 were 40 and 45, respectively. The 4.05 Å peak was therefore attributed to cristobalite which has a 100% peak has a d-spacing of 4.04 Å. The presence of cristobalite has not been reported in any key GIC glass crystallisation papers. Wood and Hill [1991a, 1991b, and 1995] discussed the crystallisation of ionomer glasses with slightly different compositions and this might explain the absence of a cristobalite peak in their results. However, the presence of a third DTA exotherm was noted and could possibly result from the formation of cristobalite [Hill and Wood 1995]. The formation of this additional phase suggested that there was excess SiO_2 in the glass after the formation of apatite and mullite.

The presence of cristobalite in the sample heat treated to 950°C was investigated using DSC. Cristobalite can exist in one of two forms α and β(ordered and disordered) and transforms from the one polymorph to the other as a function of temperature. The cristobalite inversion temperature has been shown to be in the range of 225-275°C with the endotherm on heating being observed at a higher temperature than the exotherm on cooling (Figure 4.8) [Hand *et al* 1998]. Samples of A1 previously heated to 950°C were reheated to 400°C at a heating rate of 5°C/min in a DSC. Figure 4.9 shows the DSC trace obtained, no endothermic response was noted, possible due to the presence of insufficient cristobalite.

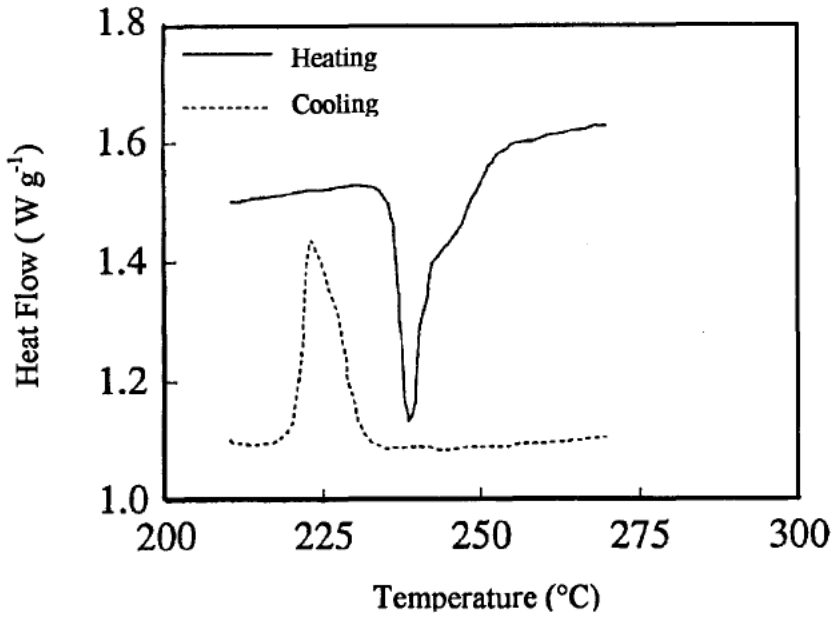

Figure 4.8: Thermal analysis (DSC) trace for cristobalite prepared from pure Iota Quartz [adapted from Hand *et al* 1998]

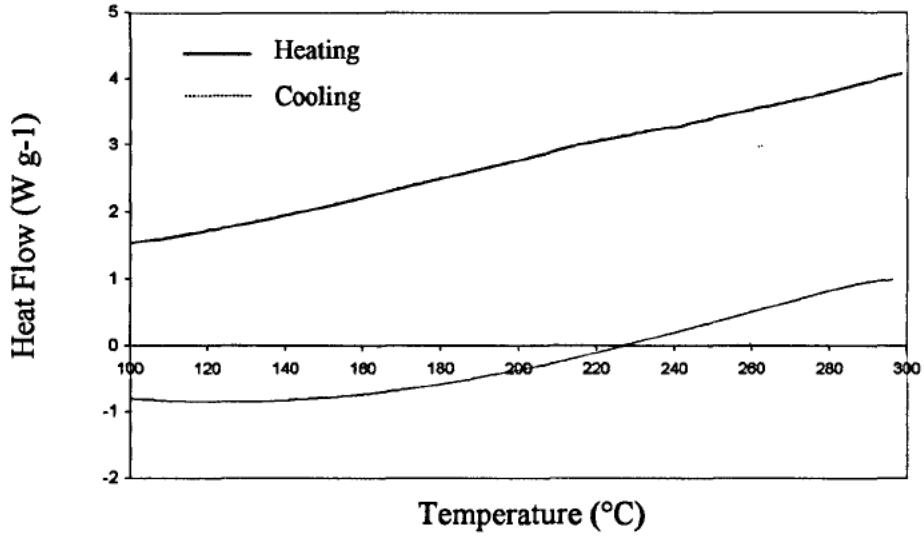

Figure 4.9: Thermal analysis (DSC) trace of glass A1 (previously heated to 950°C)

The degree of crystallinity was, however, found to differ in the two glasses. In A1 the intensity of the amorphous hump greatly decreased by 850°C whereas for SC the hump was still evident. A quantitative investigation of the percentage of devitrification was determined for the heat-treated samples using equation 4.1 devised by Ohlberg and Strickler (1962),

$$\alpha = \frac{(I_g - I_x) \times 100}{(I_g - I_b)} \qquad 4.1$$

Where I_g is the intensity of the parent glass, I_x is the intensity of the partially crystallised glass and I_b is the intensity of fully crystalline material.

The degree of crystallinity was calculated for 2θ values over the amorphous region where crystal phases were not present. A range of 2θ values were used and an average determined. The degree of crystallinity was found to increase in both glasses with increasing isothermal heat treatment temperature as shown in Table 4.4.

Table 4.4: Degree of crystallinity (α) in glasses SC and A1 over a range of isothermal heat treatment temperatures

Temperature (°C)	α SC (%)	α A1 (%)
750	25 (±7.6)	30 (±4.0)
800	34 (±7.9)	55 (±5.8)
850	46 (±3.5)	77 (±5.8)
950	62 (±9.3)	98 (±2.4)

SC was found to be less crystalline than A1 on heating to an equivalent temperature. XRF (Table 4.2) showed that SC had a lower amount of CaF_2 within the final glass composition than glass A1. CaF_2 is a known nucleating agent and a reduction in the presence of this in the glass may have retarded crystal formation.

Figures 4.10 and 4.11 show XRD traces from A2 and A3 heat treated to different temperatures. The as-cast glasses were both amorphous but on heating to 750°C, apatite was observed. At 850°C both glasses crystallised to apatite and mullite, but an additional phase was identified, fluorite (CaF_2, JCPDS – 35-816). The presence of fluorite was not easily identifiable as the two principal peaks overlap (d–spacing 3.155 (28°2θ) and 1.932 Å (47°2θ)) with those noted for apatite (d–spacing 3.167 and 1.937 Å). However, the relative intensity of these peaks was too high to be uniquely apatite and therefore the peaks were attributed to the additional presence of fluorite. In addition a minor fluorite peak at 56°2θ (d –spacing 1.647 Å) was also present.

DTA (Figure 4.4) of glass A3 exhibited three crystallisation exotherms, consistent with the formation of the three crystal phases observed during the heat treatments. T_{x1} (~750°C) could be attributed the formation of apatite, T_{x2} (~830°C) with fluorite and finally T_{x3} (~912°C) with the crystallisation of the remaining residual glass to mullite. The DTA (Figure 4.4) of glass A2 however only displayed two crystallisation exotherms. These are assigned to the apatite (T_{x1} ~760°C) and mullite phases (T_{x2} ~912°C). The absence of a third peak at ~830°C is thought to be due to the quantity of fluorite present. P_2O_5 is

known to aid retention of fluorine during glass melting. Glass A2 had less P_2O_5 than A1 and this could have resulted in increased fluorine loss during melting. Therefore, less fluorine was available to form CaF_2 and insufficient to produce an exotherm during DTA.

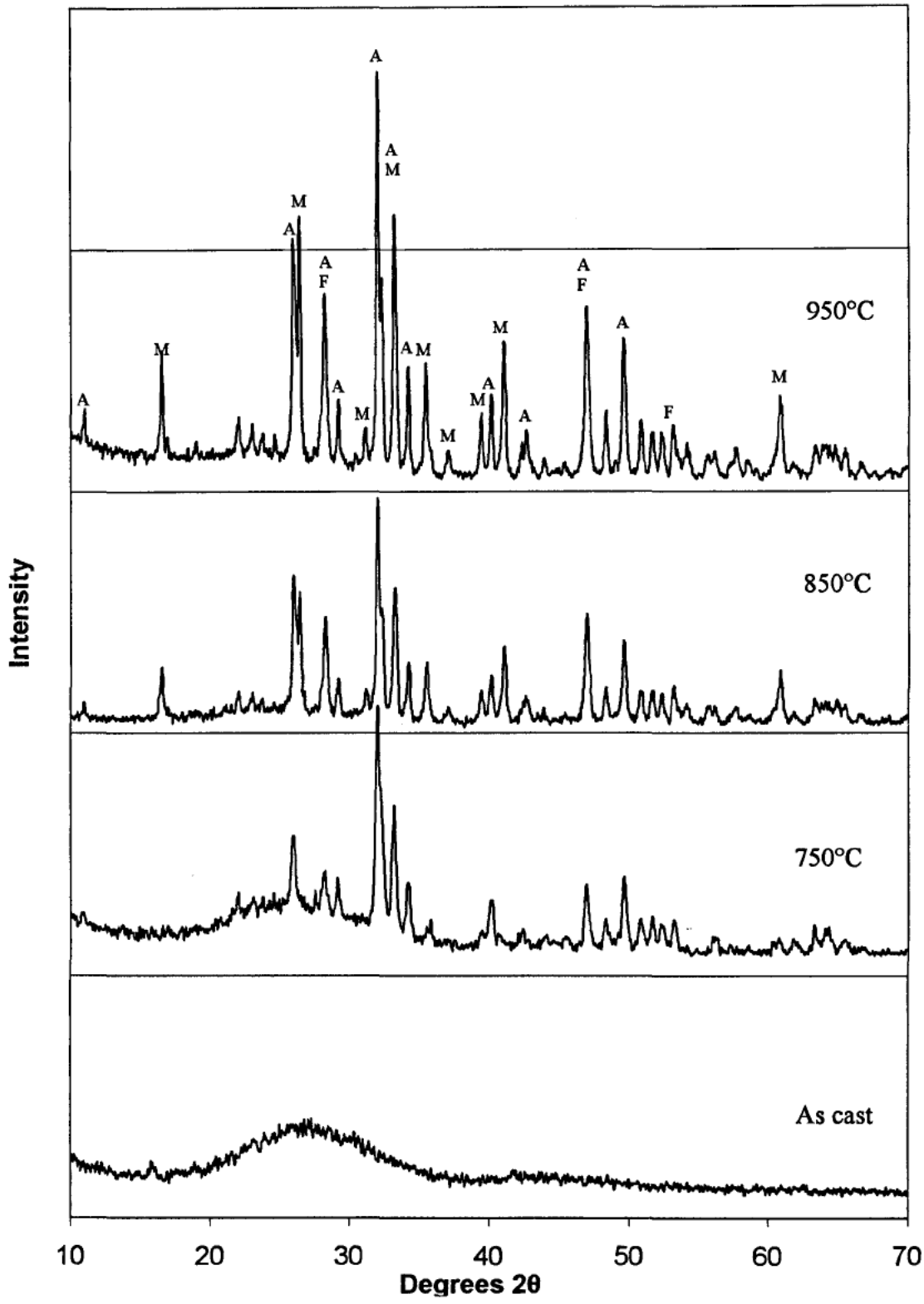

Figure 4.10: XRD spectra from the crystallisation of glass A2 using isothermal heat treatments. Principal peaks associated with the crystalline phases are labelled A – Apatite M – Mullite F - Fluorite

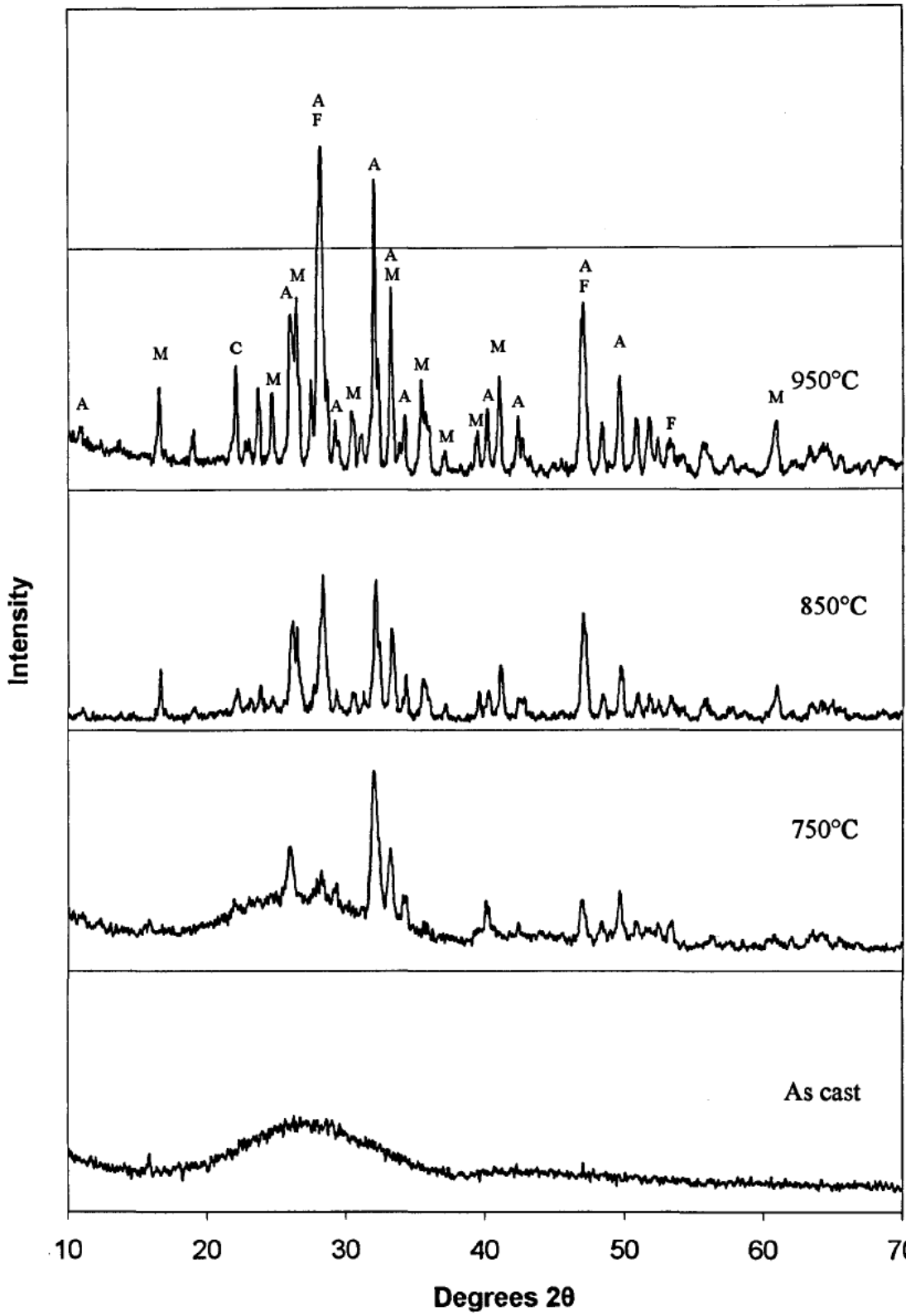

Figure 4.11: XRD spectra from the crystallisation of glass A3 using isothermal heat treatments. Principal peaks associated with the crystalline phases are labelled A – Apatite M – Mullite C – Cristobalite F - Fluorite

The DTA trace of glass A5 did not show an exotherm below 915°C but XRD traces (Figure 4.12) revealed the presence of Fluorite (CaF_2 – JCPDS #35-816) by 800°C. The absence of an exotherm close to this temperature may again be attributed to the formation of only a small number of CaF_2 crystals. XRD patterns from the sample heat treated at the temperature above the crystallisation peak (950°C) revealed anorthite ($CaAl_2Si_2O_8$ – JCPDS #41-1486). Peaks corresponding to cristobalite were noted in the glass heat treated to 950°C. The formation of fluorite occurs primarily due to the mobility of Ca^{2+} and F^- within the glass network. Anorthite requires much higher temperatures (>850°C) to form due to the greater energy required to break the bonds within the glassy network [Wood and Hill 1991a].

This crystallisation sequence is consistent with studies by Hill and Wood [1991b]. They also found that non-phosphate containing ionomer glasses readily crystallised to fluorite and anorthite. Hill and Wood [1991b] suggested that the fluorite crystals act as nuclei for anorthite crystallisaiton and proposed that these glasses are therefore self-nucleating.

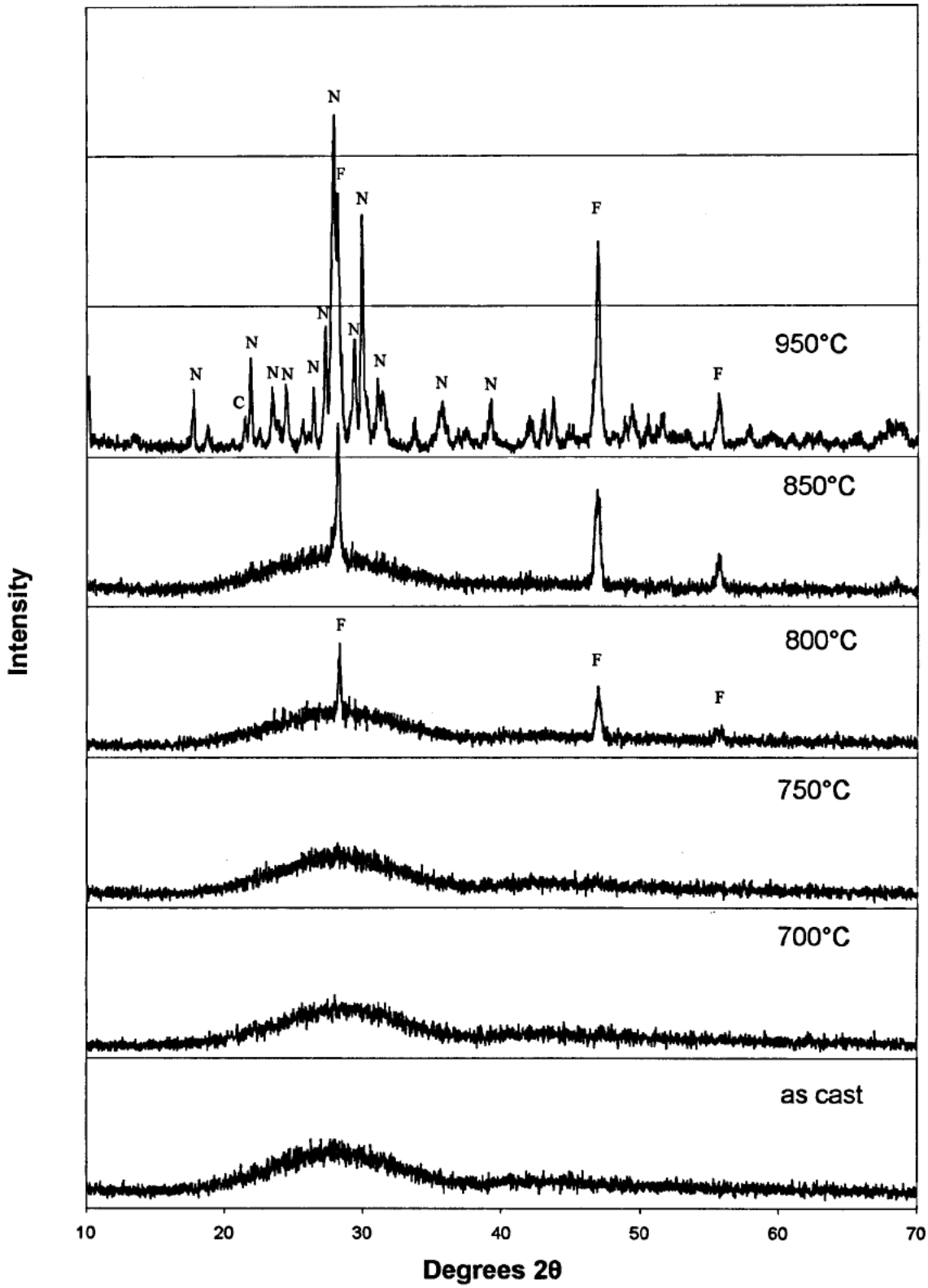

Figure 4.12: XRD spectra from the crystallisation of glass A5 using isothermal heat treatments. Principal peaks associated with the crystalline phases are labelled F – Fluorite N – Anorthite C – Cristobalite

4.3.5 Microstructural Analysis

Transmission Electron Microscopy

Heat-treated (750°C and 950°C) pieces of glass A1 were examined using TEM to study the morphology and distribution of the crystals in the microstructure. Differing microstructures were observed at the two temperatures chosen 750°C and 950°C. In the glass heat-treated at 750°C (Figure 4.13) a distribution of blocky crystals ranging in size from 0.5 – 0.1 μm were observed. Energy dispersive x-ray spectroscopy (EDS) revealed all the crystalline regions (Figure 4.14a) to be rich in Ca, P, O and F, confirming the presence of apatite detected by XRD. The residual glass (Figure 4.14b) was found to contain Si, Al, O, Ca and P but the amount of Ca and P was much lower in the glassy regions compared with the crystalline phase.

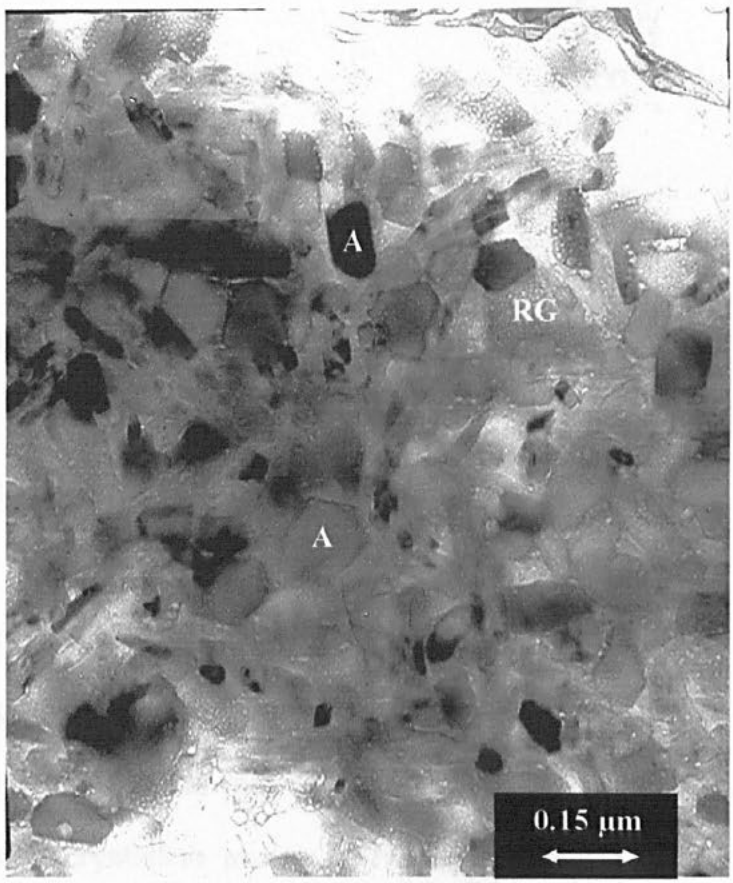

Figure 4.13: BF TEM micrograph of A1 held at 750°C for 2h showing apatite crystals (A) in a matrix of residual glass (RG).

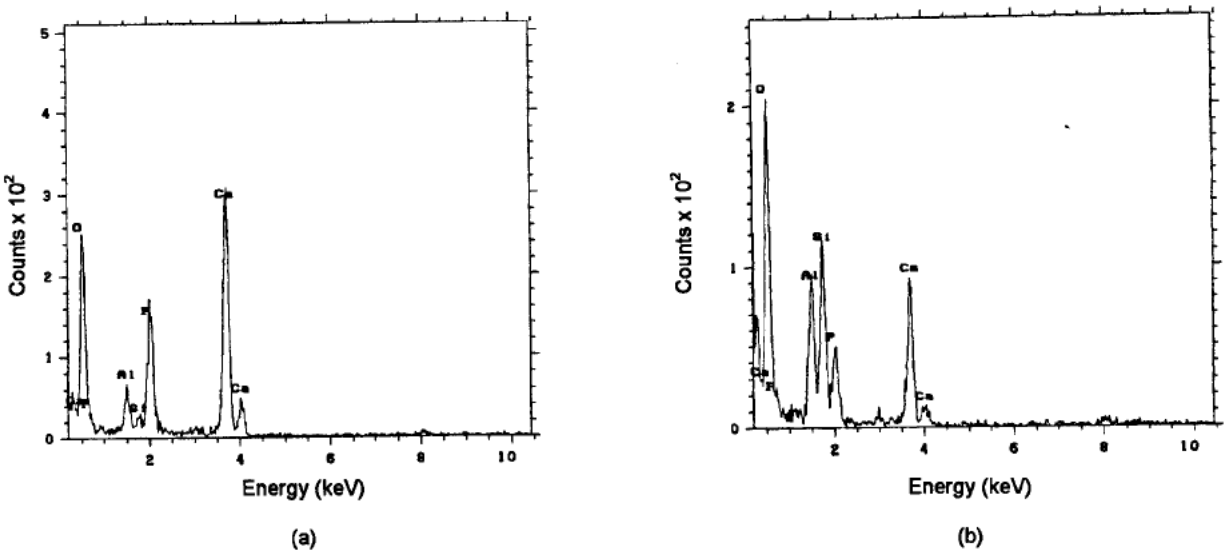

Figure 4.14: EDS spectra of glass A1 held at 750°C for 2h, spectrum (a) denotes the blocky apatite crystalline regions, showing an abundance of Ca and P and (b) shows the residual glass.

The microstructure observed in A1 heat-treated at 950°C showed blocky and lath shaped crystals in a matrix (Figure 4.15). Tilting the sample within the TEM revealed that the matrix exhibited diffraction contrast (Bragg contours) typical of a crystalline phase. The EDS analysis (Figure 4.16a) from the blocky and lath shaped regions revealed the presence of Ca, P, F, and O. Suggesting that the blocks and laths were the same crystal phase, apatite. The EDS analysis (Figure 4.16b) obtained from the diffracting matrix was found to contain the elements Al and Si in a ~6:2 ratio, although no attempt was made to perform full quantification, this ratio was consistent with mullite ($3Al_2O_3 - 2SiO_2$). Further examination revealed that there were small regions that did not diffract and were therefore assumed to be residual glass. The compositions of these regions were determined to contain predominantly Si

and O (Figure 4.16c). It was not possible however to find any regions of crystalline cristobalite but the presence of regions of glassy SiO_2 indicate that its formation may occur elsewhere in the system. It was not possible to carry out a comparative TEM study of the commercial glass system, SC, as only glass frit and powders were supplied by the manufacturers.

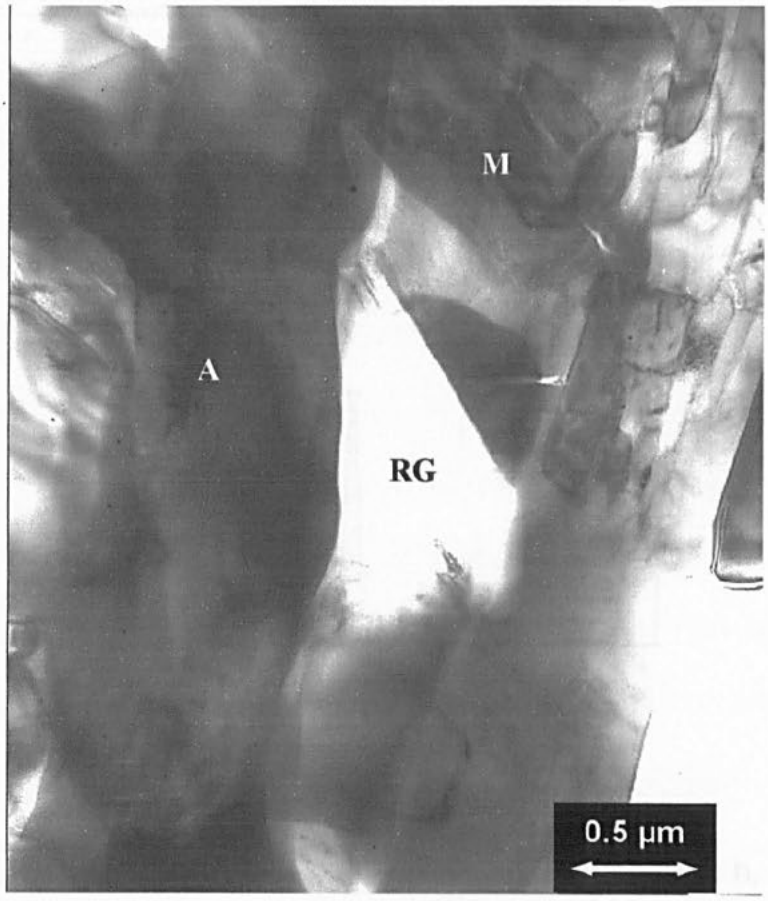

Figure 4.15: BF TEM micrograph of glass A1 held at 950°C for 2 h showing apatite crystals (A) in a mullite matrix (M) with regions of residual glass (RG).

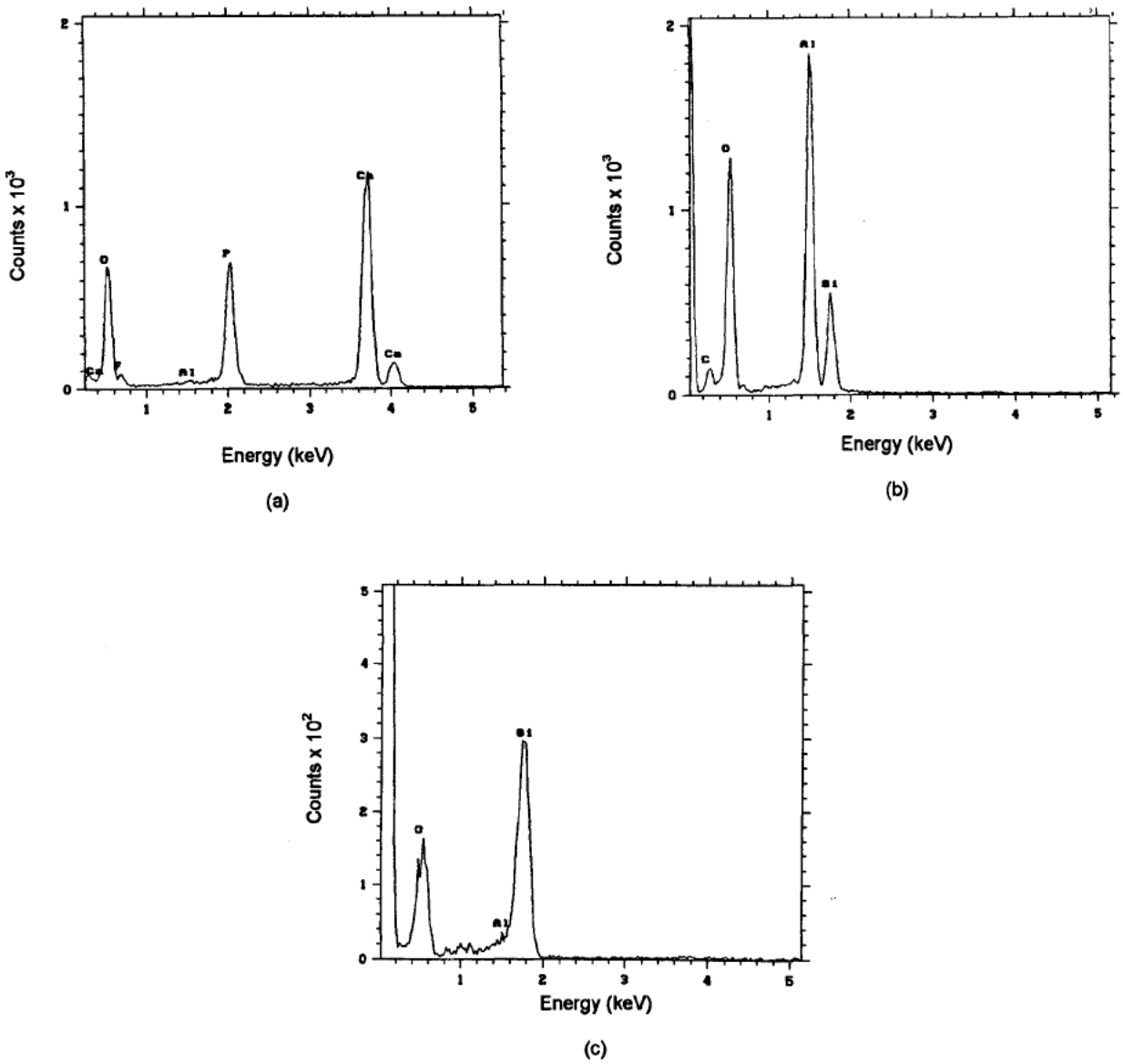

Figure 4.16: EDS spectra of glass A1 held at 950°C for 2 h, spectrum (a) denotes the blocky apatite crystalline regions, showing an abundance of Ca and P (b) mullite matrix rich in Si and Al and (c) residual glass, a small trace of Al was observed.

4.4 Glass Powder Preparation and Characterisation

4.4.1 Particle Size Analysis

The particle size distribution and morphology of the glass powders used for the cements is an important factor in cement properties. Early studies on silicate cements determined that powders must be passed through a 45 μm mesh sieve to give the best cement properties [Crisp *et al* 1975]. Silicate cements fabricated from powders containing substantial quantities of large particles (30 – 70 μm) exhibited a higher degree of porosity, resulting in a reduction in the compressive strength of the cement [Brune and Smith 1982]. A further reduction in strength is believed to be related to the glass – matrix interfacial bond, since interfacial separation appears to be greater for larger particles [Brune and Smith 1982]. Larger particles can also induce a 'gritty' texture, unappealing to the practitioner. A very fine powder is also detrimental to cement properties. Mixing would be difficult, resulting in incomplete mixing and a non-uniform paste [Kent 2002]. The distribution of particle sizes within a cement is therefore an important factor to consider when measuring mechanical properties. Both very fine and large particles can reduce strength, therefore an even distribution of glass particles is essential to obtain the optimal cement properties.

The laser particle size analysis showed that all the experimental glasses had similar particle size distributions (Figures 4.17 – 4.23). Table 4.5 gives the mean particle size and also the particle size for the 90th percentile. The mean particle size ranged from 22 μm to 28 μm for all glasses in series A. The commercial cement however exhibited a different particle size distribution, a

bimodal distribution was noted with a lower mean particle size. This may account for differences noted in mechanical properties and working and setting times (see section 4.5.1).

Table 4.5: Laser Particle size analysis showing the mean particle size and the particle size at the 90th percentile.

Glass	Particle Size	
	Mean (µm)	90th percentile (µm)
SC	18.27	36.49
A1	25.91	50.21
A2	26.07	39.84
A3	24.38	45.78
A5	27.32	52.32
A1 (750)	28.99	55.70
A1 (950)	21.99	45.64

SEM was used to assess the morphology of the milled glasses. A representative SEM micrograph showing both the distribution and the morphology of the particles are shown in Figures 4.17 – 4.23. Milled glasses were all found to have angular not spherical particles. An even distribution of particle sizes was noted. The larger particles were found to have a number of finer glass particles or 'fines' attached to their surface.

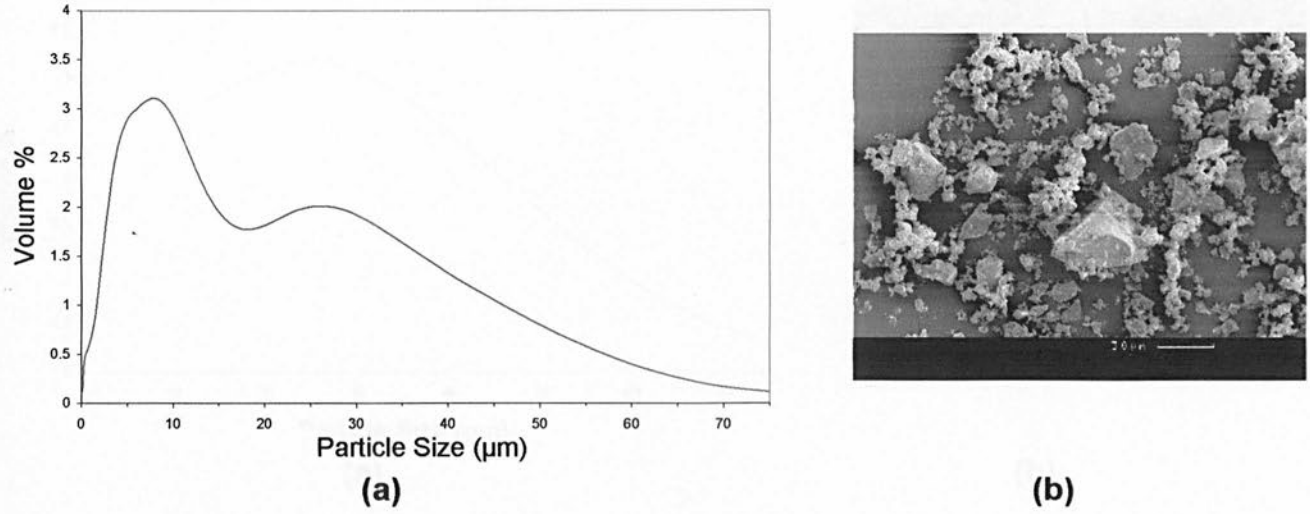

Figure 4.17: Particle size distribution for SC a. laser analysis b. SEM micrograph

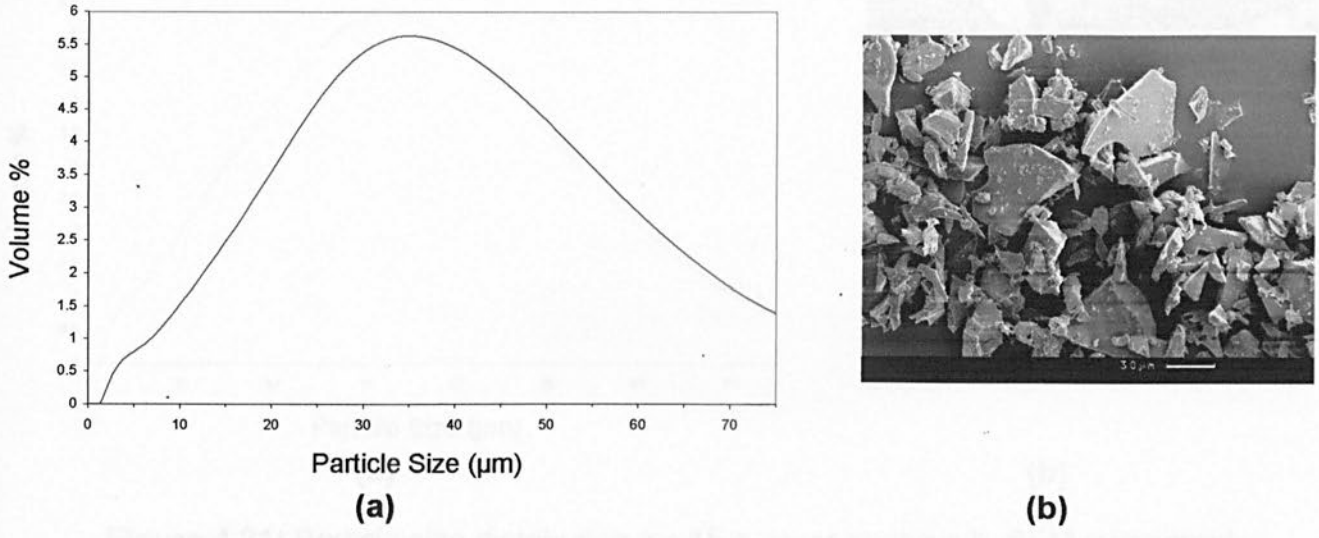

Figure 4.18: Particle size distribution for A1 a. laser analysis b. SEM micrograph

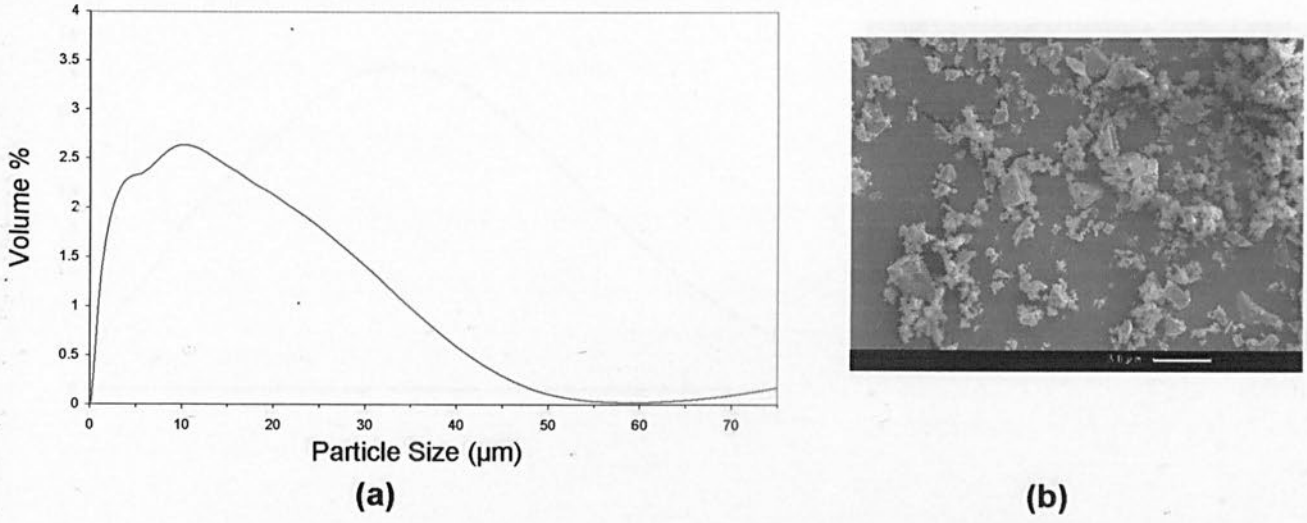

Figure 4.19: Particle size distribution for A2 a. laser analysis b. SEM micrograph

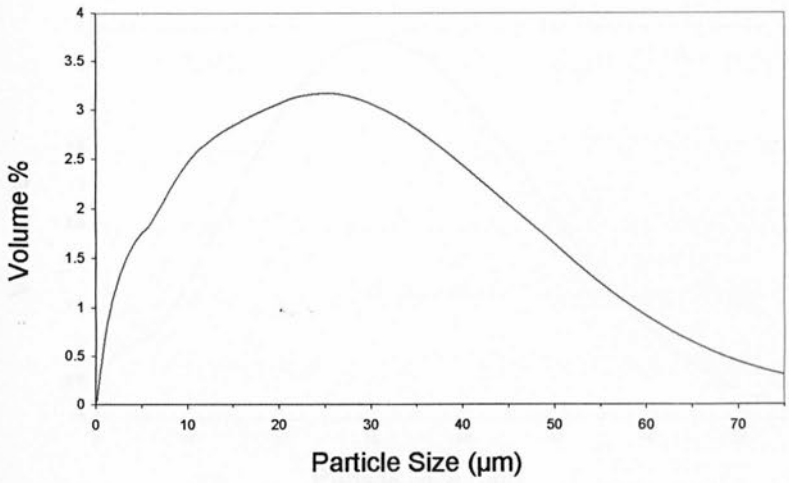

(a)

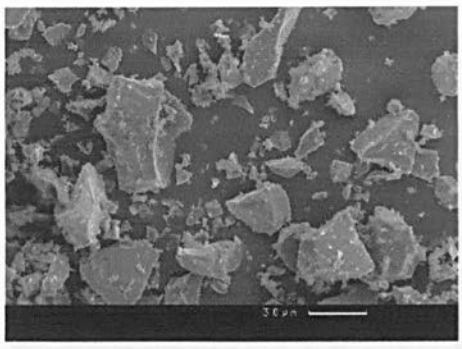

(b)

Figure 4.20: Particle size distribution for A3 a. laser analysis b. SEM micrograph

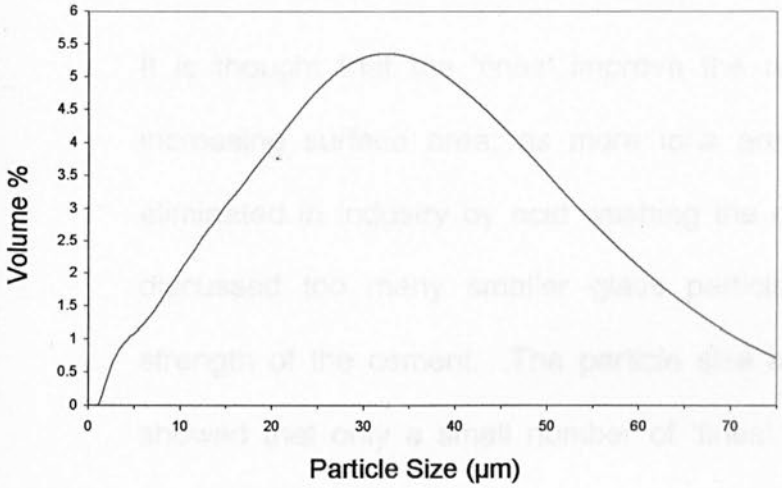

(a)

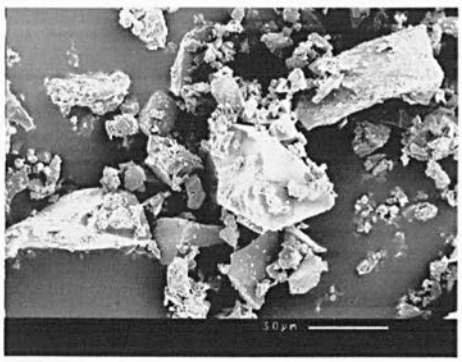

(b)

Figure 4.21: Particle size distribution for A5 a. laser analysis b. SEM micrograph

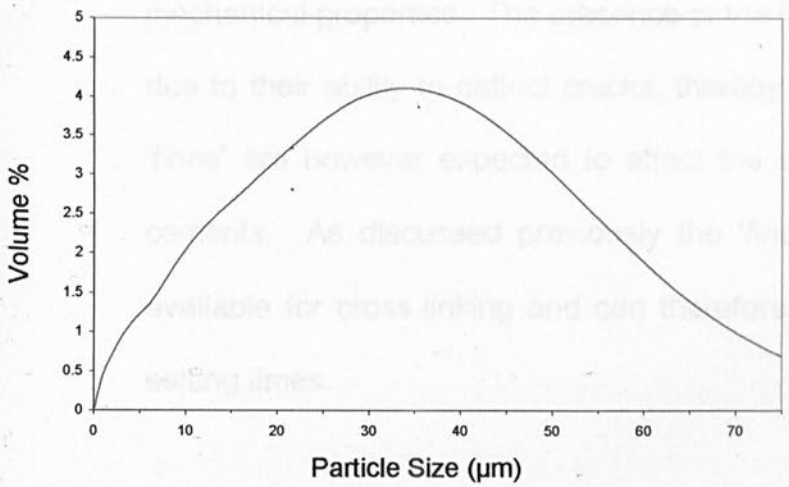

(a)

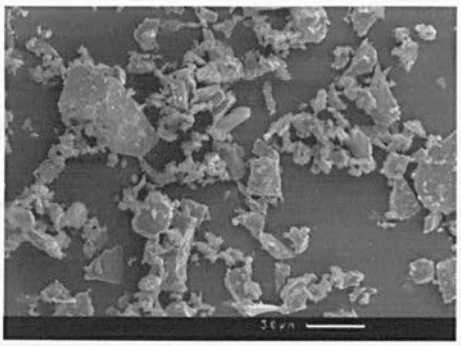

(b)

Figure 4.22: Particle size distribution for A1 (750) a. laser analysis b. SEM micrograph

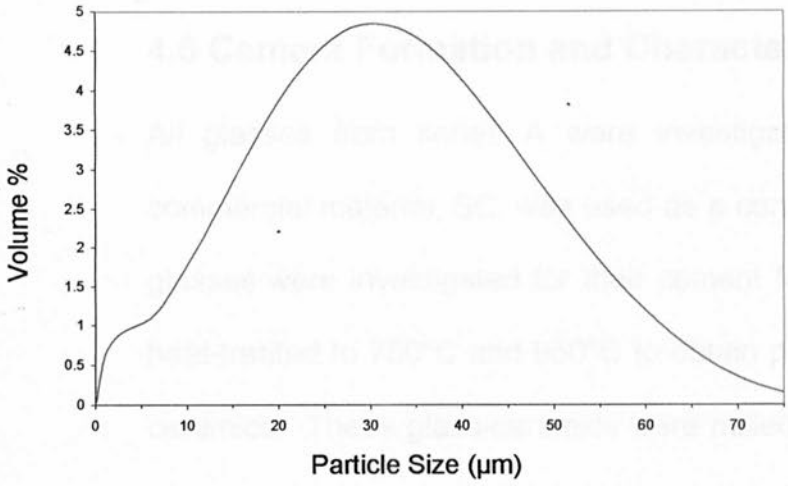

(a)

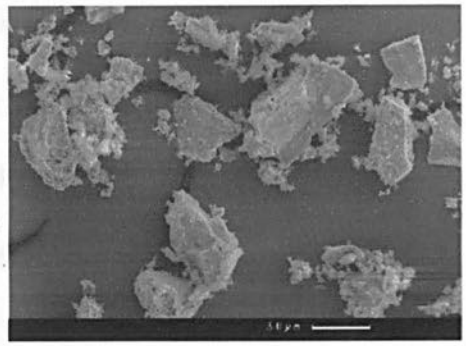

(b)

Figure 4.23: Particle size distribution for A1 (950) a. laser analysis b. SEM micrograph

It is thought that the 'fines' improve the reactivity of the cement, through increasing surface area, as more ions are available for release. This is eliminated in industry by acid washing the cement. However, as previously discussed too many smaller glass particles can compromise the overall strength of the cement. The particle size analysis of all the glass powders showed that only a small number of 'fines' were present. In addition, they were only found on the surface of larger particles rather than 'free' within the powder. It is therefore believed that these will not greatly affect the mechanical properties. The presence of the larger particles increases strength due to their ability to deflect cracks, thereby slowing crack propagation. The 'fines' are however expected to affect the setting and working times of the cements. As discussed previously the 'fines' increase the number of ions available for cross-linking and can therefore decrease both the working and setting times.

4.5 Cement Formation and Characterisation

All glasses from series A were investigated for use as cements. The commercial material, SC, was used as a control. In addition, two heat-treated glasses were investigated for their cement forming ability. Glass A1 frit was heat-treated to 750°C and 950°C to obtain partially and fully crystalline glass-ceramics. These glass-ceramics were milled and prepared for cement use in the same way as the glasses (see section 3.4). The viability of the cement was assessed using freshly mixed cements. Gilmore needle indentation tests based on the dental standard for GIC [BS 6039:1981] were used to determine setting and working times for each of the experimental glass compositions.

4.5.1 Working and Setting Time Determination

Gilmore Needle

The Gilmore needle has been employed for determining cement working and setting times for decades [BS 6039:1981]. The test although subjective gives reproducible results for the same user and offers a quick and simple analysis of cement handleablitity. Working and setting times of glass series A are given in Table 4.6. All glasses in series A were found to form cements. The working times of the cements were found to decrease with decreasing phosphate content. This is consistent with reported data [Griffin and Hill 2000, Wilson *et al* 1995].

Lowenstein's theories on alumino-silicate cements state that to maintain Al in tetrahedral co-ordination the Al:(Si+P) ratio must be <1 [Ray 1978]. In glasses A1 and A2 this criterion is met, but in A3 it is approximately equal to 1 and in

A5 >1. This results in Al no longer being in stable AlO_4^- tetrahedra but is available for release. This could account for the change in setting times. More Al^{3+} ions are available for release thereby reducing the overall setting time.

Table 4.6: Working and Setting Times for cements based on glass series A, determined using the Gilmore needle indentation test.

Cement	Working Time (sec)	Setting Time (sec)
SC	162 (±8)	348 (±8)
A1	213 (±28)	872 (±65)
A2	145 (±5)	242 (±8)
A3	144 (±2)	267 (±3)
A5	110 (±13)	180 (±13)
A1 (750)	110 (±13)	282 (±28)
A1 (950)	1025 (±5)	In excess of 30 min

Oscillating Rheometery

Oscillating rheometery allows for a more quantitative measure of the setting characteristics of cements. It is less subjective than the Gilmore needle indentation test but it is not without its faults. Reproducibility of data is possible based on measurements taken from one individual machine. However, due to the tension of the spring component differing results may be obtained on different rheometers. It is therefore essential that all measurements are carried out on the same machine. A second source of error is that the movement of the plates continues the mixing of the cement

after placement. This can therefore give lower working and setting times compared with the Gilmore needle indentation test.

Only glasses SC and A1 had the desired setting characteristics specified in section 2.4.6 based on Gilmore needle indentation testing. Their setting properties were investigated further using oscillating rheometery. However due to interest in the effect of devitrification of ionomer glasses on working and setting times, A1(750) was also assessed using rheometery. Table 4.7 shows the working and setting times obtained for the three glass compositions.

Table 4.7: Working and Setting Times for cements based on glass series A, determined using an Oscillating rheometer.

Cement	Working Time (sec)	Setting Time (sec)
SC	99 (±7.9)	178 (±6.9)
A1	82 (±19.9)	593 (±65.9)
A1 (750)	80 (±1.7)	192 (±10.4)

The working and setting times were found to be lower using this assessment method. As mentioned above this can be attributed to the motion of the plates. Secondly the setting time is carried out at 37°C; this too will decrease the time relative to setting at room temperature.

4.5.2 Mechanical Properties

The flexural strength of the cements was investigated using three-point bend testing. It was only possible to make sample rods out of SC and A1, all other

cements set too quickly to enable rods of the required test length (25 mm) to be fabricated. The mean flexural strength values and the standard deviation are given in Table 4.8. for both the unaged (24 h) and aged (4 w) samples.

Table 4.8: Flexural strength (FS) values for SC and A1 at time intervals of 24 h and 4 w, the standard deviation is given in brackets

Cement	FS at 24 h	FS at 4 w
SC	13.1 (±3.0) MPa	16.6 (±2.6) MPa
A1	10.3 (±3.0) MPa	14.9 (±1.6) MPa

Using an unpaired t-test the flexural strength of both cements was found to significantly increase over time ($P < 0.05$). This was consistent with current theories on the setting chemistry of GICs. It is hypothesised that the Ca ions cross-linking the dissociated carboxyl groups are replaced over time with Al ions, resulting in stronger bonds improving cement strength. The commercial cement was found to have slightly higher strength than the experimental equivalent (A1).

The fracture surfaces were examined after mechanical testing using SEM to ascertain the mode of failure for the cement. Figures 4.24 and 4.25 show the surfaces for the two cements at the two time intervals investigated. No differences were noted, suggesting that the failure mechanism was the same in both unaged and aged specimens. The cause of fracture was thought to be failure of the glass-matrix interface. Other authors have also reported this mode of failure. Brune and Smith [1982] and Xie *et al* [2000] reported that

fracture surfaces show that the interfacial region between the original glass particle and the cement matrix is a zone of weakness.

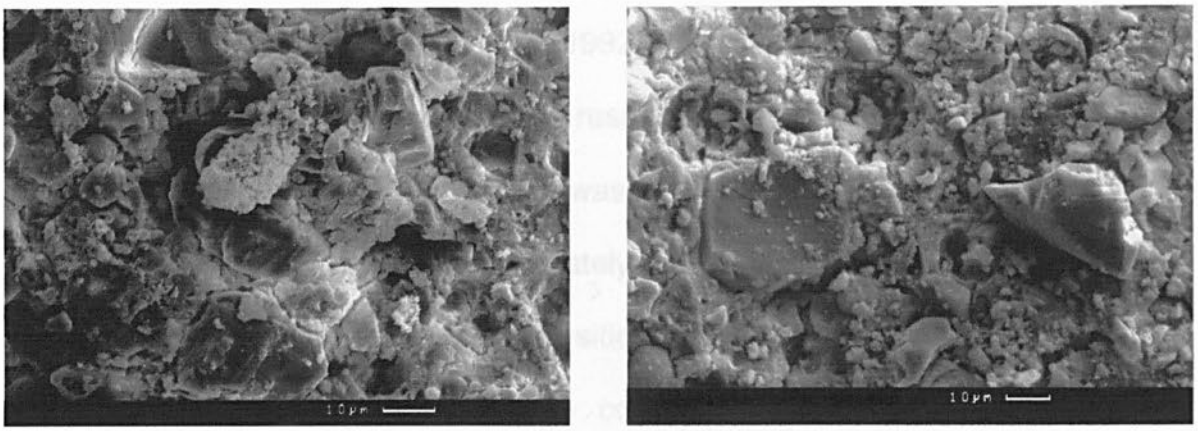

Figure 4.24: SEI SEM micrographs of fracture surfaces of SC at different time intervals a. 24 h and b. 4 w. Pits present due to glass pullout caused by a glass-matrix interface failure

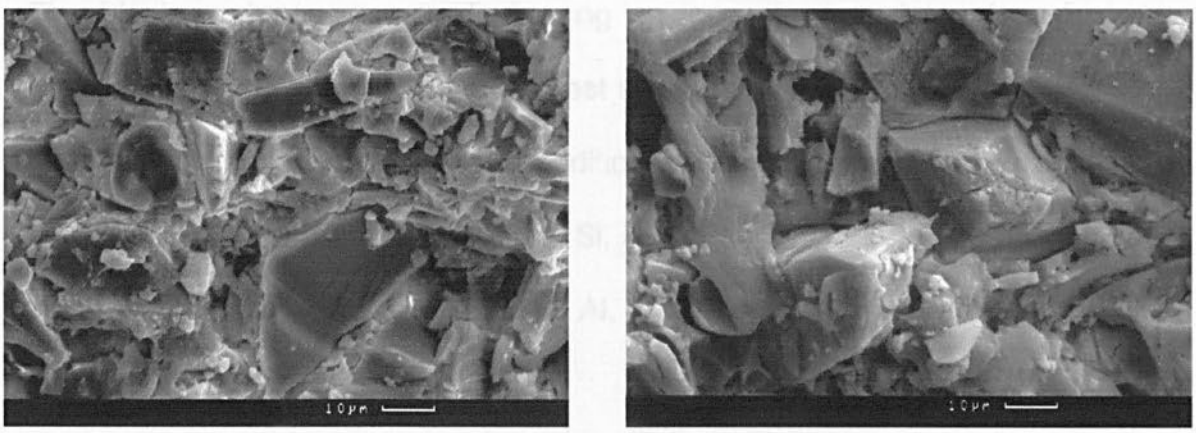

a b

Figure 4.25: SEM micrographs of fracture surfaces of A1 at different time intervals a. 24 h and b. 4 w. Pits present due to glass pullout caused by a glass-matrix interface failure

4.5.3 Ion Release

X-ray microanalytical studies of GICs have shown that ions are released from the cement and enter the polymer matrix as predicted by early models of cement studies [Hatton and Brook 1992]. Ion release from GICs has been studied extensively, particularly with respect to the release of F ions. The ion release profile of only two cements was analysed GIC A1 and GIC A1 (750). The inability to fabricate appropriately sized and smooth discs hindered investigation of other cement compositions. The commercial system was not included for comparison since the commercial glass undergoes an acid washing step prior to encapsulation. The effect of this process is to remove ions from the surface retarding the setting process. It was felt that this would affect the ion release from the cement and would not supply a fair comparison with the experimental glasses.

Fluoride ion release was studied using an ion selective electrode. A de-complexing agent was added to the test samples, as fluoride ion is known to form complexes with other ions in addition to being released as F^-. ICP-ES was used to investigate the release of Si, Al, Ca and P ions. Figures 4.26 – 4. 30 show the release profiles for the Si, Al, P, Ca and F respectively.

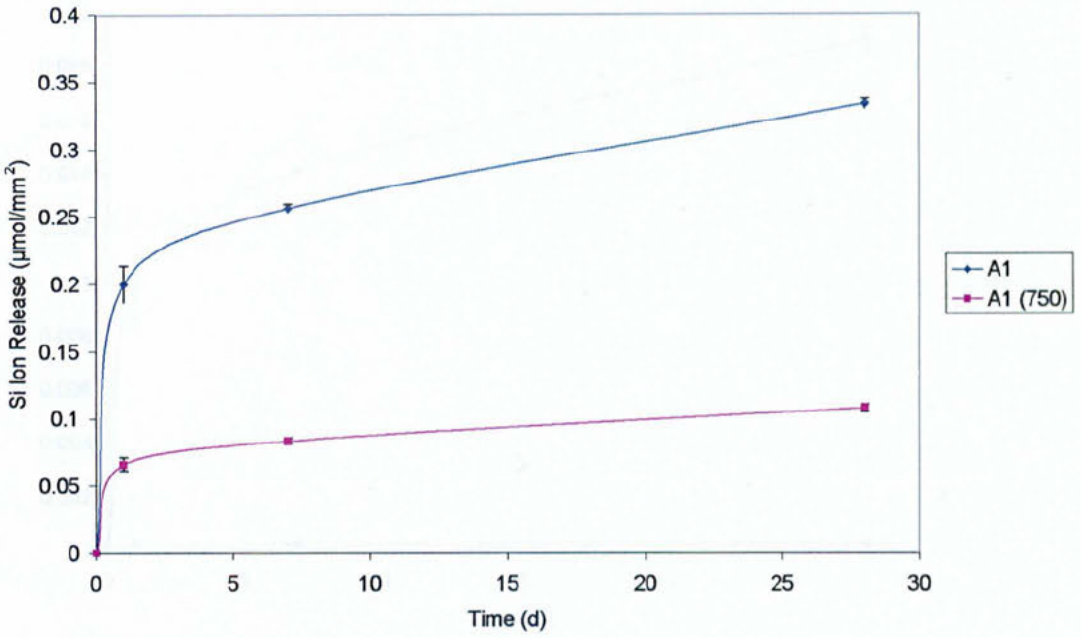

Figure 4.26: Graph showing the Si ion release profile for cements A1 and A1(750) over three time intervals (1 d, 7 d, and 28 d).

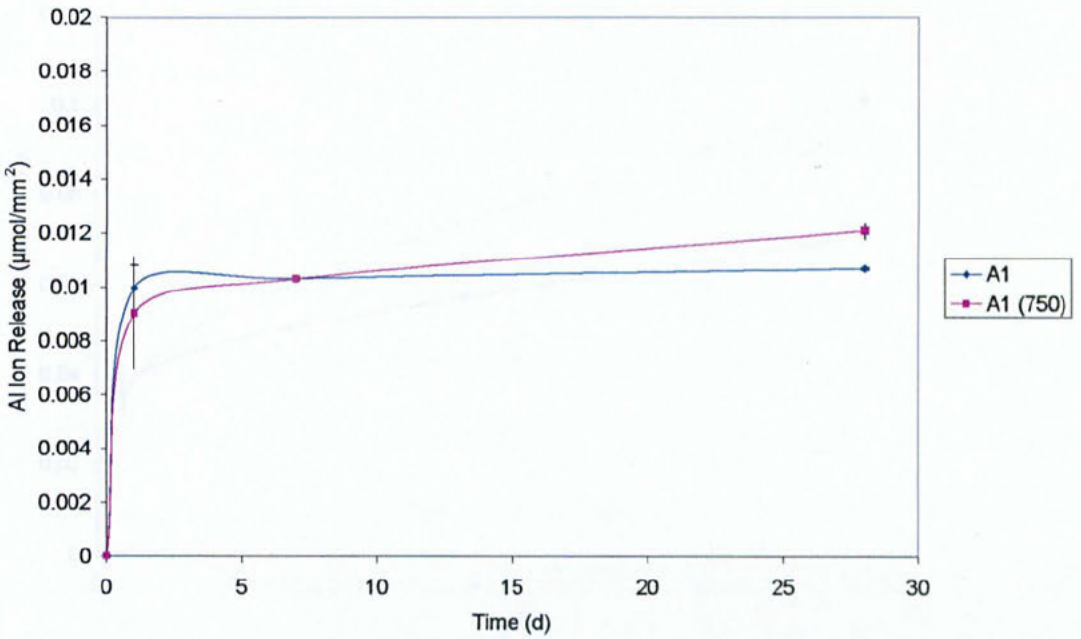

Figure 4.27: Graph showing the Al ion release profile for cements A1 and A1(750) over three time intervals (1 d, 7 d, and 28 d).

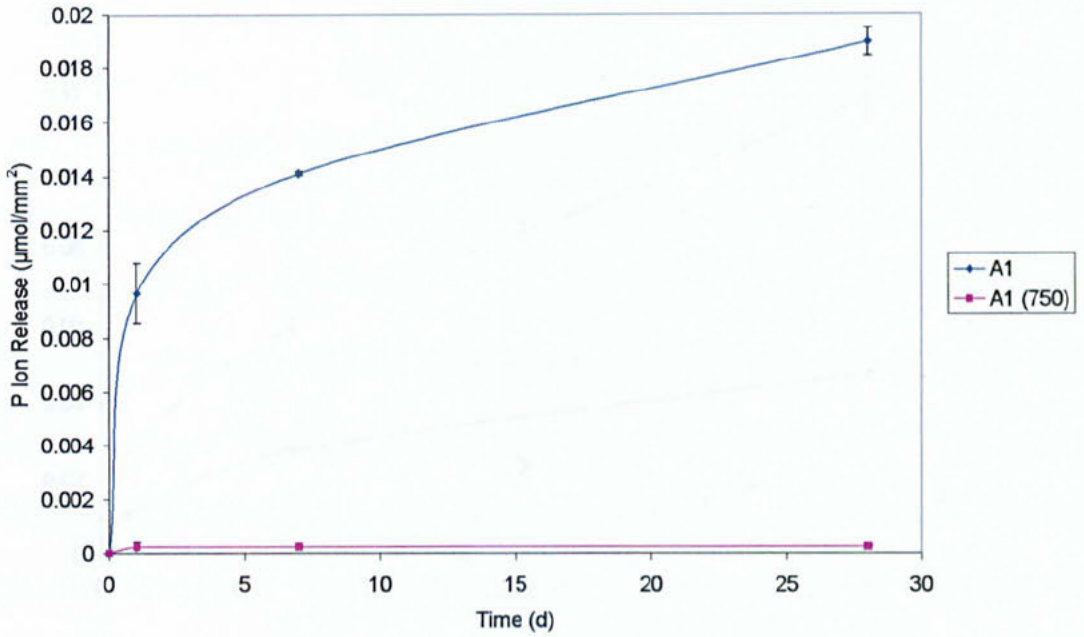

Figure 4.28: Graph showing the P ion release profile for cements A1 and A1(750) over three time intervals (1 d, 7 d, and 28 d).

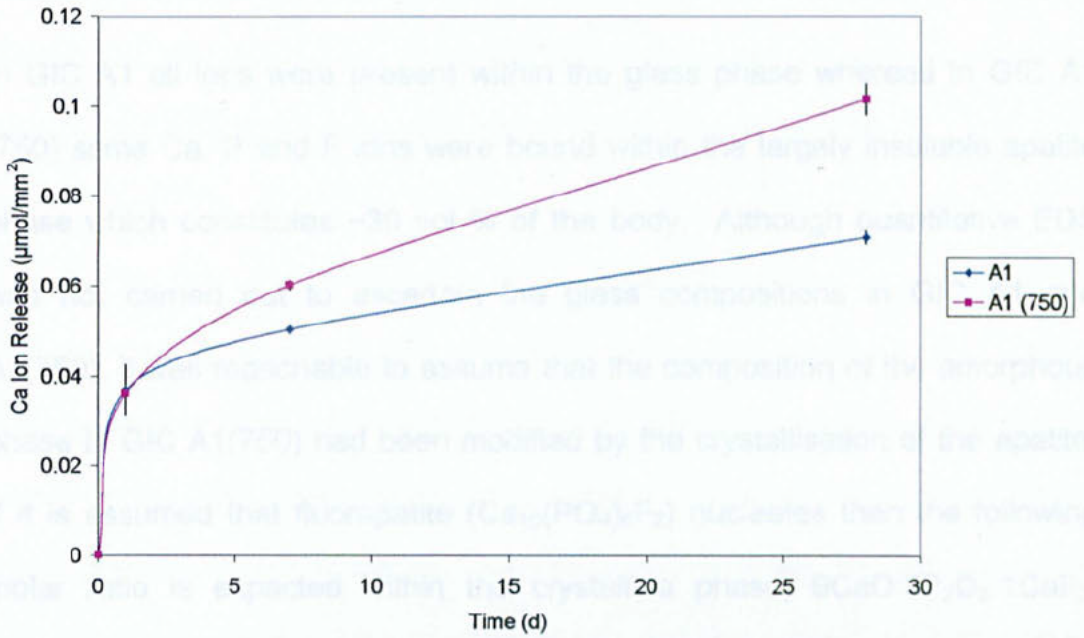

Figure 4.29: Graph showing the Ca ion release profile for cements A1 and A1(750) over three time intervals (1 d, 7 d, and 28 d).

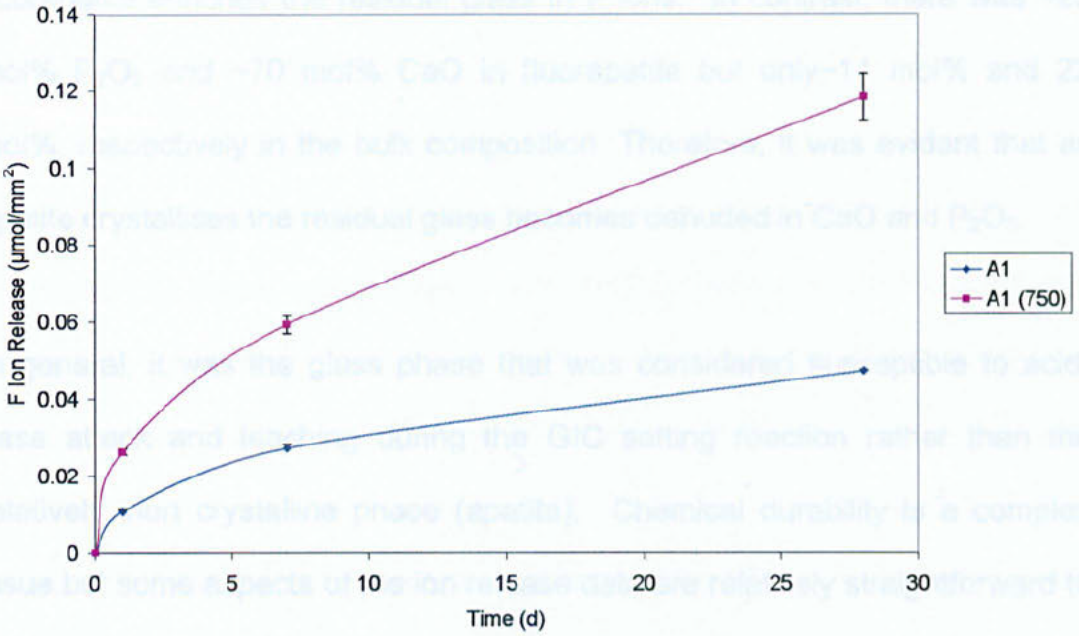

Figure 4.30: Graph showing the F ion release profile for cements A1 and A1(750) over three time intervals (1 d, 7 d, and 28 d).

In GIC A1 all ions were present within the glass phase whereas in GIC A1 (750) some Ca, P and F ions were bound within the largely insoluble apatite phase which constitutes ~30 vol % of the body. Although quantitative EDS was not carried out to ascertain the glass compositions in GIC A1 and A1(750), it was reasonable to assume that the composition of the amorphous phase in GIC A1(750) had been modified by the crystallisation of the apatite. If it is assumed that fluorapatite ($Ca_{10}(PO_4)_6F_2$) nucleates then the following molar ratio is expected within the crystalline phase, $9CaO:3P_2O_5:1CaF_2$. Therefore, from a simple molar ratio perspective, the limiting factor in the volume fraction of apatite in the final body is the concentration of CaO (~22 mol%), i.e. $22CaO:7.3P_2O_5:2.5CaF_2$. There is approximately ~7 mol% CaF_2 in fluorapatite but 14 mol% in the bulk glass. Therefore the formation of

fluorapatite enriches the residual glass in F ions. In contrast, there was ~23 mol% P_2O_5 and ~70 mol% CaO in fluorapatite but only~11 mol% and 22 mol%, respectively in the bulk composition. Therefore, it was evident that as apatite crystallises the residual glass becomes denuded in CaO and P_2O_5.

In general, it was the glass phase that was considered susceptible to acid-base attack and leaching during the GIC setting reaction rather than the relatively inert crystalline phase (apatite). Chemical durability is a complex issue but some aspects of the ion release data are relatively straightforward to explain. The P ion release was the greatest in GIC A1 rather than A1(750) because the residual glass was denuded in P_2O_5 due to the formation of the apatite phase. However, the Ca and F ion release were both greater in GIC A1(750). Si plays no role in crystallisation at 750°C but its release was more pronounced in GIC A1 rather than A1(750) and surprisingly the Al ion release was low (0.01 μmol/mm^3) and virtually identical in each sample.

The contradictory nature of these results demonstrates the complexity of the acid-base reaction and leaching process. There are, however, two key points to consider. As discussed already the GIC A1(750) had ~30 vol% apatite modifying the glass composition. In addition, it was leaching from the cross-linked polymer which contributes most strongly to the ion release data. The latter point explains the low but similar values of Al ion release for GIC A1 and A1(750). In effect, the Al ions were strongly bound within the polymer since they are inherent in the cross-linking reaction.

The increased F-ion release in GIC A1(750) could be explained by the increase in F-ions within the residual glass due to crystallisation. However, the same logic could not be applied to the Ca ion release. In GIC A1 and A1(750), the Ca ion release was similar after a short time (2 days) but the rate over a longer period was greater in GIC A1(750) even though fewer Ca-ions were present in the glass phase. The explanation for this phenomenon remains to be elucidated. To an extent the higher Si ion release in GIC A1 than GIC A1(750) might be explained by the larger volume fraction of glass phase in the former. However, the amount released was much greater than could be explained by only considering the volume fraction.

It was interesting to note that the release of Ca and F ions into the biological environment was considered to enhance biocompatibility. [Brook and Hatton, 1998]. From this perspective, GIC A1(750) should offer superior *in-vitro* and *in vivo* response compared with GIC A1 since the rate and the amount of Ca and F ion release was greater.

4.5.4 *In Vitro* Biocompatibility

Two cell culture studies were carried out on glass series A. The effect of compositional change on *in vitro* biocompatibility was investigated. Additionally a study on the effect of devitrification of glass A1 on biocompatibility was undertaken. For this study, glass frit was heated to 750°C and 950°C and glass powder prepared using the standard method. Nomenclature relating to the heat treatment undergone by the glass was used,

e.g. GIC A1 (750) and GIC A1 (950) with the number in brackets referring to the heat treatment temperature.

In vitro biocompatibility of ionomer glasses with differing P_2O_5 content.

Cells were able to grow on all cements fabricated from the glasses in series A. A non-confluent cell sheet was observed on the surface of GIC A1 (Figures 4.31 a and b). Rounded cells were present in addition to flattened ROS cells with a normal osteoblast-like appearance. The cells cultured on GIC A2 (Figure 4.32) were flattened and had pseudopodia projecting across the surface of the cement. The cell sheet was again non-confluent but the coverage was better than that observed for the surface GIC A1. Rounded cells were also visible but it was difficult to distinguish whether they were dividing or dead. A fully confluent sheet of cells was observed on the surface of GIC's A3 and A5 (Figures 4.33 and 4.34 respectively). Good biocompatibility has been related to confluent flattened sheets of cells on the surface of test materials.

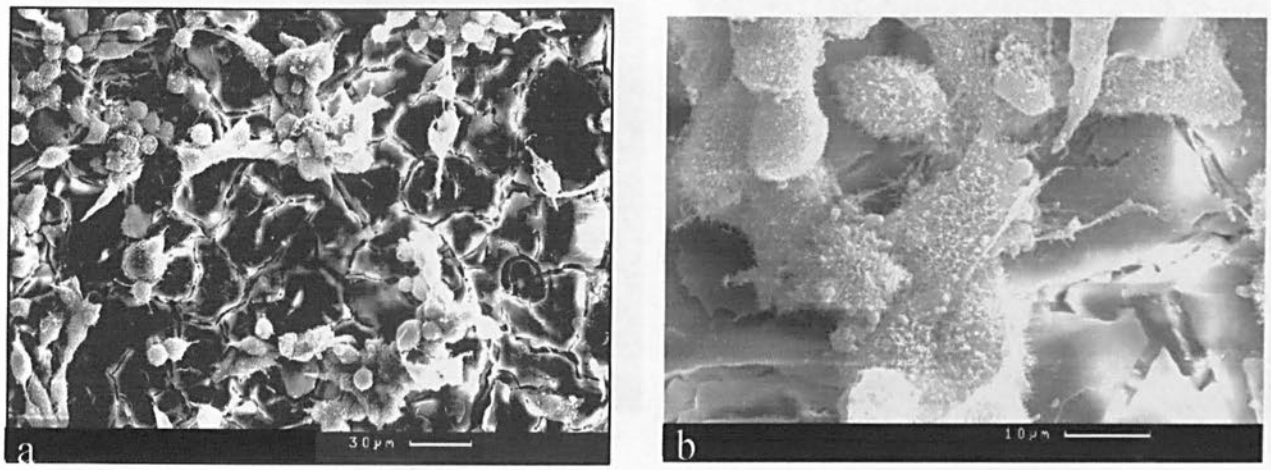

Figure 4.31: Secondary electron SEM images of cell cultured cement, GIC A1 **a.** showing cells of differing morphology, rounded and flattened **b.** GIC showing flattened cells with pseudopodia present

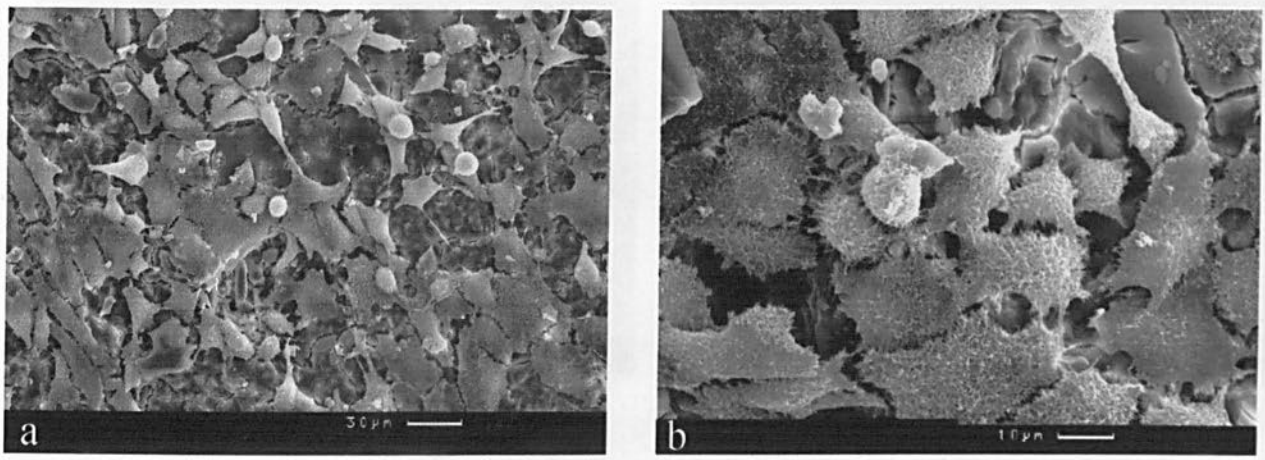

Figure 4.32: Secondary electron SEM image of cells cultured on cement based on A2, **a**. shows flattened cells with pseudopodia spreading across the cement surface b. near-confluent cell sheet.

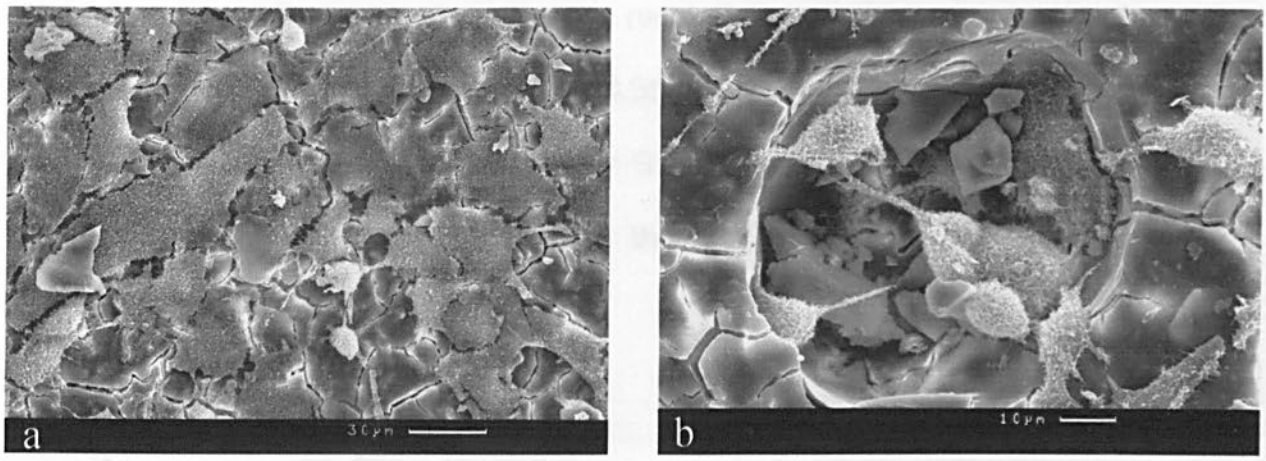

Figure 4.33: Secondary electron SEM image of cells cultured on GIC A3 **a.** shows a confluent cell sheet colonising the cement surface **b.** cells growing within a surface defect

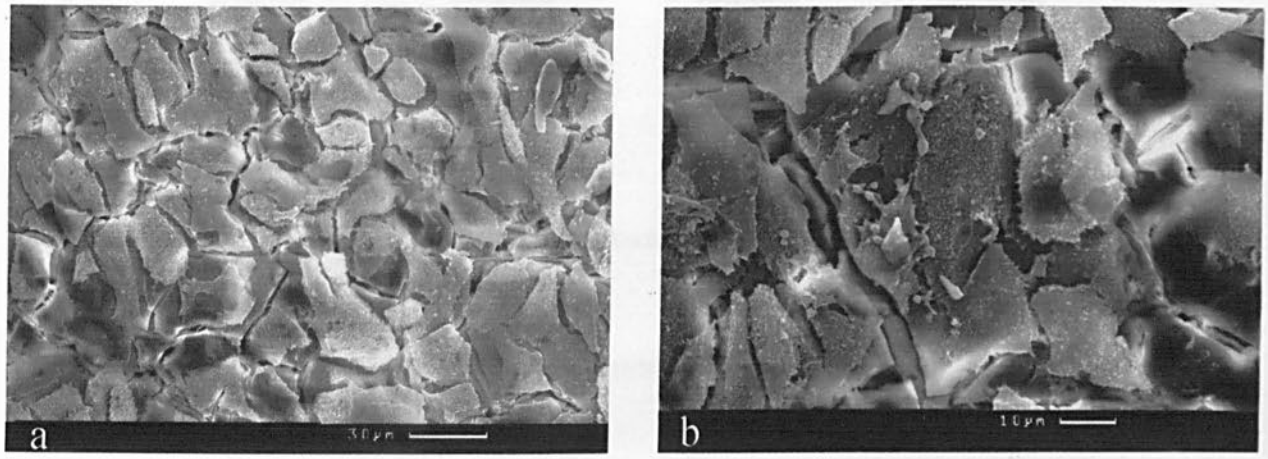

Figure 4.34: Secondary electron SEM image of cells cultured on GIC A5 **a.** confluent cell sheet **b.** confluent cell sheet. N.B. Cracks present are a processing artefact.

Quantitative MTT assay showed that respiratory activity increased with decreasing phosphate content (Figure 4.35). GIC A1 showed the poorest cellular response followed by GIC A2 with GIC A5 showing the best compared to tissue culture plastic. This confirms the qualitative SEM data reported above.

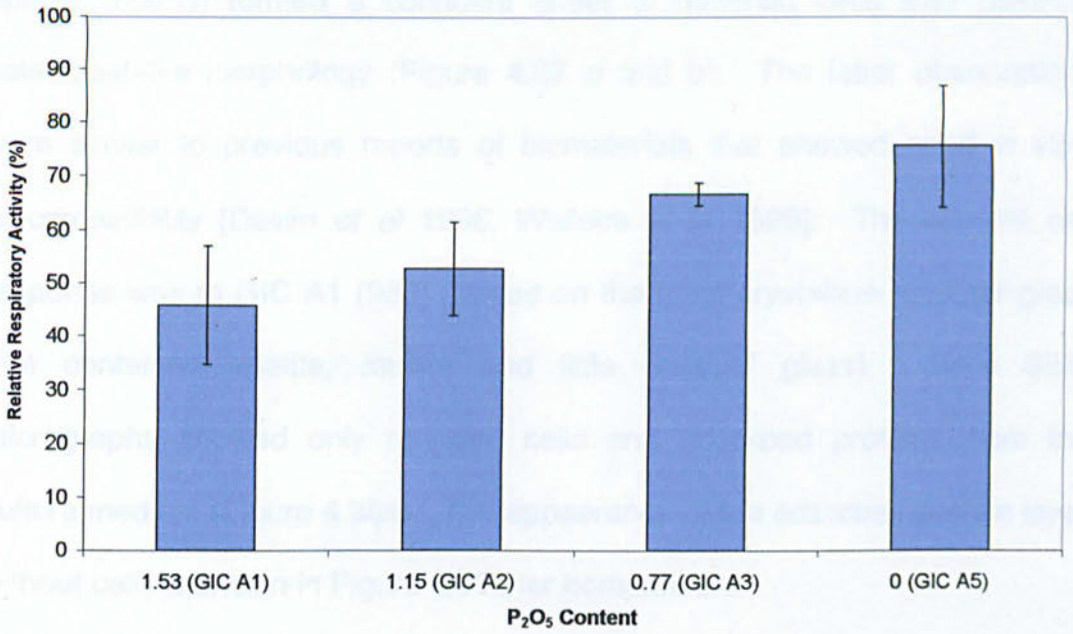

Figure 4.35: Graph showing the relative mitrochondrial activity

These data suggested that decreasing the phosphate content of the glass component could improve biocompatibility. One explanation for the improvement is that by reducing the P_2O_5 concentration the chemistry of the glass is changed. The solubility of the cements may therefore, also be affected. This might result in a higher number of other constituent ions being released. Further work needs to be carried out to study the effect of decreasing P_2O_5 on the ion release profiles of these cements.

In vitro cell culture study based on as cast and devitrified ionomer glasses

Cells were able to grow in the presence of GIC A1 (Figure 4.31 a and b). However, the cell sheet was not confluent, and rounded cells were present in addition to flattened ROS cells with a typical osteoblast-like appearance. In contrast, ROS cells cultured on GIC A1 (750) (based on A1 crystallised to apatite, 750°C) formed a confluent sheet of flattened cells with classical osteoblast-like morphology (Figure 4.37 a and b). The latter observations were similar to previous reports of biomaterials that showed good *in vitro* biocompatibility [Devlin *et al* 1998, Wallace *et al* 1999]. The poorest cell response was to GIC A1 (950) (based on the most crystalline ionomer glass that contained apatite, mullite and little residual glass). Here SEM micrographs showed only rounded cells and adsorbed proteins from the culture medium (Figure 4.38a). The appearance of the adsorbed protein layer without cells is shown in Figure 4.38b for comparison.

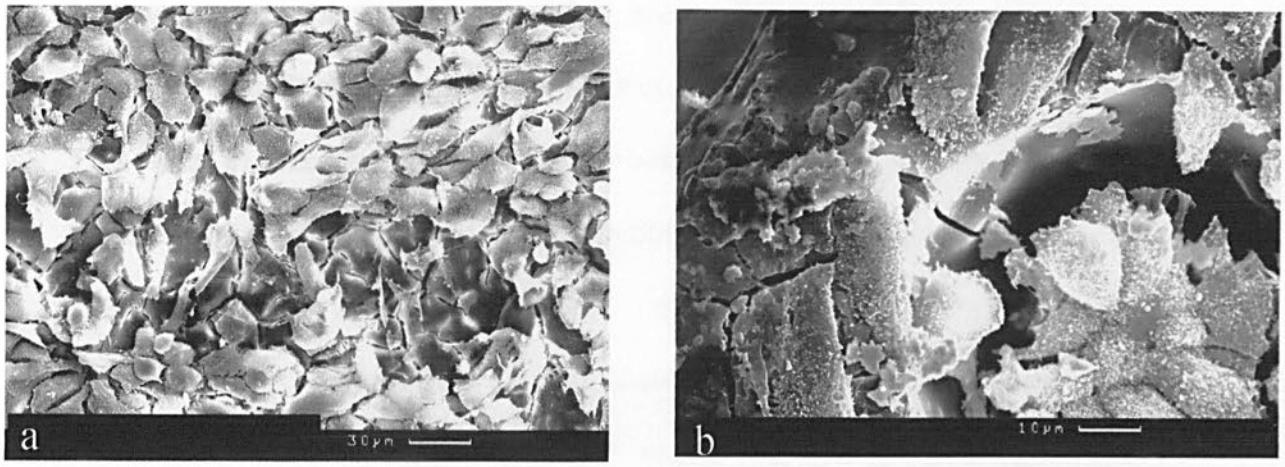

Figure 4.37: Secondary electron SEM images of cell cultured cement, GIC A1 (750) (based on apatite containing glass-ceramic) **a.** displaying a confluent sheet of cells **d.** Cells colonising a surface defect on GIC surface

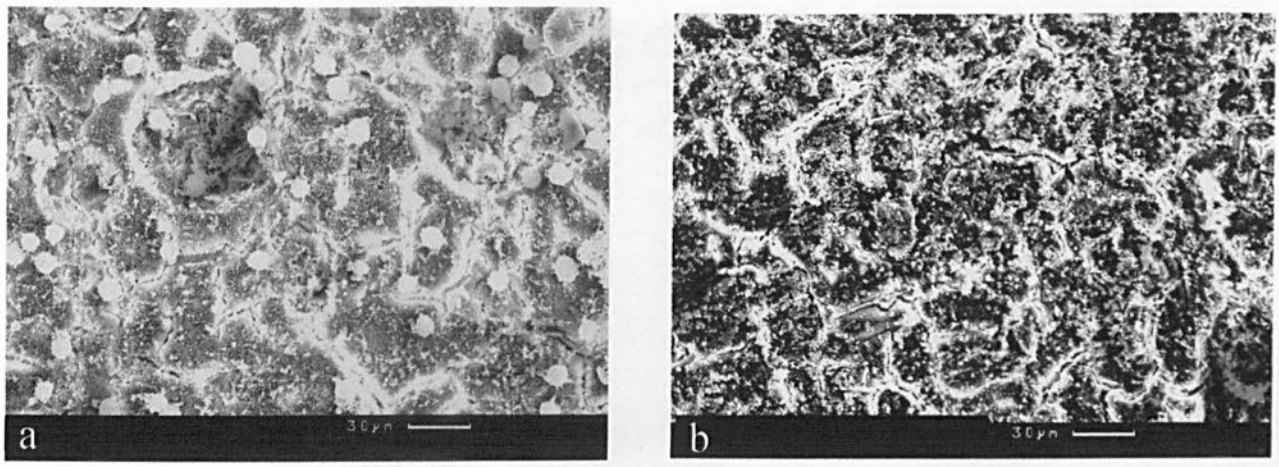

Figure 4.38: Secondary electron SEM images of cell cultured cement, GIC A1 (950) (based on apatite and mullite containing glass-ceramic) **a.** showing non-vital, rounded cells on the materials surface. **b.** from the cell-free control, post culturing showing an absorbed protein layer on the surface

Following from the quantitative MTT assay, GIC A1 showed a poorer cell response than that observed with control tissue culture plastic (Figure 4.39). This was in accordance with many previous *in vitro* evaluations of GIC biocompatibility [Brook *et al* 1992, Sasanaluckit *et al* 1993 and Devlin *et al* 1998]. In GIC A1 (750) however, the MTT assay showed excellent biocompatibility, comparable to that observed for the control tissue culture plastic. For GIC A1 (950) the MTT assay results obtained showed little evidence of cell growth and metabolism (Figure 4.39). This trend demonstrated by the quantitative MTT assay was repeated in the evaluation of total protein synthesised in the presence of test materials (Figure 4.40), with GIC A1 (950) supporting the least biosynthetic activity.

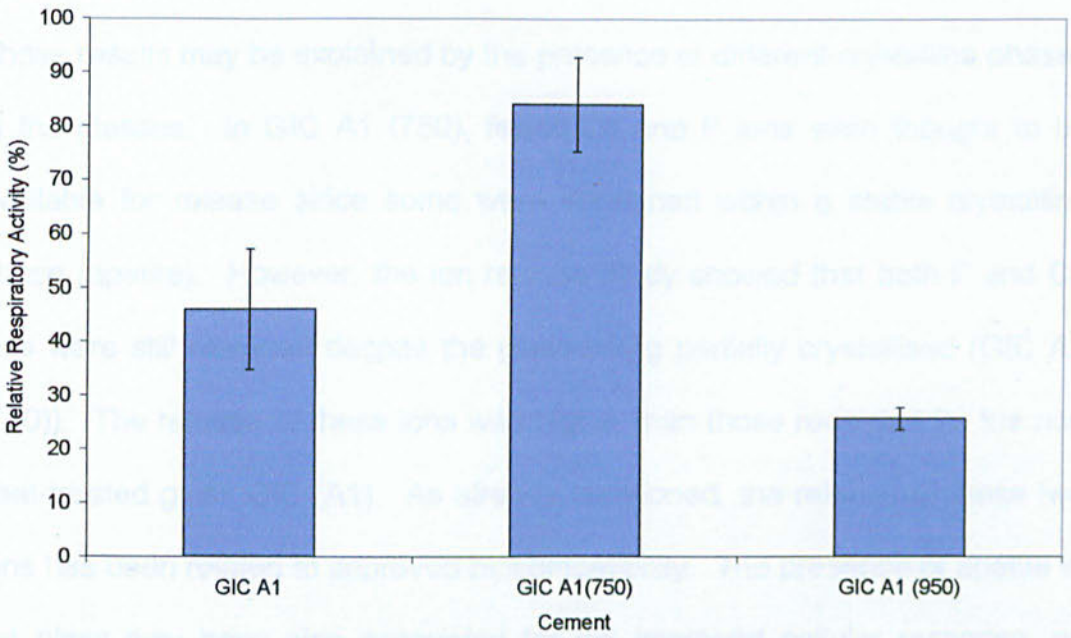

Figure 4.39: Bar Chart showing the MTT assay results for GIC based on amorphous and heat treated glasses (A1, A1 (750) and A1 (950)).

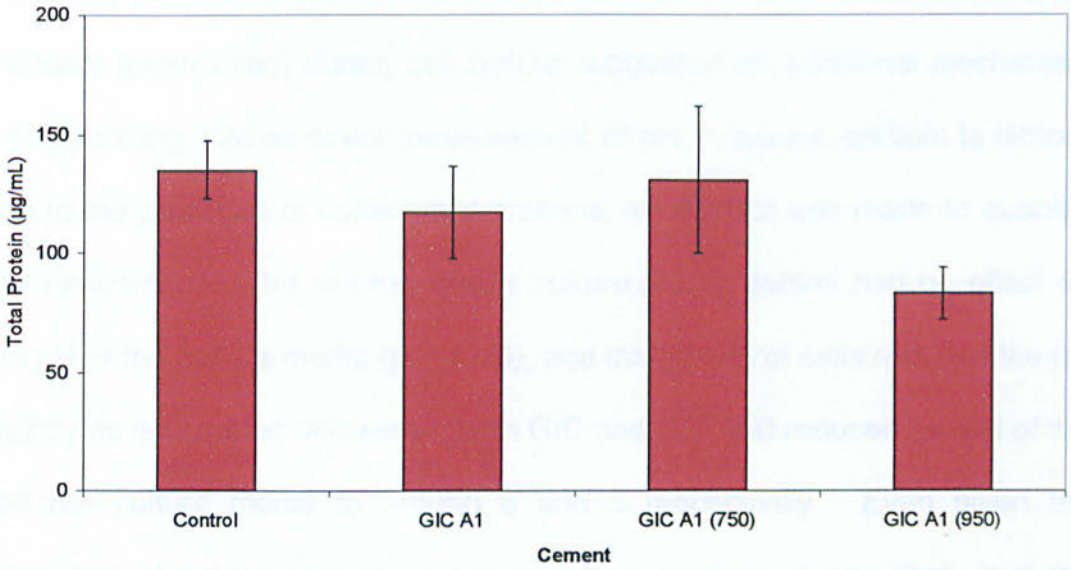

Figure 4.40: Bar chart showing the total protein found on the surfaces of cultured cements and tissue cultured plastic (control).

These results may be explained by the presence of different crystalline phases in the glasses. In GIC A1 (750), fewer Ca and P ions were thought to be available for release since some were contained within a stable crystalline phase (apatite). However, the ion release study showed that both F and Ca ions were still released despite the glass being partially crystallised (GIC A1 (750)). The release of these ions was higher than those recorded for the non heat-treated glass GIC (A1). As already mentioned, the release of these two ions has been related to improved biocompatibility. The presence of apatite in the glass may have also accounted for the improved cellular response, as apatite has long been associated with excellent biocompatibility (in particular with bone tissue) [Kokubo 1991].

However, observations of colour changes in the medium that contained a pH indicator (phenol red) during cell culture suggested an additional mechanism was operating. While direct measurement of pH in culture medium is difficult due to the presence of buffers and proteins, an attempt was made to quantify this observation. The cell-free tissue culture plastic control had no effect on the pH of the culture media (pH = 7.0), and the growth of cells reduced the pH slightly as anticipated. However, both GIC and GIC 950 reduced the pH of the cell-free culture media to around 6 and 5 respectively. Even given the difficulties of determining pH in tissue culture medium, it was likely that the reduction in the pH of culture medium by GIC and GIC 950 contributed to the relatively poor biocompatibility of these materials. In the case of GIC 950, it was suggested that unreacted poly(acrylic acid) contributed to the acidification of the culture medium [Hurrell-Gillingham *et al* 2003]. It has also been reported that a drop in pH (increased acidity) can cause an increase in the release of Al ions [Andersson and Dahl 1994]. An increase in Al ion release could cause a decrease in biocompatibility.

In the presence of GIC 750, the pH of cell-free medium was 7.2. No acidification was detected after cell culture, suggesting that the apatite-containing GIC had actually provided additional buffering capacity. Anion exchange between the GIC matrix and [$-OH^-$] in the aqueous biological environment is one event associated with acidification. A plausible mechanism for improved biocompatibility was that there were fewer phosphate ionic species available for release (Figure 4.28) when the glass was crystallised at 750°C (fluorapatite). Numerous papers have reported the

importance of F^-, Al^{3+} and pH on GIC biocompatibility but have not seriously considered the potential influence of phosphate [Brook *et al*, 1992, Sasananluckit *et al* 1993, Devlin *et al* 1998].

Both *in vitro* cell culture studies demonstrate that it is possible to modify the biocompatibility of GIC bone cement by altering the composition and controlled crystallisation of the constituent ionomer glass. While the *in vitro* data presented here is encouraging, further *in vivo* studies are required to confirm osteoconductivity. In addition, controlled clinical trials should be performed before these modified GICs are placed on the market. The clinical complications described in sections 1 and 2.4.4 should have been avoidable, as many of the features of a GIC that conspired to cause the deaths of patients were already known. Specifically, the moisture sensitivity of setting GICs, low pH, Al^{3+} release and its dose-dependent effect on nerve tissue had all been described in the literature. Together these features make GIC bone cements both technique sensitive and only biocompatible for specific clinical applications. While the modifications reported might extend the usefulness of GIC bone cements, ideally Al-free compositions need to be developed.

4.6 Summary

A more detailed discussion of this chapter is given in Chapter 6, however, to summarise, it was possible to produce all of the glasses in series A. Problems were encountered in the fabrication. Crucible selection was an important factor and sillimanite crucibles were found to be the least susceptible to

corrosion. All glasses formed cements but the setting time was found to be composition dependant. The greater the phosphate content the slower the set.

The glasses followed crystallisation sequences previously reported by Hill and Wood [1991a, 1991b and 1995]. Two glass-ceramics (A1 heated to 750°C and A1 heated to 950°C) were prepared. Glass A1(750) was found to contain only apatite and glass A1(950) contained the crystal phases apatite and mullite. It was possible to fabricate cements from these two crystallised glasses.

The ion release profiles of GICs A1 and A1(750) were investigated and it was found that partially crystallising the glass altered the ion release profiles. GIC A1(750) released more Ca and F ions than GIC A1. These ions are known to be beneficial in the biological environment. *In vitro* biocompatibility was investigated for all cements fabricated using the glasses in series A including the two devitrified glasses. The best cellular response was noted in the cements that had contained low phosphate or a phosphate containing crystal phase.

5. Results and Discussion –

Glass series B: $4.5SiO_2 \cdot 3Fe_2O_3 \cdot (1.53 - X)P_2O_5 \cdot 3CaO \cdot 2CaF_2$

Glass series C: $4.5SiO_2 \cdot 1.5Fe_2O_3 \cdot (1.53 - X)P_2O_5 \cdot 3CaO \cdot 2CaF_2$

As discussed in section 2.3.4, the presence of Al^{3+} has been related to poor biocompatibility and neurotoxicity in GICs. This chapter deals with the replacement of Al^{3+} with Fe^{3+} in ionomer glasses. Fe^{3+} was chosen because transition metals can be readily added to silicate glasses in large quantities McMillan [1962] and it is believed to not present a risk when used in biomedical devices [Nicholson 2002]. Fe is known to react with hydrogen peroxide but this reaction does not result in either mutagenicity or carcinogenicity and can be easily controlled by the body. Fe_2O_3-containing silicate glasses have also been investigated for biomedical applications, specifically for use as hyperthermal cancer seeds. A study by Kamitakahara *et al* [2000] investigated the effect of replacing Al_2O_3 with Fe_2O_3 in a calcium silicate glass. Although not a true ionomer glass composition, the Fe_2O_3–based glass did form a cement when mixed with PAA.

Sections 5.1 and 5.2 describe the fabrication of the glass series and the problems encountered in producing novel glasses. Section 5.3 covers the characterisation of the glasses, including the effect of composition on devitrification. The preparation of glass powders is discussed in section 5.4, and in section 5.5 the ability of these glass powders to form cements and their resulting properties is investigated. Finally in section 5.6 the *in vitro* biocompatibility is considered.

5.1 Glass Melting

In accordance with previous work (see section 4.1.2) the first Fe_2O_3-based glass melts were carried out in sillimanite crucibles. The resulting glasses were however found to corrode the base of the crucible (Figure 5.1). A similar pattern of corrosion was also found when mullite crucibles were used. It has been reported that alumino-silicate refractories, especially sillimanite are susceptible to attack from Fe_2O_3 containing melts [Paul 1982]. This was thought to explain the corrosion noted post melting [Vose 1980]. The different types of corrosion that may occur during glass melting are detailed in section 2.4.2. The type of corrosion believed to be responsible for the attack on both the mullite and sillimanite crucibles was either direct or congruent. This typically results in complete dissolution of all the refractory material into the glass as shown in Figure 5.1. Since the same corrosion was noted for all the glasses in the series, it was concluded that Fe_2O_3 was responsible.

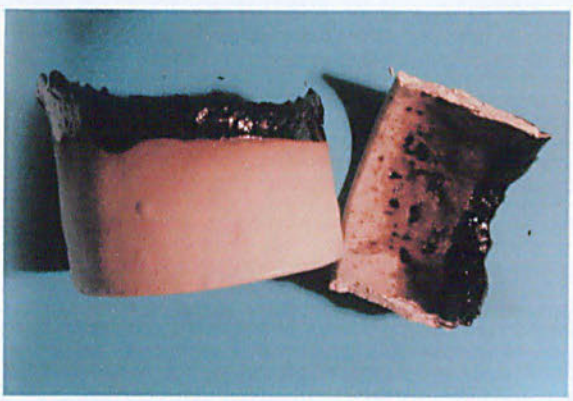

Figure 5.1: Corroded sillimanite crucible observed after melting glass B1 at 1450°C in an electric box-melting furnace for 1 h

Since alumino-silicate crucibles were completely dissolved by the glass, the use of pure Al_2O_3 and ZrO_2 crucibles was investigated. ZrO_2 crucibles routinely thermally shocked and could not be used successfully. Al_2O_3 did not thermally shock as readily as the ZrO_2 crucibles and exhibited less corrosion than alumino-silicates, as evidenced by post melt examination. They were employed for all P_2O_5-containing glasses in series B and C. Glasses B5 and C5 were P_2O_5 free and could be melted in Pt-12%Rh crucibles.

A second problem was encountered in the fabrication of glasses B2, B3, B4, C2, C3 and C4. The melts were found to foam and spill over the top of the crucible, Figure 5.2. This was initially attributed to a build up of gases beneath the lid but removal of the lid did not result in a reduction of foaming and additionally reintroduced drilling corrosion, noted in series A.

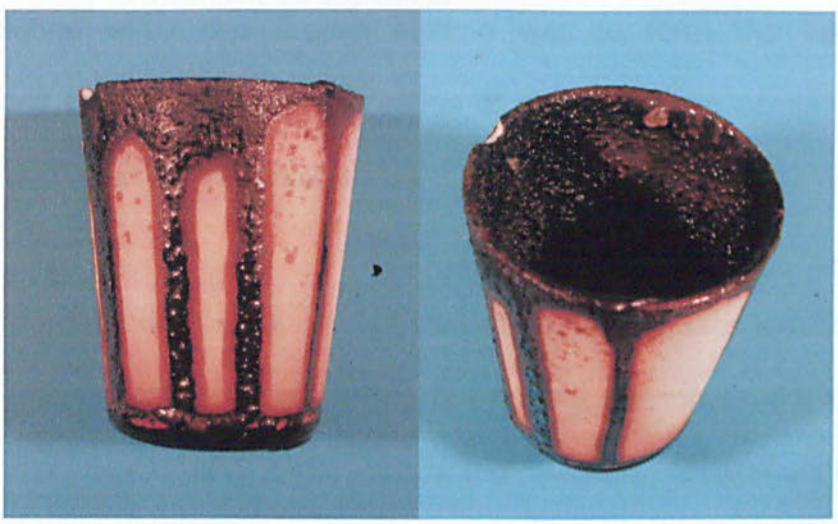

Figure 5.2: Foaming and subsequent glass spillage onto the external walls of an alumina crucible used to fabricate glass B3 (using standard melt conditions see section 3.1)

The foaming was attributed to similar reactions present during the manufacture of steel. In steel fabrication, foaming in the molten alloy is induced by the introduction of carbonates creating a H^+/CO_2 atmosphere in the reaction vessel. This atmosphere is essential in the chemical reactions required to reduce Fe oxide [Kuleva *et al* 1992, Li and Hong 1997 and Tiernan *et al* 2001]. Applying this theory to the problems encountered in glass melting, may in part explain the foaming. To make the glasses B2 – B4 and C2 – C4, $CaHPO_4$ and $CaCO_3$ are used as part of the batch. The decomposition of these raw materials results in the releases of H_2O and CO_2 and it is postulated that this causes foaming in the Fe_2O_3 containing glasses.

Preheating $CaCO_3$ to remove the CO_2 component prior to melting partially decreased the amount of foaming but gaseous products were still formed as a result of the calcination of other batch materials (e.g. $CaHPO_4$). The only viable solution within the project lifetime was to form the intermediate compositions by using appropriate ratios of glass frit from compositions B1 and B5 and C1 and C5, respectively.

On viewing post melt, it was evident that all Al_2O_3 crucibles exhibited some corrosion (insufficient to cause drilling but ridging was observed) during the fabrication of Fe_2O_3 and P_2O_5 containing glasses. Subsequently, Al_2O_3 contamination was found during analysis of these glasses (see section 5.3.1). Since no other type of crucible was successful, melting was performed in Al_2O_3 crucibles but melt times were kept to a minimum to decrease contamination.

5.2 Glass Formation

All Fe_2O_3 containing glasses were found to partially devitrify (see section 5.3.3) even when quenched into water. The use of iced brine instead of water did not significantly retard devitrification. Figure 5.3 shows a typical XRD trace for Glass B1 fabricated using both quench methods. Each contained the same crystal phases (magnetite - Fe_3O_4 and apatite - $Ca_5(PO_4)_3F$) and the amorphous humps were qualitatively similar in intensity.

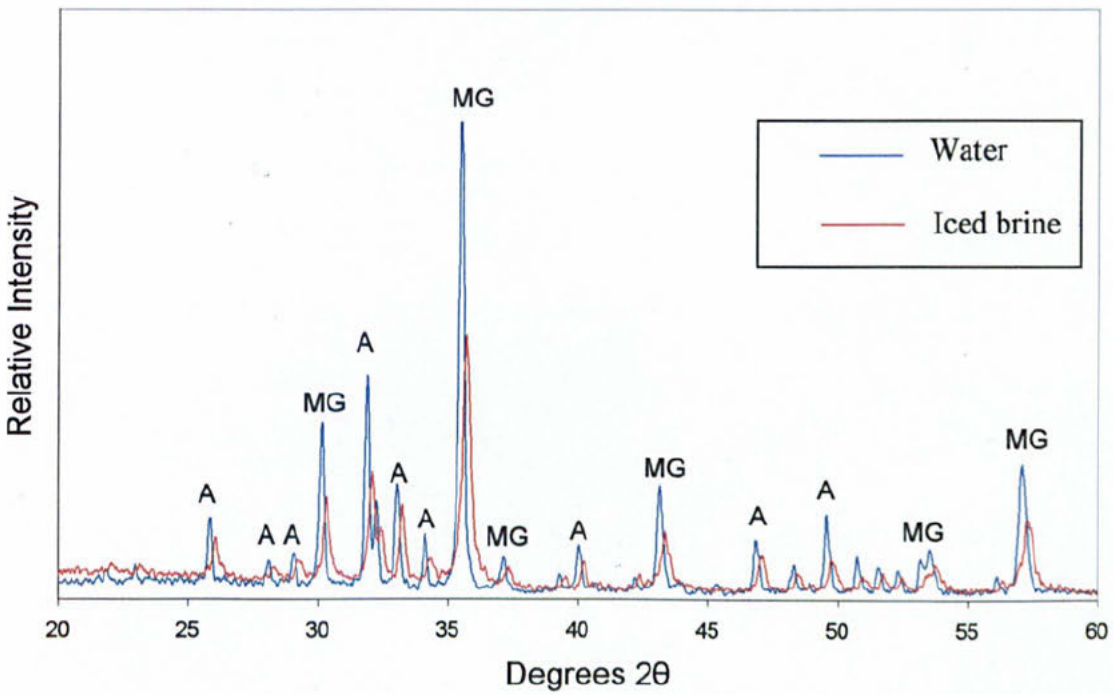

Figure 5.3: XRD trace showing glass B1 quenched using water (blue trace) and iced brine (red trace). Apatite ($Ca_5(PO_4)_3F$) and Magnetite (Fe_3O_4) are labelled A and MG respectively

5.3 Glass Characterisation

5.3.1 X-ray Fluorescence

The compositions of selected glasses (B1, B2, B3, B5 and C2; see Tables 3.6 and 3.7) were determined using X-ray fluorescence (XRF). Glasses B1 and B5 were analysed since they formed the basis of all the intermediate composition in series B. Glasses B2, B3 and C2 were investigated because of their cement forming ability (see section 5.5). XRF (Table 5.1) revealed that all glasses melted in Al_2O_3 crucibles contained Al_2O_3 contamination. Glasses melted in Pt-12%Rh crucibles (e.g. B5) had no Al_2O_3 contamination.

Table 5.1: Molar percent of glasses B1–3, 5 and C2 compared to the theoretical molar compositions.

Oxide	B1		B2		B3		B5		C2	
	XRF	*Batch*	*XRF*	*Batch*	*XRF*	*Batch*	*XRF*	*Batch*	*XRF*	*Batch*
SiO_2	28.6	31.9	28.7	32.8	29.8	33.8	36.6	35.8	31.6	36.8
Al_2O_3	7.6	0	10.7	0	11.7	0	0.4	0	11.6	0
Fe_2O_3	19.5	21.2	19.2	21.8	19.8	22.4	22.3	23.8	10.8	12.2
P_2O_5	9.9	10.9	7.0	8.4	4.4	5.8	0.1	0	7.7	9.4
CaO	30.5	21.8	30.5	22.4	31.0	23.0	34.2	24.4	34.2	25.1
CaF_2	3.9	14.2	4.0	14.6	3.3	15.0	6.5	15.9	4.1	16.4

In Table 5.1, the measured CaF_2 concentrations were lower (~10 – 12 mol%) than their batched counterparts. Similarly, the measured CaO concentration was higher (10 – 12 mol%) than anticipated. This was attributed to excessive F losses in glass series B and C, particularly when compared with series A. The loss of F was attributed to the absence of Al_2O_3. This is believed to help

retain F in GIC glass compositions. Incorporating a basic oxide into the glass network ensures that at least one non-bridging O per Si atom/ion exists, leaving sufficient Al^{3+} ions free to bind with F^- [Clifford *et al* 2001a].

Since glasses B2, B3 and C2 were fabricated using ratios of glasses B1 and B5 combined or C1 and C5 combined, the contamination and loss to atmosphere due to evaporation was greater. More F^- was lost through the secondary melt process and additional Al_2O_3 was introduced from the melt vessel.

It was concluded that the post-melt glass compositions were not the same as those batched. Moreover, it was not possible to produce on a laboratory scale the glasses without F loss and Al_2O_3 contamination. As discussed in section 5.1, alternative melt routes (i.e. use of ZrO_2 crucibles) were attempted but were not successful. The amount of Al_2O_3 was however reduced in comparison to glass series A, and these novel glasses were therefore investigated further.

5.3.2 Differential Thermal Analysis

DTA was used to assess the glass transition and crystallisation temperatures of the experimental glass series B and C (Figures 5.4 and 5.5 respectively). Due to the high levels of crystallinity found in these glasses (see section 5.3.3) any measurements made using DTA would only reflect thermal events in the residual glass component. It was not possible to determine the T_g of the

residual glass phase in glasses B1 – B4 and C1 – C5. This was probably due to the relatively small quantity of residual glass present.

B1 displayed no anomalies in its DTA trace and was believed to be essentially crystalline on casting. The remaining glasses in series B (Figure 5.4) exhibited exothermic peaks (T_x) that decreased in temperature with decreasing P_2O_5 concentration, from 905°C (B2) to 746°C (B5). In addition, glass B5 (no P_2O_5) exhibited a second broad exotherm immediately preceded in temperature by an endotherm (635°C). This anomaly was likely therefore to be the T_g for the residual glass in this composition. It was proposed that decreasing the P_2O_5 concentration increased the volume fraction of residual glass because apatite could not crystallise. A greater volume fraction of residual glass would increase the likelihood of the presence of an annealing dip associated with T_g in the DTA trace.

In contrast, glass series C exhibited a different trend compared to series B (Figure 5.5). Glass C1 had a broad, possibly multiple, exotherm at around 938°C and similar shaped exotherms were observed between 905 – 914°C in glasses C2 – C5. In addition, glasses C2 – C5 all had endotherms at approximately the same temperature (747 – 760°C), which in the case of glass C5 was preceded by an exotherm at 736°C. Such deep endotherms were unlikely to have arisen from a structural rearrangement of the glass at T_g, however the small endotherm at ~600°C was probably due to T_g. Deep endotherms may have occurred due to the melting of a crystalline phase or phase transitions between two polymorphs [McMillan 1979].

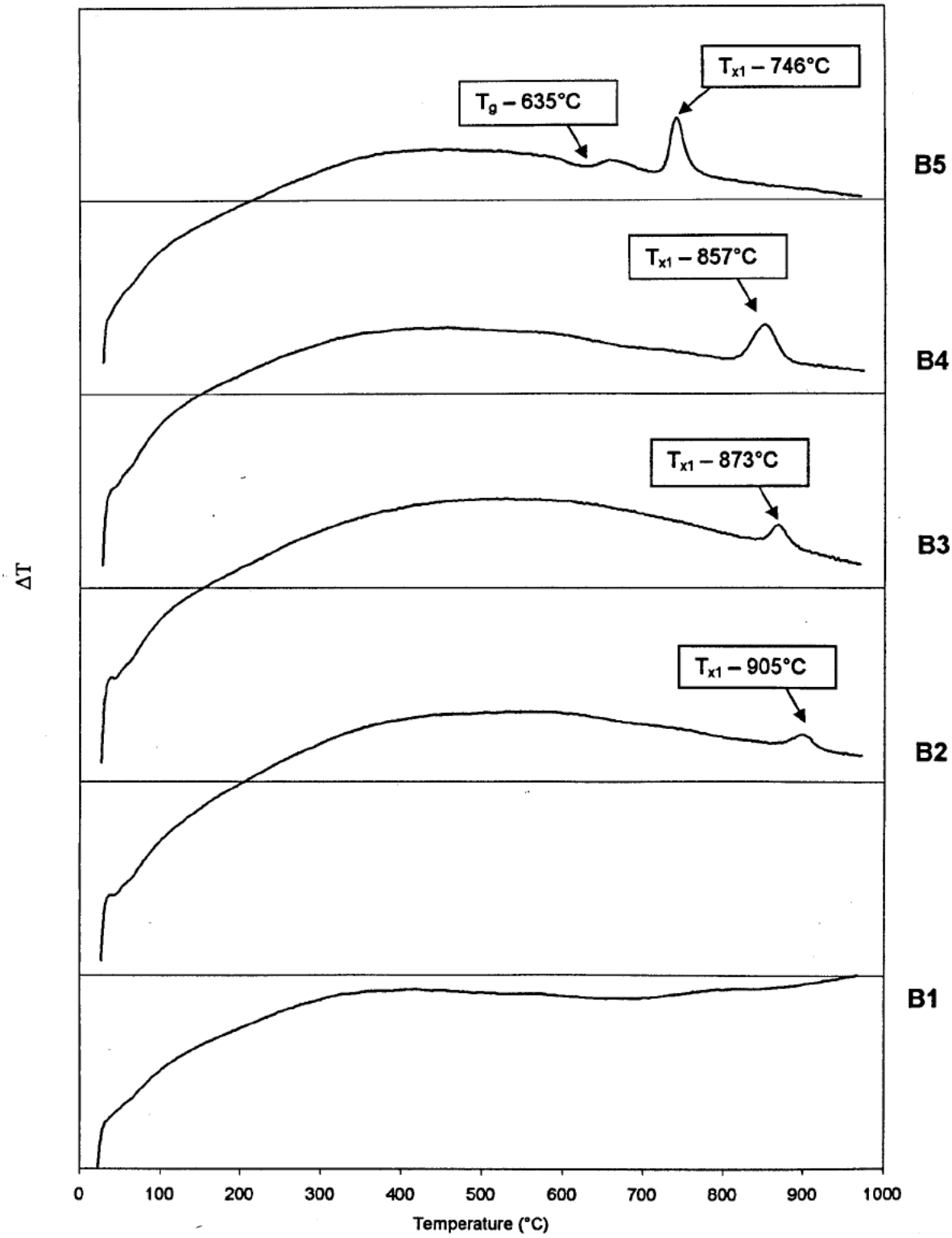

Figure 5.4: DTA traces of glass series B, showing the glass transition temperature (T_g) and crystallisation exotherms (T_{x1}).

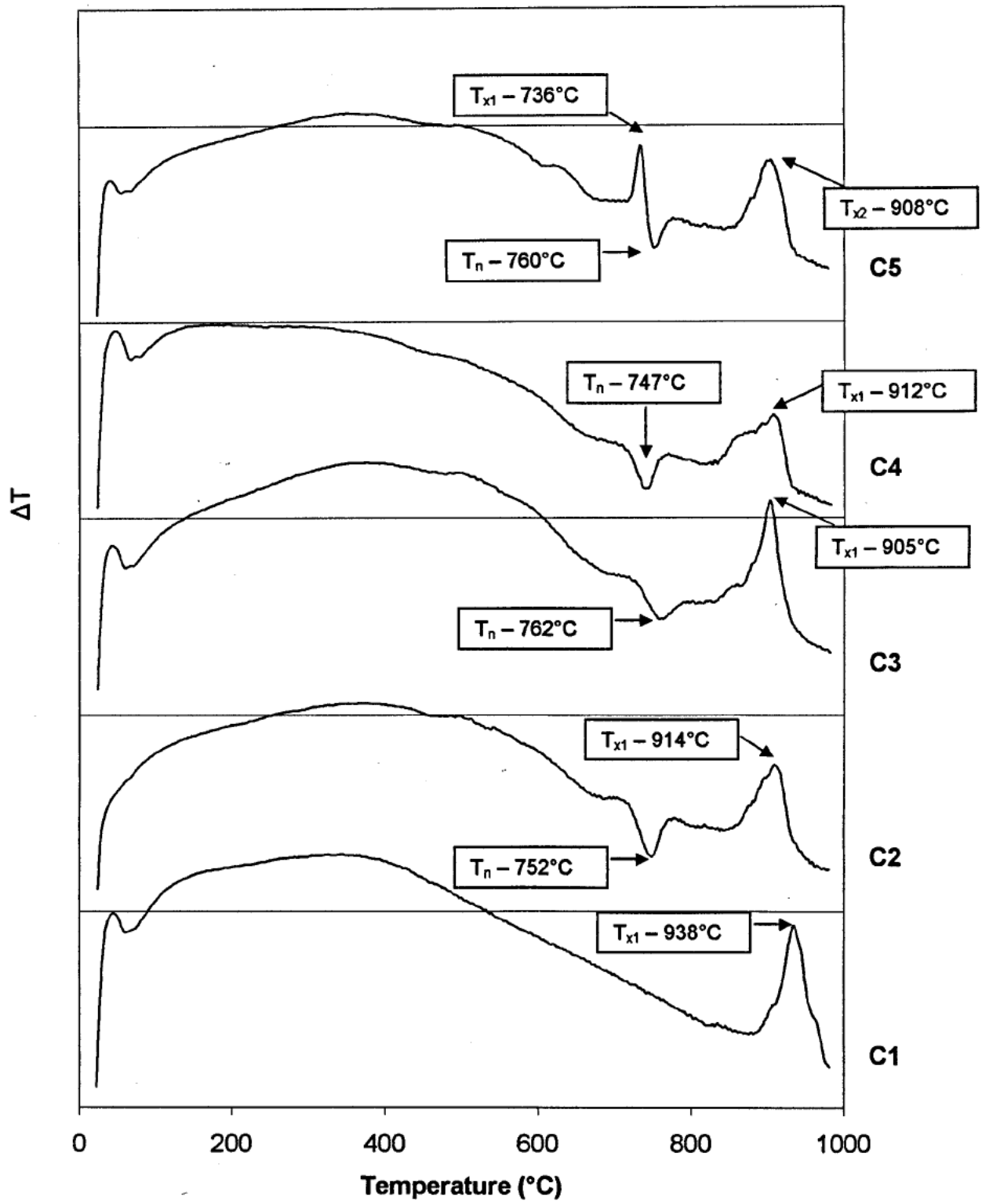

Figure 5.5: DTA traces of glass series C, showing the crystallisation exotherms T_{x1} and T_{x2} and endotherms T_n.

5.3.3 X-ray Diffraction of as Quenched Compositions

Figure 5.6 shows the XRD traces from as-quenched glasses in series B. The major crystal phase in all compositions was magnetite (Fe_3O_4), JCPDS # 19 – 629. In the phosphate containing glasses B1 – B4 an additional crystal phase was observed with peaks that corresponded to those expected for apatite ($Ca_5(PO_4)_3F$), JCPDS # 15-876. Peaks attributed to hematite (Fe_2O_3), JCPDS # 33 – 664 were also found in the XRD traces for all glasses. However, it was believed that this formed on the surface post-quenching and was caused by the reaction of the glass surface with the surrounding atmosphere.

Glass series C followed a similar crystallisation pattern, Figure 5.7, with magnetite as the major phase present in all glasses and the minor apatite phase present in the phosphate containing glasses (C1 – 3). However, the relative intensity of the amorphous hump was greater in series C than B, qualitatively suggesting that the volume fraction of glassy phase was greater in the as-cast C series. In addition the presence of an annealing dip associated with T_g also suggests a higher degree of residual glass. It was not possible to determine the exact degree of crystallinity in either glass series since a non-crystalline parent glass could not be prepared. However, from a simple visual inspection of the intensities of the crystal peaks, the overall degree of crystallinity would appear to decrease with P_2O_5 concentration.

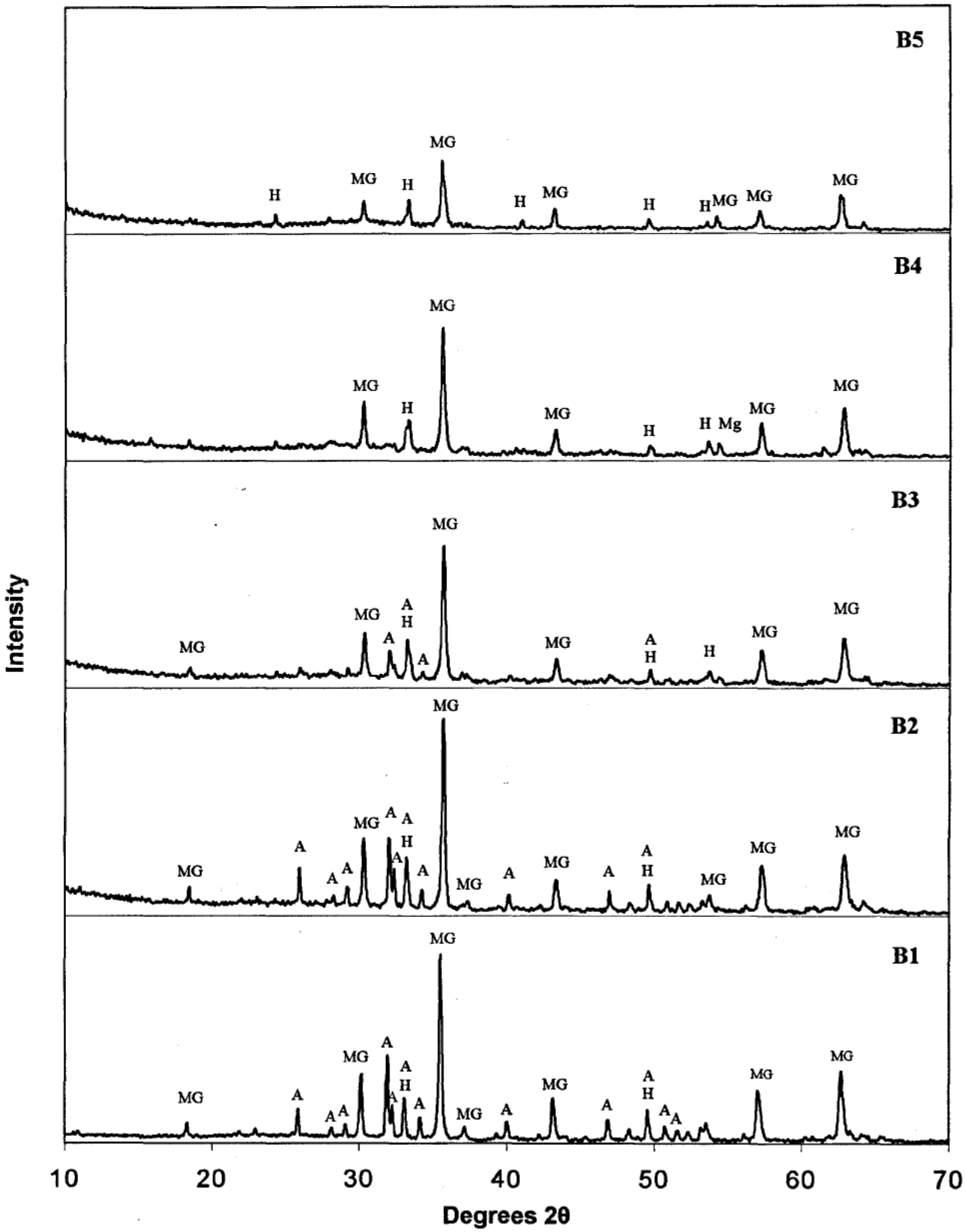

Figure 5.6: XRD spectra showing the crystal phases present in the as-cast glasses in series B melted using standard melt conditions. MG – Magnetite A – Apatite H – Hematite

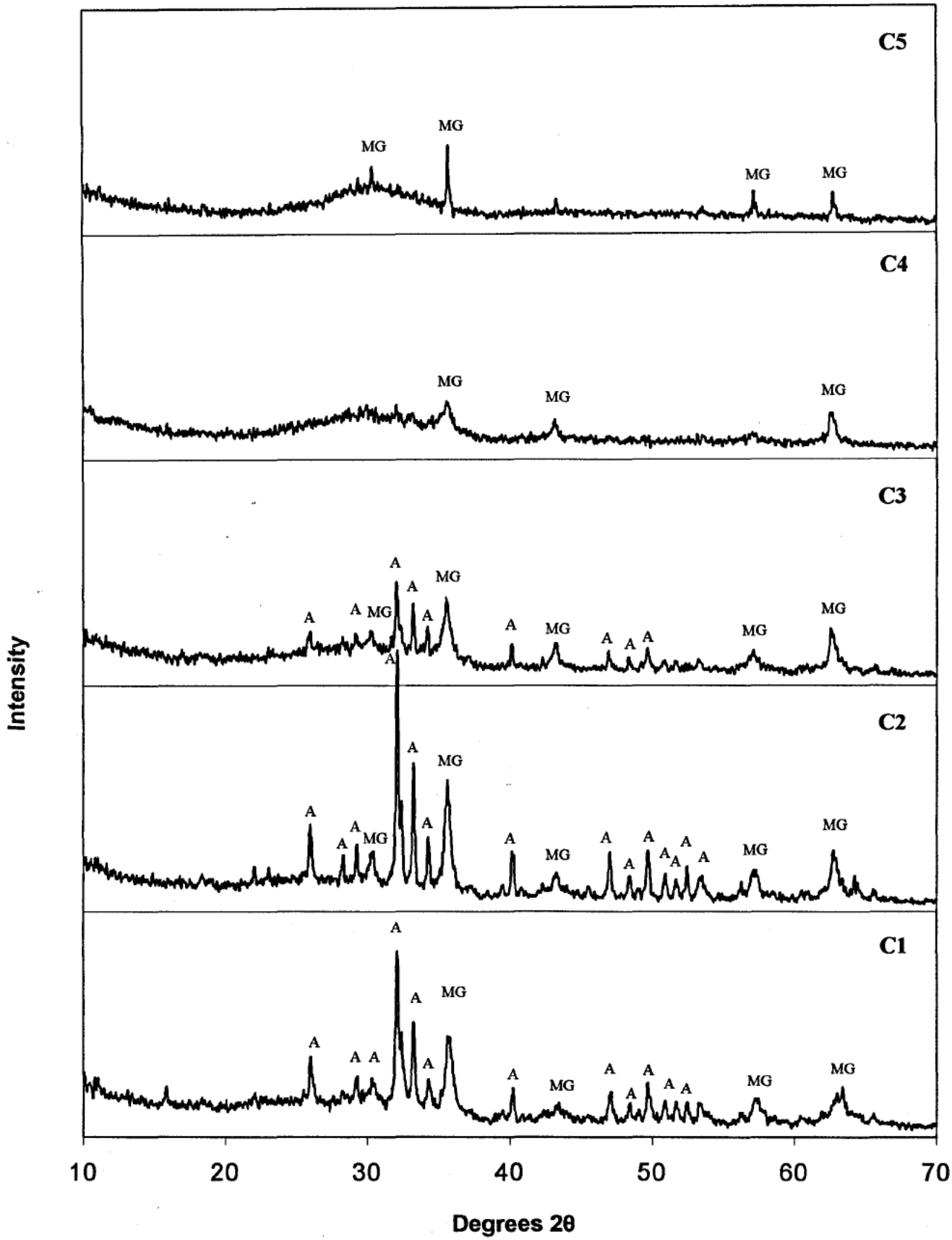

Figure 5.7: XRD spectra showing the crystal phases present in the as-cast glasses in series C melted using standard melt conditions. MG – Magnetite A – Apatite

5.3.4 Microstructural Analysis

Scanning Electron Microscopy

To determine the distribution of the crystalline phases, as cast pieces of each of the glasses were examined using SEM. All the glasses were observed using back-scattered imaging. The micrographs obtained from glass series B and C are shown in Figures 5.8 – 5.12 and Figures 5.13 – 5.17, respectively.

All the glasses in series B contained an inhomogeneous distribution of crystals. In B1 (Figure 5.8a), the microstructure was composed of regions of large crystals surrounding finer crystals. Higher magnifications (Figure 5.8b) showed that a network of dendrites was present throughout the material. In addition, an inhomogeneous distribution of blocky crystals was also noted. XRD indicated the presence of both apatite and magnetite. Since the micrographs were taken in BEI mode, it was concluded that the light dendrites were magnetite and the blocky phase was apatite. Magnetite (Fe - 7.87 g/cm^3) has a higher density than apatite (Ca – 1.53 g/cm^3) and would therefore appear lighter in BEI images. The darker regions between the two crystal types were believed to be residual glass.

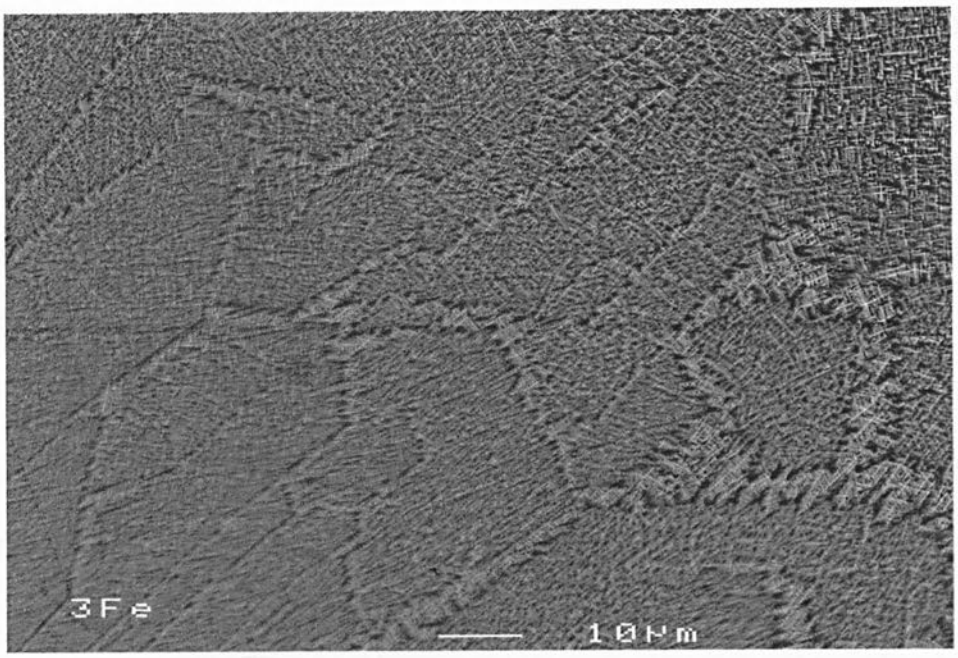

a

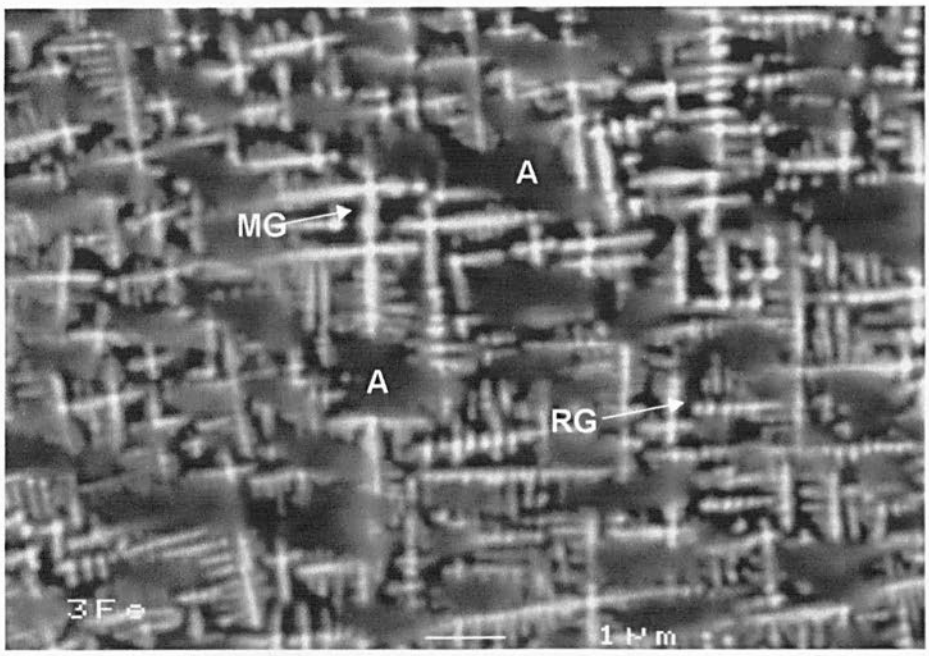

b

Figure 5.8: BEI SEM micrographs of glass B1 **a**. Low magnification image showing larger magnetite dendrites surrounding regions of finer magnetite dendrites **b**. Higher magnification revealing the presence of magnetite dendrites (MG), apatite crystals (A) and residual glass

A similar microstructure to glass B1 was also noted in B2 (Figure 5.9a), i.e. magnetite dendrites interspersed with apatite crystals. In certain areas of the glass (Figure 5.9b) apatite crystals were found to have formed channels between the magnetite dendrite arms. In glasses B3 (Figure 5.10 a and b) and B4 (Figure 5.13 a and b), the apatite crystals were no longer visible using SEM. The magnetite dendrites were however more pronounced and larger. In contrast, Glass B5 (Figure 5.12 a and b) exhibited smaller magnetite dendrites, along with clusters of whisker-like precipitates. The contrast of the latter in BEI mode was still, however, consistent with the presence of magnetite.

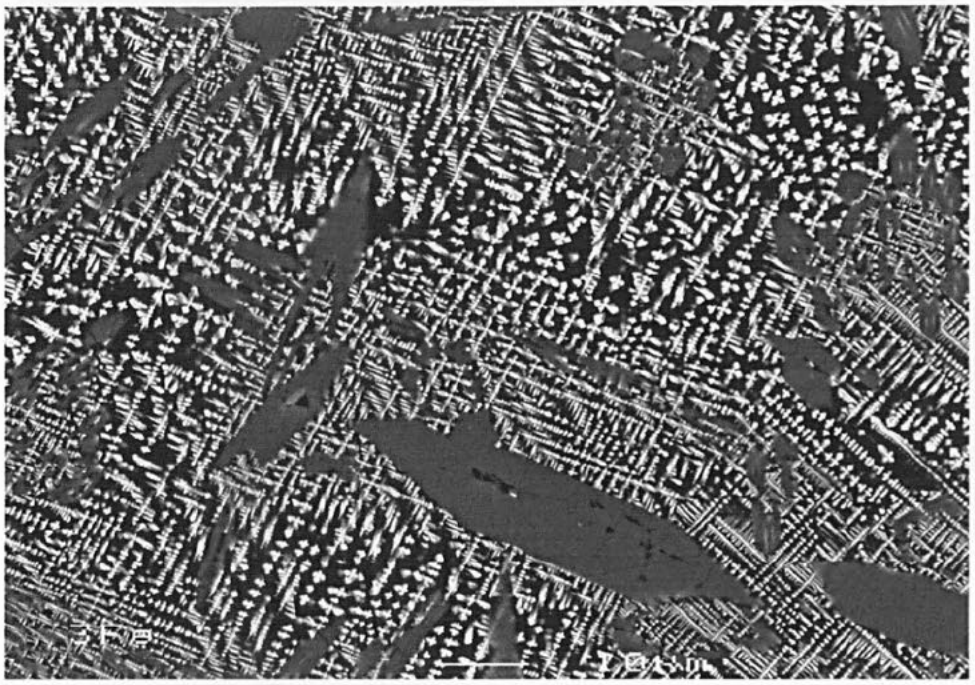

a

b

Figure 5.9: BEI SEM micrographs of Glass B2 **a.** Low magnification image showing non-homogenous structure **b.** higher magnification revealing the presence of magnetite dendrites and apatite crystals

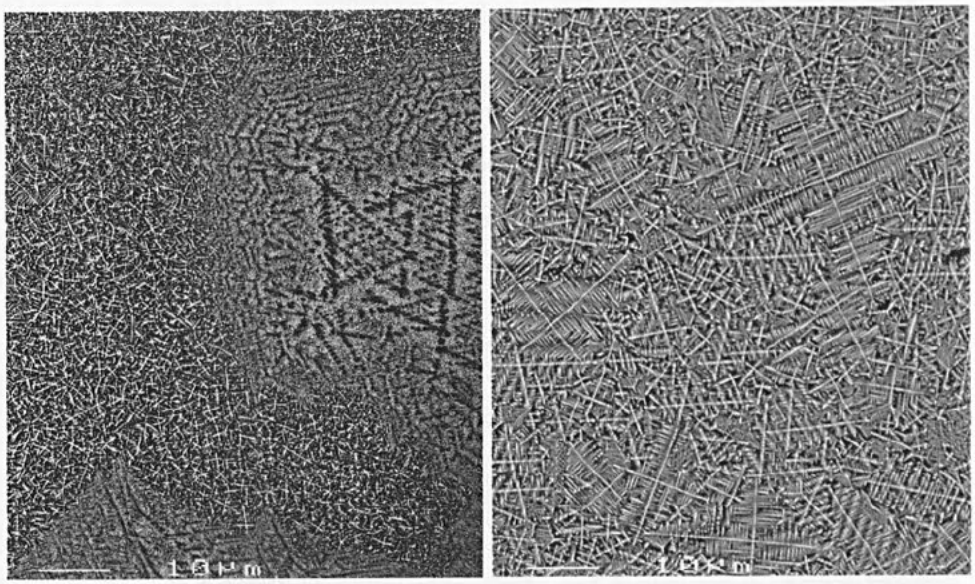

a b

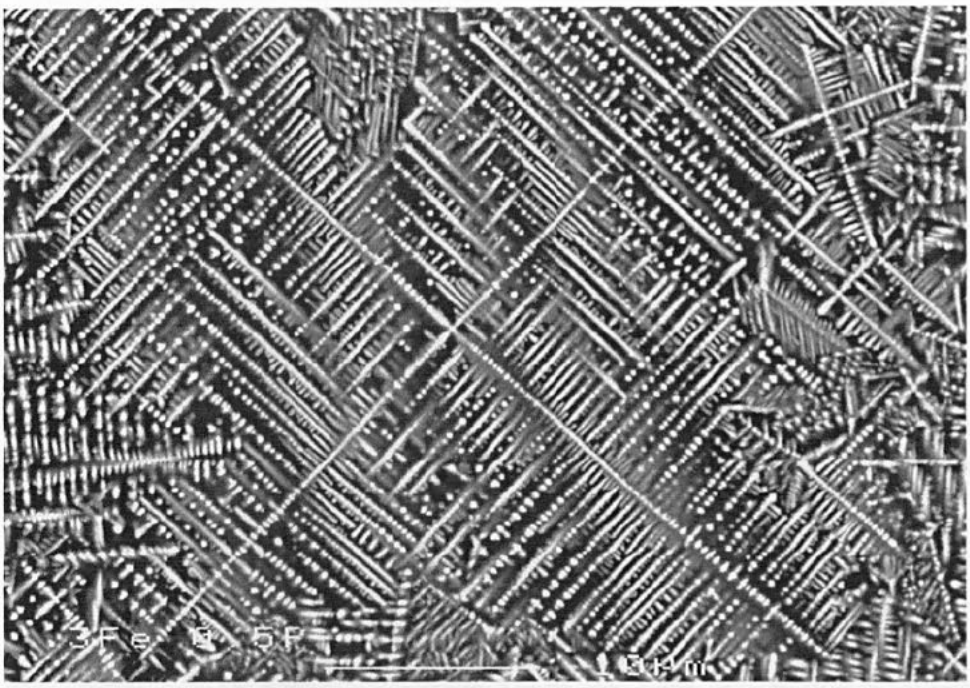

c

Figure 5.10: BEI SEM micrographs of Glass B3 **a** and **b**. Low magnification images of different regions showing the glass to be non homogeneous **c**. Higher magnification revealing the presence of magnetite dendrites

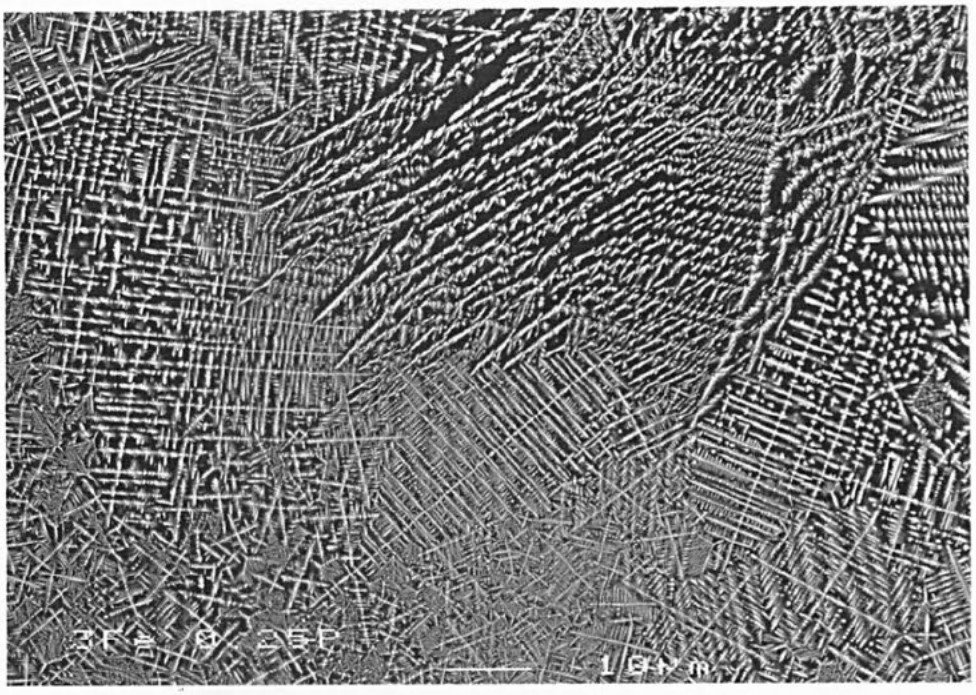

a

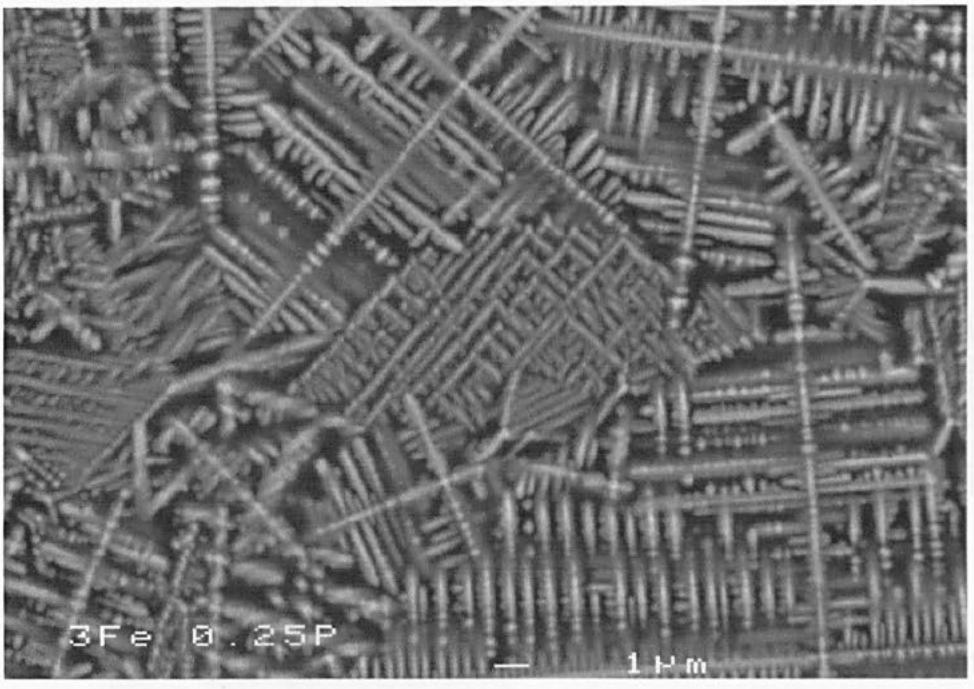

b

Figure 5.11: BEI SEM micrographs of Glass B4 **a.** Low magnification image showing non-homogenous structure **b.** higher magnification revealing the presence of magnetite dendrites

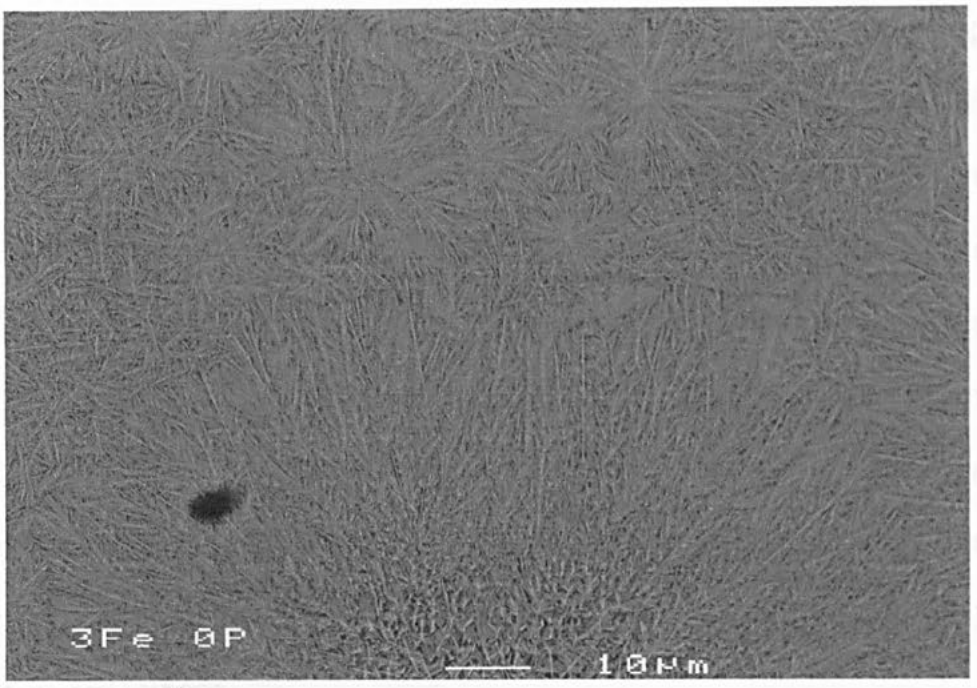

a

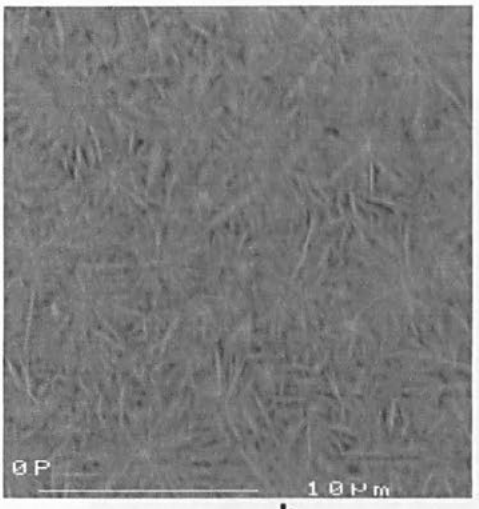

b

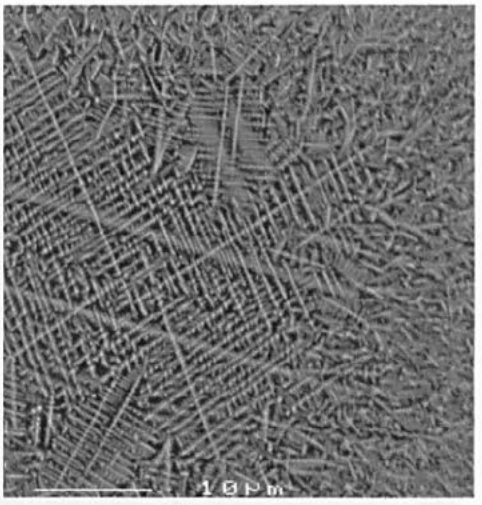

c

Figure 5.12: BEI SEM micrographs of Glass B5 **a.** Low magnification image showing non-homogenous structure **b.** higher magnification revealing the presence of magnetite dendrites

In glass series C only C1 – C3 had crystalline inclusions visible using BEI mode in SEM (Figures 5.15 – 5.17). A similar microstructure to glass series B was noted with a non-homogenous distribution of dendrites present throughout. However, the blocky crystal phase identified as apatite in some compositions of glass series B was not observed. Apatite and magnetite can both adopt a dendritic morphology and SEM was inconclusive in determining the chemical composition of the dendrites. Therefore, TEM was performed to further examine the microstructure of these glasses along with glass C4 and C5 which did not show any evidence of crystal phases in SEM but exhibited peaks in XRD traces.

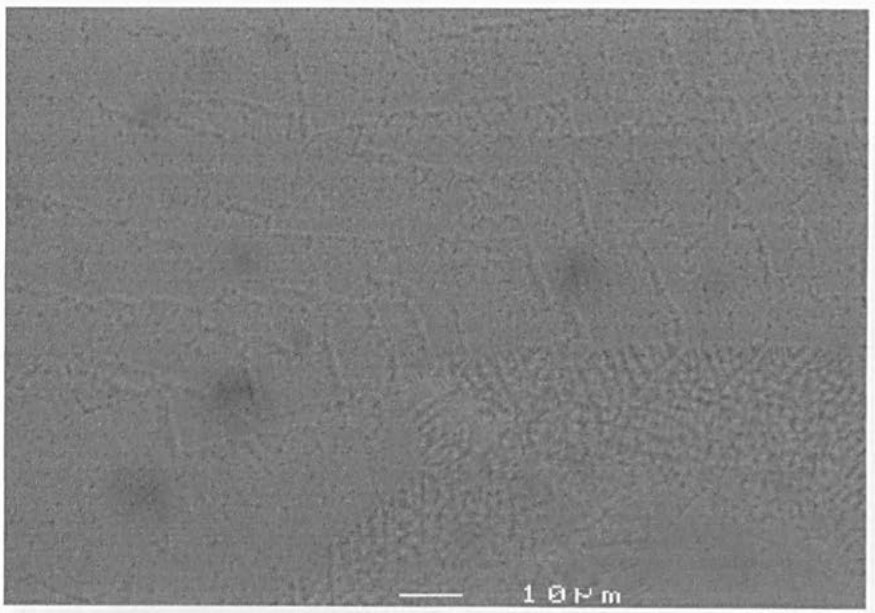

Figure 5.13: BEI SEM micrograph of Glass C1 showing the crystal structure to be non-homogenous with fine nano-dendrites (whiskers) present

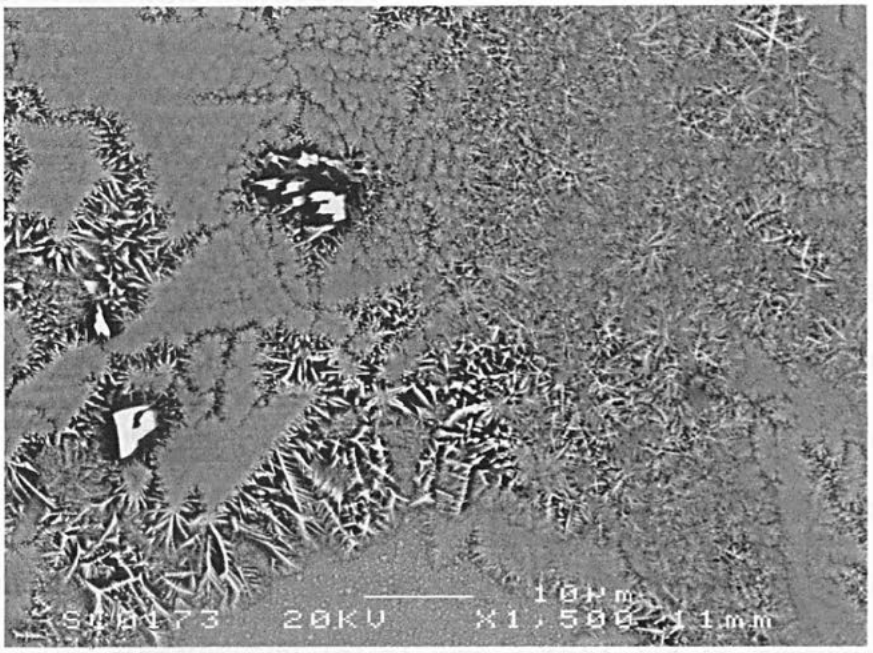

Figure 5.14: BEI SEM micrograph of Glass C2 showing the microstructure to be non-homogenous with fine nano-dendrites or clusters of whiskers and coarser dendrites

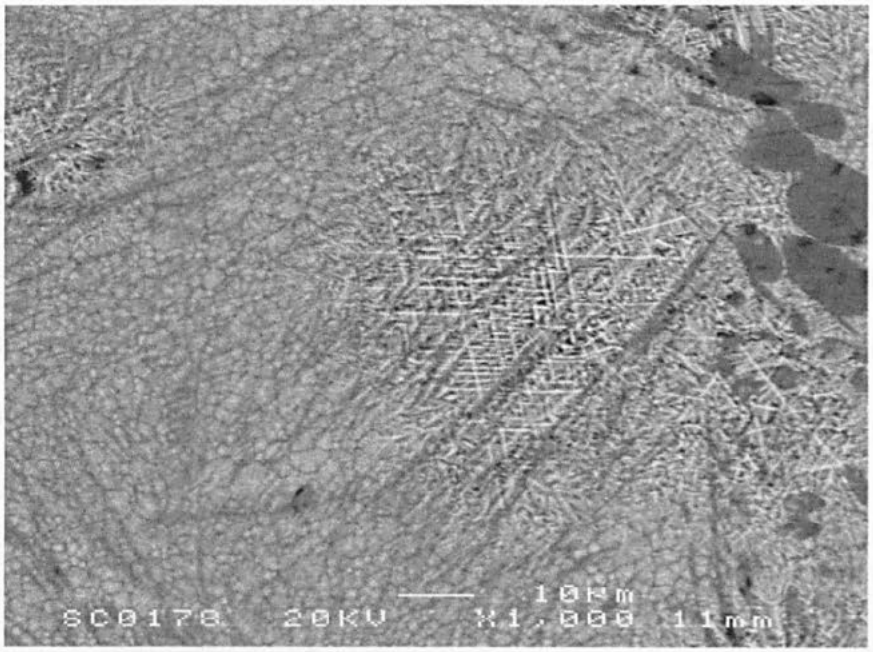

Figure 5.15: BEI SEM micrograph of Glass C3 showing a microstructure composed of both fine nano-dendrites or florets and coarser dendrites

Transmission Electron Microscopy

Transmission electron microscopy (TEM) was used to investigate further the microstructure of all the glasses in series B and selected glasses in series C. BF TEM micrographs of glasses B1 (Figure 5.16) and B2 (Figure 5.17) revealed similar microstructures. Each contained dendrites interspersed with a blocky crystal phase. However glass B2 appeared to have more residual glass than B1. These microstructures were consistent with those observed using SEM. XRD analysis showed that magnetite and apatite were present. Since apatite can have both a blocky or dendritic microstructure, energy dispersive x-ray spectroscopy (EDS) was carried out to determine the composition of the crystals.

EDS analysis from the residual glass present in glass B1 showed Al in addition to O, Fe, Si, P and Ca (Figure 5.17 a), confirming that the Al_2O_3 crucible partially dissolved during glass melting. The blocky phase was predominately composed of Ca, P O and F (Figure 5.17 b), suggesting that these crystals were apatite. In contrast, EDS of the dendrites showed them to contain Fe and O (Figure 5.17 c), consistent with magnetite. EDS analysis of glass B2 (Figure 5.18) revealed identical spectra in dendritic regions (Fe and O) and the blocky phase (Ca, P, O, F) compared with those in B1. The residual glass was also found to contain Al ions

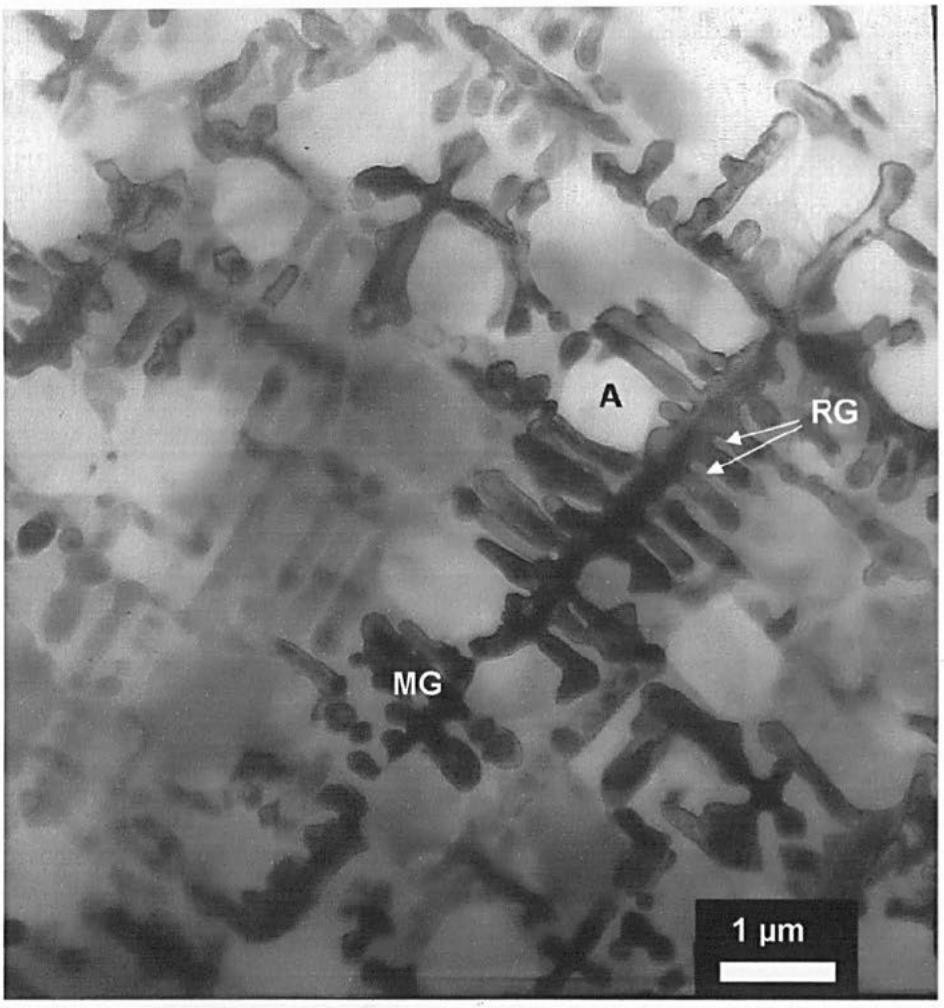

Figure 5.16: BF TEM micrograph showing the morphology of glass B1. Magnetite dendrites (MG) interspersed with apatite crystals (A) and regions of residual glass (RG).

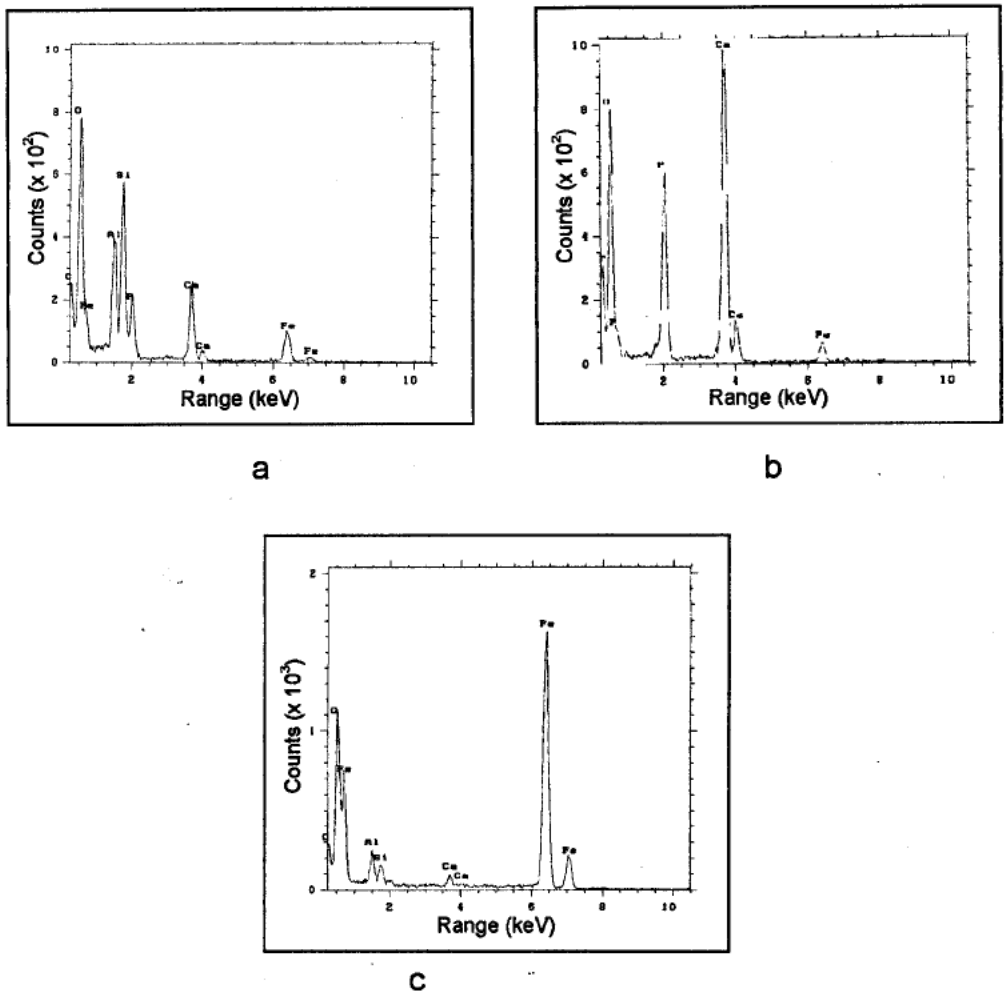

Figure 5.17: Energy dispersive spectra from different regions of glass B1 shown on Figure 5.16. **a.** residual glass (RG) showing predominately Si, Al and O present with small traces of Fe Ca and P **b.** The blocky crystals of apatite (A) showing the presence of Ca, P,O and F and **c.** Magnetite (MG) dendrites showing an abundance of Fe and O

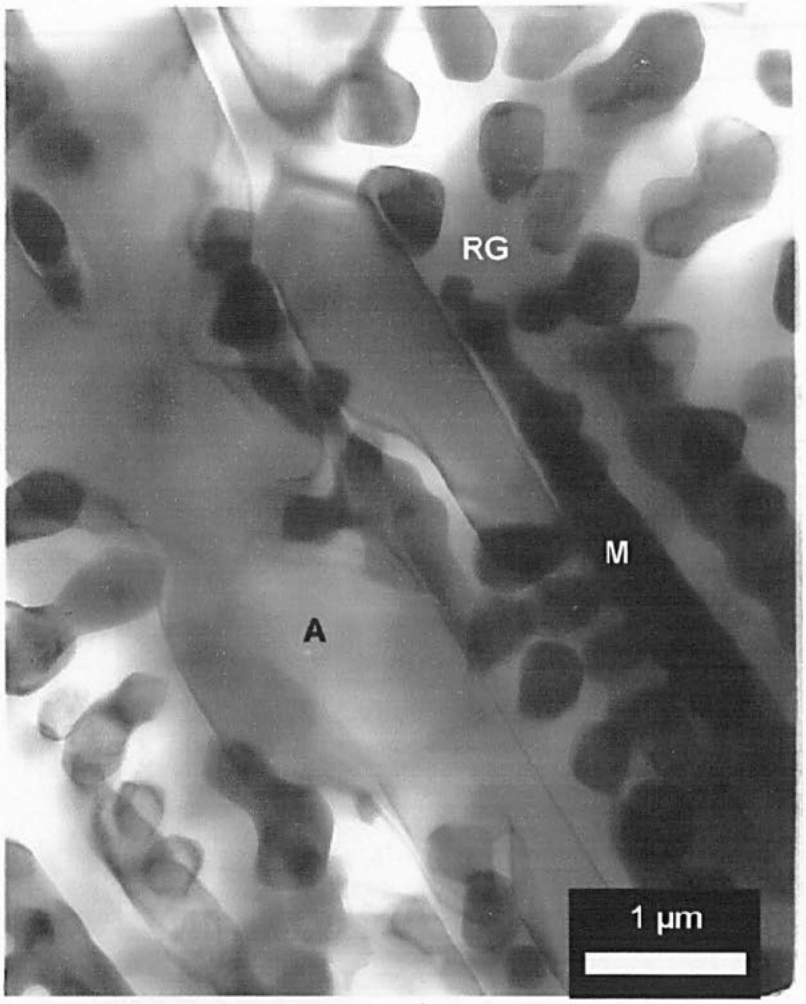

Figure 5.18: TEM micrograph showing the microstructure of glass B2 with magnetite dendrites (MG), apatite crystals (A) and residual glass (RG)

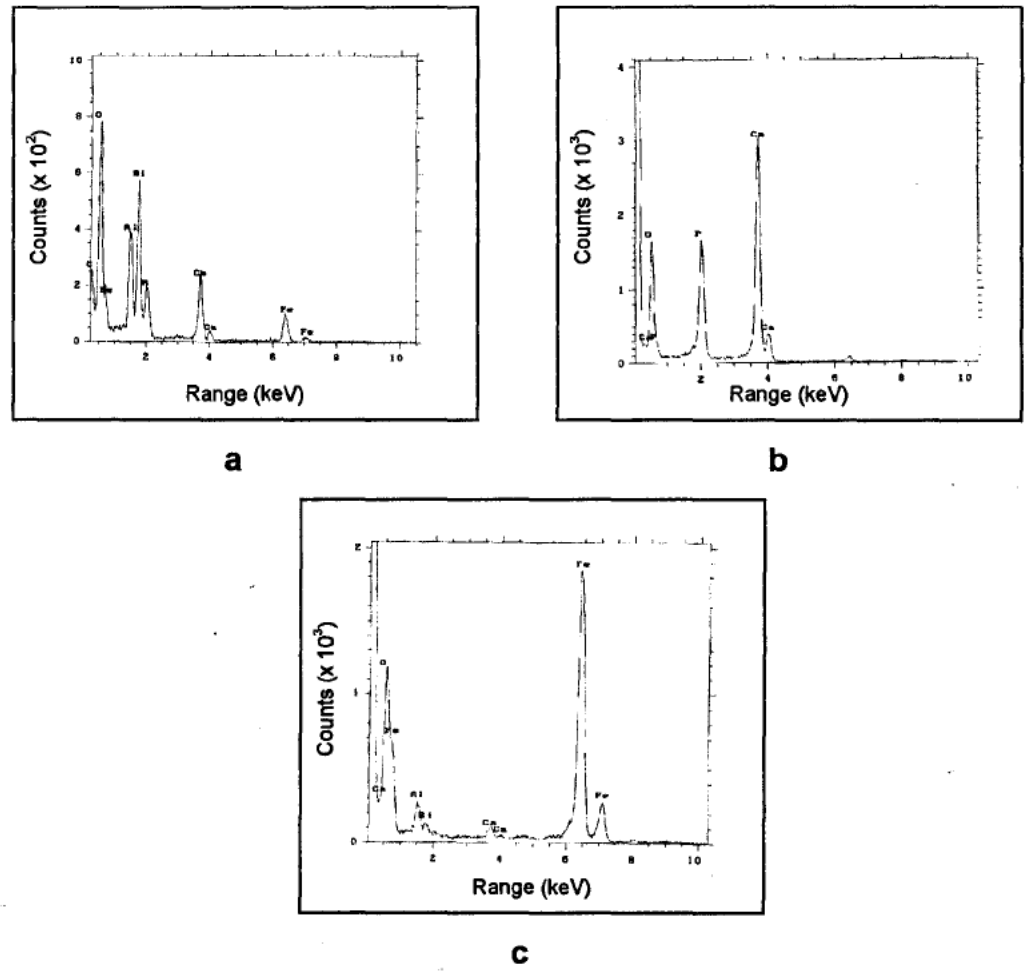

Figure 5.19: Energy dispersive spectra from different regions of glass B2 shown on Figure 5.18. **a.** residual glass (RG) showing predominately Si, Al and O present with small traces of Fe Ca and P **b.** The blocky crystals of apatite (A) showing the presence of Ca, P,O and F and **c.** Magnetite (MG) dendrites showing an abundance of Fe and O

Glass B3 was found to have a different microstructure (Figurer 5.20) from B2 and B1. Dendritic magnetite crystals were still present as the major phase but the blocky apatite was replaced with smaller spherical crystals. It was not possible to carry out EDS analysis on these small crystals because the micro-analysis probe was too large and encompassed residual glass as well as the crystal. A general EDS spectra was obtained for this glass and is given in Figure 5.21. This showed the presence of Fe, Si, Ca, P, F,O and Al confirming XRF data.

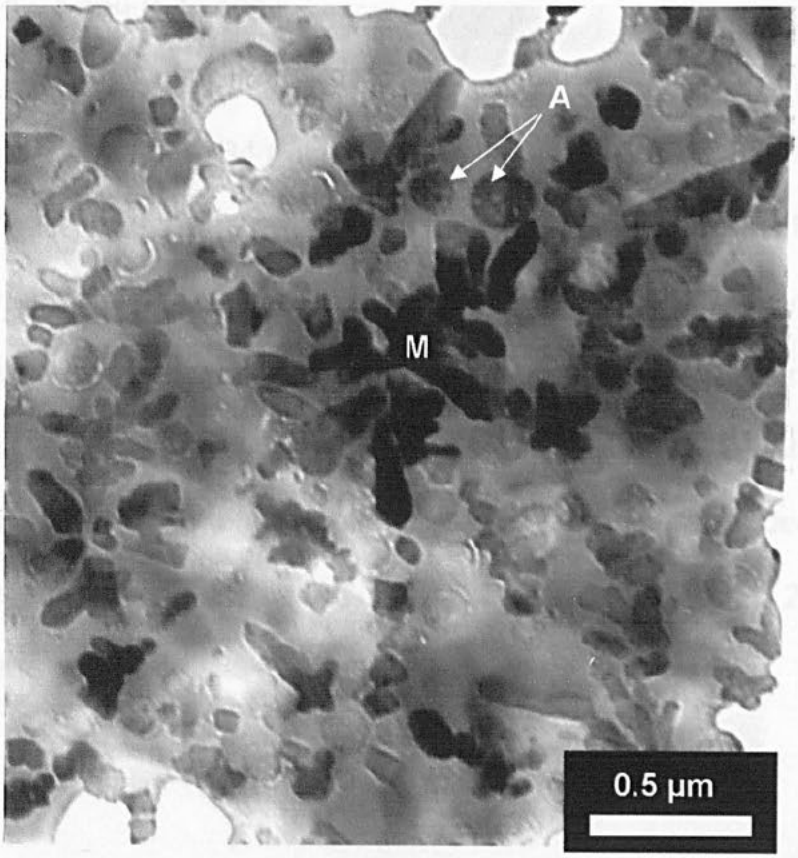

Figure 5.20: BF TEM micrograph of glass B3 showing florets of magnetite (MG) and spherical apatite crystals (A) in a residual glass matrix.

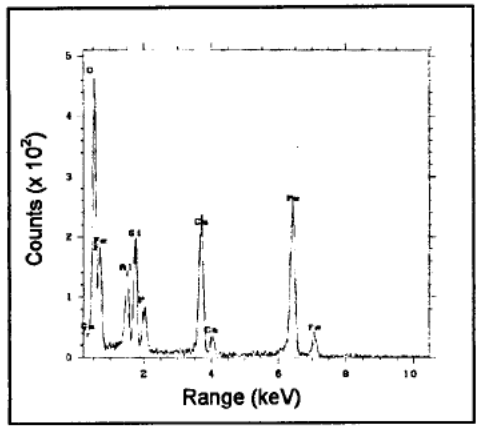

Figure 5.21: Energy dispersive spectrum from glass B3 showing the presence of Si, Al, Fe Ca and P, O and F

BF TEM images of glass B4 (Figure 5.22) showed only dendritic crystals were present. These were finer than the dendrites observed in glasses B1 – B3 and owing to their small size, it was not possible to obtain EDS analysis uniquely from these crystals. However the morphology of these dendrites was similar to those noted in the other glasses in this series and the XRD data confirmed the presence of magnetite in this glass. It was therefore concluded that these dendrites were also magnetite. General EDS traces (Figure 5.23) revealed that the glass contained Ca, Fe, Si, P, F, O and Al.

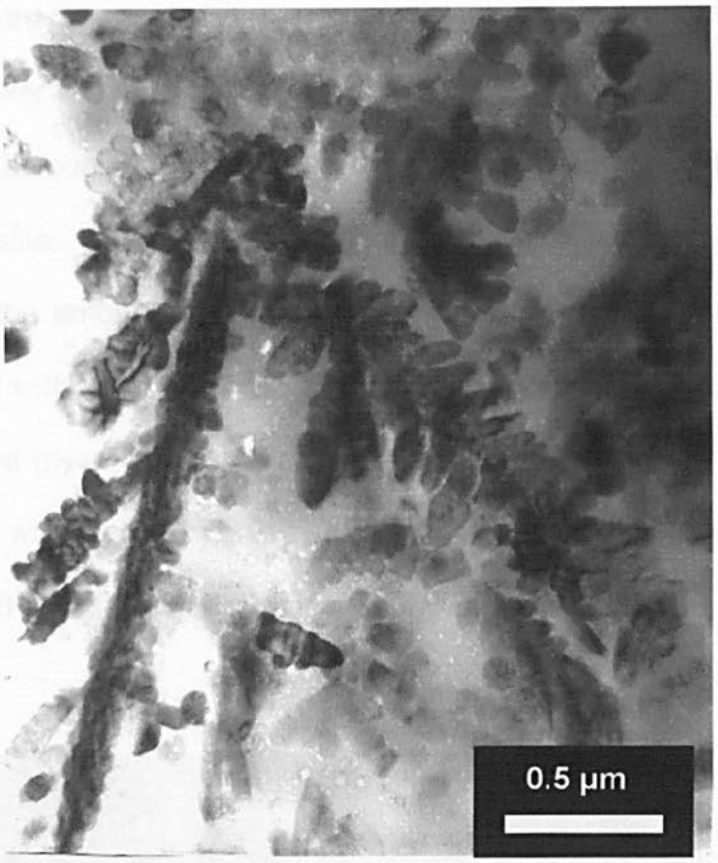

Figure 5.22: BF TEM micrograph of glass B4 showing the presence of magnetite dendrites in a residual glass matrix

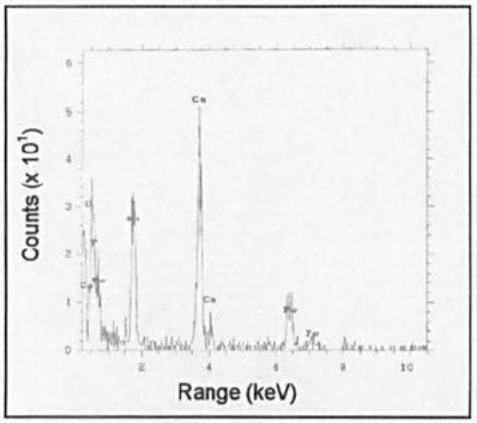

Figure 5.23: Energy dispersive spectrum from glass B4 showing the presence of Si, Al, Fe Ca and P, O and F

The microstructure of glass B5 (Figure 5.24) exhibited nano-dendrites or clusters of whisker-like crystals. The crystals were examined using EDS (Figure 5.25) that confirmed the dendrites contained Fe and O and were therefore magnetite. A qualitative inspection of the glass B5 in the TEM suggested that the amount of residual glass present was the highest in this glass, compared with B1 – B4. EDS revealed the presence of Ca, Fe, Si and O, in the residual glass (Figure 5.25). There was no Al contamination since this composition was melted in a Pt crucible, confirming that the Al ions noted in glasses B1 – B4 arose from dissolution of the Al_2O_3 crucibles.

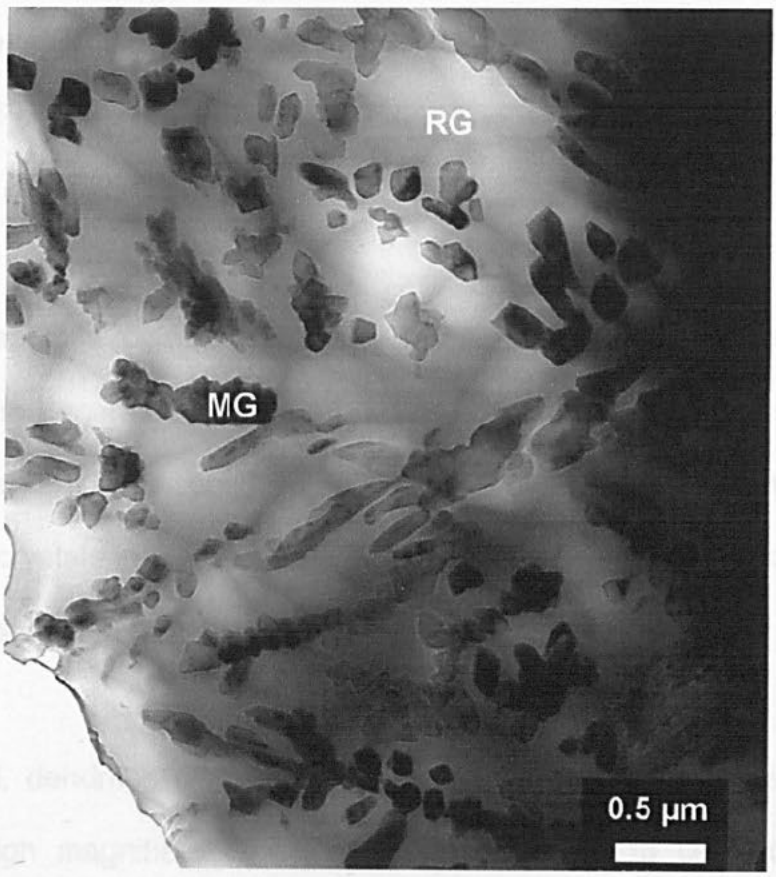

Figure 5.24: BF TEM micrograph of glass B5 showing the presence of magnetite nano-dendrites (MG) in a residual glass (RG) matrix

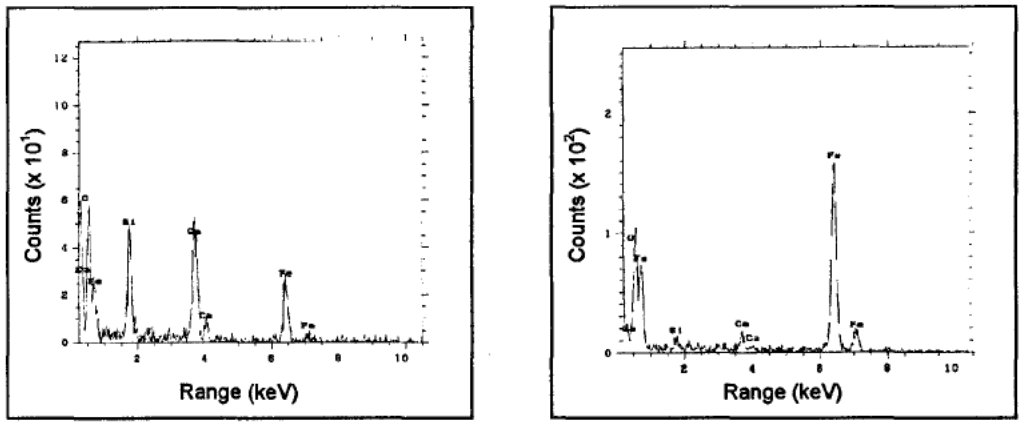

a **b**

Figure 5.25: Energy dispersive spectra from different regions of glass B5 **a.** residual glass (RG) showing predominately Si, Ca and O present with small traces of Fe and Al **b.** Magnetite nano – dendrites (MG) showing an abundance of Fe and O

Glass series C was also examined using TEM. SEM images of these compositions generally indicated that the crystallinity was not as high as in series B and it was only possible to observe some inhomogeneously distributed crystals in glasses C1, C2 and C3. Furthermore, at no stage were crystals observed in SEM images in C4 and C5.

Using TEM, dendrites and a blocky phase were noted in glass C1 (Figure 5.26) at high magnification, butit was not possible to carry out EDS on selected areas and only a general trace (Figure 5.27) was taken showing the presence of Ca, O, F, Fe, Al, Si, and P. Al was again assumed to have arisen from the dissolution of the Al_2O_3 crucibles. Although a similar microstructure

was observed in glass C2, (Figure 5.28), fewer and smaller blocky crystals were present. The dendrites were believed to be magnetite since they displayed a similar morphology to those observed in glass series B and the blocky phase was thought to be apatite for the same reasons. This was consistent with the XRD traces obtained for both these glasses.

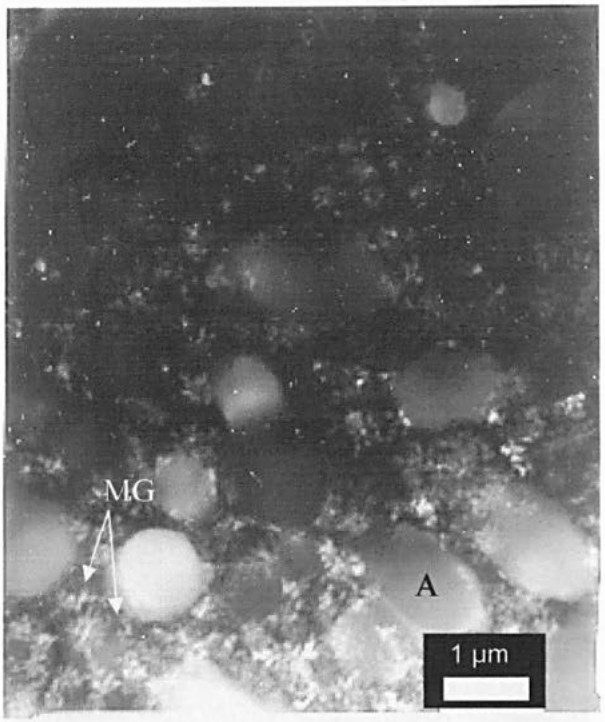

Figure 5.26: BF TEM micrograph of glass C1 showing the presence of magnetite nano-dendrites (MG) and apatite crystals (A) in a residual glass matrix

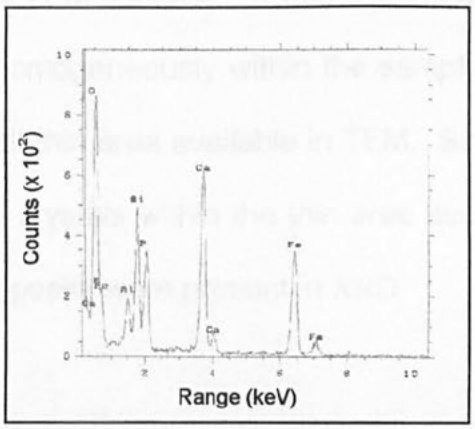

Figure 5.27: Energy dispersive spectra from glass C1 showing the presence of Si, Al, Fe Ca and P, O and F

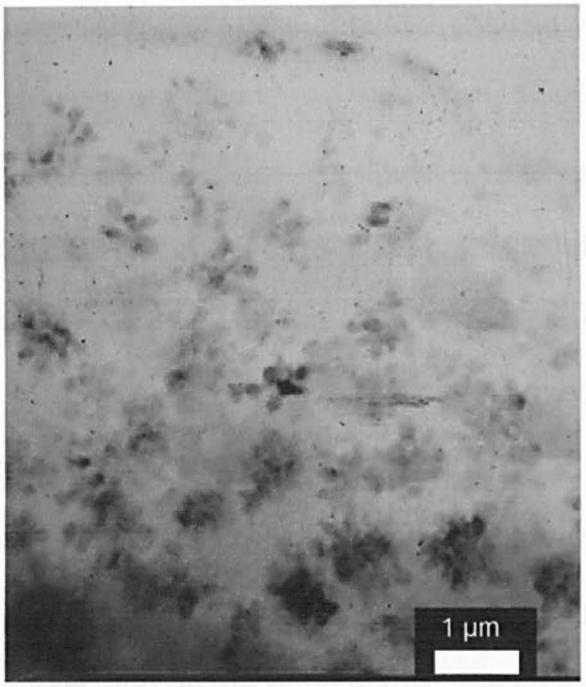

Figure 5.28: BF TEM micrograph of glass C2 showing the presence of magnetite nano-dendrites in a residual glass matrix

Although both the XRD and SEM showed crystals present in C3 these could not be found in the TEM samples. It was assumed that the crystals were few and distributed inhomogeneously within the samples and therefore difficult to find within the small thin area available in TEM. Similarly, glasses C4 and C5 did not exhibit any crystals within the thin area available in the TEM samples prepared although peaks were present in XRD.

5.3.5 Heat Treatment

Since the purpose of this project was to investigate the cement forming characteristics of Fe_2O_3 containing glasses and not their phase evolution, relatively little emphasis was placed on heat-treatment of the compositions

prepared. However, for completeness a small number of samples were studied. In many cases the XRD data obtained showed very little difference between the as–cast glasses and those that were heat-treated. In many compositions this was expected since there was a relatively small amount of residual glass present. In general, the residual glass concentration increased as P_2O_5 concentration decreased and exothermic peaks in DTA traces (Figures 5.4 and 5.5) became more intense. Typically, heat treatment (heating – 5°C min^{-1}/120 cooling – 5°C min^{-1} /25°C) of compositions with higher volume fractions of residual glass resulted in the formation of an additional crystal phase, wollastonite. However, after crystallisation, this phase also underwent a transformation as indicated by the endothermic inversion on the DTA traces (Figure 5.4 and 5.5). Figure 5.29 shows the position of XRD peaks that correspond to JCPDS cards 84-654 (wollastonite – 1T) and 43-1460 (wollastonite – 2M), illustrating how the peaks change during the phase transformation from 1T to 2M. The XRD traces from glasses when heated from 750°C to 950°C underwent changes in accordance with those seen in Figure 5.6. Figure 5.30 shows a representative XRD trace of this phase transformation as seen in C3.

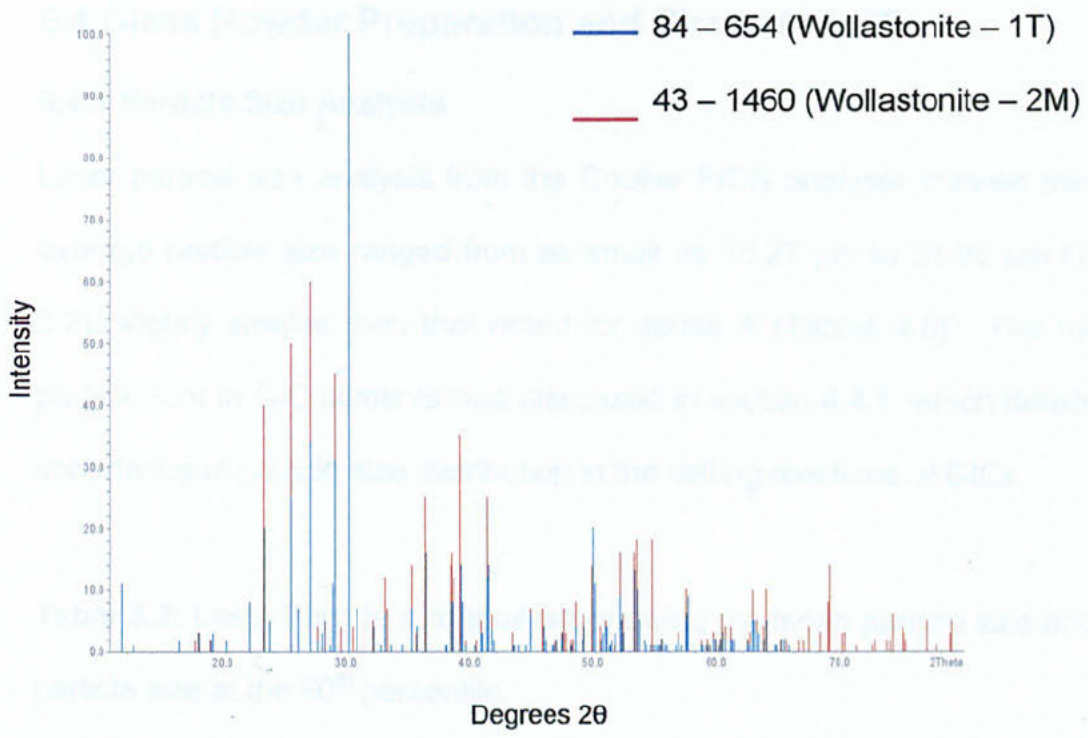

Figure 5.29: Trace showing the peaks associated with JCPSD cards 84 – 654 (Wollastonite – 1T) and 43 – 1460 (Wollastonite – 2M)

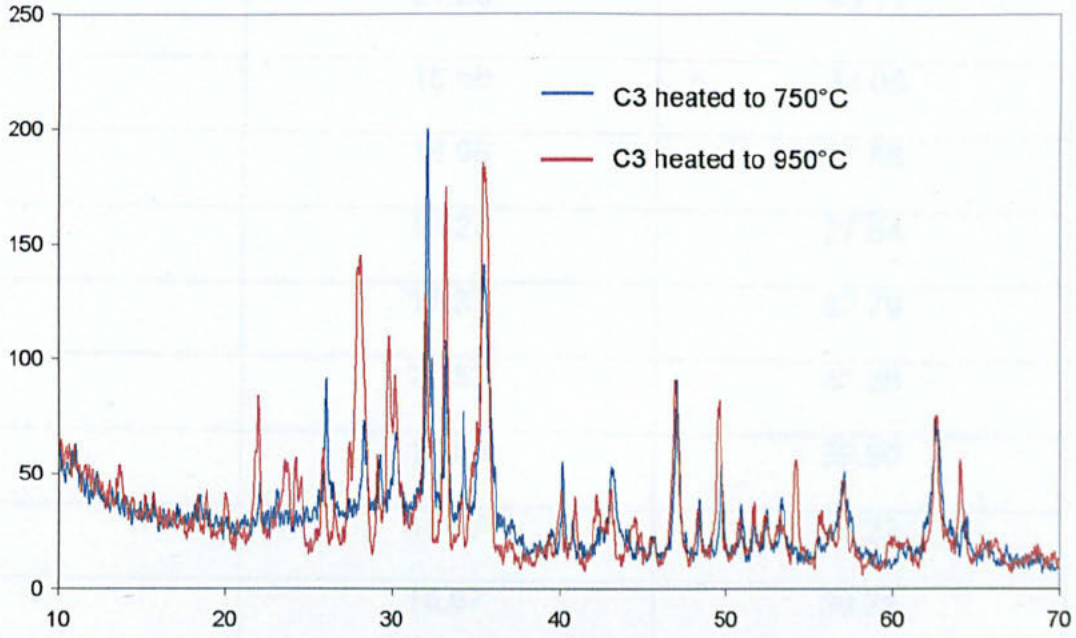

Figure 5.30: XRD traces showing the wollastonite phase transformation in glass C3 that occurs when heated to 750°C and 950°C

5.4 Glass Powder Preparation and Characterisation

5.4.1 Particle Size Analysis

Laser particle size analysis from the Coulter PIDS analyser showed that the average particle size ranged from as small as 15.27 μm to 21.25 μm (Table 5.2), slightly smaller than that noted for series A (Tables 4.5). The role of particle size in GIC cements was discussed in section 4.4.1, which details the importance of particle size distribution in the setting reactions of GICs.

Table 5.2: Laser Particle size analysis showing the mean particle size and the particle size at the 90th percentile.

Glass	Particle Size Results	
	Mean Particle Size (μm)	**90th percentile (μm)**
B1	21.25	43.11
B2	18.68	33.06
B3	18.98	37.56
B4	15.27	27.64
B5	17.37	32.79
C1	21.53	45.38
C2	17.80	39.90
C3	15.07	35.22
C4	16.67	38.71
C5	20.51	44.44

Figure 5.31 shows the quantitative particle size distribution of all the glass powders formed with series B and Figure 5.32 the glass powders of series C.

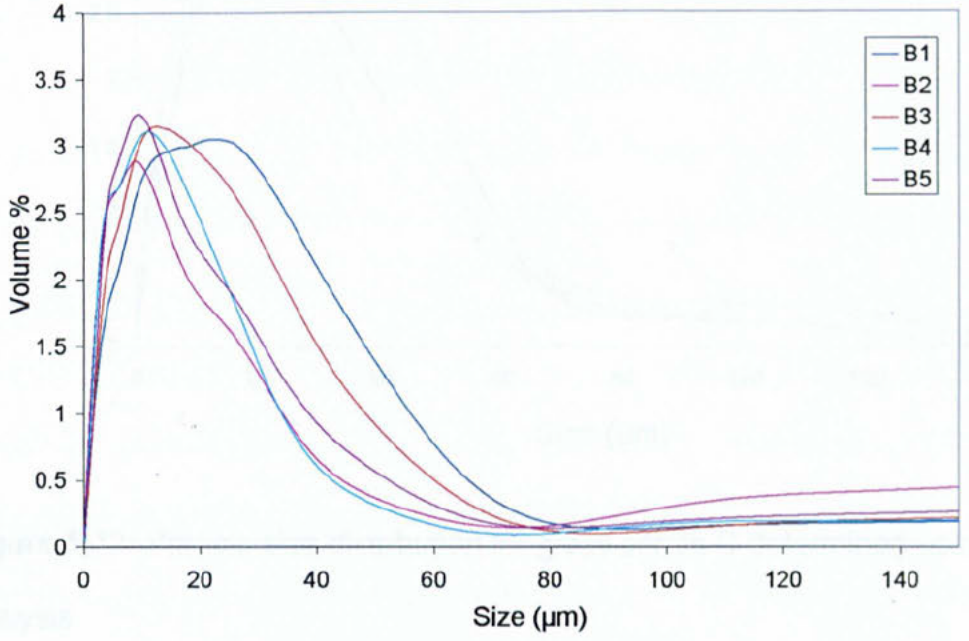

Figure 5.31: Particle size distribution for series B determined using laser analysis

The powders were also examined using SEM and a representative micrograph is shown in Figure 5.33. The glass powders of both series B and C were found to be more angular than those in series A. In glass series A most of the larger glass particles were covered with small 'fines' however the glasses in series B and C did not have the same quantity of fines. More fundamentally, the SEM images confirmed the particle size distribution obtained using laser analysis.

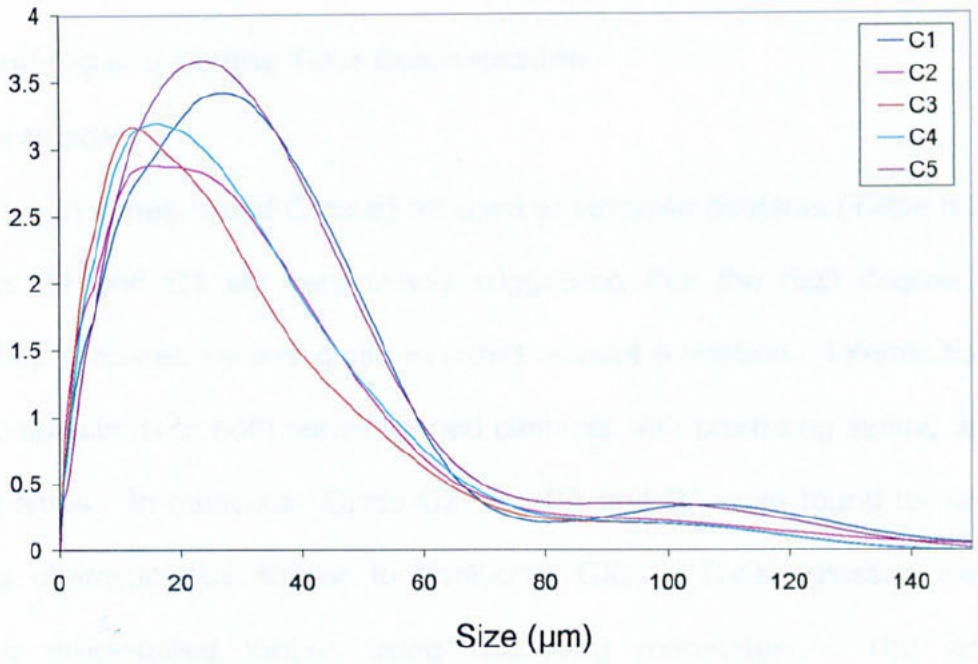

Figure 5.32: Particle size distribution for glass series C determined using laser analysis

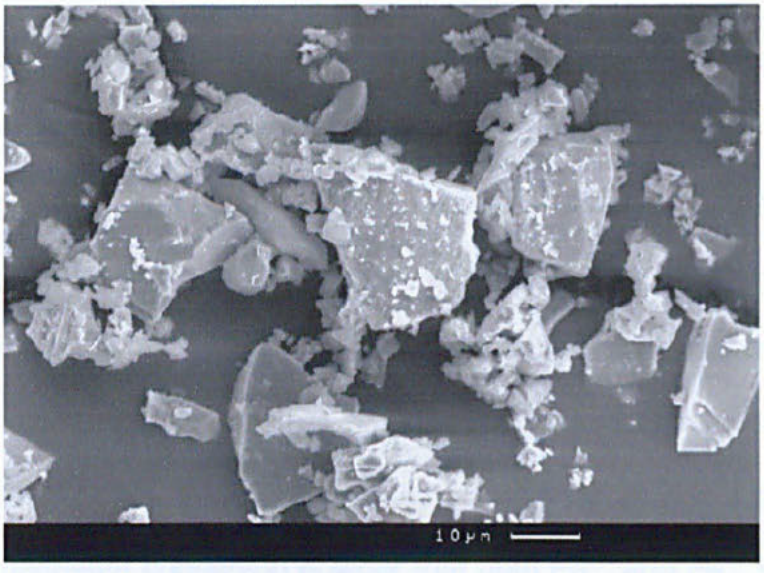

Figure 5.33: SEM micrograph showing the particle size distribution of a typical glass powder from glass series B and C

5.5 Cement Formation and Characterisation

5.5.1 Working and Setting Time Determination

Gilmore Needle

All glasses in series B and C could be used to fabricate cements (Table 5.3). Cements B1 and C1 set very slowly suggesting that the high degree of crystallinity exhibited by this glass inhibited cement formation. Intermediate glass compositions in both series formed cements with promising setting and working times. In particular, Glass C2, C3, B2 and B4 were found to have handling characteristics similar to traditional GICs. These glasses were therefore investigated further using oscillating rheometery. The only completely Al_2O_3–free glasses, B5 and C5, both formed cements but each set very quickly suggesting that Al ions are not needed for the setting reaction.

As a control experiment, an additional cement setting study was carried out using powders composed of magnetite and ratios of magnetite and apatite. Both pure magnetite and ratios of magnetite and apatite formed cements when mixed with the same ratios of PAA and water. The setting time for all the cements was in excess of 1 h and the resulting cements very brittle. Since PAA and water alone are not capable of forming cement the acid must be interacting with the crystalline magnetite and/or apatite. It is thought that in the purely magnetite containing powder that both Fe^{2+} and Fe^{3+} ions are released due to acid attack and these cross link the polymer using the same mechanism as in a conventional GIC. Likewise, the apatite powder also formed cement when mixed with PAA and water. The acid is thought to attack the apatite resulting in the release of ions that can cross-link the polymer.

Table 5.3: Setting and working times for cements made from glass series B and C determined using Gilmore needle indentation method

Cement	Working Time (sec)	Setting Time (sec)
B1	1042 (±7)	In excess of 30 min
B2	216 (±8)	785 (±31)
B3	88 (±15)	273 (±8)
B4	50 (±10)	98 (±10)
B5	Set too quickly	Set too quickly
C1	978 (±18)	In excess of 30 min
C2	242 (±18)	667 (±23)
C3	76 (±4)	210 (±5)
C4	47 (±3)	107 (±8)
C5	41 (±2))	132 (±13)

Oscillating Rheometery

As discussed in section 4.5.1, oscillating rheometery permitted a more quantitative measure of the setting characteristics of cements. Cements B2, B3, C2 and C3 had setting times that were considered viable (see section 2.4.6). However, as in Series A, the working and setting times were found to decrease with respect to the Gilmore needle studies. This was consistent with reported data on the use of oscillating rheometers and was attributed to the motion of the plates. This technique did however show that the 4 glasses selected had useful handling characteristics (Table 5.4).

Table 5.4: Setting and working times for cements made from glass series B and C determined using oscillating rheometery method

Cement	Working Time (sec)	Setting Time (sec)
B2	108 (±15.9)	132 (0)
B3	68 (±11.4)	295 (±32.1)
C2	98 (±4.6)	234 (±25.5)
C3	56 (±3.5)	112 (±6.9)

As with the glasses in series A, P_2O_5 content was found to be influential in the working and setting times. The higher the P_2O_5 content in the glass the slower the setting time. This was consistent with reported data [Griffin and Hill 2000, Wilson *et al* 1995]. It was discussed in section 5.3.2 that phosphate can disrupt the glass network and it is proposed that this in addition to affecting the T_g and T_x of the glass this could modify the rate of dissolution of cations from the glasses and therefore the handling characteristics.

5.5.2 Mechanical Properties

The flexural strength of the cements was investigated using three-point bend testing. It was only possible to make sample rods out of B2, B3 and C2 all other cements set too quickly to allow rods of the required test length (25 mm) to be fabricated. The mean flexural strength values and the standard deviation are given in Table 5.5 for both the unaged (24 h) and aged (4 w) samples.

All three Fe_2O_3 – containing cements were found to have higher FS values than those reported in section 4.5.2 for the Al_2O_3 – containing cements. In addition, GIC B2 was found to have increased FS values after 28 d. An increase in FS over time is consistent with an acid – base setting reaction. The initial FS of GIC C3 was higher than those measured in GIC's B2 and C2. However, the standard deviation was considerably greater, indicating that one rod may have had a disproportionally higher FS than the others, thereby skewing the data. GIC's B3 and C2 did not exhibit an increase in FS over time suggesting that these GIC's might mature in a different manner to conventional GIC's.

Table 5.5: Flexural strength (FS) values for B2, B3 and C2 at time intervals of 24 h and 4 w, the standard deviation is given in brackets

Cement	FS at 1 d	FS at 28 d
B2	13.6 (±0.8) MPa	18.9 (±3.2) MPa
B3	16.9 (±2.7) MPa	16.1 (±0.9) MPa
C2	13.0 (±1.2) MPa	13.1 (±2.1) MPa

After testing, the fracture surfaces were examined using SEM to determine the nature of the failure. Figures 5.34 – 5.36 shows the fracture surfaces at 1 d and 28 d. No difference was noted and it was assumed that the same mode of failure occurred. As with series A the cause of fracture was thought to be a failure of the glass-matrix interface. This mode of failure has also been reported by other authors [Brune and Smith 1982 and Xie *et al* 2000].

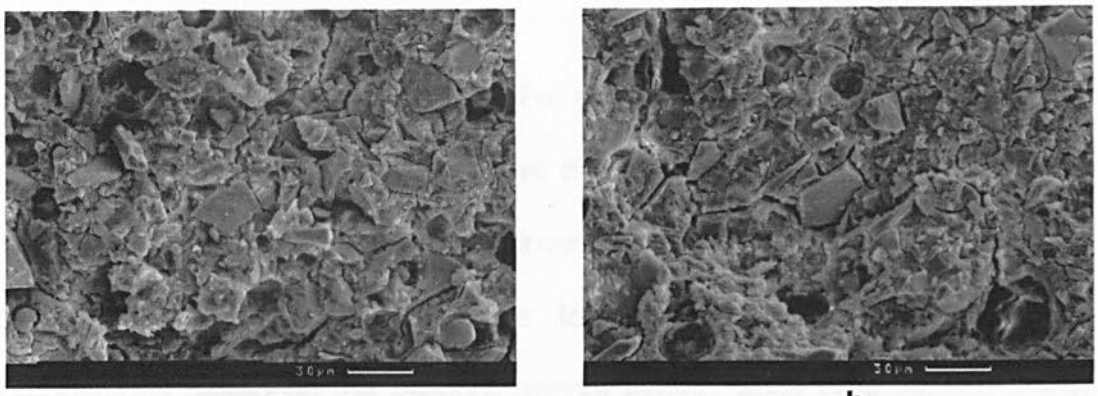

a b

Figure 5.34: SEM micrographs of fracture surfaces of B2 at different time intervals a. 24h and b. 4 w.

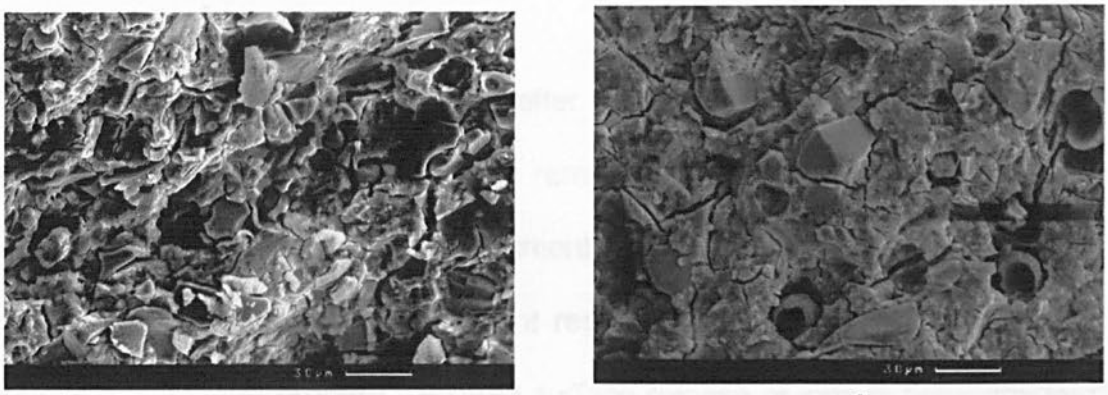

a b

Figure 5.35: SEM micrographs of fracture surfaces of B3 at different time intervals a. 24h and b. 4 w.

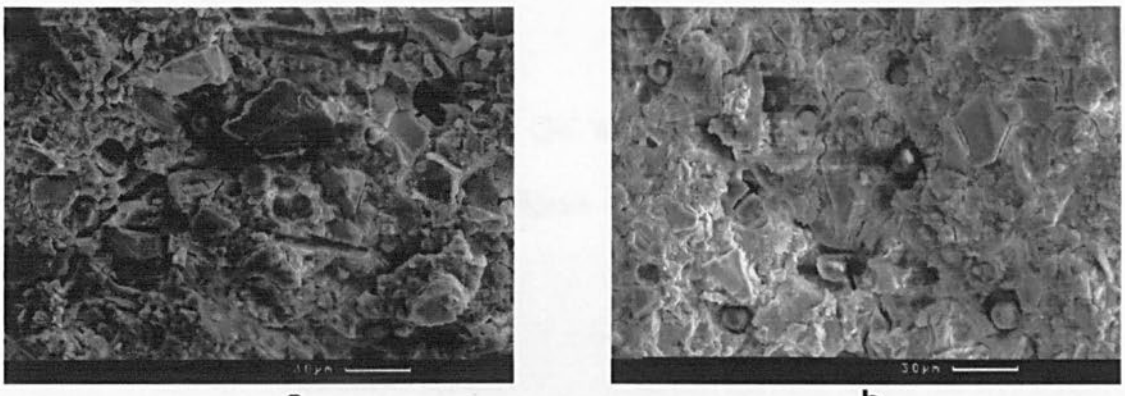

a b

Figure 5.36: SEM micrographs of fracture surfaces of C2 at different time intervals a. 24h and b. 4 w.

5.5.3 Ion Release

The release of ions from these novel Fe–containing cements was investigated using both ICP-ES and an ion selective electrode but only cements fabricated from glasses B2, B3 and C2 were investigated. This was partially due to fabrication difficulties but also due to poor cement viability for other compositions based on the Gilmore needle setting study (see section 2.4.6). As with glass series A, all ions present in the glasses were found to leach from the set cements. Figures 5.37 – 5.42 show the release of ions in weight per surface area ($\mu mol.mm^{-2}$) over time (d).

In traditional Al-containing GICs, after the gelation stage in the setting reaction, the ions within the cement remain mobile. These ions are able to exchange with the aqueous environment causing leeching. This effect has been extensively studied and current research suggests that the release of ions is a two-stage process. A rapid surface release of ions is noted followed by a slower bulk diffusion of ions [Wilson *et al* 1993]. Going from a high concentration (the cement) to a low concentration (aqueous environment) is the driving force for the diffusion.

The release of Si (Figure 5.37) from GIC's B2 B3 and C2 was found to follow the same profile as Al, as shown in Figure 4.26 (GIC A1).

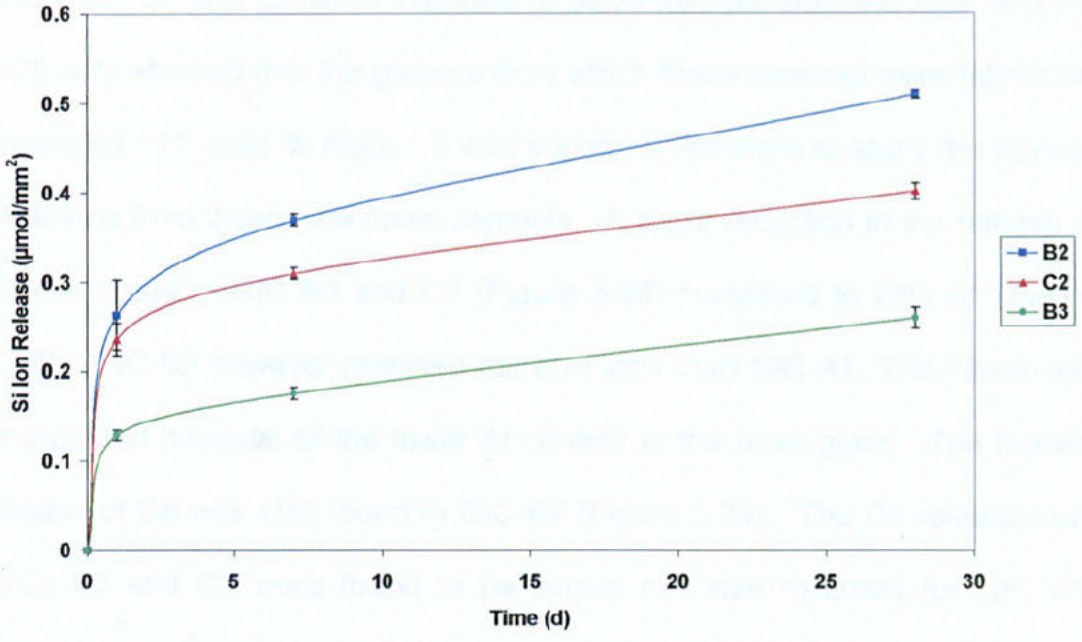

Figure 5.37 : Graph showing the Si ion release profile for cements B2, B3 and C2 over three time intervals (1 d, 7 d, and 28 d).

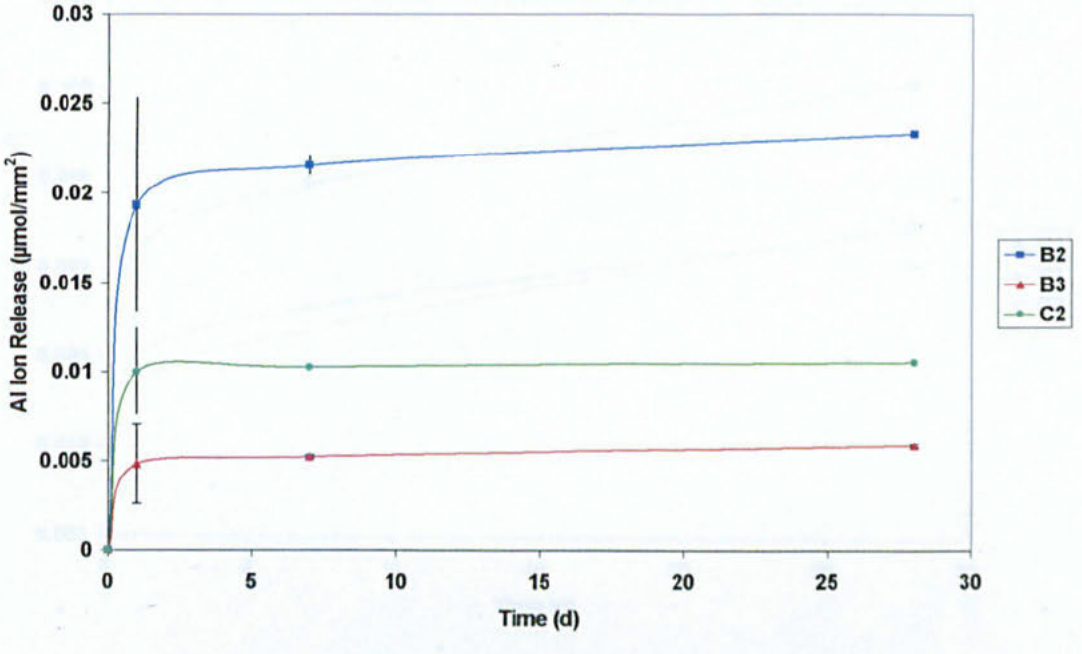

Figure 5.38: Graph showing the Al ion release profile for cements B2, B3 and C2 over three time intervals (1 d, 7 d, and 28 d).

GIC's B2, B3 and C2 were intended to be Al free but both the XRF and the EDS data showed that the glasses from which these cements were fabricated contained ~11 mole % Al_2O_3. It was important therefore to study the release of Al ions from these new novel cements. A slight reduction in the release of Al was noted in GIC B3 and C2 (Figure 5.38) compared to GIC A1 (Figure 4.27). GIC B2 however released more Al ions than GIC A1. This result was unexpected because of the lower Al content in the base glass. The highest release of Ca was also found in GIC B2 (Figure 5.39). The Ca release from GICs B3 and C2 were found to be similar to those recorded for GIC A1. These increases were believed to be due to the solubility of glass B2. It was possible that this cement may have been more susceptible to aqueous dissolution, resulting in higher ion release.

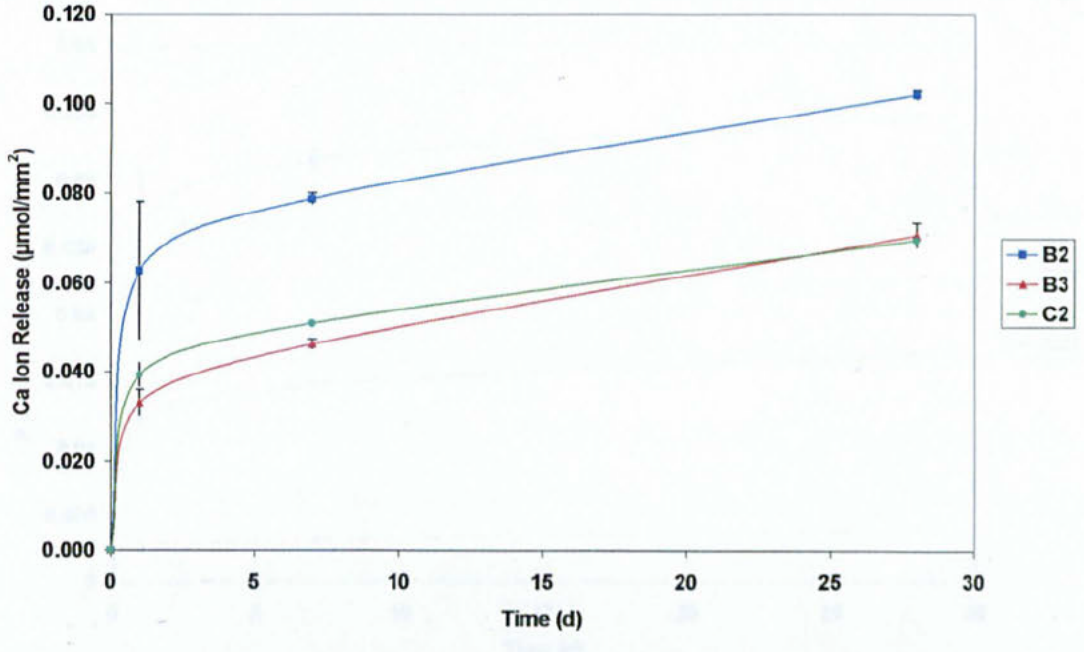

Figure 5.39: Graph showing the Ca ion release profile for cements B2, B3 and C2 over three time intervals (1 d, 7 d, and 28 d).

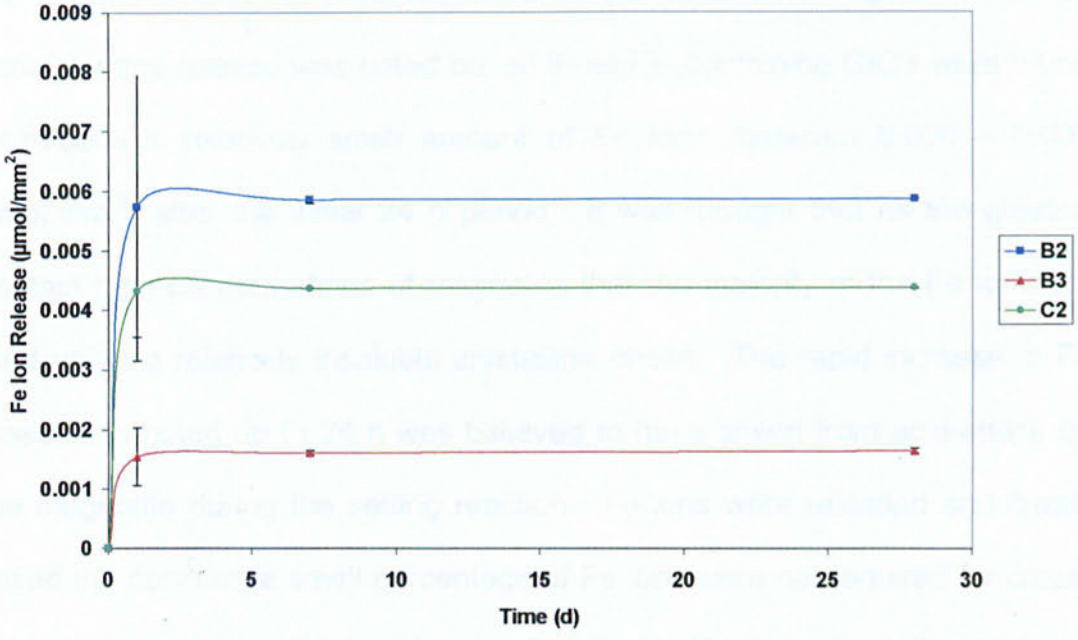

Figure 5.40: Graph showing the Fe ion release profile for cements B2, B3 and C2 over three time intervals (1 d, 7 d, and 28 d).

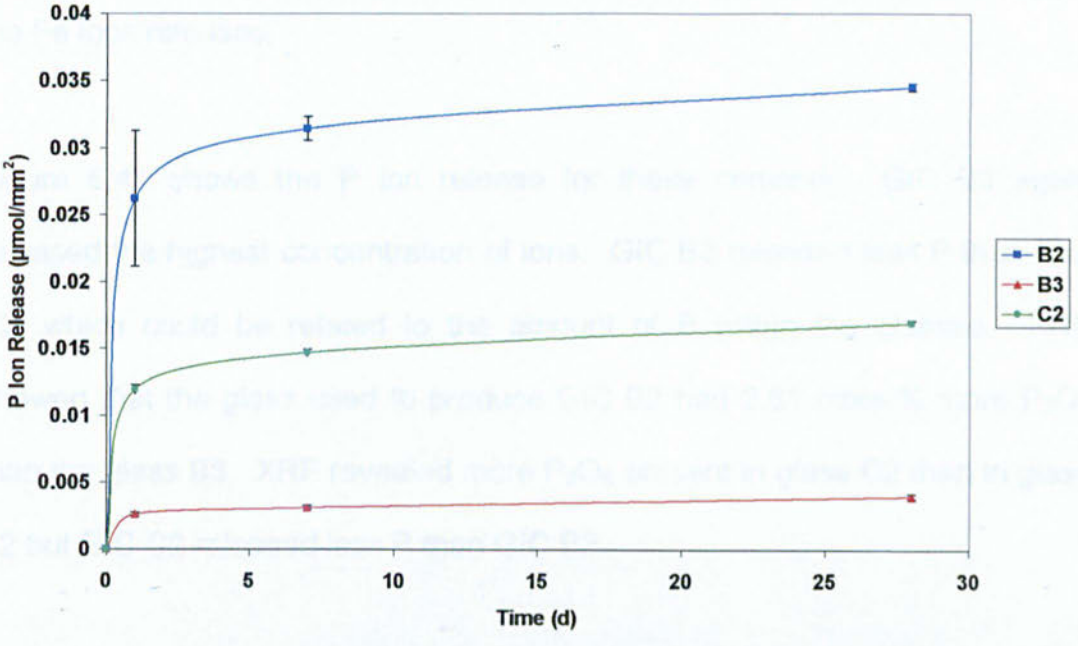

Figure 5.41: Graph showing the P ion release profile for cements B2, B3 and C2 over three time intervals (1 d, 7 d, and 28 d).

The release of Fe ions from these novel cements would not appear to adopt the traditional leaching patterns noted for the other ions (Figure 5.40). An initial surface release was noted but all three Fe–containing GIC's were found to release a relatively small amount of Fe ions (between 0.006 – 0.001 $\mu mol.mm^{-2}$) after the initial 24 h period. It was thought that as the glasses contain high concentrations of magnetite that the majority of the Fe ions are 'tied up' in a relatively insoluble crystalline phase. The rapid increase in Fe dissolution noted up to 24 h was believed to have arisen from acid-attack on the magnetite during the setting reaction. Fe ions were released and cross-linked the polymer, a small percentage of Fe ions were not required for cross-linking and were released during the first 24 h. However once the acid had been neutralised no further Fe ions were leached and unlike other ions present in the cements it was not able to exchange with the aqueous environment. It was not possible to distinguish between the valence states of the Fe ions released

Figure 5.41 shows the P ion release for these cements. GIC B2 again released the highest concentration of ions. GIC B3 released less P than GIC B2, which could be related to the amount of P within the glasses. XRF showed that the glass used to produce GIC B2 had 2.61 mole % more P_2O_5 than the glass B3. XRF revealed more P_2O_5 present in glass C2 than in glass B2 but GIC C2 released less P than GIC B2.

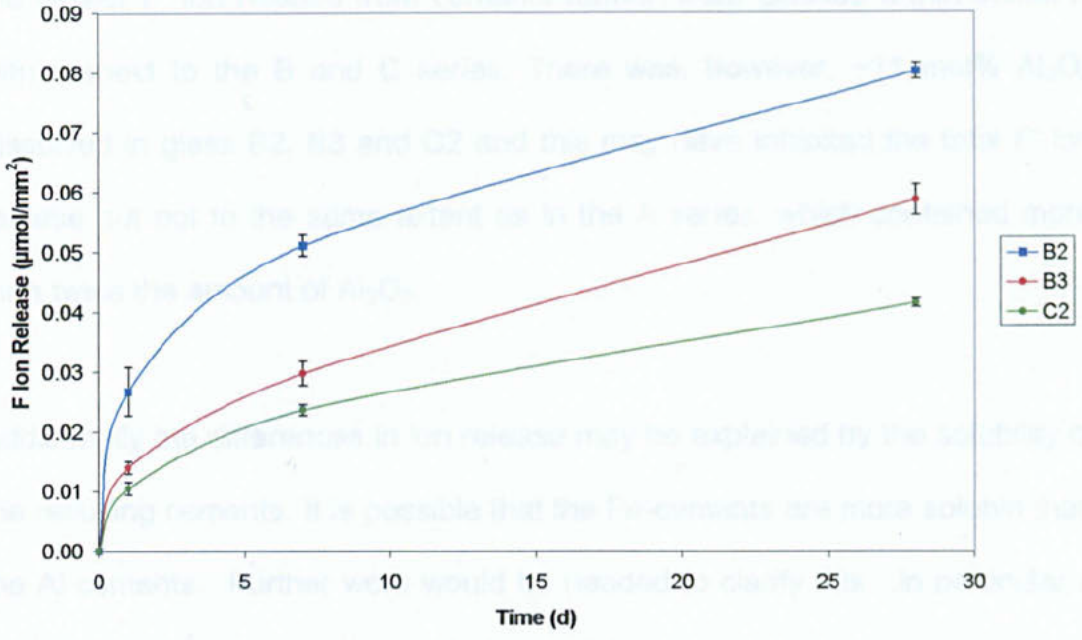

Figure 5.42: Graph showing the F ion release profile for cements B2, B3 and C2 over three time intervals (1d, 7d, and 28d).

Despite having less F in the glass components (Table 5.1), the GICs fabricated using the Fe_2O_3–containing glasses were found to release substantially more F than GIC A1 (Figure 5.42). All three Fe_2O_3–containing glasses used to form cements were highly crystalline and contained less glassy phase than in the A-series.

One possible explanation is that only the regions of residual glass contained ions capable of exchanging with the aqueous environment. Based on this concept, and the fact that more F^- is present in A1, GIC A1 should release more F^- than the B and C series cements. However, the presence of Al^{3+} ions within the glass is known to inhibit F^- evaporation during melting [Clifford *et al* 2001a]. The higher concentration of Al^{3+} ions could have been responsible for

the slower F^- ion release from cements formed from glasses within series A with respect to the B and C series. There was, however, ~11 mol% Al_2O_3 dissolved in glass B2, B3 and C2 and this may have inhibited the total F^- ion release but not to the same extent as in the A series, which contained more than twice the amount of Al_2O_3.

Additionally the differences in ion release may be explained by the solubility of the resulting cements. It is possible that the Fe-cements are more soluble than the Al-cements. Further work would be needed to clarify this. In particular a study of mass loss over time would be useful.

5.5.4 *In Vitro* Biocompatibility

GICs B1–B3 and B5 and C1–C3 were studied using an *in vitro* biocompatibility model. GICs B4, C4 and C5 were not investigated partially due to fabrication difficulties, but also due to their poor viability as commercial cements. GIC B5 was included as it was possible to form a disc and was the only completely Al–free GIC. SEM, MTT and total protein assays were employed to study the cellular interactions between the test materials and the cells. Results were obtained using both SEM and MTT assays but the total protein assay interacted with the cements. The reagents used to carry out the total protein assay were found to attack the surfaces of the cements causing dissolution of some material. This resulted in a discolouration of the test solution. Since protein content is measured using photospectrometery this gave a distorted result.

SEM showed that flattened cells were visible on all the surfaces of cement series B. GIC B1 had a confluent sheet of flattened cells present on the surface (Figure 5.43). As discussed in section 4.6.4 this was concurrent with good biocompatibility. GIC B2 had flattened cells throughout the surface but the sheet was not confluent (Figure 5.44). A near confluent sheet of cells was observed growing on the surface of GIC B3 (Figure 5.45) but in addition to flattened cells a few round cells were found to be present. On closer inspection these were thought to be dividing. Figure 5.44c shows two daughter cells that have just formed on the cement surface. GIC B5 (Figure 5.45) had a confluent sheet of cells present on the cement surface. The processing technique can cause cracking in the cell's sheet. Where this was visible it was possible to observe a glass particle near the surface that had magnetite crystals present.

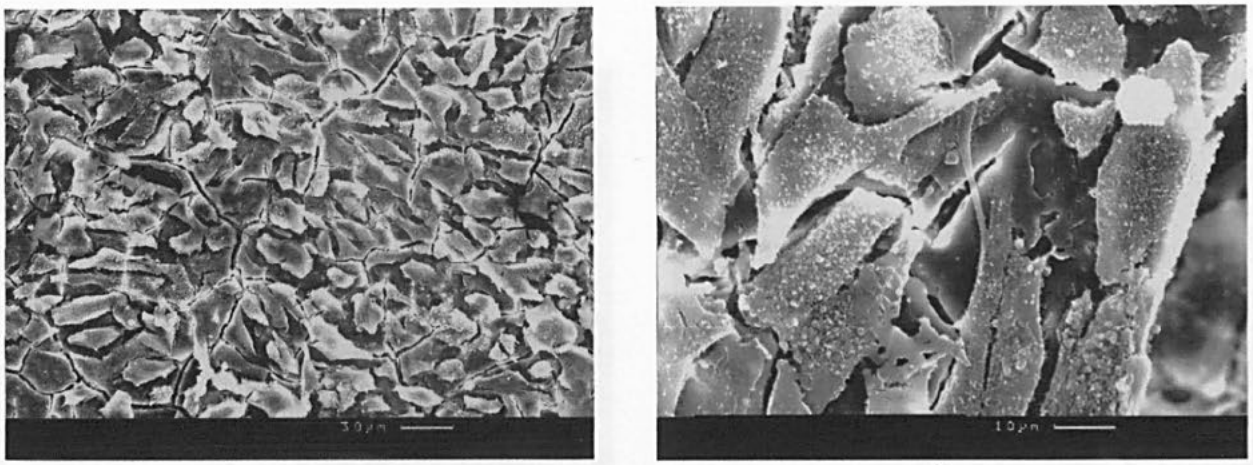

a b

Figure 5.43: Secondary electron SEM image of cells cultured on GIC B1 **a.** confluent cell sheet **b.** confluent cell sheet.

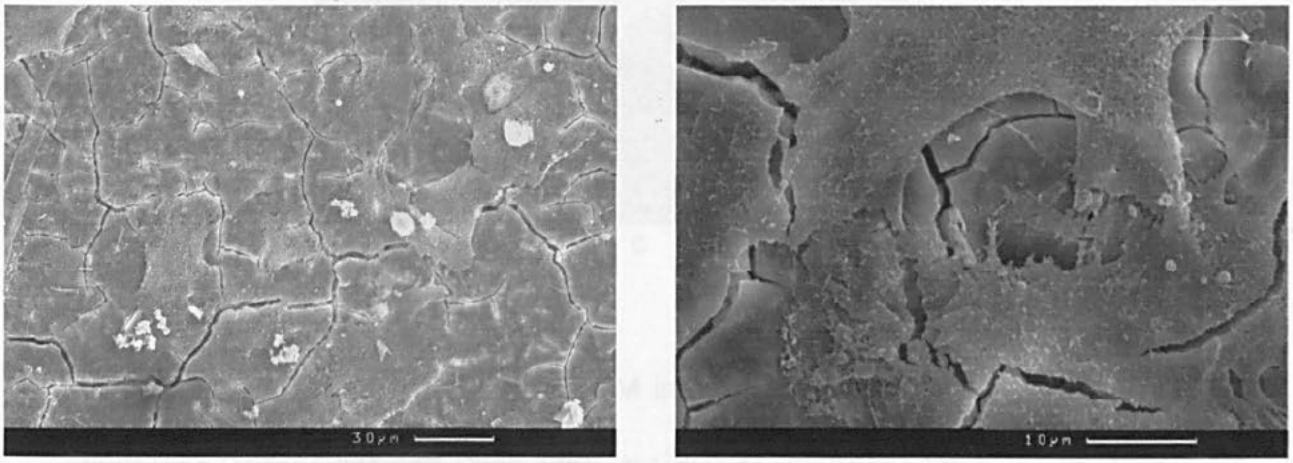

a b

Figure 5.44: Secondary electron SEM image of cells cultured on GIC B2 **a.** flattened osteoblasts-like cells over surface **b.** flattened cells on the material surface

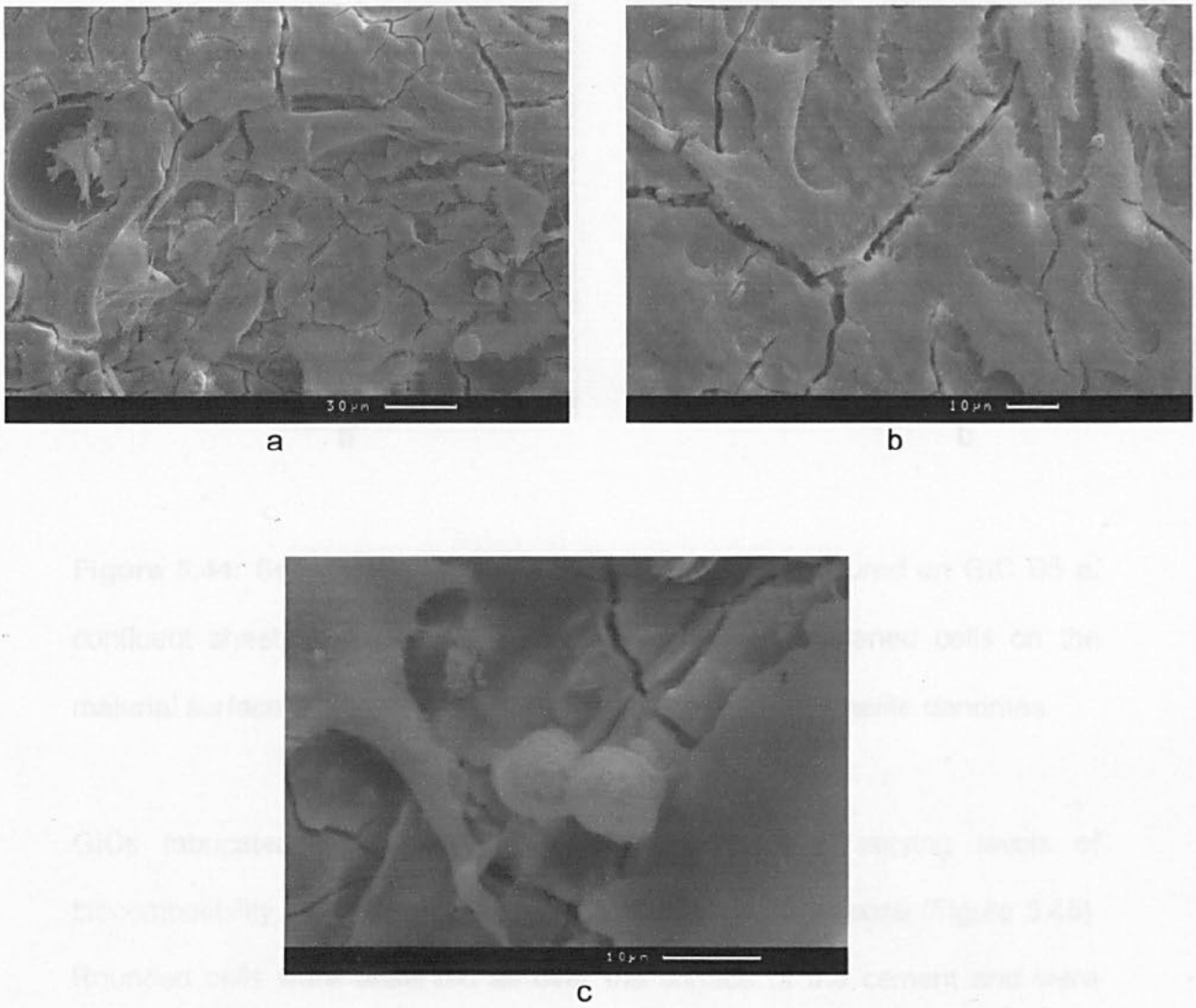

a b c

Figure 5.44: Secondary electron SEM image of cells cultured on GIC B3 **a.** flattened osteoblasts-like cells over surface **b.** flattened cells on materia'ls surface with psuedopodia present, **c.** Two daughter cells post dividing

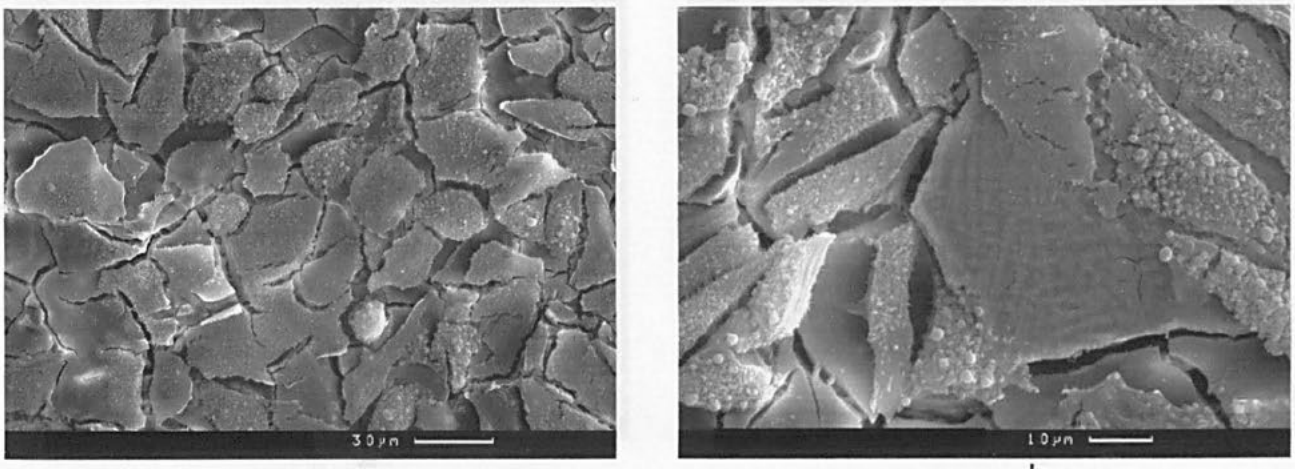

a b

Figure 5.44: Secondary electron SEM image of cells cultured on GIC B5 **a.** confluent sheet of flattened osteoblasts-like cells **b.** flattened cells on the material surface with a glass particle present; note the magnetite dendrites.

GICs fabricated from the glasses of series C had varying levels of biocompatibility. GIC C1 showed a very poor cellular response (Figure 5.45). Rounded cells were observed all over the surface of the cement and were thought to be non-vital or dead. There were a few more osteoblast – like cells present but these were in the minority. In contrast GIC C2 had a large number of flattened cells evenly distributed over the cement surface (Figure 5.46). Although the cell sheet was not confluent, it is felt that this would have occurred had the experiment been continued for a longer period. The presence of pseudopodia branching across the gaps between whole cells suggests that the surface is non-toxic to the growing cell population. The cells found on GIC C3 had a similar morphology although in addition a few rounded cells were present (Figure 5.47).

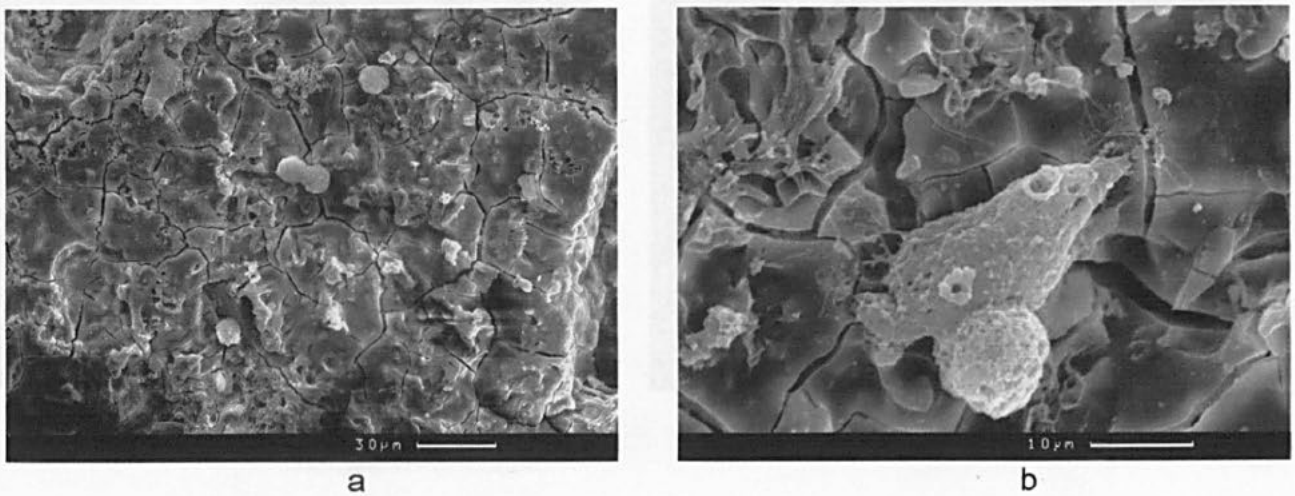

a b

Figure 5.45: Secondary electron SEM image of cells cultured on GIC C1 **a.and b.** rounded cells on the cement surface

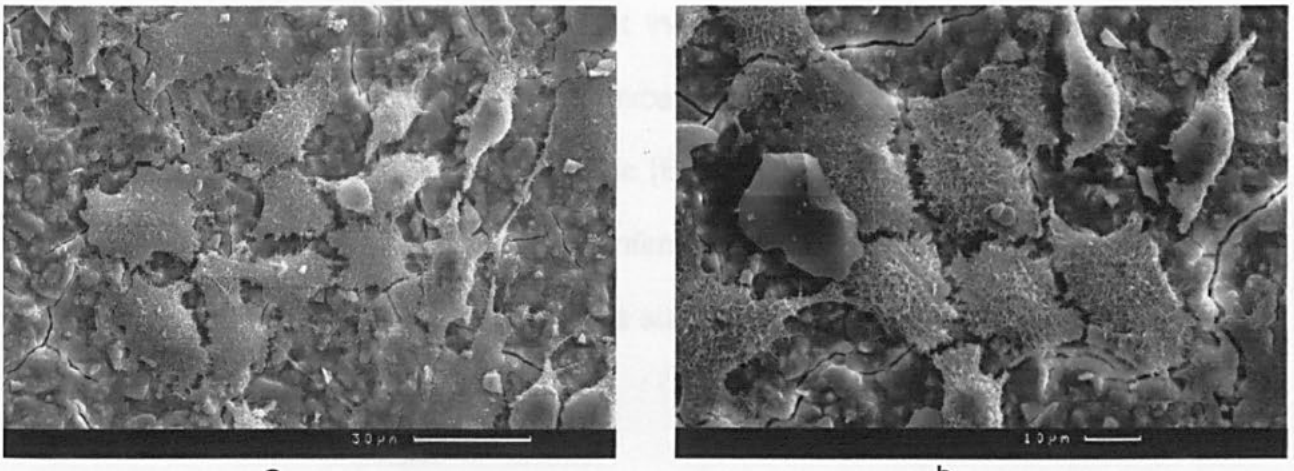

a b

Figure 5.46: Secondary electron SEM image of cells cultured on GIC C2 **a.** confluent sheet of flattened osteoblasts-like cells **b.** flattened cells on material's surface.

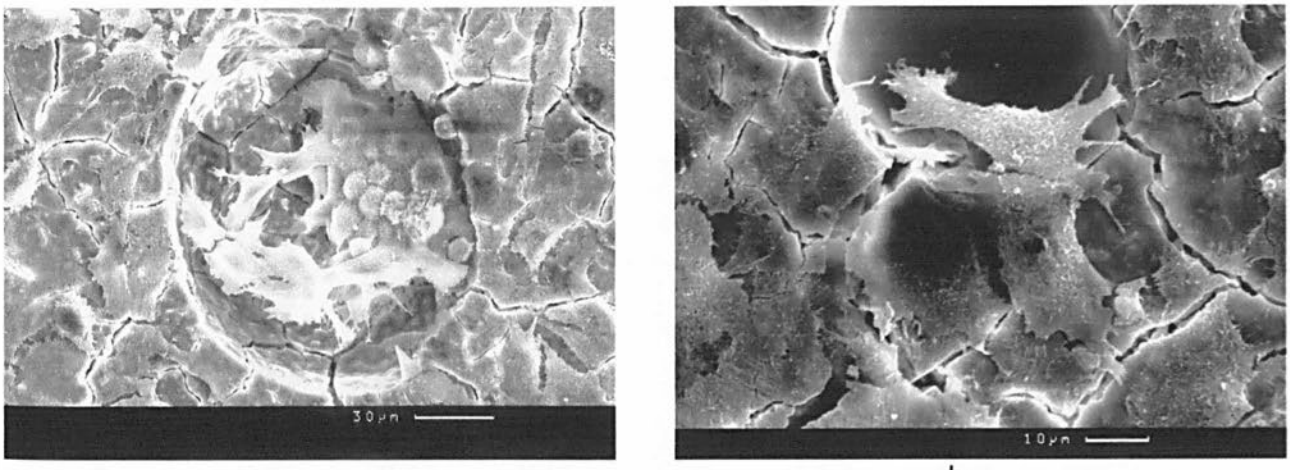

a b

Figure 5.47: Secondary electron SEM image of cells cultured on GIC C3 **a.** confluent sheet of flattened osteoblasts-like cells **b.** flattened cells on material's surface.

MTT assay (Figure 5.48) showed that the poorest cellular response was to GIC C1. All the other cements had excellent biocompatibility comparable to those reported for tissue culture plastic [Brook *et al* 1992, Sasanaluckit *et al* 1993 and Devlin *et al* 1998]. This confirms the SEM data, with only GIC C1 exhibiting rounded non-vital cells on the surface.

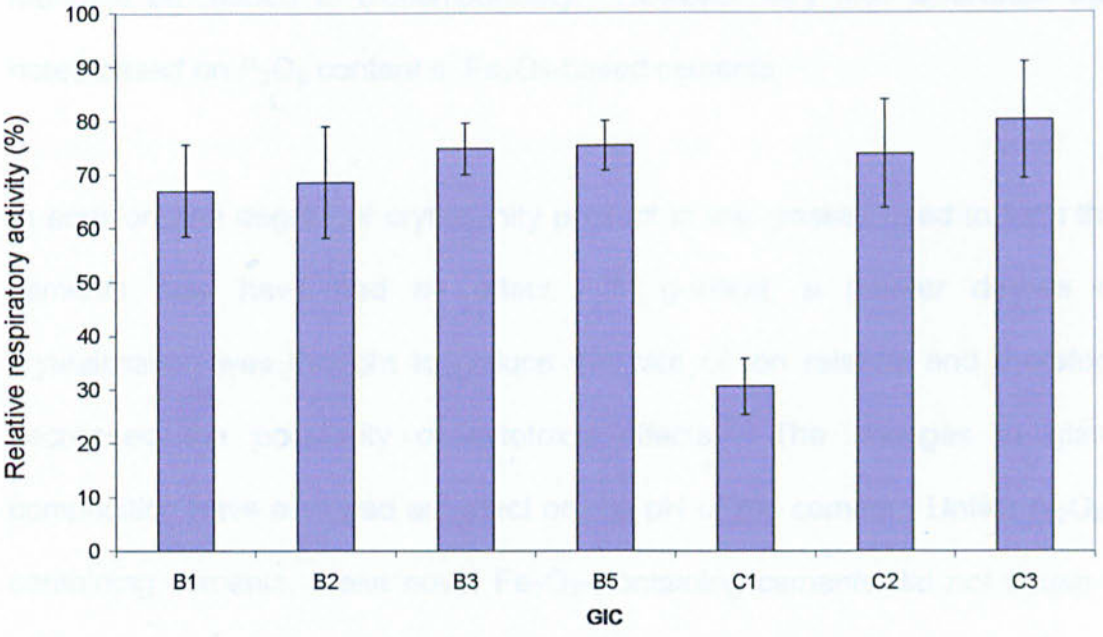

Figure 5.48: Graph showing the relative mitrochondrial activity in the presence of Fe – containing cements

Quantitative biocompatibility results (Figure 5.48) showed that all the cements had a similar mitrochondrial activity except C1. The responses to the cell culture experiments may be explained by a number of possible causes. The compositional variation may have contributed to the change. The presence of Fe_2O_3 and the reduction in the Al_2O_3 content of the glasses used to fabricate the cements may have improved the biocompatibility. Al ion release has been repeatedly reported as being cytotoxic (see section 2.3.4). It might have been expected that GIC B5 would have had the highest biocompatibility because it contained the least Al_2O_3 but this was not found. All the Fe_2O_3-based cements except C1 had improved biocompatibility. A second compositional variation was investigated, change in P_2O_5 content. In series A, P_2O_5 content was

found to be related to biocompatibility. However very little difference was noted based on P_2O_5 content in Fe_2O_3-based cements.

In addition, the degree of crystallinity present in the glasses used to form the cements may have had an effect. In general, a greater degree of crystallisation was thought to reduce the rate of ion release and therefore decreased the possibility of cytotoxic effects. The changes in glass composition have also had an effect on the pH of the cement. Unlike Al_2O_3–containing cements, these novel Fe_2O_3–containing cements did not cause a colour change in the buffering medium used for cell culture. As was discussed in section 4.6.4 pH can contribute to the release of Al ions from GIC. Although these cements do contain Al it is thought that the release is reduced because the cements are not as acidic as their Al counterparts.

The exact mechanism responsible for the changes observed in cellular response is not known. Further work is needed to investigate the roles of P_2O_5 and Fe_2O_3 in the biological environment.

5.6 Summary

A more detailed discussion of this chapter is given in Chapter 6, however, to summarise, it was possible to produce all of the glasses in series B and C. As with series A, glasses were difficult to fabricate due to crucible corrosion. All glasses were found to contain a degree of crystallinity. All glasses in series B and C contained magnetite, in addition phosphate containing glasses also contained crystalline apatite.

All glasses formed cements when mixed with PAA and a TA solution. The setting times were again found to be composition dependent. The presence of crystalline phases within these glasses was thought to slow the ion release and therefore cause the cements to set more slowly. The ion release of three cements (GIC B2, B3 and C2) was investigated. All ions were found to be released. The Fe ion release was found to have a relatively high initial rate of release but after 24 h the rate decreased substantially. In GIC's B3 and C2 the Al ion release was found to be greatly reduced. Cell culture studies showed that GIC's fabricated from Fe_2O_3 based glasses had greatly improved biocompatibility.

6. General Discussion

6.1 Glass Formation

It was possible to produce all of the glasses in each of the three series. However difficulties were experienced in the fabrication process. The glasses in series A were found to be very corrosive to mullite and alumina crucibles and therefore sillimanite crucibles were employed. The opposite was noted in series B and C; the Fe–containing glasses readily corroded sillimanite crucibles but minimal corrosion was noted in alumina. The addition of a lid was found to be important when melting all glass compositions. All glasses were fast-quenched in an attempt to avoid devitrification but this was only achieved sucessfully in series A.

The reduction of the amount of Fe_2O_3 in the glass was studied in an attempt to retard crystallisation. Glass series B contained more Fe_2O_3 than series C. However, further reducing the Fe_2O_3 concentration resulted in compositions that would not form a homogeneous melt and therefore could not be cast. By XRD, quenched glasses in series C contained a greater volume fraction of amorphous phase and therefore lower crystallinity than equivalent compositions in series B.

Glass series A exhibited very little variation between batched and post melt composition, whereas glass series B exhibited ~11 mol % of Al_2O_3 contamination and a considerable reduction in F^- (~10 mol %) concentration. The contamination of Fe_2O_3 based compositions was an inevitable consequence of melting in Al_2O_3 crucibles and could only be avoided by

melting in Pt. The volatilisation of F^- however, was directly linked to the replacement of Al_2O_3 by Fe_2O_3. The presence of non-bridging oxygen atoms leaves sufficient Al^{3+} free to bind with the F^- [Clifford *et al* 2001a]. Consequently, the incorporation Al_2O_3 arrests F^- volatilisation. However, replacing Al_2O_3 with Fe_2O_3 was not found to produce the same result. This suggests that Fe_2O_3 does not occupy the same sites or provide the same 'role' within the glassy network as Al_2O_3. Although the Fe_2O_3–containing glass compositions were not the same as those batched they offered insight into potential new GIC glass compositions.

All glasses in series A were amorphous when the melt was cast as frit into water or quenched between two steel plates. If boules were cast and allowed to cool to room temperature, apatite was always present and the glass became opalescent. GIC glasses contain high concentrations of P_2O_5 and CaF_2 traditionally used as nucleating agents, which readily induce crystallisation on cooling [Hill and Wood 1995]. Irrespective of quench rate, glass series B and C devitrified on cooling and were all found to contain magnetite and hematite. The glasses that contained P_2O_5 additionally formed apatite. The mechanism for the crystallisation in the Fe_2O_3-based glasses is unknown and requires further work. A detailed understanding of the crystallisation in these glass systems may offer a route to producing an amorphous Fe_2O_3-based glass.

Controlled crystallisation of series A showed that these glasses readily crystallised to form apatite and mullite and in the non - P_2O_5 containing glass

fluorite and anorthite. Hill and co-workers [1995] have described crystallisation following heat treatment of a number of ionomer glasses. They reported that most compositions crystallised to apatite and mullite, consistent with the results obtained for glass series A. Decreasing the P_2O_5 concentration of the glasses reduced the amount of apatite and increased the likelihood of fluorite formation with compositions such as A4 exhibiting both phases.

6.2 Cement Formation

All glasses formed cements with PAA and TA solution but the working and setting times were found to be dependent on the glass composition. In all glass series, reducing the P_2O_5 concentration reduced both the working and setting time of the cements. The acid degradability of the glass is altered by the presence of phosphate. According to Lowenstein's theories of acid-base cements, a change in P content alters the coordination of the Al. Increased P content aids the retention of Al in a stable tetrahedral coordination [Griffin and Hill 2000a].

The effect was greater in series B and C because decreasing the P_2O_5 concentration also increased the volume fraction of the amorphous phase. The presence of crystalline phases within the glasses is believed to affect the ion release. The lower the degree of crystallinity, the greater the amorphous regions, the greater the number of ions available for release. In addition Ca^{2+} ions are known to be very mobile and therefore in GIC C5, where no Ca^{2+}

containing crystal phases are present, more are available for release and a 'quick' set is noted.

As discussed above, Al-ions play an important role in the setting of traditional GICs. The majority of the Fe_2O_3-containing glasses also contained significant quantities of Al-ions (~11 mol %) due to contamination from the Al_2O_3 crucibles during melting. As discussed above all the glasses formed cements and it could be postulated that the Fe-ions are not involved in the setting reaction. Instead, contaminant Al^{3+} ions dissolve from the glass and cross-link the polymer. However, glasses B5 and C5 readily formed cements but contained no contaminant Al^{3+} ions since they were melted in Pt crucibles. In addition, when the mineral magnetite was ground and mixed in the appropriate ratios with PAA and TA, a cement resulted. This conclusively demonstrates that Fe_3O_4 is also susceptible to acid attack and is able to cross link PAA, thereby setting the cement.

The Al and Fe cements had similar mechanical properties. Moreover all the cements had flexural strengths comparable to the commercial material. The mode of fracture was thought to be failure of the glass-matrix interface, a similar mechanism to commercial compositions that has been reported by other authors, Brune and Smith [1982], Xie and co-workers [2000].

Ion release profiles from the cements showed that all cations present in the glasses were released over a period of time. The major difference between the Al_2O_3 and Fe_2O_3 containing cements was the release profile of Fe ions.

The release of Fe ions did not adopt the usual leaching reported by Wilson *et al* [1993] as a rapid surface release of ions followed by a slower bulk diffusion of ions. The Fe ions initially were found to have a high rate of release but after 24 h the rate decreased to virtually zero. It is proposed that initially excess Fe-ions unused during the setting reaction are leached from the cement. Once this initial release is complete, no further leaching occurs since the magnetite is effectively insoluble.

The highest rate of Al ion release was in GIC B2, and the lowest in GIC B3. The high rate of release is thought to be due to two possible reasons. Firstly the high quantities of magnetite and apatite crystals present within the bulk and secondly the solubility of the glass. B1 has a similar level of crystallisation but is only melted once whereas B2 has been manufactured by re-melting the appropriate ratios of B5 and B1, therefore increasing the Al_2O_3 contamination. The crystallisation of magnetite and apatite results in a residual glass supersaturated with Al_2O_3. Consequently, the Al ion release is enhanced from these regions. Other Fe_2O_3-containing glasses were found to release less Al than the Al_2O_3-based cements, probably due to lower crystallinity in these compositions and therefore a lower molar volume of Al_2O_3 in the residual glass. GIC B2 had the highest release rates for all ionic species. It is believed that this cement may be more soluble than the other Fe-based cements. Further work is needed to determine the mass losses over time to see whether solubility is a contributing factor for the higher ion release. Although the release of Al was undesirable the amount leached was generally reduced in Fe_2O_3 based cements.

6.3 Biocompatibility

Biocompatibility was investigated for all cements where fabrication of suitable discs was possible. Figure 6.1 shows the relative mitochondrial activity noted after 72 h post culturing with the cement discs. The best cellular response from a non-heat treated glass was noted in GIC C3, a Fe_2O_3-containing GIC. However all the Fe-based cement exhibited very similar results except GIC C1.

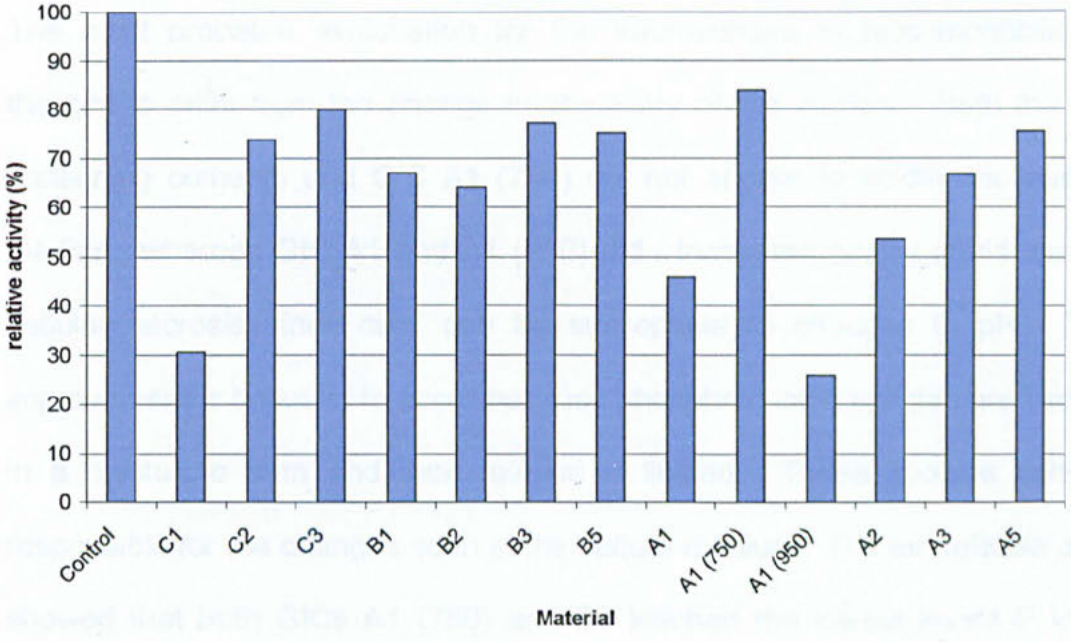

Figure 6.1: Graph showing MTT assay results for all test cements.

In addition to the use of Fe_2O_3, a low P_2O_5 concentration improved biocompatibility. In all cements the best cellular response was found in the GICs fabricated from glasses that contained low or no phosphate. This phenomenon was greater in series A than in series B or C. However, series B and C crystallise on cooling to magnetite and apatite, whereas series A may be quenched into an amorphous solid. It is therefore difficult to compare the

effect of P_2O_3 between the series. However, the presence of apatite within the cement is thought to contribute to an improvement in biocompatibility. GIC A1 (750) contained apatite crystals and exhibited excellent biocompatibility compared with GIC A1. The presence of apatite in the glass may have accounted for the improved cellular response, as apatite has long been associated with excellent biocompatibility (in particular with bone tissue) [Kokubo 1991].

The most probable explanation for the improvement in biocompatibility is thought to arise from the change in chemistry of the cement. Both the Fe-containing cements and GIC A1 (750) did not appear to acidify the culture medium, whereas GIC A1 and A1 (950) did. Increased acidity could lead to cellular necrosis since cells can be susceptible to changes in pH. The improvement is believed to occur because phosphate ionic species are tied up in a crystalline form and their release is limited. These species can be responsible for the changes seen in the culture medium. The ion release data showed that both GICs A1 (750) and B3 leached the lowest levels P ions, confirming the above observation.

7. Conclusions

7.1 Glass series A: $4.5SiO_2 \cdot 3Al_2O_3 \cdot (1.53 - X)P_2O_5 \cdot 3CaO \cdot 2CaF_2$

(i) Despite fabrication difficulties, it was possible to produce a glass of similar composition to that used in a commercial bone cement (SerenoCem®). Moreover, glasses were also fabricated with reductions of P_2O_5 (mole %).

(ii) All P_2O_5–containing compositions crystallised to form apatite and mullite, and sometimes cristobalite. Glasses that did not contain P_2O_5 formed fluorite and anorthite. Glass A4 contained both apatite and fluorite. This was generally consistent with previous work reported by Hill and co-workers. However, data in this thesis also provides new evidence for the crystallisation of cristobalite under certain conditions.

(iii) All glasses formed cements when mixed with PAA and dilute TA solution. Furthermore, devitrified glass (A1 heat treated to 750°C and 950°C) also formed cements. GIC A1 had mechanical properties similar to the commercial cement and exhibited an ion release profile consistent with similar GIC compositions.

(iv) Decreasing P_2O_5 content increased *in vitro* biocompatibility. In addition, devitrification at 750°C, improved the *in vitro* response. These data are highly significant in that this is the first demonstration of improving cement biocompatibility by using a crystallised ionomer glass (i.e. a glass-ceramic).

7.2 Glass series B: $4.5SiO_2 \cdot 3Fe_2O_3 \cdot (1.53 - X)P_2O_5 \cdot 3CaO \cdot 2CaF_2$

(i) All glasses were fabricated, although glasses B2, B3 and B4 required an additional melt process. All glasses devitrified to form magnetite and hematite on cooling and all P_2O_5–containing glasses formed apatite on cooling. All glasses melted in alumina crucibles were found to contain ~ 11 mol% Al_2O_3 contamination. This is the first reported fabrication of a true ionomer glass where all or a substantial proportion of Al_2O_3 has been replaced by Fe_2O_3.

(ii) All glasses formed cements when mixed with PAA and dilute TA solution but two cements GICs B2 and B3 had good handling properties. GICs B2 and B3 had improved mechanical properties with respect to series A. Unlike Al_2O_3 based cements, Fe ion release only occurred at 24 h after which there was no prolonged release as noted for other ions. GICs B2 and B3 had similar ion release profiles, although B2 released considerably more ions.

(iii) Improved biocompatibility was seen in all GICs fabricated from Fe_2O_3 based glasses as opposed to Al_2O_3. Decreasing P_2O_5 content had no effect on the biocompatibility of cements produced from this series of glasses. This is the first reported study of the *in vitro* biocompatibility of Fe-based GICs.

7.3 Glass series C: $4.5SiO_2 \cdot 1.5Fe_2O_3 \cdot (1.53 - X)P_2O_5 \cdot 3CaO \cdot 2CaF_2$

(i) All glasses were fabricated, although glasses C2, C3 and C4 required an additional melt. However, devitrification to form magnetite and hematite could not be suppressed. P_2O_5–containing glasses formed

apatite as well as magnetite on cooling whereas P_2O_3 free glasses precipitated CaF_2.

(ii) All glasses formed cements when mixed with PAA and dilute TA solution but only GIC C2 had adequate working and setting times. Moreover, GIC C2 had better mechanical properties than the commercial GIC and exhibited good biocompatibility

In conclusion, this research has added significantly to our knowledge of glass-ionomer cements. The replacement of Al_2O_3 by Fe_2O_3 was successful in that viable cements with improved biocompatibility were produced. These Fe-containing ionomer cements have properties which are desirable for medical applications, especially the reduction in Al ion release. In addition, the controlled crystallisation of Al-containing glasses was also shown to be an effective route to improve biocompatibility without compromising cement properties. It is anticipated that this research will have a major impact on the fabrication of ionomer glasses for medical applications.

8. Future Work

The following work is thought to be needed to further investigate Al–free GICs.

i. A production route that does not use an alumina crucible, to eliminate Al_2O_3 contamination from the glasses. Potential crucibles include Y_2O_3 stabilized zirconia and fused silica/zirconia, these both offer excellent thermal shock and chemical attack resistance.

ii. Additional biocompatibility studies including *in vivo* testing to investigate further the biocompatibility and osteoconductivity of Fe_2O_3-containing GICs.

iii. Consider other ionic species which can substitute for Al_2O_3 and which can induce a setting reaction in GIC's. In a recent publication Towler *et al* [2002] have investigated the substitution of Al by Zn, but it did not improve the biocompatibility of the cements.

iv. Study the release of Si ions from both conventional and Fe_2O_3 based GICs. There is a large debate about the role of Si in the setting and maturation of GICs, further clarification is required.

v. Study the magnetic properties of the Fe_2O_3 based GIC's with a view to understanding their interaction with a large magnetic field such as those generated by nuclear magnetic resonance scanners. In addition study the heating characteristics of Fe_2O_3 based GIC's to investigate their potential for use in hypothermic treatment of tumours. There have been a number of reports on the potential use of magnetite in the treatment of bone cancer [Ikenaga *et al* 1991, Ebisawa *et al* 1992 & 1997, Lee and Choi 1992 & 1997 and Lee *et al* 2000].

9. References

9.1 Papers

Andersson O.H & Dahl J.E, *Aluminium release from glass ionomer cements during early water exposure in vitro*, Biomaterials, 1994, **15**, 882-888

Barra E.D & Hill R.G, *Influence of glass composition on the properties of glass polyalkenoate cements. Part 3: influence of fluorine content*, Biomaterials, 2000, **21**, 693-698

Blades M.C, Moore D.P, Revell P.A & Hill R, *In vivo skeletal response and biomechanical assessment of two novel polyalkenoate cements following femoral implantation in the female New Zealand white rabbit*, Journal of Materials Science: Materials in Medicine, 1998, **9**, 701-706

Brook I.M, Craig G.T & Lamb D.J, *In vitro interaction between primary bone organ cultures, glass-ionomer cements and hydroxyapatite/triclacium phospahte ceramics*, Biomaterials, 1991a, **12**, 179-186

Brook I.M, Craig G.T & Lamb D.J, *Initial in-vivo evalution of glass-ionomer cements for use as alveolar bone substitutes*, Clinical Materials, 1991b, **7**, 295-300

Brook I.M, Craig G.T, Hatton P.V & Jonck L.M, *Bone cell interactions with a granular glass-ionomer bone substitute material: in vivo and in vito culture models*, Biomaterials, 1992, **13**, 721-725

Brook I.M. & Hatton P.V., *Glass-Ionomers: bioactive implant materials*, Biomaterials, 1998, **19**, 565-571

Brune D and Smith D, *Microstructure and strength properties of silicate and glass ionomer cements*, Acta Odontology Scandinavia, 1982, **40**, 389-396

BS 6039:1981, *Specification for Dental Glass Ionomer Cements*, British Standards Institution, 1981, ,

Cable M, *A century of developments in glassmelting research*, Journal of American Ceramic Society, 1998, **81**, 1083-1094

Carter D.H, Sloan P, Brook I.M & Hatton P.V, *Role of exchanegs ions in the integration of ionomeric (glass polyalkenoate) bone substitutes*, Biomaterials, 1997, **18**, 459-466

Charnley J, *Arthoplasty of the Hip- a New Operation*, Lancet, 1961, **1**, 1129-1132

Clifford A, Hill R, Towler M.R & Wood D.J, *The Crystallisation of Glasses from the Ternary CaF_2-$CaAl_2Si_2O_8$-P_2O_5 System*, Journal of Materials Science, 2001a, **36**, 3955-3961

Clifford A, Hill R, Rafferty A, Mooney P, Wood D, Samuneva B & Maysuya S, *The Influence of Calcium to Phosphate Ratio on the Nucleation and Crystallization of Apatite Glass-Ceramics*, Journal of Materials Science: Materials in Medicine, 2001b, **12**, 461-469

Cook W.D & Brockhurst P, *The Oscillating Rheometer - What does it measure?*, Journal of Dental Research, 1980, **59**, 795-799

Crisp S. Ferner AJ. Lewis BG. Wilson AD. *Properties of improved glass-ionomer cement formulations.* Journal of Dentistry. 1975, **3,** 125-30

Crisp S, Merson S.A & Wilson A.D, *Modification of ionomer cements by the addition of simple metal salts*, Ind. Eng. Chem. Prod. Res. Dev., 1980, **19**, 403-408

Culbertson B, *Glass-ionomer dental restoratives*, Progress in Polymer Science, 2001, **26**, 577-604

Devlin A.J, Hatton P.V & Brook I.M, *Dependence of in vitro biocompatibility of ionomeric cements on ion release*, Journal of Materials Science: Materials in Medicine, 1998, **9**, 737-741

Ducheyne P and Qui Q, *Bioactive Ceramics: the effect of surface reactivity on bone formation and bone cell function*, Biomaterials, 1999, **20**, 2287-2303

Ebisawa Y, Kokubo T, Ohura K & Yamamuro T, *Bioactivity of Fe2O3 - Containing CaO-SiO2 glasses: in vitro evaluation*, Journal of Materials Science: Materials in Medicine, 1992, **4**, 225-232

Ebisawa Y, Miyaji F Kokubo T, Ohura K & Nakamura T, *Surface reaction of bioactive and ferrimagnetic glass-ceramics in the system FeO-Fe2O3-CaO-SiO2*, Journal of the Ceramic Society of Japan, 1997, **105**, 947-951

Ellis J. Anstice M. Wilson AD, *The glass polyphosphonate cement: a novel glass-ionomer cement based on poly(vinyl phosphonic acid)*, Clinical Materials, 1991, **7**, 341-346

EN 29917:1994, *Dental Water-Based Cements*, British Standards Institution, 1994,

Engelbrecht E, von Foerster G & Delling G, *Ionogram in Revision Arthroplasty*, The Journal of Bone and Joint Surgery, 2000, **82**, 192-199

Finkemeier C.G, *Bone Grafting and Bone Graft Substitutes*, Journal of Bone and Joint Surgery - American Volume, 2002, **50**, 454-464

Geyer G and Helms J, *Ionomer-based cement as a bone substitute in reconstructive middle ear surgery*, HNO, 1997, **45**, 442-447

Giles H.L, Hurley P.W & Webster H.W.M, *Simple Approach to the Analysis of Oides, Silicates and Carbonates Using X-Ray Fluorescence Spectrometry*, X-Ray Spectrometry, 1995, **24**, 205-218

Griffin S.G & Hill R.G, *Influence of glass composition on the properties of glass polyalkenoate cements. Part 1: influence of aluminium to silicon ratio*, Biomaterials, 1999, **20**, 1579-1586

Griffin S.G & Hill R.G, *Influence of glass composition on the properties of glass polyalkenoate cements. Part 2: influence of phosphate content*, Biomaterials, 2000a, **21**, 399-403

Griffin S.G & Hill R.G, *Influence of glass composition on the properties of glass polyalkenoate cements. Part 3: influence of fluorite content*, Biomaterials, 2000b, **21**, 563-569

Hand R.J Stevens S.J & Sharp J.H, *Characterisation of fired silicas*, Thermochimica acta, 1998, **318**, 115-123

Hantson P.H, Mahieu P, Gersdorff M, Sindic C.J.M & Lauwerys R, *Encephalopathy with seizures after use of aluminium-containing bone cement*, The Lancet, 1994, **344**, 1647

Hatton P.V & Brook I.M, *Characterisation of the ultrastructure of glass-ionomer (poly-alkenoate) cement*, British Dental Journal, 1992, **173**, 275-277

Hench L.L, *Biocermics - From Conecpt to Clinic*, American Ceramic Society Bulletin, 1993, **72**, 93-98

Higgs W.A.J, Lucksanasombool P, Higgs R.J.E.D & Swain M.V, *A Simple Method of Determining the Modulus of Orthopedic Bone Cement*, Journal of Biomedical Materials Research (Applied Biomaterials), 2001, **58**, 188-195

Hill R & Wood D, *Apatite-Mullite glass-ceramics*, Journal of Materials Science: Materials in Medicine, 1995, **6**, 311-318

Hill R.G & Wilson A.D, *Some Strucural aspects of glasses used in ionomer cements*, Glass Technology, 1988, **29**, 150-158

Hurrell-Gillingham K.E, Reaney I.M, Miller C.A, Crawford A and Hatton P.V, *Devitrification of Ionomer Glass and its Effect on the In Vitro Biocompatibility of Glass Ionomer Cements*, Biomaterials, 2003, **24**, 3153-3160

Ikenaga M, Ohura K, Nakamura T, Kotoura Y, Yamamuro T, Oka M, Ebisawa Y & Kokubo T, *Hyperthermia Treatment of Experimental Bone Tumours with a Bioactive Ferromagnetic Glass-Ceramic*, Bioceramics, 1991, **4**, 255-262

Johal K.K, Mendoza-Suarez G, Escalante-Garcia J.I, Hill R.G, & Brook I.M, *In vivo response of strontium and zinc-based ionomeric cement implants in bone*, Journal of Materials Science: Materials in Medicine, 2002, **13**, 375-379

Jonck L.M, Grobbelaar C.J & Strating H, *Biological Evalution of glass-ionomer Cement (Ketac-0) as an interface material in total joint replacement. A screening Test*, Clinical Materials, 1989, **4**, 201-224

Jonck L.M. Grobbelaar C.J., *Ionos bone cement (glass-ionomer): an experimental and clinical evaluation in joint replacement.*, Clinical Materials, 1990, **6**, 323-59

Jonck LM. Grobbelaar CJ, *A glass ionomer for reconstructive surgery. Ionogran--an ionomeric micro implant. A biological evaluation*, Clinical Materials, 1992, **9**, 85-103

Kamitakahara M, Kawashita M, Kokubo T, Nakamura T,, *Effect of Polyacrykic Acid on the Apatite Formation of a Bioactive Ceramic in a Simulated Body Fluid: Fundamental Examination of the Possibility of Obtaining Bioactive Glass-Ionomer Cements for Orthopaedic Use*, Biomaterials, 2001, **22**, 3191-3196

Kamitakahara M, Kim H.M, Miyaji F, Kokubo T, Nakamura T,, *Preparation of Al-Free Glass Ionomer Cement*, Journal of the Ceramic Society of Japan, 2000, **108**, 1117-1118

Kenny SM, Buggy M, *Bone cements and fillers: A review*, Journal of Materials Science: Materials in Medicine, 2003, **14**, 923-938

Kent B, Private Correspondence, 2002

Kokubo T, *Bioactive Glass-Ceramics - Properties and Applications*, Biomaterials, 1991, **12**, 155-163

Konaka H, Miyaji F & Kokubo T, *Preparation and Magnetic Properties of glass-ceramics containing a-Fe for hyperthermia*, Journal of the Ceramic Society of Japan, 1997, **105**, 833-836

Kuleva A.E, Pankova N.A & Orlova L.A, *Causes of Foaming of Iron-Containing Melts*, Glass and Ceramics, 1999, **0**, 210-215

Lee Y.K & Choi S.Y, *Crystallization and Properties of Fe_2O_3-CaO-SiO_2 Glasses*, Journal of the American Cermic Society, 1992, **79**, 992-996

Lee Y.K & Choi S.Y, *Controlled nucleation and crystallization in Fe_2O_3-CaO-SiO_2 glass*, Journal of Materials Science, 1997, **32**, 431-436

Lee Y.K, Kim K N Choi S.E & Kim C.S, *Effect of iron state on crystallization and dissolution in Fe_2O_3-CaO-SiO_2 glasses*, Journal of Materials Science: Materials in Medicine, 2000, **11**, 511-515

Li C & Hong Z, *Kinetics for Reduction of Aciculate Ultrafine alpha-Fe_2O_3 Particles to Fe_3O_4 Particles*, Journal of Solid State Chemistry, 1997, **134**, 248-252

Loescher A.R, Robinson P.P & Brook I.M, *The effect of implanted inomeric and acrylic bone cements on peripheral nerve function*, Journal of Materials Science: Materials in Medicine, 1994a, **5**, 108-112

Loescher A.R, Robinson P.P & Brook I.M, *The immediate effects of ionomeric and acrylic bone cements on peripheral nerve function*, Journal of Materials Science: Materials in Medicine, 1994b, **5**, 551-556

Matsuya S, Maeda T and Ohta M, *IR and NMR analyses of hardening and maturation of glass-ionomer cement*, Journal of Dental Research, 1996, **75**, 1920-1927

Milne K.A, Calos N.J, O'Donnell J.H, Kennard C.H.L, Vega S & Marks D, *Glass-Ionomers dental restoratives. Part 1: a structural study*, Journal of Materials Science: Materials in Medicine, 1997, **8**, 349-356

Mount GJ, *Clinical performance of glass-ionomers*, Biomaterials, 1998, **19**, 573-579

Neve A.D, Piddock V & Combe E.C, *The Effect of Glass Heat Treatment on the Properties of a Novel Polyalkenoate Cement*, Clinical Materials, 1993, **12**, 133-115

Nicholson J.W, *Chemistry of glass-ionomer cements: a review*, Biomaterials, 1998a, **19**, 485-494

Nicholson J.W, *Glass-Ionomers in Medicine and Dentistry*, Proceedings of the Institute of Mechanical Engineers, 1998b, **212**, 121-126

Nicholson J.W, *Adhesive dental materials and their durability*, International Journal of Adhesion & Adhesives, 2000, **20**, .11-16

Oh S.H, Choi S.Y, Lee Y.K & Kim K.N, *Research on Annihilation of Cancer Cells by Glass-Ceramics for Cancer Treatment with External Magnetic Field I. Preparation and Cytotoxicity*, Journal Biomedical Materials Research, 2001, **54**, 360-365

Ohlberg S.M & Strickler D.W, *Determination of Percent Crystallinity in Partly Devitrified Glass by X-Ray Diffraction*, Journal of the American Cermic Society, 1962, **45**, 170-171

Ohura K, Ikenaga M, Nakamura T, Yamamuro T, Ebisawa Y, Kokubo T, Kotoura Y & Oka M, *A Heat-Generating Bioactive Glass-Ceramic for Hyperthermia*, Journal of Applied Biomaterials, 1991a, **2**, 153-159

Ohura K, Nakamura T, Yamamuro T, Ebisawa Y, Kokubo T, Kotoura Y & Oka M, *A Bioactive Ferromagnetic Glass-Ceramic for Hyperthermia*, Ceramics in Substitutive and Reconstructive Surgery, 1991b, , 131-136

Rafferty A, Hill R & Wood D, *Amorphous Phase Separation of Ionomer Glasses*, Journal of Materials Science, 2000, **35**, 3863-3869

Renard JL, Felten D, and Bequet D, *Post-Otoneurosurgery Aluminium Encephalopathy*, Lancet, 1994, **344**, 63-64

Reushe E, Pilz P, Oberascher G, Linder B, Egensperger R, Gloeckner K, Trinka E & Iglsedeer B, *Subacute fatal aluminium encephalopathy after reconstructive otoneurosurgery*, Human Pathology, 2001, **32**, 1136-1140

Santos L A, Carrodeguas R G, Boschi A O, and Arruda C, , 27 (2003) 412, *Dual-Setting Calcium Phosphate Cement Modified with Ammonium*, Artificial Organs, 2003, **27**, 412

Sasanaluckit P, Albustany K.R, Doherty P.J & Williams D.F, *Biocompatility of glass ionomer cements*, Biomaterials, 1993, **14**, 906-916

Takegami K, Sano T, Wakabayashi H, Sonoda J, Yamazaki T, Morita A, Shibuya T & Uchida A, *New ferromagnetic bone cement for local hyperthermia*, Journal of Biomedical Materials Research, 1998, **43**, 210-214

Tartaro G.P, D'Amato S, Itro A, Cartotenuto G, Gallo A & Nicolais L, *Characterization of glass ionomers for surgical application*, Journal of Materials Science: Materials in Medicine, 1996, **7**, 431-438

Tiernan M.J, Barnes P.A & Parkes G.M.B, *Reduction of Iron Oxide Catalysts: The Investigation of Kinetic Parameters Using Rate Perturbation and Linear Heating Thermoanalytical Techniques*, Journal of Physics and Chemistry, 2001, **105**, 220-228

Towler MR, Crowley CM, Murphy D, O'Callaghan AMC, *A preliminary study of an aluminum-free glass polyalkenoate cement*, Journal of Materials Science Letters, 2002, **21**, 1123-1126

Wallace K.E, Hill R.G, Pembroke J.T, Brown C.J & Hatton P.V, *Influence of Sodium Oxide Content on Bioactive Glass Properties*, Journal of Materials Science: Materials in Medicine, 1999, **10**, 697-701

Walls A.W.G, *Glass polyalkenoate (glass-ionomer) cements: a review*, Journal of Dentistry, 1986, **14**, 231-243

Wasson E.A & Nicholson J.W, *Studies on the setting chemistry of glass-ionomer cements*, Clinical Materials, 1991, **7**, 289-293

Wasson E.A and Nicholson J.W, *A Study of the Relationship Between Setting Chemistry and Properties of Modified Glass Poly(Alkenoate) Cements*, British Polymer Journal, 1990, **23**, 179-183

Williams D.F, *Tissue Biomaterial Interactions*, Journal of Materials Science, 1987, **22**, 3421-3445

Wilson A.D, *Glass-ionomer cement - origins, development and future*, Clinical Materials, 1991, **7**, 275-282

Wilson A.D, *A hard decade's work: steps in the invention of the glass-ionomer cement*, Journal of Dental Research, 1996, **75**, 1723-1727

Wilson A.D, Crisp S & Ferner A.J, *Reactions in glass-ionomer cements: IV. Effects of chelating comonomers on setting behavior*, Journal of Dental Research, 1976, **55**, 489-495

Wilson A.D, Crisp S Prosser H.J Lewis B.G & Merson S.A, *Aluminosilicate glasses for polyelectrolye cements*, Ind. Eng. Chem. Prod. Res. Dev., 1980, **19**, 263-270

Wilson A.D, Kent B.E, Clinton D & Miller, *The formation and microstructure of dental silicate cements*, Journal of Materials Science, 1972, **7**, 220-238

Wood D & Hill R, *Glass ceramic approach to controlling the properties of a glass-ionomer bone cement*, Biomaterials, 1991a, **12**, 164-170

Wood D & Hill R, *Structure-Property Relationships in Ionomer Glasses*, Clinical Materials, 1991b, **7**, 301-312

Xie D, Brantley W.A, Culbertson B.M & Wang G, *Mechanical properties and microstructures of glass-ionomer cements*, Dental Materials, 2000, **16**, 129-138

9.2 Books

Abercrombie M, Hickman C.J, and Johnson M.L, Dictionary of Biology, Penguin Reference, Aylesbury UK, 1984

Alberts B, Bray D, Lewis J, Raff M, Roberts K and Watson J.D, Molecular Biology of the Cell, Garland Publishing Inc., London UK, 1994

Babcock C.L, Silicate Glass Technology Methods, John Wiley and Sons, NewYork USA, 1977

Beall G.H and Duke D.A, in Glass science and technology ; Vol.1. Glass-forming systems edited by. Uhlmann D.R, Kreidl N.J, London Academic Press, NewYork USA, 1983

Begley E.R, in "The Handbook of Glass Manufacture: Volume 1", ed. Tooley F.V., Books for Industry, NewYork USA, 1974

Hench L.L, in Biomaterials Science: An introduction to materials in medicine eds Ratner B.D, Hoffman A.S, Schoen F.J and Lemons J.E, Academic Press,, San Diego USA, 1996

Hench L.L and Ethridge E.C, Biomaterials: An interfacial Approach, Academic Press Inc, New York USA, 1982

Hench L.L and Wilson J, Introduction to Bioceramics, World Scientific Publishers, Singapore, 1993

Issels R.D, Application of Hyperthermia in the Treatment of Cancer, Springer-Verlag, NewYork USA, 1988

Katz J.W, in Biomaterials Science: An introduction to materials in medicine eds Ratner B.D, Hoffman A.S, Schoen F.J and Lemons J.E, Academic Press,, San Diego USA, 1996

Kreidl N.J, in Glass science and technology ; Vol.1. Glass-forming systems edited by. Uhlmann D.R, Kreidl N.J, London Academic Press, NewYork USA, 1983

Kuhn K.D, Bone Cements, Springer, Berlin Germany, 2000

Marieb E.N, Human Anatomy and Physiology, Benjamin/Cummings Science Publishing, California USA, 1998

McCauley R.A, Corrosion of Materials by Molten Glass" Eds. Pecoraro G.A., Marra J.C. and Wenzel J.T, The American Ceramic Society, Ohio USA, 1996

McMillan P.W, Advanced Glass Technology, Plenum Press,, NewYork USA, 1962

McMillan, P. W., Glass-ceramics.(1st and 2nd Editions), Academic Press, NewYork USA, 0

Nicholson J.W, The Chemistry of Medical and Dental Materials, Royal Society of Chemistry, Canterbury UK, 2002

Paul A, Chemistry of Glasses - 2nd Edition, Chapman and Hall, London UK, 1990

Ratner B.D, in Biomaterials Science: An introduction to materials in medicine eds Ratner B.D, Hoffman A.S, Schoen F.J and Lemons J.E, Academic Press,, San Diego USA, 1996

Rawson H, Inorganic Glass-Forming Systems, Academic Press, London UK, 1967

Schoen A.S, in Biomaterials Science: An introduction to materials in medicine eds Ratner B.D, Hoffman A.S, Schoen F.J and Lemons J.E, Academic Press,, San Diego USA, 1996

Shackleford J.F, Introduction to Materials Science for Engineers - 4th Edition, Prentice and Hall, London UK, 1996

Shelby J.E, Introduction to Glass Technology, Royal Society of Chemistry, Cambridge UK, 1997

Uhlmann D.R and Yinnon H, in Glass science and technology ; Vol.1. Glass-forming systems edited by. Uhlmann D.R, Kreidl N.J, London Academic Press, NewYork USA, 1983

van Noort, Introduction to Dental Materials, Mosby, London UK, 1994

Volf M.B, Chemical Approach to Glasses, Elsevier, NewYork USA, 1984

Vose R.H, Glass, Collins, London UK, 1980

Wilson A.D and Nicholson J.W, Acid-Base Cements Their Biomedical and Industrial Application, Cambridge University Press, Cambridge UK, 1993

Appendix I

Commercial BioCem

Mat	Wt	SiO2	oxides Al2O3	in P2O5	glass CaO	CaF2
SiO2	2160	2160				
Al2O3	1190		1190			
AlPO4	2984		1247.492	1736.903		
CaCO3	2420				1355.742	
CaF2	1247					1247
Total	10001	2160	2437.492	1736.903	1355.742	1247
					Total	8937.137

Oxide	Wt% = wt/	Wt%	RMM
SiO2	2160/8937	24.16881	60.08
Al2O3	2437.49/8	27.27374	101.96
P2O5	1736.69/8	19.43467	141.92
CaO	1355.92/8	15.16976	56.08
CaF2	1247/8937	13.95301	78.08
Total		100	

2AlPO4 = Al2O3 + P2O5
2AlPO4 = Al2O3 raw material factor = 2.392
2AlPO4 = P2O5 raw material factor = 1.718

CaCO3 = CaO + CO2
CaCO3 = CaO raw material factor = 1.785

2Al(OH)3 = Al2O3 + 3H2O
2Al(OH)3 = Al2O3 raw material factor = 1.530

2CaHPO4 = 2CaO + P2O5 + H2O
2CaHPO4 = 2CaO raw material factor = 2.426
2CaHPO4 = P2O5 raw material factor = 1.917

A1

Raw mat	Wt oxide	wt %
SiO2	24.169 x 1	24.169
Al(OH)3	27.274 x 1	41.729
CaHPO4	19.434 x 1	37.251
CaCO3		
CaF2	13.953 x 1	13.953

nb 37.251g of CaHPO4 gives 15.355g of CaO therefore no CaCO3 added

A2

Oxide	mol	mol%	mol ratio	RMM	Wt = mol	wt%
SiO2	0.402	32.823	4.50	60.08	1972.007	25.343
Al203	0.267	21.800	2.99	101.96	2222.765	28.566
P2O5	0.10275	8.389	1.15	141.92	1190.633	15.301
CaO	0.274	22.372	3.07	56.08	1254.617	16.124
CaF2	0.179	14.615	2.00	78.08	1141.157	14.666
	1.22475	100			7781.180	

Raw Mat	Wt for 100g	
SiO2	25.343	
al(oh)2	43.706	
CaHPO4	29.333	12.09105
CaCO3	7.198	
CaF2	14.666	

A3

Oxide	mol	mol%	mol ratio	RMM	Wt = mol	wt%
SiO2	0.402	33.767	4.50	60.08	2028.741	26.705
al203	0.267	22.428	2.99	101.96	2286.713	30.101
P2O5	0.0685	5.754	0.77	141.92	816.591	10.749
CaO	0.274	23.016	3.07	56.08	1290.711	16.990
CaF2	0.179	15.036	2.00	78.08	1173.987	15.454
	1.1905	100			7596.744	

Raw Mat	Wt for 100g	
SiO2	26.705	
al(oh)2	46.055	
CaHPO4	20.606	8.493928
CaCO3	15.164	
CaF2	15.454	

A5

Oxide	mol	mol%	mol ratio	RMM	Wt = mol	wt%
SiO2	0.402	33.767	4.50	60.08	2028.741	29.922
al203	0.267	22.428	2.99	101.96	2286.713	33.727
P2O5	0.0685	0.000	0.77	141.92	0.000	0.000
CaO	0.274	23.016	3.07	56.08	1290.711	19.037
CaF2	0.179	15.036	2.00	78.08	1173.987	17.315
	1.1905	94.24612			6780.153	

Raw Mat	Wt for 100g	
SiO2	29.922	
al(oh)2	51.602	
CaHPO4	0.000	0
CaCO3	33.977	
CaF2	17.315	

Batch Calculations

Fe2O3 Substitution

Oxide	mol		RMM	Wt = mol	wt%
SiO2		0.402	60.08	24.152	20.897
Fe2O3		0.267	159.69	42.637	36.892
P2O5		0.137	141.92	19.443	16.823
CaO		0.274	56.08	15.366	13.295
CaF2		0.179	78.08	13.976	12.093
				115.575	

Oxide	Oxide x Factor	Weight for 100g of glass
SiO2	20.897 x 1	**20.8975**
Fe2O3	36.892 x 1	**36.8915**
P2O5	16.823 x 1.917	**32.2497**
CaO		
CaF2	12.093 x 1	**12.0929**

33.15813 CaHPO4 gives 13.2933g of CaO therefore no need to add CaCO3

B1

Oxide	mol		mol%	mol ratio	RMM	Wt = mol x RMM	wt%
SiO2		0.402	31.930	4.50	60.08	1918.360604	20.8975
Fe2O3		0.267	21.207	2.99	159.69	3386.594917	36.8915
P2O5		0.137	10.882	1.53	141.92	1544.324067	16.8229
CaO		0.274	21.763	3.07	56.08	1220.4861	13.2952
CaF2		0.179	14.218	2.00	78.08	1110.112788	12.0929
		1.259	100			9179.878475	

Raw Mat	Wt for 100g		
SiO2	20.897451		
Fe2O3	36.891501		
CaHPO4	32.249547		
CaCO3	0.003	giving CaO	13.2933
CaF2	12.092892		

B2

Oxide	mol		mol%	mol ratio	RMM	Wt = mol x RMM	wt%
SiO2		0.402	32.823	4.50	60.08	1972.007	21.815
Fe2O3		0.267	21.800	2.99	159.69	3481.301	38.511
P2O5		0.10275	8.389	1.15	141.92	1190.633	13.171
CaO		0.274	22.372	3.07	56.08	1254.617	13.879
CaF2		0.179	14.615	2.00	78.08	1141.157	12.624
		1.22475	100			9039.715	

Raw Mat	Wt for 100g		
SiO2	21.815		
Fe2O3	38.511		
CaHPO4	25.249	giving CaO	10.408
CaCO3	6.195		
CaF2	12.624		

B3

Oxide	mol		mol%	mol ratio	RMM	Wt = mol x RMM	wt%
SiO2		0.402	33.767	4.50	60.08	2028.741	22.817
Fe2O3		0.267	22.428	2.99	159.69	3581.456	40.280
P2O5		0.0685	5.754	0.77	141.92	816.591	9.184
CaO		0.274	23.016	3.07	56.08	1290.711	14.516
CaF2		0.179	15.036	2.00	78.08	1173.987	13.203
		1.1905	100			8891.487	

Raw Mat	Wt for 100g		
SiO2	22.817		
Fe2O3	40.280		
CaHPO4	17.606	giving CaO	7.257
CaCO3	12.956		
CaF2	13.203		

B4

Oxide	mol		mol%	mol ratio	RMM	Wt = mol x RMM	wt%
SiO2		0.402	34.768	4.50	60.08	2088.835	23.915
Fe2O3		0.267	23.092	2.99	159.69	3687.544	42.218
P2O5		0.03425	2.962	0.38	141.92	420.390	4.813
CaO		0.274	23.697	3.07	56.08	1328.944	15.215
CaF2		0.179	15.481	2.00	78.08	1208.763	13.839
		1.15625	100			8734.477	

Raw Mat	Wt for 100g		
SiO2	23.915		
Fe2O3	42.218		
CaHPO4	9.227	giving CaO	3.803
CaCO3	20.368		
CaF2	13.839		

B5

Oxide	mol		mol%	mol ratio	RMM	Wt = mol x RMM	wt%
SiO2		0.402	35.829	4.50	60.08	2152.599	25.124
Fe2O3		0.267	23.797	2.99	159.69	3800.110	44.353
P2O5		0	0.000	0.00	141.92	0.000	0.000
CaO		0.274	24.421	3.07	56.08	1369.512	15.984
CaF2		0.179	15.954	2.00	78.08	1245.661	14.539
		1.122	100			8567.881	

Raw Mat	Wt for 100g		
SiO2	25.124		
Fe2O3	44.353		
CaHPO4	0.000	giving CaO	0.000
CaCO3	28.529		
CaF2	14.539		

Batch Calculation

B1											
Oxide	mol	mol%	mol ratio	RMM	Wt = mol x	wt%		Raw Mat	Wt for 100g		
SiO2	0.402	31.930	4.50	60.08	1918.361	20.89745		SiO2	20.89745		
Fe2O3	0.267	21.207	2.99	159.69	3386.595	36.8915		Fe2O3	36.8915		
P2O5	0.137	10.882	1.53	141.92	1544.324	16.82292		CaHPO4	32.24955		
CaO	0.274	21.763	3.07	56.08	1220.486	13.29523		CaCO3	0.003	giving CaO	13.2933
CaF2	0.179	14.218	2.00	78.08	1110.113	12.09289		CaF2	12.09289		
	1.259	100			9179.878						
C1											
Oxide	mol	mol%	mol ratio	RMM	Wt = mol x	wt%		Raw Mat	Wt for 100g		
SiO2	0.402	35.717	4.50	60.08	2145.905	25.62399		SiO2	25.62399		
Fe2O3	0.1335	11.861	1.49	159.69	1894.146	22.61777		Fe2O3	22.61777		
P2O5	0.137	12.172	1.53	141.92	1727.502	20.62789		CaHPO4	39.54367		
CaO	0.274	24.345	3.07	56.08	1365.253	16.30232		CaCO3	0.004	giving CaO	16.29995
CaF2	0.179	15.904	2.00	78.08	1241.788	14.82803		CaF2	14.82803		
	1.1255	100			8374.594						
C2											
Oxide	mol	mol%	mol ratio	RMM	Wt = mol x	wt%		Raw Mat	Wt for 100g		
SiO2	0.402	36.838	4.50	60.08	2213.256	27.01726		SiO2	27.01726		
Fe2O3	0.1335	12.234	1.49	159.69	1953.596	23.84758		Fe2O3	23.84758		
P2O5	0.10275	9.416	1.15	141.92	1336.291	16.31213		CaHPO4	31.27036		
CaO	0.274	25.109	3.07	56.08	1408.103	17.18873		CaCO3	7.673	giving CaO	12.88968
CaF2	0.179	16.403	2.00	78.08	1280.762	15.63429		CaF2	15.63429		
	1.09125	100			8192.009						
C3											
Oxide	mol	mol%	mol ratio	RMM	Wt = mol x	wt%		Raw Mat	Wt for 100g		
SiO2	0.402	38.032	4.50	60.08	2284.973	28.57076		SiO2	28.57076		
Fe2O3	0.1335	12.630	1.49	159.69	2016.898	25.21882		Fe2O3	25.21882		
P2O5	0.0685	6.481	0.77	141.92	919.7275	11.50006		CaHPO4	22.04561		
CaO	0.274	25.922	3.07	56.08	1453.729	18.17709		CaCO3	16.224	giving CaO	9.087226
CaF2	0.179	16.935	2.00	78.08	1322.263	16.53327		CaF2	16.53327		
	1.057	100			7997.591						
C4											
Oxide	mol	mol%	mol ratio	RMM	Wt = mol x	wt%		Raw Mat	Wt for 100g		
SiO2	0.402	39.306	4.50	60.08	2361.492	30.31381		SiO2	30.31381		
Fe2O3	0.1335	13.053	1.49	159.69	2084.44	26.75738		Fe2O3	26.75738		
P2O5	0.03425	3.349	0.38	141.92	475.2637	6.100828		CaHPO4	11.69529		
CaO	0.274	26.791	3.07	56.08	1502.412	19.28604		CaCO3	25.818	giving CaO	4.820811
CaF2	0.179	17.502	2.00	78.08	1366.543	17.54193		CaF2	17.54193		
	1.02275	100			7790.152						
C5											
Oxide	mol	mol%	mol ratio	RMM	Wt = mol x	wt%		Raw Mat	Wt for 100g		
SiO2	0.402	40.668	4.50	60.08	2443.314	32.28337		SiO2	32.28337		
Fe2O3	0.1335	13.505	1.49	159.69	2156.663	28.49586		Fe2O3	28.49586		
P2O5	0	0.000	0.00	141.92	0	0		CaHPO4	0		
CaO	0.274	27.719	3.07	56.08	1554.468	20.5391		CaCO3	36.658	giving CaO	0
CaF2	0.179	18.108	2.00	78.08	1413.892	18.68167		CaF2	18.68167		
	0.9885	100			7568.337						

Appendix II

Cell Culture – ROS cells

Prep for SEM

Require:

Plates of cultured cells, 0.1M-cacodylate buffer, plastic pipettes, gluteraldehyde in buffer, osmium tetra oxide,

Method:

1. Remove media from cells
2. Add 2 ml of 0.1M cacodylate buffer (washes off residual protein) leave for 3 – 5 mins
3. Remove cacodylate buffer
4. Gently add 1 – 2 ml of gluteraldehyde in buffer (fixative) leave for 30 mins
5. Remove gluteraldehyde
6. Add 1ml of cacodylate buffer to rinse residual gluteraldehyde from surface and remove
7. Add ~ ½ ml of osmium tetra oxide just enough to cover material surface (take care use fume cupboard – can cause blindness if comes in contact with eyes) leave for 1 –2 hours
8. Remove osmium tetra oxide
9. Add 2 ml of 0.1M cacodylate buffer leave for 10 – 15 mins
10. If need to be stored then replace cacodylate buffer with fresh buffer
11. Proceed with John Procter's protocol (steps 12 – 29)
12. Remove buffer
13. Add 75% ethanol leave for 15 mins
14. Remove 75% ethanol
15. Add 95% ethanol leave for 15 mins.
16. Remove 95% ethanol
17. Add 100% ethanol leave for 15 mins.
18. Remove 100% ethanol
19. Add100% ethanol dried over anhydrous Copper sulphate leave for 15 mins.
20. Remove 100% ethanol dried over anhydrous Copper sulphate
21. Add a 50/50 mixture of 100% ethanol and hexamethyldisilazane and leave for 30 mins
22. Remove 50/50 mixture
23. Add 100% hexamethyldisilazane and leave for 30 mins.
24. Samples air dried overnight in fume cupboard
25. Mount onto 12.5mm diameter stubs
26. Coat sides and base with silver dag
27. Carbon or Gold Coat

Appendix III

Available online at www.sciencedirect.com
SCIENCE DIRECT
ELSEVIER
Biomaterials 24 (2003) 3153–3160
Biomaterials
www.elsevier.com/locate/biomaterials

Devitrification of ionomer glass and its effect on the in vitro biocompatibility of glass-ionomer cements

K. Hurrell-Gillingham[a,b], I.M. Reaney[a,b], C.A. Miller[a], A. Crawford[b], P.V. Hatton[b,*]

[a] *Department of Engineering Materials, Sir Robert Hadfield Building, University of Sheffield, Sheffield S1 3JD, UK*
[b] *Centre for Biomaterials and Tissue Engineering, School of Clinical Dentistry, Claremont Crescent, University of Sheffield, Sheffield S10 2TA, UK*

Received 8 February 2003; accepted 20 February 2003

Abstract

The effects of devitrification of an ionomer glass with a molar composition $4.5SiO_2 \cdot 3Al_2O_3 \cdot 1.5P_2O_5 \cdot 3CaO \cdot 2CaF_2$ on cement formation and in vitro biocompatibility were investigated. Differential thermal analysis was used to study the phase evolution in the glass, and to determine the heat treatments for production of glass-ceramics. X-ray diffraction patterns from glass frit heat-treated at 750°C for 2 h contained peaks corresponding to apatite (JCPDS 15-876), whereas for samples heat-treated at 950°C for 2 h apatite and mullite (JCPDS 15-776) were the major phases detected. Transmission electron microscopy (TEM) confirmed that apatite and apatite–mullite phases were present after heat treatments at 750°C and 950°C respectively. Glass and glass-ceramics were ground to prepare $<45\,\mu m$ powders and glass ionomer cements were produced using a ratio of 1 g powder: 0.2 g PAA: 0.3 g 10% m/v tartaric acid solution in water. In vitro biocompatibility was evaluated using cultured rat osteosarcoma (ROS) cells. Scanning electron microscopy (SEM) showed that cells colonised the surfaces of cements prepared using untreated ionomer glass and glass crystallised to form apatite (750°C/2 h). However, quantitative evaluation using MTT and total protein assays indicated that more cell growth occurred in the presence of cements prepared using ionomer glasses crystallised to apatite than cements prepared using untreated glass. The least cell growth and respiratory activity was observed on cements made with crystallised glass containing both apatite and mullite. It was concluded that the controlled devitrification of ionomer glasses could be used to produce GIC bone cements with improved biocompatibility.

Keywords: Glass-ionomer cement; Devitrification; Crystallisation; Apatite; Apatite–mullite glass-ceramic

1. Introduction

Glass-ionomer cements (GICs) have been used extensively as restorative materials in dentistry for over 30 years [1]. They are made by combining a basic fluoroaluminosilicate glass, an acidic polymer (e.g. polyacrylic acid), and water or a dilute solution of tartaric acid. The cement sets via a neutralisation reaction between these components. It is generally believed that acidic degradation of the glass powder results in ion release, with cations (Ca^{2+} and Al^{3+}) then cross-linking ionised carboxylic acid groups in the polymer chains, causing the cement to set by gelation [2]. The properties associated with this class of biomaterial include adhesion to mineralised tissues, good biocompatibility, and a minimal exotherm during setting [3–6]. These properties led in turn to the development of GIC bone cements for wider surgical applications, including applications in otology where they are used for reconstruction of the ossicular chain and cementation of implants [4–6].

While GICs have been used successfully for over 30 years in dentistry, there are still concerns regarding GIC biocompatibility in non-dental applications. In particular, Al^{3+} release has been associated with poor local bone mineralisation and local neurotoxicity [7–10]. Numerous cell culture studies of cytotoxicity have reported cell inhibition by specific GIC compositions, and Brook and Hatton reviewed this work in 1998 [11]. It appeared that the in vitro toxicity of GICs was due to a complex mechanism based on both ion release (in particular, Al^{3+} and F^-) and pH effects [11–14]. Early animal studies of GIC bone cements provided evidence of good biocompatibility [12,15–17]. However, subsequent work that employed more careful specimen

*Corresponding author.
E-mail address: p.v.hatton@sheffield.ac.uk (P.V. Hatton).

0142-9612/03/$ - see front matter
doi:10.1016/S0142-9612(03)00124-8

preparation showed a mineral defect in bone adjacent to GICs caused by Al^{3+} release [7,8]. Of greater concern were reports of in vivo neurotoxicity of freshly mixed GIC bone cements [9,10]. The most serious manifestations of this problem were clinical reports of complications, and even death following skull base surgery where relatively large volumes of a GIC bone cement were apparently placed in direct contact with cerebral spinal fluid (CSF) or brain tissue [18–20]. While doubts have been expressed over the surgical approach taken, and current GIC bone cements are contra-indicated for these clinical applications, concerns remain regarding the biocompatibility of these biomaterials. Surprisingly, little effort has been directed at understanding the interaction of these biomaterials with tissues, or the design of safer bone cements, despite the current debate concerning GIC bone cement biocompatibility. Further research is clearly desirable.

Hill and co-workers have described crystallisation following heat treatment of a number of ionomer glasses. They reported that most compositions crystallised to apatite and mullite, with occasional formation of fluorite and anorthite [21,22]. While much of this work has focussed on the development of castable glass-ceramics for medical and dental applications, it seems likely that devitrification of ionomer glasses represents a route to modify and study GIC properties including biocompatibility [22]. However, no attempts to modify the biocompatibility of a medical grade GIC using this approach have been reported. The aim of this study was therefore to demonstrate crystallisation in an ionomer glass composition used in the manufacture of a commercial GIC bone cement, and to evaluate the effects of devitrification on in vitro biocompatibility. If successful, devitrification could provide a route for the development of GIC bone cements with improved biocompatibility.

2. Experimental procedure

2.1. Materials

An ionomer glass composition used in the manufacture of commercial GIC bone cement (SerenoCem®, Corinthian Medical, UK) was prepared *in-house* according to the following pre-melt molar oxide ratio:

$4.5SiO_2 \cdot 3Al_2O_3 \cdot 1.5P_2O_5 \cdot 3CaO \cdot 2CaF_2$.

The glass was produced by mixing appropriate amounts of silica (Loch Aline sand 99.5%) $CaHPO_4$, $Al(OH)_3$ (Standard laboratory grade chemicals, Fisher Scientific ltd., UK), and CaF_2 (Aldrich Chemical Company, USA). The oxide powders were melted in a covered sillimanite crucible at 1450°C for 3 h using an electrically heated box glass-melting furnace. Water-cooled granular frit and steel quenched pieces of glass were produced. The crucible and glass were weighed before and after melting and the losses were determined.

2.2. Characterisation

2.2.1. X-ray fluorescence (XRF)

The composition of the glass was verified by X-ray fluorescence (Philips PW2400 X-ray fluorescence spectrometer). Samples were prepared by fusing powdered glass with a flux producing a glass-like bead, which was then irradiated with high-energy primary X-ray photons. The weight percent of the oxides present were determined and the fluoride content calculated.

2.2.2. Differential thermal analysis (DTA) and heat treatment

Differential thermal analysis (Perkin-Elmer DTA7 running Pyris thermal analysis software in Unix) at a heating rate of 10°C min^{-1} to 1000°C was performed to determine the onset of crystallisation. In accordance with the exothermic peaks observed crystallised glass was prepared. Fast-quenched pieces of glass were heated to 750°C and 950°C at 5°C min^{-1} respectively and held for 120 min before cooling at 5°C min^{-1}.

2.2.3. X-ray diffraction (XRD)

X-ray powder diffraction (Philips diffractometer, Holland) was used to identify the crystal phases present in the heat-treated glasses. The samples were placed in Al holders and analysed using Cu radiation ($\lambda = 1.5406$ Å) with an angle range of 10°2θ to 70°2θ in 0.2°2θ intervals with a speed of 2°2θ/min.

2.2.4. Transmission electron microscopy (TEM)

Samples were ground and polished to less than 30 μm, a Cu support ring was then attached using epoxy resin. Thinning to perforation was achieved using an ion beam miller (Gatan dual ion beam miller) operating at an incidence angle of 15°, an accelerating voltage of 6 kV and a combined gun current of 6 mA. Samples were analysed using a Philips EM420 TEM operating at 120 kV which was equipped with link eXL energy dispersive detection and analytical software.

2.3. Cement preparation

Glasses and heat-treated glasses (glass-ceramics) were ground and sieved to prepare a <45 μm powder. Commercial Mercaptan-free poly(acrylic acid) (PAA) with a mean molecular weight of 52,000 (batch 079915-2, Advanced Healthcare, Tonbridge, Kent, UK) was employed. Cement discs (9 mm × 1.5 mm) were made using a ratio of 1 g glass powder: 0.2 g PAA (batch 079915-2, Advanced Healthcare, UK): 0.3 g 10% m/v tartaric acid solution. The ratios are in accordance with

the commercial system. The components were mixed thoroughly, placed into a silicone mould and left to set at ambient temperature (21 ± 2°C) until fully hardened. Cement discs were sterilised by autoclaving (15 min at 121°C). The resulting cements were named GIC, GIC 750 and GIC 950 in accordance with the heat treatment schedule.

2.4. In vitro biocompatibility

Biocompatibility was investigated using rat osteosarcoma (ROS 17/2.8, Merck Inc.) cells seeded into wells of a 24 well-plate containing test samples (seeding density of 1.25×10^4 cells/ml) with a total well volume of 1 ml. A non-material control was included for comparison. The materials and cells were incubated at 37°C in a 5% CO_2 atmosphere for 72 h. MTT assay (3-(4,5-dimethylthiazol-2-yl)-2,5-diphenyltetrazolium bromide) was carried out on cells cultured on samples of each cement composition ($n = 4$). Total protein assay was also performed on cultures using the Biruet method ($n = 4$). In addition, scanning electron microscopy (SEM) was used to observe cell morphology on the GIC discs. These methods have been reported previously for the evaluation of in vitro biocompatibility [14,23].

3. Results and discussion

3.1. Glass characterisation

XRF data demonstrated a close similarity between the pre-melt molar composition and the glass frit. Table 1 indicated that very little volatilisation occurred during melting. The potential for fluorine loss in the form of SiF_4 from ionomer glass melts has been widely reported [21,24–27]. However, the glass composition used in this study had been optimised for minimal fluoride losses. Incorporating a basic oxide into the glass ensures that there is at least one non-bridging oxygen per silicon, leaving sufficient aluminium atoms free to bind with the fluorine [26]. DTA was used to determine the temperature of the onset of crystallisation. Two crystallisation exothermic peaks (T_1 at 725°C and T_2 at 916°C) were observed (Fig. 1) from this the heat treatment schedule was derived. It was not possible to determine a glass transition temperature.

XRD (Fig. 2) showed that the quenched glass was amorphous, but on heating to 750°C peaks were recorded that corresponded to the presence of apatite ($Ca_5(PO_4)_3(F)$—JCPDS #15-876). At 950°C, mullite ($Al_6Si_2O_{13}$—JCPDS #15-776) was the major phase present in addition to apatite and cristobalite (SiO_2—JCPDS #39-1425). This was largely in accordance with previous reports of crystallisation in ionomer glasses [21]. The degree of crystallinity was also calculated using

Table 1
XRF data showing the oxides present in the glass post-melting compared with pre-melt molar oxide ratios in the batch

Oxides	Mole percent	
	Pre-melt glass composition	Post-melt glass composition
SiO_2	32.01	31.55
Al_2O_3	21.29	21.96
P_2O_5	10.90	9.23
CaO	21.56	25.96
CaF_2	14.24	11.26

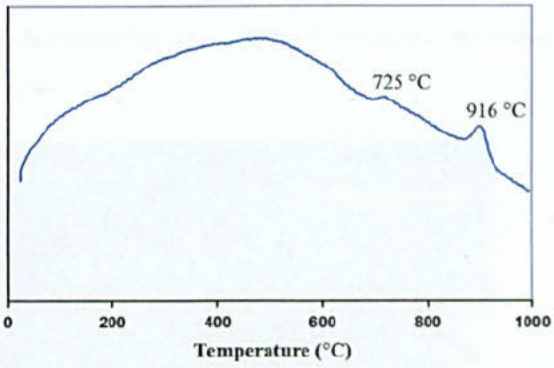

Fig. 1. Differential thermal analysis showing exotherms at 725°C and 916°C.

XRD data. The intensity of the amorphous hump greatly decreased with increasing heat treatment temperature. A quantitative investigation of the percentage of devitrification was determined for the heat-treated samples using Eq. (1) devised by Ohlberg and Strickler [28]:

$$\alpha = \frac{(I_g - I_x)}{(I_g - I_b)} \times 100 \quad (1)$$

I_g is the intensity of the parent glass, I_x is the intensity of the partially crystallised glass and I_b is the intensity of fully crystalline material. The degree of crystallinity was calculated for 2θ values over the amorphous region but not where crystal phases were present. At 750°C the glass contained only 30% crystallinity due to the development of an apatite phase. However, by 950°C the glass was almost entirely crystalline (98%).

TEM showed changes in microstructures that developed at 750°C and 950°C. A distribution of blocky crystals ranging in size from 0.5–0.1 μm was observed in the glass heat-treated at 750°C (Figs. 3a and b). Energy dispersive X-ray spectroscopy (EDS) indicated that the crystalline regions (Fig. 3c) were rich in Ca, P, O and F. The residual glass (Fig. 3d) contained Si, Al, O, Ca and P. However, the amount of Ca and P was much lower in these glassy regions compared with the

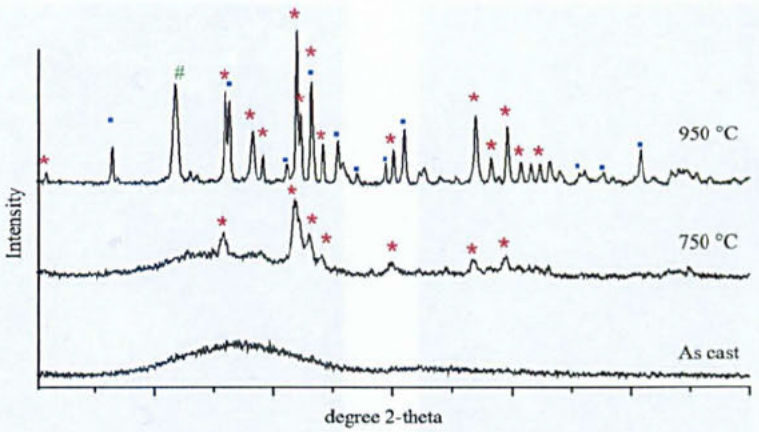

Fig. 2. X-ray diffraction traces obtained from the amorphous glass, and glasses heat-treated to 750°C and 950°C: (*) apatite, (■) mullite, (#) cristobalite.

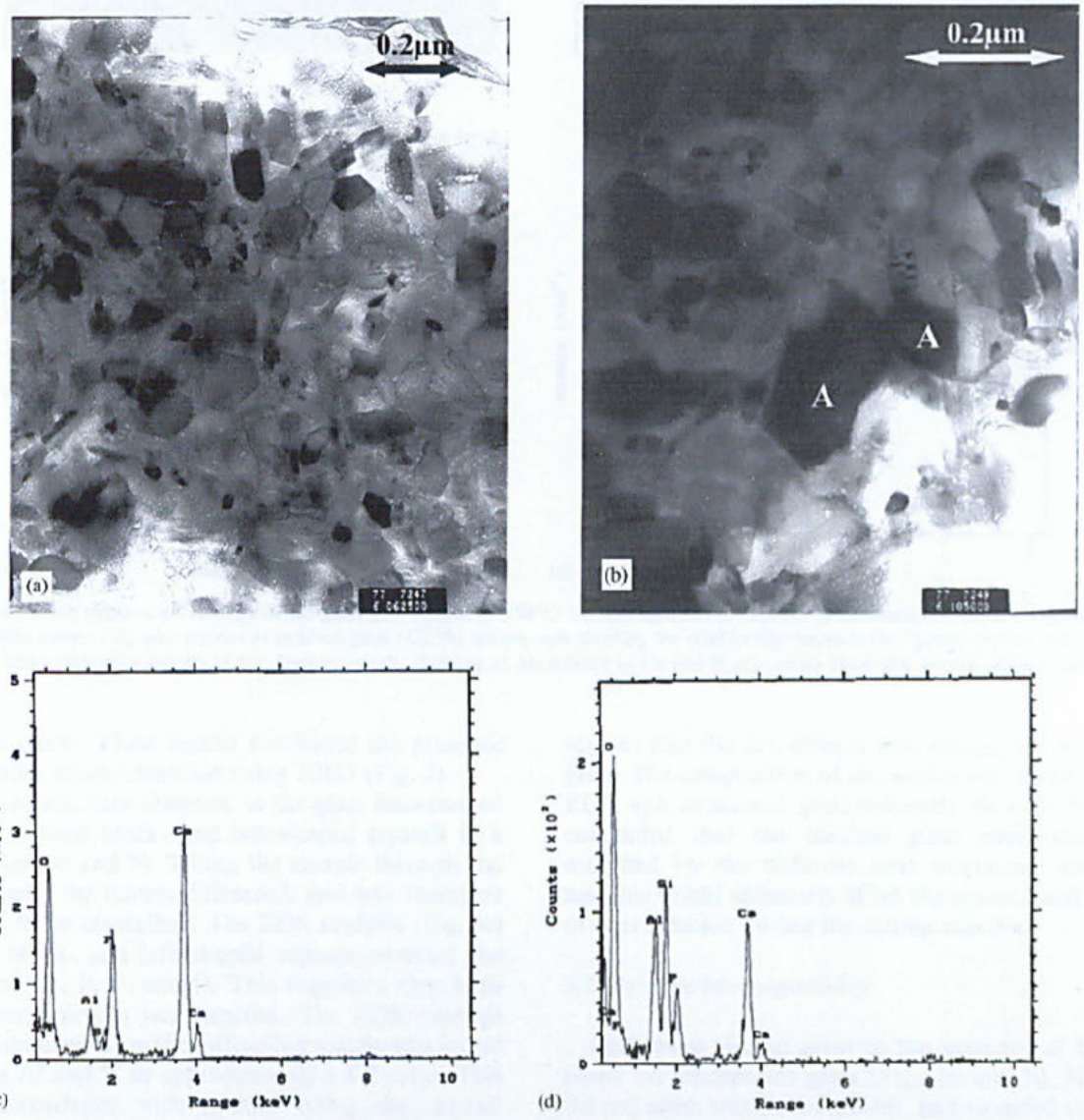

Fig. 3. Transmission electron microscopy of the glass heat-treated to 750°C: (a) micrograph showing the general microstructure of apatite crystals with regions of residual glass; (b) micrograph showing the apatite crystals and the residual glass; (c) energy dispersive spectra of the blocky crystalline regions, showing an abundance of Ca and P; (d) energy dispersive spectra of the residual glass.

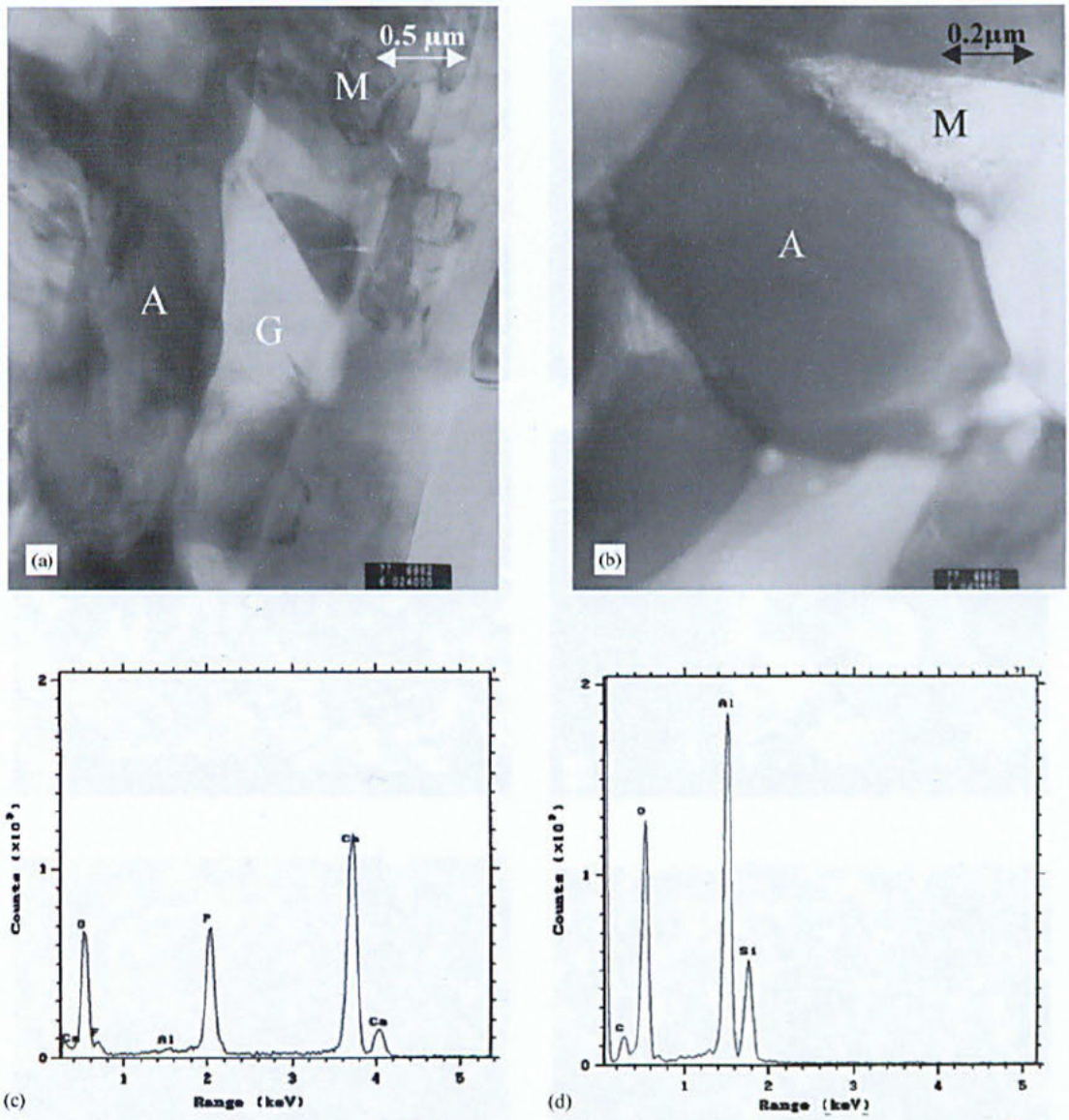

Fig. 4. Transmission electron microscopy of the glass heat-treated to 950°C: (a) micrograph showing the general microstructure of apatite crystals (A) in a mullite matrix (M) with regions of residual glass (G); (b) micrograph showing the relationship between the apatite crystals and the mullite matrix; (c) energy dispersive spectra of the apatite crystals, showing an abundance of Ca and P; (d) energy dispersive spectra of the mullite matrix.

crystalline phase. These results confirmed the presence of the apatite phase identified using XRD (Fig. 2).

The microstructure observed in the glass heat-treated to 950°C showed block- and lath-shaped crystals in a matrix (Figs. 4a and b). Tilting the sample through the x-axis showed the matrix diffracted, and was therefore concluded to be crystalline. The EDS analysis (Fig. 4c) from the block- and lath-shaped regions revealed the presence of Ca, P, F, and O. This suggested that both crystal morphologies were apatite. The EDS analysis (Fig. 4d) obtained from the diffracting matrix was found to contain Al and Si in approximately a 6:2 ratio. This was in accordance with mullite being the second crystalline phase as identified by XRD. Remaining regions that did not diffract were designated as residual glass. The composition of this region was determined by EDS and contained predominantly Si and O. It was concluded that the residual glass composition was modified by the different heat treatments described, and this would ultimately affect the amount and identity of ions released during the setting reaction.

3.2. *In vitro biocompatibility*

Cells were able to grow in the presence of the GIC based on amorphous glass (Figs. 5a and b). However, the cell sheet was not confluent, and rounded cells were present in addition to flattened ROS cells with a normal

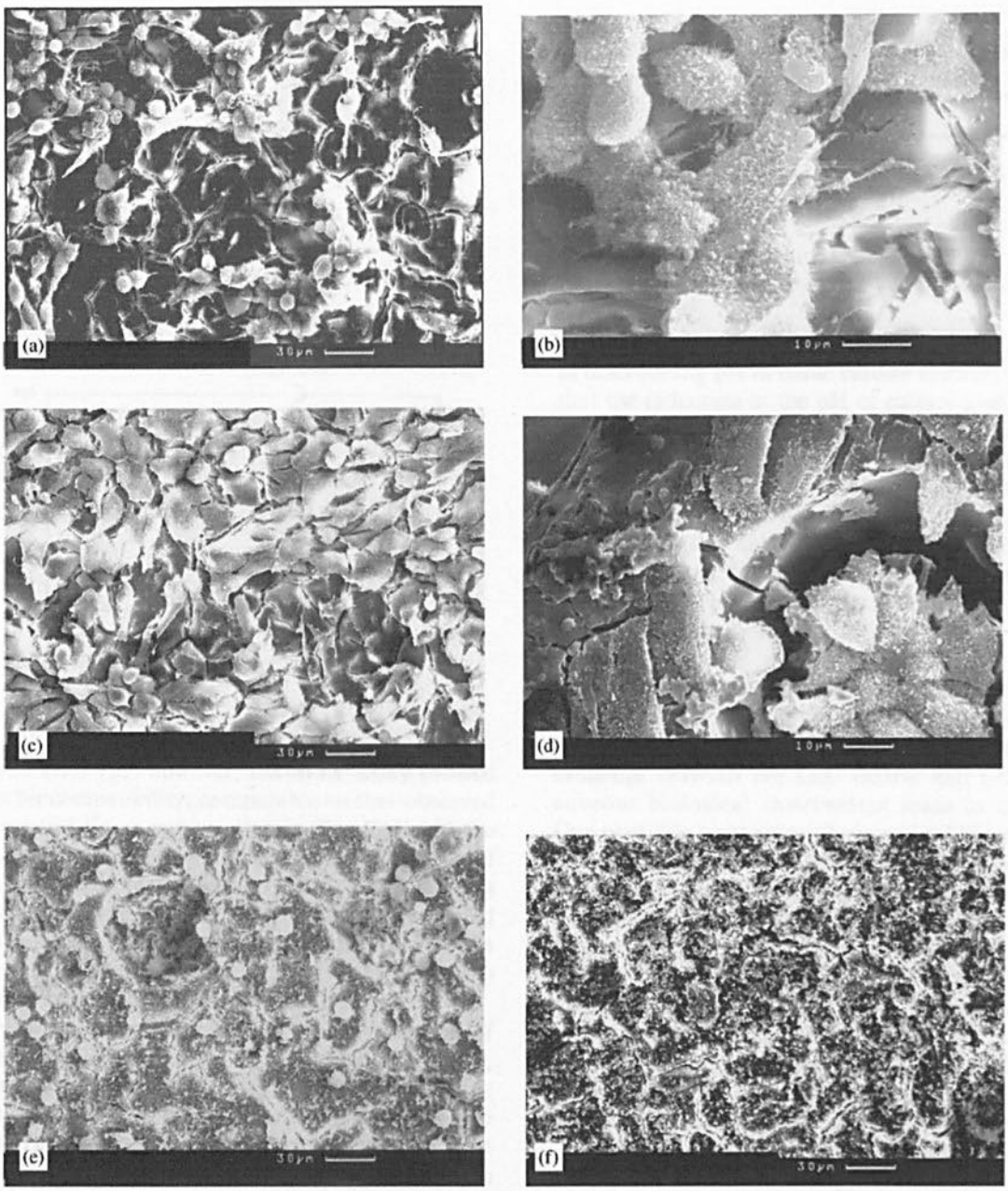

Fig. 5. Secondary electron SEM images of cell cultured cements: (a) GIC (based on amorphous glass) showing cells of differing morphology, rounded and flattend; (b) GIC showing flattened cells with pseudopodia present; (c) GIC 750 displaying a confluent sheet of cells; (d) cells colonising a surface defect on GIC 750; (e) GIC 950 showing non-vital, rounded cells on the materials surface; (f) GIC (950) from the cell-free control, post culturing showing an absorbed protein layer on the surface.

osteoblast-like appearance. In contrast, ROS cells cultured on GIC 750 (based on an ionomer glass crystallised to apatite) formed a confluent sheet of flattened cells with classical osteoblast-like morphology (Figs. 5c and d). The latter observations were similar to previous reports of biomaterials that showed good in vitro biocompatibility [14,23]. The poorest cell response was to GIC 950 (based on the most crystalline ionomer glass that contained apatite, mullite and little residual glass). Here SEM micrographs showed only rounded cells and adsorbed proteins from the culture medium (Fig. 5e). The appearance of the adsorbed protein layer without cells is shown in Fig. 5f for comparison.

Following the quantitative MTT assay, normal GIC (formed with amorphous glass) showed a poorer cell response than that observed with control tissue culture plastic (Fig. 6). This was in accordance with many previous in vitro evaluations of GIC biocompatibility

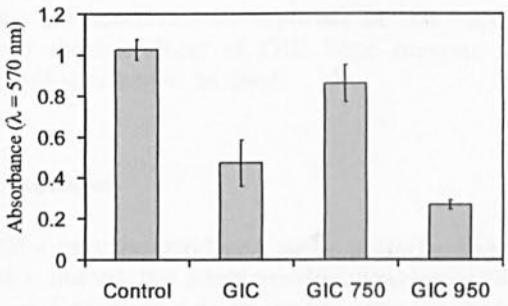

Fig. 6. Bar chart showing MTT assay results.

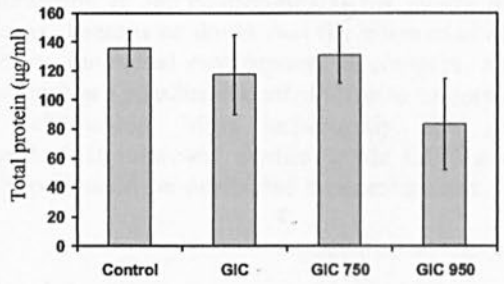

Fig. 7. Bar chart showing total protein results.

[12–14]. In GIC 750, however, the MTT assay showed excellent biocompatibility, comparable to that observed for the control tissue culture plastic. For GIC 950 the MTT assay results obtained showed little evidence of cell growth and metabolism (Fig. 6). This trends demonstrated by quantitative MTT assay were repeated in the evaluation of total protein synthesised in the presence of test materials (Fig. 7), with GIC 950 supporting the least biosynthetic activity.

These results may be explained by the presence of different crystalline phases in the glasses. In GIC 750, Ca, F and P ions were not available for release since they were contained largely within a stable crystalline phase (apatite). The presence of apatite in the glass may have accounted for the improved cellular response, as apatite has long been associated with excellent biocompatibility (in particular with bone tissue) [29]. However, observations of colour changes in the medium that contained a pH indicator (phenol red) during cell culture suggested an additional mechanism was operating. While direct measurement of pH in culture medium is difficult due to the presence of buffers and proteins, an attempt was made to quantify this observation. Table 2 gives the pH of media after the 72 h culture period, determined in the presence of and without cells. The cell-free tissue culture plastic control had no effect on the pH of the culture media (pH = 7.0), and the growth of cells reduced the pH slightly as anticipated. However, both GIC and GIC 950 reduced the pH of the cell-free culture media to around 6 and 5, respectively. Even given the difficulties

Table 2
Effect of cement discs on pH of culture media in the presence and absences of cells

Material	pH	
	With cells	Without cells
Material free control	6.6	7.0
GIC	5.9	5.9
GIC 750	7.2	7.3
GIC 950	5.1	5.1

of determining pH in tissue culture medium, it was likely that the reduction in the pH of culture medium by GIC and GIC 950 contributed to the poor biocompatibility of these materials. In the case of GIC 950, relatively little residual glass was available for reaction. It was therefore likely that unreacted poly(acrylic acid) contributed to the acidification of the culture medium and the poorer biocompatibility of this material (see Section 3.1). This was not the case for GIC 750 where only 30% crystallinity was determined.

In the presence of GIC 750, the pH of cell-free medium was 7.2. No acidification was detected after cell culture, suggesting that the apatite-containing GIC had actually provided additional buffering capacity. Anion exchange between the GIC matrix and [-OH^-] in the aqueous biological environment leads to acidification. One plausible mechanism for improved biocompatibility was therefore that less fluoride and phosphate ionic species were available for release when crystallised as fluorapatite. While further work is necessary, it is interesting that the numerous papers that have reported GIC biocompatibility have not considered the potential influence of phosphate [12–14]. This research did not provide evidence for specific in vitro cytotoxicity mediated by Al^{3+}. The authors consider Al^{3+} release to be an in vivo problem, causing poor local bone mineralisation and neurotoxicity [7–11,13–14].

This research has demonstrated that it is possible to modify the biocompatibility of GIC bone cement by controlled crystallisation of the constituent ionomer glass. While the in vitro data presented here is encouraging, further in vivo studies are required to confirm osteoconductivity. In addition, controlled clinical trials should be performed before these modified GICs are placed on the market. The clinical complications described in the introduction to this paper should have been avoidable, as many of the features of a GIC that conspired to cause the deaths of patients were already known. Specifically, the moisture sensitivity of setting GICs, low pH, Al^{3+} release and its dose-dependent effect on nerve tissue had all been described in the literature [7–11,13–14]. Together these features make GIC bone cements both technique-sensitive and only biocompatible in specific clinical applications.

While the modifications reported in this paper may extend the usefulness of GIC bone cements, Al-free compositions would be ideal.

4. Conclusion

GICs may be produced using partially crystallised glasses. Indeed, this study provides convincing evidence that devitrification may be used to improve the in vitro biocompatibility of GICs. The mechanism is most likely based on the formation of an apatite phase, and the modification of the environmental pH effects of these cements. There is no doubt that the interaction of GICs with the biological environment is complex, and this paper makes a significant contribution to understanding this relationship. More importantly, this research suggests that improved medical-grade GICs could be developed based on devitrified ionomer glasses.

Acknowledgements

The authors would like to acknowledge the EPSRC for funding this research project. Ian Watts and Dean Haycock for help in making the glass and John Procter for preparation of specimens for scanning electron microscopy. The authors would like to thank Merck Inc. for permission to use the ROS 17/2.8 cell line.

References

[1] Wilson AD. Glass-ionomer cement—origins development and future. Clin Mater 1991;7:275–82.
[2] Hatton PV, Brook IM. Characterisation of the ultrastructure of glass-ionomer (poly alkenoate) cement. Br Dent J 1992;173:275–7.
[3] Walls AWG. Glass polyalkenoate (glass-ionomer) cements: a review. J Dent 1986;14:231–43.
[4] Higgs WAJ, Lucksanasombool P, Higgs RJED, Swain MV. A simple method of determining the modulus of orthopedic bone cement. J Biomed Mater Res (Appl Biomater) 2001;58:188–95.
[5] Geyer G, Helms J. Ionomer-based bone substitute in otologic surgery. J Eur Arch Otorhinolaryngol 1993;250:253–6.
[6] Ramsden RT. Cochlear implant fixation with ionomeric bone glue. Adv Otorhinolaryngol 1995;50:51–3.
[7] Carter DH, Sloan P, Brook IM, Hatton PV. Role of exchanged ions in the integration of ionomeric (glass polyalkenoate) bone substitutes. Biomaterials 1997;18:459–66.
[8] Blades MC, Moore DP, Revell PA, Hill R. In vivo skeletal response and biomechanical assessment of two novel polyalkenoate cements following femoral implantation in the female new zealand white rabbit. J Mater Sci: Mater Med 1998;9:701–6.
[9] Loescher AR, Robinson PP, Brook IM. The effect of implanted inomeric and acrylic bone cements on peripheral nerve function. J Mater Sci: Mater Med 1994;5:108–12.
[10] Loescher AR, Robinson PP, Brook IM. The immediate effects of ionomeric and acrylic bone cements on peripheral nerve function. J Mater Sci: Mater Med 1994;5:551–6.
[11] Brook IM, Hatton PV. Glass-ionomers: bioactive implant materials. Biomaterials 1998;19:565–71.
[12] Brook IM, Craig GT, Hatton PV, Jonck LM. Bone cell interactions with a granular glass-ionomer bone substitute material: in vivo and in vito culture models. Biomaterials 1992;13: 721–5.
[13] Sasanaluckit P, Albustany KR, Doherty PJ, Williams DF. Biocompatility of glass ionomer cements. Biomaterials 1993;14: 906–16.
[14] Devlin AJ, Hatton PV, Brook IM. Dependence of in vitro biocompatibility of ionomeric cements on ion release. J Mater Sci: Mater Med 1998;9:737–41.
[15] Jonck LM, Grobbelaar CJ, Strating H. Biological evalution of glass-ionomer cement (Ketac-0) as an interface material in total joint replacement. A screening test. Clin Mater 1989;4:201–24.
[16] Jonck LM, Grobbelaar CJ. Ionos bone cement (glass-ionomer): an experimental and clinical evaluation in joint replacement. Clin Mater 1990;6:323–59.
[17] Jonck LM, Grobbelaar CJ. A glass ionomer for reconstructive surgery Ionogran—an ionomeric micro implant. A biological evaluation. Clin Mater 1992;9:85–103.
[18] Hantson PH, Mahieu P, Gersdorff M, Sindic CJM, Lauwerys R. Encephalopathy with seizures after use of aluminium-containing bone cement. The Lancet 1994;344:1647.
[19] Renard JL, Felten D, Bequet D. Post-otoneurosurgery aluminium encephalopathy. Lancet 1994;344:63–4.
[20] Reusche E, Pilz P, Oberascher G, Lindner B, Egensperger R, Gloeckner KL, Trinka E, Iglseder B. Subacute fatal aluminum encephalopathy after reconstructive otoneurosurgery: a case report. Hum Pathol 2001;32:1136–40.
[21] Wood D, Hill R. Glass ceramic approach to controlling the properties of a glass-ionomer bone cement. Biomaterials 1991;12: 164–70.
[22] Hill R, Wood D. Apatite-mullite glass-ceramics. J Mater Sci: Mater Med 1995;6:311–8.
[23] Wallace KE, Hill RG, Pembroke JT, Brown CJ, Hatton PV. Influence of sodium oxide content on bioactive glass properties. J Mater Sci: Mater Med 1999;10:697–701.
[24] Barra ED, Hill RG. Influence of glass composition on the properties of glass polyalkenoate cements. Part 3: influence of fluorine content. Biomaterials 2000;21:693–8.
[25] Wilson AD, Nicholson JW. Acid-base Cements: Their Industrial Applications. Cambridge: Cambridge University Press, 1993.
[26] Clifford A, Hill R, Towler MR, Wood DJ. The crystallisation of glasses from the ternary CaF_2-$CaAl_2Si_2O_8$-P_2O_5 system. J Mater Sci 2001;36:3955–61.
[27] Clifford A, Rafferty A, Hill R, Mooney P, Wood D, Samuneva B, Maysuya S. The influence of calcium to phosphate ratio on the nucleation and crystallization of apatite glass-ceramics. J Mater Sci: Mater Med 2001;12:461–9.
[28] Ohlberg SM, Strickler DW. Determination of percent crystallinity in partly devitrified glass by X-ray diffraction. J Am Ceram Soc 1962;45:170–1.
[29] Kokubo T. Bioactive glass-ceramics—properties and applications. Biomaterials 1991;12:155–63.